Mechanogrowth factor (IGF-1Ec) and fluorescent nanoparticles in colorectal cancer

Swethan Alagaratnam

A thesis submitted to the University College London for the degree of

Doctor of Medicine (Research)

2020

UCL Center for Nanotechnology and Regenerative Medicine

Division of Surgery & Interventional Science

University College London

Declaration of originality

I, Swethan Alagaratnam, confirm that the work presented in this thesis is my own. I have outlined all contributions by others to this work in the acknowledgement sections. Information derived from other sources is indicated in the thesis.

Abstract

The IGF-1 axis was an area of significant interest in cancer therapy following promising preclinical studies but led to disappointing clinical trials. Further scrutinization of this pathway is, therefore, warranted. The IGF-1 axis has been demonstrated to inhibit autophagy via the Akt/PI3K pathway and induce autophagy via the ERK pathway. Autophagy has been associated with chemotherapy resistance in tumour cells. My work in this thesis involved investigating the expression of an isoform of IGF-1 referred to as IGF1-Ec or Mechanogrowth Factor (MGF) in colorectal cancer tissues and polyps with immunohistochemistry. Further work was done with fluorescent nanoparticles which have exciting potential to improve the diagnostic yield of investigations including colonoscopy, improve immunohistochemistry assessment of tissue biopsies and help in surgery with intraoperative delineation of tumours. In addition, I investigated the relationship between autophagy and apoptosis with a view towards developing a model for further work in investigating the effect of MGF in autophagy.

Semi-quantitative immunohistochemistry for MGF on colonic tissues including normal, polyp and cancer tissues demonstrated a significantly higher expression of MGF in colonic polyps (with higher expression with worsening dysplasia, $p=0.001$) and cancer compared to normal colon tissues ($p<0.001$). Semiconductor CdTe quantum dots and gold nanoparticles were synthesised and conjugated to the MGF peptide and antibody. Gold nanoparticles were successfully characterised with immunodots and applied to the HT29 and SW620 colorectal cancer cell lines and to tissues including normal, colon cancer and polyp tissues reflecting the results from conventional immunohistochemistry.

Autophagy inducers were administered to the cell lines HT29 and SW620 and inhibited with the use of Bafilomycin and 3-MA. Immunohistochemistry for LC3B was used to confirm the induction of autophagy, and cell viability studies were used to demonstrate significantly increased cell viability with autophagy induction and significant reduction of cell viability with inhibition of autophagy ($p<0.01$ at 24 hours). This model can be subjected to the application of MGF and assess its effects on cell viability.

MGF is overexpressed in colonic polyps and cancer with low levels of expression in normal colon tissues offering an opportunity for the use of fluorescent gold nanoparticles to augment polyp and cancer detection in colonoscopy and intraoperative tumour delineation.

Impact statement

Colorectal cancer is the third most prevalent cancer diagnosed worldwide with an early diagnosis associated with better outcomes and patients presenting with features such as involvement of draining lymph nodes demonstrating higher rates of cancer recurrence. Chemotherapy can reduce the risk of recurrence, but its efficacy is limited by toxicity due to interactions with healthy tissues. This emphasises the importance of 'targets' expressed at significantly higher levels in tumour tissues compared to healthy tissues thereby enabling drug delivery agents to accumulate chemotherapy drugs in tumours. In addition, the efficacy of chemotherapy can be affected by the expression of factors such as *KRAS*, emphasising the importance of accurate quantitative immunohistochemistry techniques to guide treatments. Chemotherapy agents have also been demonstrated to induce autophagy in colorectal cancer tissues, which acts as a protective mechanism for cancer cells at the later stages of cancer pathogenesis and a cause for resistance to chemotherapy.

My work has identified the overexpression of Mechanogrowth factor (MGF) expression in primary colorectal cancer tissues and polyps compared to normal colon tissues, thereby offering a target for drug delivery and imaging agents in colorectal cancer. MGF is expressed at low levels in healthy tissues in the body, and therefore, this would reduce the systemic distribution of targeting drug delivery agents. Further research work in this area would include the application of fluorescent gold nanoparticles conjugated to MGF antibody in xenograft models of colorectal cancer *in vivo* and investigating the efficacy of drug delivery and systemic toxicity. The advantage of fluorescent gold nanoparticles is that it provides a dual capability of tumour imaging and drug delivery alongside its low inherent toxicity. This can be further applied to prostate cancer and osteosarcomas, which have been reported in the literature to overexpress MGF. There is also a potential for application of MGF antibodies conjugated to gold nanoparticles in reducing missed lesion rates in colonoscopy, which has recently been estimated as high as 25%. The benefit of intravenously or locally administering this nanoparticle and performing colonoscopy with appropriate excitation energy will help identify these lesions with fluorescence.

Finally, improving understanding of autophagy and apoptosis is essential to help further improve the efficacy of chemotherapy agents. IGF-1 has been demonstrated to induce autophagy via the ERK pathway and inhibit autophagy via the Akt/PI3K pathway. My work demonstrating the successful induction of autophagy and inhibition in colorectal cancer cell lines provides the groundwork for investigating this with the administration of the isoforms of IGF-1.

Acknowledgements

I am very grateful to my supervisors Dr Shi-Yu Yang and Professor Barry Fuller for their guidance, help and patience throughout this research project, mainly due to the trying circumstances during my experiments with changes in my supervisors and their job roles. I am particularly grateful to Professor Loizidou for her time and help with my thesis and submission for this degree despite her busy schedule.

I would like to thank and acknowledge Dr Bala Ramesh for his invaluable support, expertise, guidance and constant encouragement without whom this may never have been possible. In particular, his work in synthesis, functionalization and conjugation of the fluorescent nanoparticles, which was a crucial part of my thesis. I would also like to acknowledge the work done by Dr Jessica Broni and Dr Francesca Launchbury with the immunohistochemistry experiments at the UCL Institute of Neurology. In addition, I would like to acknowledge Professor Fuller's MSc student, Ajit Abraham Nirmal, for his help with the autophagy experiments and Dr Richard Thorogate for his help with atomic force microscopy.

I would like to extend my gratitude to my clinical supervisors over the years including Mr David Stoker, Mr Saswata Banerjee, Mr Michael Dworkin and Mr Chetan Bhan for their persistent belief, understanding and support through this process, and Professor Marc Winslet for his guidance over the years.

Finally, I would like to dedicate this thesis to my family for their unwavering support over the years.

Table of Contents

List of Figures

List of tables

Abbreviations

3T3	Fibroblast cell line
5-FU	5-fluorouracil
AFM	Atomic force microscopy
AFP	Alpha-fetoprotein
AMPK	AMP-activated protein kinase
ATG	Autophagy related gene
BAD	Bcl-2-associated death
BAX	BCL2 Associated X
BCL2	B-cell lymphoma 2
BID	BH3 interacting-domain death agonist
BIM	Bcl-2-like protein 11
Cd	Cadmium
CEA	Carcinoembryonic antigen
CIN	Chromosome instability
CMC	Critical micelle concentration
CNT	Carbon nanotube
CpG	CpG island methylator phenotype
CRC	Colorectal cancer
CT	Computer Tomography
Cu	Copper
DAB	3,3’-Diaminobenzidine
DAPK	Death-associated protein kinase
DCC	Deleted colon cancer gene
DLD1	Colorectal adenocarcinoma cell line
DMEM	Dulbecco's Modified Eagle's Medium
DMSO	Dimethyl sulfoxide
DNA	Deoxyribonucleic acid
DNX	Liposomal daunorubicin
ECACC	European Collection of Cell Cultures
EDC	1-ethyl-3-(3-dimethylaminopropyl) carbodiimide
EDTA	Ethylenediaminetetraacetic acid
EGFP	Enhanced green fluorescent protein
EGFR	Epidermal growth factor receptor
EGTM	European Group on Tumour markers
EPR	Enhanced permeability and retention
EZH2	Enhancer of zeste homolog 2
FBS	Fetal bovine serum
FDA	Food and Drug Administration
FFPE	Formalin-fixed paraffin-embedded
FIT	Faecal immunochemical test
FOB	Faecal occult blood
FRET	Fluorescence resonance energy transfer
GLL19	Melanoma cell line
GT	Guaiac test

HeLa	Cervical cancer cell line
HepG2	Hepatocellular carcinoma cell line
HER2	human epidermal growth factor receptor 2
Hg	Mercury
HRP	horseradish peroxidase
HT29	Colorectal cancer cell line
IGF	Insulin-like growth factor
IR	Infra-red
JNK	Jun N-terminal kinases
K562	Myelogenous leukaemia line
KLE	Endometrial cancer cell line
LEA	Large external antigen
LHRH	luteinizing hormone-releasing hormone
LOH	Loss of heterozygosity
LS	Lynch syndrome
MCF 7	Breast adenocarcinoma cell line
MDA-MB-231	Breast adenocarcinoma cell line
MG-63	Osteosarcoma cell line
MGF	Mechanogrowth factor
Mhos	Osteosarcoma cell line
MLH	MutL-homolog
MMR	Mismatch repair genes
MOMP	Major outer membrane protein
MRI	Magnetic resonance imaging
MSA	Mercaptosuccinic acid
MSH	MutS Homolog
MSI	Microsatellite instability
MWCNT	Multi-walled carbon nanotube
NICE	National Institute of Clinical Excellence
NIR	Near-infrared
NPV	Negative predictive value
PAGE	Polyacrylamide gel electrophoresis
PBS	Phosphate-buffered saline
PCDA	Pentacosadiynoic acid
PCL	Polycaprolactone
PCR	Polymerase chain reaction
PDLLA	Poly-DL-lactide
PDT	Photodynamic therapy
PEG	Polyethylene glycol
PI3K	Phosphatidylinositol-4,5-bisphosphate 3-kinase
PIK3CA	Phosphatidylinositol-4,5-Bisphosphate 3-Kinase Catalytic Subunit Alpha
PLD	PEGylated liposomal doxorubicin
PLGA	Poly(lactic-co-glycolic acid)
PPO	Propylene oxide
PPV	Positive predictive value
PTEN	Phosphatase and tensin homolog
PUMA	p53 upregulated modulator of apoptosis

PVDF	Polyvinylidene difluoride
PVDR	Disperse Red 1-functionalized PVK copolymer
QD	Quantum dot
RES	Reticuloendothelial system
RIPA	Radioimmunoprecipitation assay
RNA	Ribonucleic acid
S	Sulphur
SCC	Squamous cell carcinoma
SDS	Sodium dodecyl sulfate
SPIO	Superparamagnetic iron oxide
SPR	surface plasmon resonance phenomenon
SW620	Colorectal cancer cell line
SWCNT	Single-walled carbon nanotube
Te	Telluride
TGF	Transforming growth factor
TNM	Tumour-Node-Metastasis staging system
TOP	Trioctylphosphine
TOPO	Trioctylphosphine oxide
U20s	Bone osteosarcoma cell line
UK	United Kingdom
US	Ultrasound
USA	United States of America
USPIO	Ultra small Superparamagnetic Iron Oxide
VCAM	Vascular cell adhesion molecule 1
VEGF	Vascular endothelial growth factor
Zn	Zinc

1 CHAPTER 1: Introduction into molecular pathways in colorectal cancer, biomarkers and the Mechanogrowth factor

1.1 Colorectal cancer

1.1.1 Introduction/demographics

Colorectal cancer (CRC) is the third most commonly diagnosed cancer in males, and the second in females worldwide with an estimated 1.36 million new cancer cases and 694,000 deaths in 2012 ("Fact Sheets by Cancer," 2016). In the UK, bowel cancer accounts for the third commonest cancer diagnosis (13% of all new cases), third commonest in males and in women with a slight male preponderance of 12:10 ("Bowel cancer statistics," 2015). The five-year survival rate for colorectal cancer is 54.2% in males and 55.6% in females ("Cancer survival in England - Office for National Statistics," 2016). The incidence of colorectal cancer is highest in the western world in countries such as the United States, United Kingdom, Australia and New Zealand and is almost 30 fold lower in countries such as India, South America and Africa (Turner, 2009). In absolute numbers, colorectal cancer affects approximately 40 per 100,000 people in the United States, Australia and Europe compared to 5 per 100,000 people in Africa and parts of Asia (Haggar and Boushey, 2009; "Second Expert Report | World Cancer Research Fund International," 2016).

1.1.2 Pathology

1.1.2.1 Adenoma-carcinoma sequence

Few discrete pathways have been described with regards to the genetic events leading to colorectal malignancies. The model of the 'adenoma-carcinoma' sequence describes the development of invasive cancer from colorectal polyps through a progressive accumulation of genetic and epigenetic mutations (Figure 1.1). This 'adenoma-carcinoma' sequence has been reported to account for approximately 80% of sporadic colorectal cancers. This is supported by findings of higher risk of cancer in larger adenomatous polyps, the observation of benign

polyps developing into cancers, the increased prevalence of adenomas in patients with colorectal carcinomas and the reduced incidence of carcinomas in patients who undergo resection of polyps compared to patients who did not have their polyps excised (Fry and Maron, 2012). The initial description of the 'adenoma-carcinoma' sequence by Fearon and Volgenstein in 1990 was based on four mutations causing progression from normal colonic mucosa to invasive cancer (Fry and Maron, 2012.). It is now recognised that the molecular pathogenesis of colorectal cancer is far more complicated, with over 50 genes implicated. Three molecular pathways have been described in colorectal cancer, and these are not mutually exclusive in tumours involving different genes and likely to impact on the efficacy of different chemotherapy regimens. Therefore, a clear understanding of these pathways is essential to improve treatments for colorectal cancer. These pathways are chromosomal instability (CIN), microsatellite instability (MSI) and CpG island methylator phenotype (CIMP). These pathways inactivate tumour suppressor genes and promote the activity of proto-oncogenes, thereby leading to uncontrolled cell division leading to carcinogenesis.

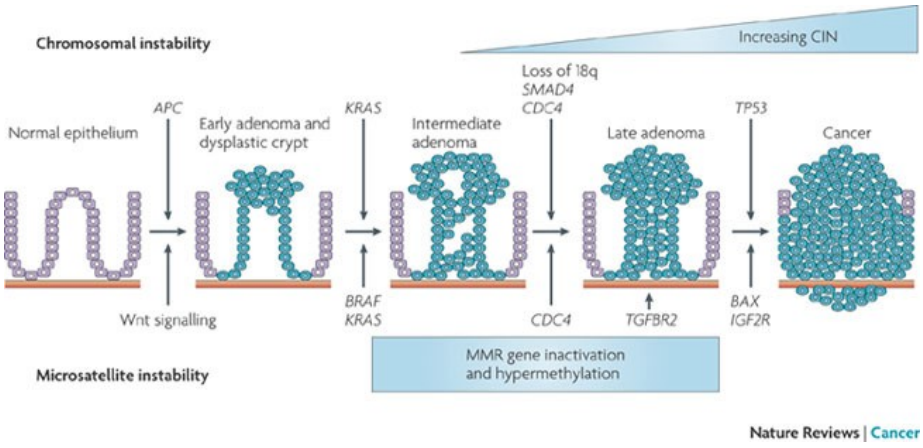

Figure 1.1: Adenoma-Carcinoma sequence in colorectal carcinogenesis (Walther et al., 2009)

1.1.2.2 Chromosomal instability (CIN)

CIN has been demonstrated to be the most frequent cause of genomic instability and accounts for 65% – 70% of colorectal cancer cases (Al-Sohaily et al., 2012). This pathway is characterised by karyotypic variability of chromosomes, which arises from either gains or losses of chromosomes (partial or whole). CIN positive tumours have been identified to occur more distally in the colon and rectum (Pino and Chung, 2010). The allele loss of 18q referred to as the loss of heterozygosity (LOH), is found in as high as 70% of colorectal cancers and is strongly associated with CIN. It hosts genes such as Deleted in Colorectal Cancer (DCC), SMAD4 and SMAD2 and has been associated with a poorer prognosis in colorectal cancer (Pino and Chung, 2010; Reimers et al., 2013). CIN positive tumours have been demonstrated to be independently negatively prognostic, and Mouradov et al. reported assessing samples directly for CIN rather than the markers such as the LOH had a stronger association with prognosis, and its use may be useful in the decision making for adjunct treatments for stage II/III colorectal cancer (Mouradov et al., 2013).

1.1.2.3 Microsatellite instability pathway (MSI)

Microsatellites are lengths of DNA containing a tandem repeat of a pattern of nucleotides found throughout the genome. These sections of DNA are monitored by mismatch repair genes (MMR) responsible for correcting base-base DNA replication errors. Inactivation of these repair genes can lead to elongation or shortening of the microsatellites, thereby resulting in microsatellite instability (Kanthan et al., 2012; Worthley and Leggett, 2010). Inherited mutations of MMR genes have been identified to be the cause of Lynch syndrome, while somatic mutations have been implicated in approximately 15% of cases of sporadic colorectal cancer (Kanthan et al., 2012; Worthley and Leggett, 2010). MSI testing involves a

panel of five microsatellite loci and has been graded as MSI-high (instability in at least two markers), MSI-low (instability in one marker) and microsatellite stable (MSS) in the absence of instability. MSI-high tumours are commoner in older females with a predisposition for right colonic tumours proximal to the splenic flexure with increased lymphocytic infiltration, mucinous histology and poor differentiation(Boland and Goel, 2010; Iacopetta et al., 2010; Jass, 2004). These tumours have been demonstrated to have better overall survival compared to MSS tumours though there have been reports that MSI-high tumours have resistance to chemotherapy agents such as 5-fluorouracil (5-FU) and cisplatin (Aebi et al., 1996; Guastadisegni et al., 2010). The incidence of *K-ras* and *p53* mutations are lower in MSI-high tumours but a long list of genes involved include those involved in DNA repair (*RAD50, MSH3, MSH6, MLH3),* apoptosis (*BAX, BCL-10, caspase 5)*, signal transduction (*TGFβRII, IGFIIR*) and cell cycle genes (*PTEN*) (Iacopetta et al., 2010). *TGFβRII* mutations have been observed in approximately 90% of colorectal cancer arising from MSI (Parsons et al., 1995).

1.1.2.4 CpG Island Methylator Phenotype (CIMP) and serrated neoplastic pathway

The CpG island Methylator phenotype involves widespread hypermethylation of numerous promotor CpG island loci, which are usually protected from methylation in normal cells (Rhee et al., 2017). CIMP has been demonstrated to be an important molecular pathway in colorectal cancer by silencing tumour suppressor genes such as p16, p14, MGMT and hMLH1 (Goel et al., 2007; Worthley and Leggett, 2010). This process increases with age and in patients with chronic inflammation and has been identified to be the second most frequent cause of sporadic CRC with 35-40% of CRC positive for CIMP (Boland and Goel, 2010). CIMP-high tumours are now considered to predominantly develop via the serrated neoplastic pathway (Rhee et al., 2017). The serrated neoplastic pathway has been identified to be a separate pathway for progression of colonic polyps to cancers and involves characteristic serrated

polyps. The serrated polyps include typical hyperplastic polyps, sessile serrated adenomas and dysplastic serrated polyps which are characterised by infoldings in the epithelial surface thereby providing the 'serrated' appearance (Kanthan et al., 2012; Snover, 2011). It is estimated that 20% of CRC develop from this pathway, and is identified predominantly in females with an average age of 61 years (Kanthan et al., 2012).

1.1.3 Management of colorectal cancer

1.1.3.1 Diagnostic investigations to confirm the cancer

The diagnosis of colorectal cancer is made predominantly using endoscopic examinations with a colonoscope ("Overview | Colorectal cancer," n.d.). Colonoscopy is the gold standard investigation for bowel cancer as it can directly visualise the tumour and obtain biopsies to provide histological confirmation of the underlying malignancy. The main alternative to colonoscopy is CT colonoscopy which is a relatively non-invasive investigation with an 89% sensitivity and 75% specificity for detection of adenomas >6mm and cancers (Plumb et al., 2014). CT colonoscopy does not provide histological confirmation of identified lesions, and therefore, patients identified to have abnormalities on CT imaging often require colonoscopy to confirm the diagnosis visually and for biopsies. Tattooing of the bowel is now standard practice when a colonic tumour is identified to aid future localisation of the tumour. This procedure involves the submucosal injection of a tattoo, commonly Spot®/india ink, approximately 2 cm distal to the tumour. Identification of the tattoo is vital for the operating surgeon to identify the site of the tumour during the operation, particularly in minimally invasive surgery where palpating the tumour is not possible, and therefore ensure that the bowel removed includes the tumour. The importance of this has been illustrated by recent studies demonstrating approximately 20% - 33% of cancers being incorrectly recorded by the endoscopist with regards to the location of the tumour due to the lack of reliable intraluminal

landmarks during colonoscopy (Blum-Guzman and Wanderley de Melo, 2017; Yap et al., 2016). Complications from placement of tattoos has been reported to be very low (0.22% (Nizam et al., 1996)) including intramural injections (injections too deep into the bowel wall) resulting in spillage of the tattoo intraperitoneally resulting in focal peritonitis, haematomas with localized abscesses, adhesions and very rarely tumour inoculation (Trakarnsanga and Akaraviputh, 2011). Additionally, incorrect placement of the tattoo proximal to the tumour as opposed to distal to the tumour can cause confusion between the operating surgeon and the endoscopist and therefore lead to bowel resections without the tumour. Tattooing rectal tumours are not performed due to concerns of deeper infiltration affecting the surgical planes, and therefore this requires the use of other techniques such as endoscopy during the operation to accurately localize the rectal tumour which increases operating time. Therefore, despite the advantages of tattoing the bowel, there remains scope for improvement for techniques of 'marking' the site of tumours prior to surgery.

Colonoscopy additionally plays a vital role in the detection and removal of colorectal polyps, thereby preventing the progression of these lesions to cancers. However, there is increasing recognition of missed lesions during colonoscopy, which develop into cancers. The rate of missed lesions, particularly small and flat adenomas, has been estimated to be as high as 10 - 25% (Libânio and Azevedo, 2016; Zhao et al., 2019). Further adjuncts to colonoscopy, to improve detection rates of lesions, include the use of a 'cap' at the end of the endoscope to help visualization around the folds of the bowel and techniques such as narrow-band imaging and chromoendoscopy which utilizes spraying dyes such as Indigocarmine green onto the colonic mucosa help by improving detection rates of these polyps (Brown et al., 2016).

1.1.3.2 Current staging systems in colorectal cancer and its limitations

The management options for colorectal cancer include curative surgery, palliative surgery (if the tumour cannot be removed entirely), chemotherapy and radiotherapy. The stage of the tumour determines the choice of treatment modality offered and this is currently based on the Tumour, Node and Metastasis (TNM) classification of the Union for International Cancer Control (UICC) (Greene and Sobin, 2008). The TNM classification (Table 1.1 includes the traditional Dukes staging system) has undergone many revisions, and it has a few limitations. Currently, surgery is the predominant modality offering cure for colorectal cancer and the role of adjuvant, and neo-adjuvant therapies with chemoradiotherapy are dictated by the TNM stage. However, given our growing understanding of the complexity of colorectal cancer, treatments based on a comparatively simple clinical staging system such as the TNM system has been recognised to either over-treat or under-treat certain patient groups. Stage II colon cancer, in particular, remains an area of uncertainty. The use of adjuvant chemotherapy (i.e. after surgical excision) to reduce the risk of a recurrent tumour is predominantly reserved for patients identified to have lymph node metastases, supported by substantial evidence in the literature for reduction of recurrence rates ("Colorectal cancer," 2011). The role of chemotherapy in stage II colon cancer, where the tumour has breached the wall of the bowel but not spread to the lymph nodes remains unclear. The incidence of recurrent disease in these patients has been demonstrated to be approximately 20%-25% within five years with outcomes for these patients similar to those with stage III disease where lymph nodes are involved (Chen and Bilchik, 2006; Davies et al., 2008). The use of chemotherapy in all patients with stage II colorectal cancer has not been demonstrated to be beneficial, and therefore arises the need to identify the subgroup of patients with stage II cancer who would benefit from chemotherapy thereby avoiding over or undertreating patients with adjuvant therapies

and their associated side effects and complications. This emphasises the importance of biomarkers to help identify patients who would benefit from different adjuvant therapies.

Stage	T	N	M
0	Tis	N0	M0
I	T1	N0	N0
	T2	N0	M0
IIA	T3	N0	M0
IIB	T4a	N0	M0
IIC	T4b	N0	M0
IIIA	T1-T2	N1	M0
	T1	N2a	M0
IIIB	T3-T4a	N1	M0
	T2-T3	N2a	M0
	T1-T2	N2b	M0
IIIC	T4a	N2a	M0
	T3-T4a	N2b	M0
	T4b	N1-N2	M0
IVA	Any T	Any N	M1a
IVB	Any T	Any N	M1b
IVC	Any T	Any N	M1c

Table 1.1: *TNM 8th edition staging system for colorectal cancer (Bertero et al., 2018)*

Tx (Tumour cannot be assessed) T0 (no evidence of the primary tumour) Tis (Carcinoma in situ) T1 (tumour invades submucosa) T2 (tumour invades muscularis propria) T3 (tumour invades subserosa or into non-peritonealised pericolic or perirectal tissues) T4 (Tumour directly invades other organs or structures and/or perforates the visceral peritoneum) T4a (Tumour penetrates to the surface of the visceral peritoneum) T4b (tumour directly invades other organs or structures) NX (regional nodes cannot be assessed) N0 (no lymph node involvement) N1 (metastasis in 1-3 regional lymph nodes) N1a (metastasis in one regional lymph node), N1b (metastasis in 2-3 regional lymph nodes) N1c (tumour deposit in subserosa or in non-peritonealised pericolic or perirectal soft tissue without regional lymph node metastasis) N2 (metastasis in 4 or more regional lymph nodes) N2a (metastasis in 4-6 regional lymph nodes) N2b (metastasis in 7 or more regional lymph nodes). M0 (no distant metastasis) M1 (distant metastasis) M1a (metastasis confined to one organ without peritoneal metastases) M1b (metastasis in more than one organ) M1c (Metastasis to the peritoneum with or without organ involvement)

1.2 Biomarkers

A biomarker is a characteristic that is objectively measured and evaluated as an indicator of normal biological processes, pathogenic processes or pharmacologic responses to a therapeutic intervention (Biomarkers Definitions Working Group., 2001). Biomarkers are classified as prognostic, predictive and surrogate endpoint markers.

- Prognostic biomarkers predict the natural course of the disease process, regardless of treatments. Therefore, these are utilised to aid the decision process for appropriateness of potentially toxic treatments compared to conservative management. Examples of these markers include HER2/neu in breast cancer (Ludwig and Weinstein, 2005).
- Predictive biomarkers predict the effectiveness of specific treatments for the individual patient. The presence of the marker will guide the use of medications, and the absence of the marker will avoid the potentially toxic effects of the therapy. Examples of these markers in clinical practice include the oestrogen receptor status in breast cancer, which predicts the response to hormonal therapy and HER2/neu expression in breast cancer for trastuzumab (Shi et al., 2012).
- Surrogate endpoints replace primary clinical outcomes such as 5-year survival in the evaluation of the efficacy of treatments.

The use of biomarkers in colorectal cancer in clinical practice is currently limited. Biomarkers currently in clinical use in the NHS are listed in Table 1.2. There is an abundance of research in genomics and proteomics research to identify suitable biomarkers.

1.2.1 Biomarkers in current clinical practice

1.2.1.1 Faecal occult bloods (FoB)

Faecal occult blood tests have become established as screening tests for bowel cancer. The NHS bowel cancer screening program invites men and women between the ages of 60 – 69 to provide stool samples for testing every two years. Beyond this age group, screening tests are provided on the patient's request (Choices, 2015). The test is sensitive but not specific for

colorectal cancer, and therefore, any positive result will require luminal investigations of the patient with endoscopy or radiology.

The initial test used for FoB was the guaiac test, which detected the pseudo peroxidase activity of haemoglobin. This was limited by its lack of specificity for human haemoglobin (thereby affected by certain food substances and medications), and low clinical sensitivity and specificity for colorectal cancer (Allison et al., 2007; Duffy et al., 2014). The guaiac test is now being replaced by the faecal immunochemical test (FiT) which detects the globin component of haemoglobin. The FiT is more sensitive and specific than the guaiac test and can be performed at an automated level, thereby making it more suitable for large population screening (Allison et al., 2007; Duffy et al., 2014).

1.2.1.2 Carcinoembryonic antigen (CEA)

CEA is a serum glycoprotein with a molecular weight of 180kd, and functions as an intercellular adhesion molecule which promotes aggregation of human carcinoma cells and can be raised in smokers with no underlying colorectal pathology (Bolocan et al., 2012). CEA has been demonstrated to be an adverse prognostic marker in colorectal cancer with elevated CEA levels demonstrated to be negatively prognostic in colorectal cancer, especially in stage II colorectal cancer (Duffy et al., 2014; Huh et al., 2010; Park et al., 2009; Peng et al., 2013; Sun et al., 2009; Thirunavukarasu et al., 2011). However, studies have not demonstrated any benefit in the use of CEA to select patients for adjuvant therapies in stage II colorectal cancer (Duffy et al., 2014). CEA is now in routine clinical use as a surveillance marker for recurrent cancer following surgery for colorectal cancer. CEA measurements have been demonstrated to be the most sensitive investigation for the detection of early recurrent disease compared to radiological and endoscopic investigations (Duffy et al., 2014; Tsikitis et al., 2009). The

European Group on Tumour Markers (EGTM) recommends baseline measurement of CEA, followed by 2-3 monthly postoperative measurements for at least three years, and after that six-monthly for five years (Duffy et al., 2014).

1.2.1.3 K-RAS

K-Ras is located on chromosome 12p12 and belongs to the ras family of oncogenes. The oncogene encodes a 21-kD protein involved in the G-protein signal transduction pathway (Molnar et al., 2003). K-Ras mutations have been identified to be present in greater than 50% of colorectal adenomas and carcinomas with codon 12 of the oncogene most commonly affected (Duffy et al., 2014). Mutations of the oncogene have not been demonstrated to be independently prognostic, and almost 97% of genetic events within KRAS are caused by DNA base-pair substitutions within codon 12 and 13 (Bendardaf et al., 2004).

KRAS mutations have been demonstrated to be negative predictive biomarkers for the efficacy of anti-EGFR (Epidermal growth factor) monoclonal antibodies in advanced colorectal cancer. Cetuximab and panitumumab are immunoglobulin antibodies directed against EGFR and have been demonstrated to improve survival in patients with metastatic colorectal cancer as single agents or combination chemotherapy (Van Cutsem et al., 2010). Mutations of the K-RAS oncogene in codons 12 and 13 have been demonstrated to be significant predictive biomarkers for resistance to these anti-EGFR therapies. The use of anti-EGFR therapies as single or combination therapies, in early clinical studies, for all patients with metastatic colorectal cancer demonstrated benefit in only 10 – 15% of patients (Dahabreh et al., 2011). Retrospective analysis of phase II and III randomised control trials which investigated the efficacy of anti-EGFR therapies in metastatic colorectal cancer demonstrated that these therapies had no benefit in patients with K-RAS mutations (Bokemeyer et al., 2009; Karapetis

et al., 2008). Following these studies, the European Society for Medical Oncology in 2010 and the American Society of Clinical Oncology in 2009 recommended that anti-EGFR therapies be restricted to patients with wild type KRAS tumours (codons 12 and 13) (Allegra et al., 2009; Van Cutsem et al., 2010). It is important to note that the efficacy of anti-EGFR therapies in wild type KRAS tumours is 15-20% alone, and up to 35-40% when treated with combination therapies and this lack of response in patients has been attributed to further mutations in genes such as BRAF, PIK3CA and PTEN (Di Nicolantonio et al., 2008; Er et al., 2014; Linardou et al., 2011). There has been some recent conflicting evidence with regards to the efficacy of Cetuximab in codon 13 K-Ras mutations with studies demonstrating an increase in overall survival, and progression-free survival (Er et al., 2014; Mao et al., 2013). This remains an area which requires further research to elucidate the true predictive nature of K-RAS mutations for the efficacy of anti-EGFR therapies.

1.2.1.4 Microsatellite instability

The detection for microsatellite instability and DNA mismatch repair has been recommended for clinical use to prescreen patients with colorectal cancer for Lynch syndrome which has been attributed to approximately 3% of colorectal cancers (Duffy et al., 2014). Lynch syndrome, previously referred to as hereditary non-polyposis coli, is an autosomal inherited disorder which is associated with the risk of developing different cancers including colon, rectum, endometrium, stomach and small bowel (Duffy et al., 2014; Hewish et al., 2010). Lynch syndrome is associated with mutations of the mismatch repair (MMR) genes, which leads to microsatellite instability. Criteria such as the Amsterdam and Bethesda criteria have been developed as guides for patients who should be screened for Lynch syndrome targeting patients who are diagnosed at a young age with colorectal cancer, with a strong family history or affected by LS related tumours (Duffy et al., 2014). However, recent expert groups have

suggested that screening should extend to patients under the age of 70 due to concerns that this condition remains underdiagnosed, and recent NICE guidance recommends testing for MSI in all new cases of colorectal cancer ("Molecular testing strategies for Lynch syndrome in people with colorectal cancer | Guidance and guidelines | NICE," n.d.; Moreira et al., 2012). The presence of MSI or defective MMR has been demonstrated to be a positive prognostic biomarker in colorectal cancer especially in patients with stage II and III colon cancer (Duffy et al., 2014; Roth et al., 2012; Sargent et al., 2010). A role for MSI/MMR as a predictive biomarker in adjuvant 5-FU therapy in patients with stage II colon cancer was suggested in a systemic review from 2009 which demonstrated MSI high tumours to be negatively associated with efficacy (Des Guetz et al., 2009).

Biomarker	Clinical use	Evidence
CEA	Postoperative surveillance for recurrent cancer. Recommended to be measured every 2-3 months for at least 3 years, thereafter, every 6 months for 5 years (Duffy et al., 2014).	A meta-analysis of randomised controlled studies demonstrated a significant impact on overall mortality. Asymptomatic recurrences identified earlier, and therefore more amenable to surgical resection — no difference in cancer-related mortality (Tjandra and Chan, 2007).
FoB	Screening test for colorectal cancer Faecal immunochemical testing (FIT) is superior to guaiac faecal occult blood test (GT)	Cochrane review of 4 RCTs demonstrated a 16% reduction in risk of CRC mortality (Hewitson et al., 2008). A prospective cohort study of 139 patients reported the sensitivity for detecting colorectal cancer for FIT to be 81.8% (95% confidence interval 47.8% - 96.8%) and GT to be 64.3% (95% confidence interval 35.6% - 86%) (Allison et al., 2007).
KRAS	Predictive biomarker for the effectiveness of anti-EGFR antibodies in metastatic colorectal cancer in KRAS wild-type tumours (specifically codon 12) (Duffy et al., 2014)	A meta-analysis of eight RCTs demonstrated significant improvement in PFS and OS in KRAS wild-type patients, and a detrimental outcome on patients with KRAS mutations when treated with anti-EGFR therapy (Loupakis et al., 2012).
BRAF	Predictive biomarker in anti-EGFR therapy for metastatic CRC, in patients with wild-type KRAS tumours	A meta-analysis of 21 trials demonstrated BRAF mutations to be a predictive biomarker for anti-EGFR therapy in patients with metastatic CRC. There was an improved overall survival and progression-free survival in BRAF wild type tumours, and this was improved further in KRAS wild type tumours (Yuan et al., 2013).
MSI/MMR	Screening test for Lynch syndrome	The use of the Amsterdam and Bethesda criteria was initially used to identify individuals who would benefit from screening for Lynch syndrome (Umar et al., 2004; Vasen et al., 1999). Universal testing of all patients with CRC is now being recommended due to cost-effectiveness (Duffy et al., 2014; Ladabaum et al., 2011).

Table 1.2: Biomarkers in current practice for colorectal cancer

1.2.2 Biomarkers in research

1.2.2.1 Oncotype Dx test

The Onco*type* DX colon cancer recurrence score assay was developed using tumour gene expression data from patients with stage II and III colon cancer in four large independent studies (Yothers et al., 2013). This score involves assessing for 12 genes (seven cancer-related genes and five reference genes) in paraffin-embedded primary colon tumour tissues and produces a Recurrence score. Validation studies have confirmed the ability of the Recurrence score to predict recurrence in stage II and III colon cancer (Gray et al., 2011; Yothers et al., 2013). Currently, the test is available commercially, though not in routine practice in the UK.

1.2.2.2 Apoptosis related biomarkers

The epithelial lining of colorectal tissues is an area of very high cell turnover rate, and normal tissues are maintained by a balance between proliferation and apoptosis (programmed cell death) (Alcaide et al., 2013). The downregulation of apoptosis leads to uncontrolled cell proliferation and tumour development, and at least 26 different biomarkers of the complex apoptotic pathway have been investigated for effects on prognosis, but currently, no individual marker has been identified to provide clinically useful prognostic information (Zeestraten et al., 2013).

1.2.2.3 Vascular Endothelial Growth Factor (VEGF)

VEGF and its receptor play an essential role in angiogenesis, which is vital in tumour growth. This growth factor has mainly been identified to be significant in advanced cancer, and anti-VEGF monoclonal antibodies such as Bevacizumab are currently in routine clinical practice for metastatic colorectal cancer. The use of Bevacizumab, in combination with chemotherapy agents, has been demonstrated to be the optimal regime by phase III clinical trials (Hurwitz

et al., 2004; Saltz et al., 2008). However, the role of VEGF as a prognostic factor in colorectal cancer is unclear with conflicting evidence in the literature (Beştaş et al., 2014; Doger et al., 2006; Khorana et al., 2003).

1.2.2.4 p53 mutation

Mutation of the tumour suppressor gene p53 is the most frequent mutation found in cancers earning its reference as the 'guardian of the genome' (Lane, 1992; Petitjean et al., 2007; Suppiah and Greenman, 2013). The detection of serum anti-p53 autoantibody has been demonstrated to be associated with p53 mutations and is easier to perform compared to DNA sequencing (Suppiah and Greenman, 2013). Measuring anti-p53 auto-antibody as a screening marker for colorectal cancer has been identified to be of limited use due to its low sensitivity (15%) despite its high specificity and positive predictive value (95% – 100%) (Broll et al., 2001; Lane, 1992; Suppiah and Greenman, 2013). Shiota et al (Shiota et al., 2000) reported p53 mutations to be an independently prognostic factor for colorectal cancer on multivariate analysis, though these findings have been disputed in other studies which have not been able to demonstrate the prognostic role of p53 on multivariate analysis (Chang et al., 2005; Suppiah et al., 2008; Suppiah and Greenman, 2013).

1.2.2.5 Ki67

The Ki67 antigen is a proliferation marker expressed in all cell cycle phases, except during the G_0 phase. High expression of Ki67 has been demonstrated to be prognostic in breast cancer, malignant lymphoma, astrocytoma and renal cell carcinoma (Bui et al., 2004; Kirla et al., n.d.; Reimers et al., 2013). However, in colorectal cancer the evidence is not conclusive as some studies looking at Ki67 in colorectal cancer reported over-expression of the Ki-67 antigen to be a positive predictor of survival on multivariate analysis (Ivanecz et al., 2014; Salminen et

al., 2005; Weber et al., 2001), while other studies dispute this finding (Kimura et al., 2000; Reimers et al., 2013).

1.2.2.6 PIK3CA (Phosphatidylinositol-4,5-bisphosphate 3-kinase catalytic subunit alpha) mutations

PIK3CA gene encodes the p110 alpha catalytic subunit of phosphatidylinositol 3-kinase (PI3K) which is an important cell membrane component and second messenger involved in cell signalling (Vivanco and Sawyers, 2002). PI3K has been identified to play a role in regulating, proliferation, apoptosis and cell survival. Mutations of the PIK3CA gene has been identified in 10-30% of all colorectal cancers with over 80% of mutations been identified in 2 specific areas: exon 9 and exon 20 (George and Kopetz, 2011; Samuels et al., 2004). Mutations confined to exon 20 appear to be relevant towards prognosis in colorectal cancer, and PI3KCA mutations have been identified to be negative prognostic in patients specifically with wild type KRAS mutations (Cathomas, 2014; Ogino et al., 2009). PI3KCA has also been identified to be a potential predictive biomarker for anti-EGFR therapy with mutations causing resistance to this treatment (Cathomas, 2014; Sartore-Bianchi et al., 2009).

1.2.3 Conclusions

Our growing understanding of the complexity of colorectal cancer and its underlying pathways has provided opportunities to identify the heterogeneity of the underlying process resulting in patients responding differently to the same treatments. The need for individualised treatments for patients is now accepted, and the identification of biomarkers appears to be the key to this objective particularly in stage II colorectal cancer, where the use of chemotherapy remains under scrutiny. A single ‘magic bullet’ may not exist for cancers, but a series of ‘magic bullets’ guided by biomarkers may hold the key for better outcomes.

Biomarker	Role	Evidence
CEA	Preoperative prognostic marker	Retrospective reviews of CEA levels preoperatively and survival of patients demonstrated raised CEA levels to be independently negatively prognostic. Variation in cut-off limits for abnormal CEA levels in different studies, but negative prognostic impact identified regardless (Thirunavukarasu et al., 2011). Independently prognostic in stage II colorectal cancer (Huh et al., 2010).
MSI	Prognostic marker Predictive marker for 5-FU chemotherapy	A meta-analysis of 31 studies demonstrated a favourable prognosis with reference to overall survival and disease-free progression (Guastadisegni et al., 2010). A significant benefit of 5-FU therapy in patients with MSS tumours, though further studies were recommended (Guastadisegni et al., 2010). A further meta-analysis of 8 studies in 2009 did not demonstrate any benefit of metastatic chemotherapy based on MSI status (Des Guetz et al., 2009). Further research required.
KRAS	Prognostic marker	Conflicting outcomes with studies suggesting prognostic value (Hutchins et al., 2011), with others(Roth et al., 2010) suggesting no prognostic value of KRAS.
BRAF	Prognostic marker	BRAF mutation is associated with a poor prognosis and overall survival independent of treatment with anti-EGFR therapies (Bokemeyer et al., 2012).
Oncotype DX colon cancer	The continuous Recurrence Score based on the Oncotype Dx colon cancer test is a prognostic marker for recurrence following surgery in stage II colon cancer	Retrospective analysis of stage II colon cancer patients who underwent surgery in 2 studies have confirmed the Recurrence score predicts the risk of recurrence in stage II and III colon cancer (Gray et al., 2011; Yothers et al., 2013).
TP553	Prognostic marker	Conflicting outcomes in the literature. Shiota et al. (Shiota et al., 2000) identified p53 to be an independent prognostic factor on COX regression analysis following 89 patients with reduced overall survival in patients with p53 mutations. Suppiah et al. (Suppiah et al., 2008) and Chang et al. (Chang et al., 2005) identified p53 was not an independent prognostic factor for colorectal cancer on multi-variate analyses.
Apoptosis related biomarkers	Prognostic markers	A recent review of the literature by Zeestraten et al. (Zeestraten et al., 2013) identified 26 markers for apoptosis, but none of which were individually identified to be prognostic markers. A combined profile of markers was recommended.
Ki67	Prognostic marker	Conflicting evidence. Most studies report Ki67 index to be a positive prognostic marker (Ivanecz et al., 2014; Salminen et al., 2005; Weber et al., 2001), though some studies have not identified this (Kimura et al., 2000; Reimers et al., 2013).
PIK3CA	Prognostic marker Predictive marker	Little prognostic effect (negative) demonstrated in patients with wild type KRAS tumours, and negative predictive marker for the efficacy of anti-EGFR therapy in patients with metastatic colorectal cancer (Cathomas, 2014; Ogino et al., 2009; Sartore-Bianchi et al., 2009).

Table 1.3: Biomarkers in colorectal cancer under research

1.3 The Mechanogrowth factor: an isoform of Insulin-like growth factor-1

1.3.1 Introduction

Insulin-like growth factor 1Ec, initially identified in skeletal muscle and therefore earned the title 'Mechanogrowth Factor', is an isoform of Insulin-like growth factor -1 (IGF-1). IGF-1 is a circulating autocrine and paracrine factor regulating pre and post-natal growth in most tissues (Brisson and Barton, 2012). IGF-1 affects a variety of bioactivities including induction of growth, differentiation of target cells, cell survival and maintenance of cell function (Hakuno and Takahashi, 2018). Its vital role has been illustrated in studies demonstrating IGF-1 knockout mice rarely surviving beyond birth, and the mice surviving birth demonstrating significant growth retardation, infertility and bone development (Baker et al., 1993; Liu et al., 1993). IGF-1 is predominantly synthesized in the liver, regulated by the growth hormone and is also synthesized locally in tissues (Wrigley et al., 2017).

The actions of IGF-1 are mediated through the IGF-1 receptor (IGF-1R), a tyrosine kinase receptor, which undergoes autophosphorylation on binding with IGF-1 leading to a cascade of complex pathways downstream (briefly summarized in Figure 1.2). These include the activation of the PI 3-kinase cascade and the MAP Kinase cascade. The PI3K/AKT/mTOR pathway is an essential intracellular pathway regulating survival, cell growth, proliferation, metabolism and inhibition of apoptosis (Noorolyai et al., 2019). Mutations in this pathway have been implicated in multiple solid tumours including breast, prostate, hepatocellular carcinoma, colorectal carcinoma and haematological malignancies (Mayer and Arteaga, 2016). Currently, drugs targeting this pathway for cancer therapy are undergoing clinical trials in phase 2 and 3 trials (Mayer and Arteaga, 2016). The MAP kinases include ERK 1/2, p38 kinase and c-Jun amino (N)-terminal kinases (JNK)

regulate gene expression, mitosis, metabolism, motility, survival, apoptosis and differentiation (Cargnello and Roux, 2011). Dysregulation of the RAS/RAF/MAPK/ERK pathway kinase and the ERK 1/2 have been implicated in many human cancers including breast cancer, prostate cancer, colorectal cancer and lung cancer (Rezatabar et al., 2019).

IGF-1 axis involvement in tumorigenesis, cancer growth and invasion has been demonstrated *in vitro* and *in vivo* (Bowers et al., 2015). Numerous studies from as early as the 1980s have demonstrated aberrant IGF-1 signalling in colon cancer, prostatic cancer, pancreatic cancer, osteosarcoma, melanoma and childhood malignancies (Denduluri et al., 2015; Beckwith and Yee, 2015; Sachdev and Yee, 2007). This led to the development of multiple agents targeting the IGF-1 axis, including receptor targeting agents and drugs, reducing ligand bioactivity (Beckwith and Yee, 2015; Bowers et al., 2015). However, despite promising preclinical trials with xenograft *in vivo* models and early phase clinical trials, the results were not replicated in later phase clinical human trials leading to multiple pharmaceutical companies discontinuing these agents from further research (Beckwith and Yee, 2015; Bowers et al., 2015). The failure to reflect these results in large scale clinical trials is likely related to the complexity of the IGF-1 signalling axis and its interplay with other growth factor pathways. Clearly, further scrutinization of this pathway is required, and amongst this is the growing research into the different isoforms of IGF-1 and its implications for tumorigenesis and cancer progression. The current evidence for the role of IGF-1Ec isoform in cancer is described below.

The IGF-1 gene accommodates more than 90kb of genomic DNA containing six exons (Matheny et al., 2010). Alternative splicing of the exons generates multiple mRNA sequences which encode different isoforms of IGF-1 (Figure 1.3) (Matheny et al., 2010). Post translational cleavage of the

IGF-1 precursor protein produces different isoforms containing a signal peptide, a mature IGF-1 peptide and a different E domain at the COOH terminus (Dai et al., 2010). The mature IGF-1 peptide is preserved for all isoforms of IGF-1, while the E-domain introduces the highest variability to the IGF-1 transcripts (Oberbauer, 2013). Exons 1 and 2 act as alternative leader exons at the 5' end of the mRNA. Transcripts containing exon 1 are defined as Class 1 transcripts, while transcripts containing exon 2 are referred to as Class 2 transcripts. Exons 3 and 4 are common to all splice variants coding the mature IGF-1 peptide which contains the B, C, A and D domains of the IGF-1 peptide. Splicing of exon 4 and 6 produces IGF-1Ea which has a 35 amino acid E-peptide, while the splicing of exon 4 and exon 5 generates IGF-1Eb which has a 77 amino acid E peptide(Vassilakos et al., 2014). The IGF-1Ec E peptide contains 40 amino acids and arises from the splicing of exons 4,5 and 6(Vassilakos et al., 2014). (Figure 1.3)

The role and significance of the different isoforms are unclear and under research. Class 1 isoforms have been regarded to be associated with the autocrine/paracrine form of IGF-1 used by most tissues and expressed mainly in extrahepatic tissues, while Class 2 transcripts with its endocrine form with expression mainly in the liver and kidney (Adamo et al., 1991; Matheny et al., 2010; Philippou et al., 2007). The mature IGF-1 peptide is thought to play a predominant role in the biological activity of IGF-1, however different biological actions have been demonstrated for the isoforms and the E peptides with a differential expression profile shown in various conditions and pathologies in humans including cancers (Philippou et al., 2014; Vassilakos et al., 2014). The IGF-1Ea isoform is the most widely expressed isoform accounting for more than 90% of IGF-1 expression in the liver, while the expression of IGF-1Ec is approximately 10% of IGF-1Ea in the liver (Oberbauer, 2013; Philippou et al., 2014).

The IGF-1Ec isoform was referred to as the Mechanogrowth factor by Yang et al. (Yang et al., 1996) after they demonstrated the rapid increase in levels of this isoform of IGF-1 in muscles subjected to mechanical stress**.** IGF-1Ec has been demonstrated to act as a local tissue repair factor in skeletal and cardiac muscle, bone and neurons. Compared to IGF-1Ea, IGF-1Ec lacks glycosylation sites thereby being less stable in interstitial fluid and is therefore presumed to act via autocrine/paracrine modalities (Dai et al., 2010; Yang et al., 1996). Though the pro-IGF-1Ec isoform has been demonstrated in cells and tissues, the independent actions of the E peptides were initially based on the use of a synthetic peptide analogous to the E peptide. Recently, direct evidence for the presence of E peptides was reported in human and rat tissues. In 2017, Vassilakos et al. (Vassilakos et al., 2017) reported, with the use of immunoblotting, the expression of the Ec peptide in human skeletal muscle and liver tissues and the Eb peptide in rat heart, liver, lung, muscle and kidney tissues. Interestingly, the Ec peptide was the only form of the IGF-1Ec expressed in the rat muscle and kidney with the absence of the expression of the proIGF-1Ec peptide. The expression of the Ec peptide was demonstrated to be noticeably higher 48 hours after muscle exercise in the human tissues(Vassilakos et al., 2017).

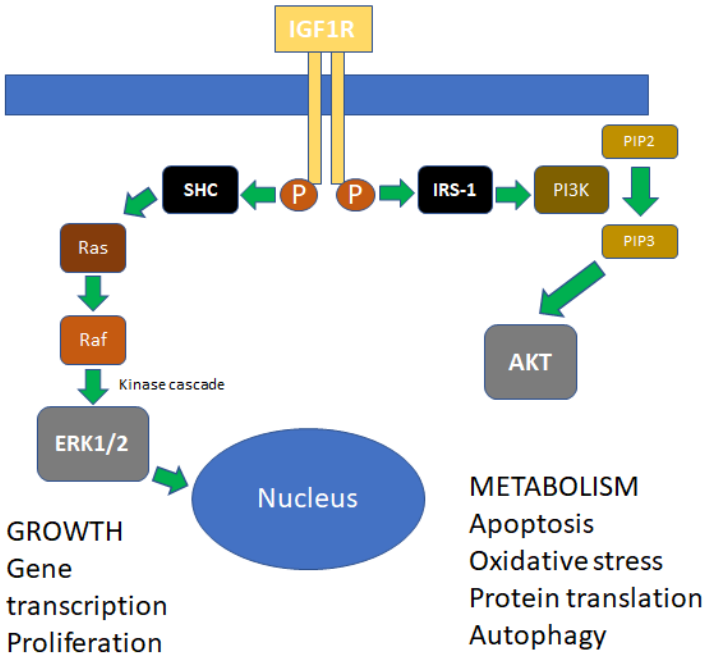

Figure 1.2*:* Brief overview of the IGF-1 signalling axis from the IGF-1R with downstream signalling

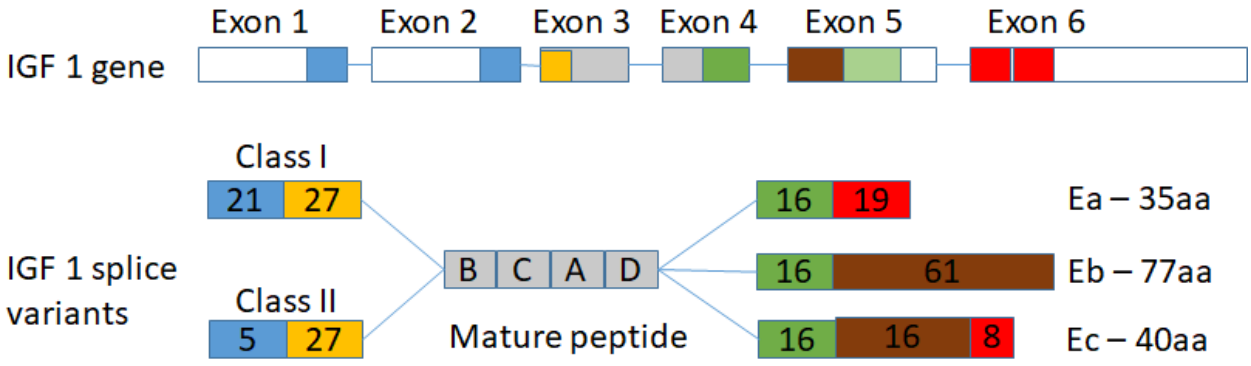

Figure 1.3*:* IGF-1 gene and its splice variants. IGF-1Ea is generated by the splicing of exons 4 and exons 6, IGF-1Eb result from splicing of exons 4 and exons 5 and IGF-1Ec (MGF) generated by exons 4, exons 5 and exons 6. Class 1 transcripts are generated from exons 1 while class II transcripts from exons 2.

1.3.2 The physiological role of MGF and involvement in human diseases

1.3.2.1 Skeletal muscle

A bulk of the initial research into MGF has been in skeletal muscles. MGF and IGF-1Ea have both been demonstrated to be expressed in resting skeletal muscle tissues (Dai et al., 2010). MGF expression was identified to be several orders of magnitude lower than IGF-1Ea, and approximately one order of magnitude lower in females compared to males (Cheema et al., 2005; Dai et al., 2010; Greig et al., 2006). Autocrine secretion of IGF1 occurs in response to muscle injury, and exercise and MGF has been hypothesized to play a role in muscle repair (Zanou and Gailly, 2013). Expression of MGF rises rapidly after exercise for several days, and thereafter its levels decrease as splicing of IGF1 switches to the expression of IGF-1Ea, which increases over the pre-injury levels. However, even at its peak, MGF levels have not been demonstrated to be near the levels of IGF-1Ea (Matheny et al., 2010). The actions of MGF in the setting of muscle repair appears to be through the activation of satellite cells which proliferate to provide myogenic precursor cells for muscle repair, and it inhibits the differentiation of the precursor cells (Hill et al., 2003; Yang and Goldspink, 2002). IGF-1Ea is then responsible for the myoblast differentiation reflecting its rise while MGF levels decline after a few days (Yang and Goldspink, 2002). In addition, MGF has been demonstrated to increase the activity of superoxide dismutase, which reduces free radicals and thereby limiting muscle damage (Dobrowolny et al., 2005; Zanou and Gailly, 2013).

1.3.2.2 Brain

There is evidence to suggest that MGF plays a neuroprotective role. While normal brain tissues have not been identified to express MGF, areas of brain ischaemia have demonstrated MGF

expression as early as three hours after transient global ischaemia and specifically in the neurons resistant to ischaemic insults (Carro et al., 2003; Dai et al., 2010; Dluzniewska et al., 2005). Intravascular injection of the C-terminal peptide of MGF in a gerbil model of brain ischaemia demonstrated significant neuroprotection compared to the full-length IGF 1 peptide, and further *in-vitro* studies have demonstrated that this appears to act independently of the IGF-1 receptor (Dluzniewska et al., 2005; Górecki et al., 2007). Tang et al. (Tang et al., 2017) demonstrated ,with the use of transgenic mice overexpressing MGF, an increase in the neural progenitor cells and neurogenesis with a potential role for MGF to prevent age-related neuronal loss.

1.3.2.3 Bone and cartilage

MGF expression has been demonstrated to be upregulated in osteoblast cell lines in response to mechanical overload, whilst not being present when mechanical stress is not administered (Tang et al., 2006). The C-terminal peptide of MGF has been demonstrated *invivo* to promote bone defect healing and osteoblastic proliferation (Deng et al., 2011). *Invivo* models have demonstrated evidence that MGF administration local to damaged cartilage with TGF-β3 in silk fibroin scaffolds promotes cartilage regeneration in rabbit models with osteochondral defects and delays osteoarthritic degeneration (Z. Luo et al., 2015; Song et al., 2017).

1.3.2.4 Heart

MGF appears to be expressed in cardiac tissues in response to ischaemic damage (Dai et al., 2010; Stavropoulou et al., 2009). This has been demonstrated in animal models where induced ischaemic damage to the myocardium was associated with a significantly higher expression of MGF compared to IGF-1Ea at 4 and 8 weeks post-infarction (Dai et al., 2010; Stavropoulou et al., 2009). The delivery of a synthetic peptide corresponding to the E peptide of IGF1Ec via systemic

and intra-coronary methods have both demonstrated preservation of cardiac function, and prevention of pathological remodelling in animal models (Carpenter et al., 2008; Mavrommatis et al., 2013; Peña et al., 2015).

1.3.2.5 Inflammatory bowel disease

IGF1 has been demonstrated to be associated with the smooth muscle hypertrophy of intestinal muscle in Crohn's disease with resulting stricture formation (Li et al., 2015). The expression of IGF1 in Crohn's disease is regulated by TGF-β1, TNF-α and IL-6, which are products of inflammation. MGF expression has been demonstrated to be significantly increased in bowel affected by Crohn's disease compared to healthy bowel, and it appears to be via a TGF-β1 pathway (Li et al., 2015).

1.3.2.6 Endometriosis

IGF-1 has been demonstrated to inhibit apoptosis and promote the proliferation of endometrial cells *in-vitro*, with increased levels of IGF-1 demonstrated in the peritoneal fluid of women affected by endometriosis compared to controls (Kim et al., 2000; Koutsilieris et al., 2001). MGF has been demonstrated to be expressed by ectopic endometrial cells, while no expression of IGF-1 isoforms identified in eutopic endometrium (Dimitrios S Milingos et al., 2011). In addition, MGF has been demonstrated to have a mitogenic effect on the growth of endometrial cell lines, and therefore the potential role of MGF in endometriosis pathogenesis has been postulated (Dimitrios S Milingos et al., 2011).

1.3.3 Possible mechanisms of action for MGF

Currently, there is no clear consensus for the mechanisms of action of the IGF-1Ec isoform. This may be due to studies using different synthetic peptides resembling the E domain of IGF-1Ec, the age of the cell cultures used, the choice of different inhibitors for the IGF-1 axis and cell media (Vassilakos et al., 2014). Table 1.4 outlines a brief overview of the different pathways postulated to be involved in the actions of IGF-1Ec. Most studies have demonstrated IGF1-Ec to promote proliferation and migration of different cell lines via an IGF-1 receptor-independent pathway(Armakolas et al., 2015; Ates et al., 2007; Dluzniewska et al., 2005; Mavrommatis et al., 2013; Mills et al., 2007; Quesada et al., 2009; Yang and Goldspink, 2002; Yi et al., 2017, p. 12). Some of these studies further identified that IGF-1Ec effects were independent of the insulin receptor (INSR) and IGF-1R/INSR hybrid receptors which are the other vital receptors in the IGF-1 pathway (Armakolas et al., 2010a; Philippou et al., 2014). This would suggest that the Ec peptide acts via an alternative receptor which has not yet been characterized. However, this has been disputed by studies reporting IGF1-Ec activity to be dependent on the IGF1R (Brisson and Barton, 2012; Yi et al., 2017). Brisson et al. (Brisson and Barton, 2012) demonstrated that blocking IGF-1R resulted in no activity by the E peptides, and in the absence of mature IGF-1 peptide, the E peptides failed to increase receptor activation independently (Brisson and Barton, 2013). The suggestion from this group was that the E peptides modulate the activity of IGF-1 but may not act independently of the mature IGF-1 peptide, postulating that both the mature IGF-1 peptide and the E peptides interact and converge on the IGF1-R pathway (Brisson and Barton, 2013). A majority of studies (Deng et al., 2012; Sha et al., 2017a; Xin et al., 2012; B. Zhang et al., 2016, 2014) have demonstrated ERK 1/2 phosphorylation to be the most frequent pathway affected by

IGF-1Ec, though Fornaro et al. (Fornaro et al., 2014) specifically found no evidence of ERK 1/2 phosphorylation on human and mouse myoblast cell lines, though intriguingly they were also unable to demonstrate any evidence of increased cell proliferation in these cell lines which have been demonstrated in other studies. A few studies have demonstrated the involvement of the PI3K/Akt pathway, though this has been contradicted by other studies as outlined in Table 1.4. It is likely that standardization of the methodology used to investigate the pathways involved, including the synthetic peptides utilized will be required before a broad consensus can be reached regarding the mechanism of action of IGF-1Ec.

1.3.4 Current evidence for MGF in cancer

There are increasing numbers of research groups investigating the role of IGF-1 isoforms in different human cancers (Table 1.5). Christopoulos et al. (Christopoulos et al., 2015) performed real-time PCR quantification of mRNA for the IGF-1 isoforms extracted from different human cancer and non-cancer cell lines. Class I transcripts was the predominantly expressed variants of all isoforms except for the colon cancer cell line DLD1 which expressed class I and class II variants equally. The endometrial cell line, KLE, was identified to have the highest levels of expression of IGF-1Ec, while the breast cancer cell line MCF7 had the lowest level of expression of IGF-1Ec (Christopoulos et al., 2015). The results published for the colon cancer cell line, DLD1, were conflicting as the overall expression of IGF-1Ec was identified to be much lower than the other isoforms, though the results for Class I IGF-1Ec was higher than IGF-1Ea and IGF-1Eb, and Class II IGF-1Ec was marginally lower than IGF-1Ea and higher than IGF-1Eb. No explanation for this finding was offered in this paper. Durzyńska et al (Durzyńska and Barton, 2014a) published interesting data for the expression of mRNA transcripts of IGF-1 isoforms using quantitative real-

time PCR (qRT-PCR) and the peptide expression of the isoforms using immunoblotting for four cell lines including HeLa (cervical adenocarcinoma), U20S (osteosarcoma), HepG2 (Hepatocellular adenocarcinoma) and K562 (human myelogenous leukemia). There was a complete discordance between the mRNA and peptide expression for the isoforms. IGF-1Ea, in its transcript form, was expressed significantly higher in the K652 cell line compared to other cell lines, while IGF-1Ea peptide was highest in the HeLa cells in which its transcript expression was significantly lower. Similarly, IGF-1Eb expression in HepG2 and K562 cells were reversed with regards to transcript and peptide levels. IGF-1Ec peptide expression was not achieved due to very low expression in all the cell lines utilized. This study reflected the likely crucial role for post translational processing of mRNA affecting peptide production and confirms the limitations of using transcript levels as a surrogate measure of gene expression. Control of translation has a physiological role in cells to enable the cell to adapt swiftly to stress conditions by controlling protein synthesis from an existing pool of mRNAs (Vaklavas et al., 2017). Dysregulation of translation has been confirmed to be a critical nexus for cancer cells to enable cancer cells to overcome the array of stress conditions including that of the tumor microenvironment, immune recognition and anti-tumour therapies (Vaklavas et al., 2017).

The potential role of IGF-1Ec in prostate cancer has predominantly been demonstrated by the Department of Experimental Physiology at the University of Athens (Armakolas et al., 2015, 2010a; Philippou et al., 2013; Savvani et al., 2013). Their published work spanning over a few years initially reported higher IGF-1Ec peptide expression, using immunohistochemistry, in prostate cancer tissues compared to normal prostate tissue (Savvani et al., 2013). Subsequent work with semi-quantitative PCR demonstrated increased expression of IGF-1Ec in prostate

cancer and intra-epithelial neoplasia (very early stage/insitu cancer) compared to normal prostate tissues and demonstrated Ec peptide's mitogenic effects act through a pathway independent of IGF-1R and insulin receptor (Armakolas et al., 2015, 2010a). In 2015, Armakolas et al. (Armakolas et al., 2015) focused on the actions of the Ec peptide in prostate cancer. They demonstrated a correlation with the level of expression of IGF-1Ec peptide with the stage of prostate cancer and reported that the exogenous administration of synthetic Ec peptide increased PC-3 cellular proliferation via the ERK1/2 pathway but not the Akt pathway (Armakolas et al., 2015). In addition, this study demonstrated the endogenous production of Ec peptide in the PC-3 cell line driving proliferation through an autocrine/paracrine mode of action and inducing the Epithelial-Mesenchymal Transition phenomenon (a recognized path for cancer progression) via an IGF-1R independent pathway (Armakolas et al., 2015). In 2018, Armakolas et al. (Armakolas et al., 2018) reported interesting data by focusing on the immune response in tumorigenesis of prostate cancer. Activation of the immune response by incubating prostate cancer cell lines (PC3 and DU145) with SCID mouse blood cells and human white blood cells in separate experiments, demonstrated significantly increased IGF-1Ec expression. They demonstrated IL-6, secreted by the immune response cells, activated the JAK/STAT signaling pathway leading to increased secretion to the Ec peptide. The Ec peptide was then identified to induce the migration and invasion of human mesenchymal stem cells which are likely to be involved in the tumour repair process.

Mourmouras et al. (Mourmouras et al., 2018) investigated the expression of the RNA transcripts of all IGF-1 isoforms in bladder cancer in comparison to adjacent normal uroepithelium using semi-quantitative real-time PCR. IGF-1Ea and IGF-1Eb were identified to be marginally increased

in expression in bladder cancer tissues compared to normal tissues though the results did not reach statistical significance. IGF-1Ec mRNA transcripts, interestingly, were expressed at a significantly decreased level in bladder cancer tissues compared to normal tissues and the study suggested a positive correlation for this with histological and clinical characteristics suggestive of advanced disease. Other cancers investigated for IGF-1Ec expression include osteosarcoma, neuroendocrine tumours, hepatocellular tumours and colon cancer. These studies are summarised in Table 1.5.

IGF-1Ec expression in osteosarcomas was confirmed *in vitro* with the cell lines MG-63 and Mhos (Philippou et al., 2011; Shang et al., 2015). Quantitative PCR, western blotting and immunohistochemistry confirmed the over-expression of mRNA IGF-1Ec transcripts in the malignant cell lines (MG-63) compared to 'less' malignant cell lines (Mhos), and exogenous administration of a synthetic peptide Ec peptide demonstrated significantly increased the proliferation index compared to controls with increased migration distances and invasion (through an 8µm pore of polycarbonate membrane) in a dose-dependent manner (Shang et al., 2015). Work on hepatocellular tumours suggested that the RNA expression of all IGF-1 isoforms including IGF-1Ec was lower in tumours compared to control tissues, though the levels were higher in the normal liver tissue adjacent to the tumour compared to the tumour and control tissues. Alexandraki et al. (Alexandraki et al., 2017) reported IGF-1Ec peptide expression in neuroendocrine tumours was more prevalent in metastatic tumours with higher proliferation indices compared to primary neuroendocrine tumours with lower proliferation indices. Koczorowksa et al. (Koczorowska et al., 2011) performed real-time PCR to quantify the expression of the RNA transcripts of IGF-1 isoforms in pre-cancerous, cancerous and normal cervical tissues.

The three isoforms were universally significantly higher in the pre-cancerous tissues compared to the cancerous and control tissues, with IGF-1Ea accounting for over 85% of expression and IGF-1Ec accounting for approximately 1%. The proportion of IGF-1Eb (with regards to contribution to total IGF-1) in cervical cancer tissues was higher compared to normal and precancerous tissues, therefore raising the suggestion that IGF-1Eb may play a role in cancer progression and potentially a prognostic marker.

Kasprzak et al. (Kasprzak et al., 2013, 2012) published two reports in 2012 and 2013 on the expression of mRNA IGF-1 isoforms in colorectal cancers. The first paper involved 13 tissue pairs of colorectal cancer and normal adjacent colon tissue. Immunocytochemical studies demonstrated cellular expression of IGF-1 in 69% of patients, while control tissues did not demonstrate any significant expression. In tumour tissues, expression of the IGF-1Ea isoform mRNA was the most prevalent followed by IGF-1Eb and then IGF-1Ec with significantly higher levels of class II transcripts compared to class I transcripts. This latter finding of significantly higher class II transcripts was also identified in normal/control tissues. The overall expression of IGF-1 mRNAs was significantly lower in the colorectal cancer tissues compared to control tissues; however the expression of IGF-1Ea was significantly higher in the cancer tissues compared to control. IGF-1Eb was significantly lower in colorectal cancer tissues, and no significant differences were identified for IGF-1Ec compared to normal colon tissues. The second report by Kasprzak et al. (Kasprzak et al., 2013) investigated tissue samples from 28 patients which included paired tumour and normal colorectal tissues. The immunocytochemical analysis (for IGF-1 and not the isoforms) of these tissues demonstrated IGF-1 protein expression in 50% of colorectal cancer tissues and 39% of control tissues with cytoplasmic expression. The intensity of the stain was of

moderate density with no quantitative differences between the control tissues and cancer tissues, and the Ki-67 index was higher in the colorectal cancer tissues. Significantly higher IGF-1Ea and IGF-1Eb mRNA transcripts were identified compared to IGF-1Ec mRNA in both normal and tumour tissues. Comparison of colorectal cancer tissues and control tissues demonstrated significantly higher IGF-1Ea mRNA levels and significantly lower IGF-1Eb mRNA levels in cancer tissues. IGF-1Ec mRNA levels were low for both cancer and control tissues and significantly lower in cancer tissues

1.3.5 The rationale for further investigation of MGF in colorectal cancer

MGF was initially identified to play an essential role in tissue repair and regeneration. There is now growing evidence that it may be involved in cancer progression, notably confirmed in prostate and osteosarcomas. Its role in colorectal cancer remains unclear and therefore warrants further investigation, particularly at the post-translational level.

Pathway	Cell lines
ERK1/2 dependent	Human vascular EC line (Deng et al., 2012), rat tenocyte(B. Zhang et al., 2016, 2014), osteoblasts (Xin et al., 2012), anterior cruciate ligament (ACL) fibroblast(Sha et al., 2017a), mesenchymal cells (Wu et al., 2013), breast cancer(Christopoulos et al., 2017)
PI3K dependent	Mesenchymal stem cells(Tong et al., 2015)
ERK1/2 and PI3K pathways	Bone marrow-derived stem cells(Sha et al., 2017b), ACL fibroblasts (Sha et al., 2019)
ERK1/2 and independent of the PI3K pathway	Prostate cancer(Armakolas et al., 2010a), Neuroblastoma(Quesada et al., 2009), Myocardium(Stavropoulou et al., 2009)
Hippo pathway effector Yap	Growth plate chondrocytes(Jing et al., 2018)
Stromal cell-derived factor 1α /CXCr4 axis	ACL fibroblasts(Sha et al., 2019), Mesenchymal stem cells(Q. Luo et al., 2015)
ERK5-MEF2C	Crohns disease intestinal muscle cells (Li et al., 2015)
Haemoxygenase pathway (HO-1) and independent of the PI3K pathway	Neuroblastoma (Quesada et al., 2009)
No effect on ERK1/2 or PI3K pathways	Human and mouse myoblast cells(Fornaro et al., 2014)
IGFR1 independent	Prostate cancer(Armakolas et al., 2010a), Myoblast(Ates et al., 2007; Mavrommatis et al., 2013; Mills et al., 2007; Yang and Goldspink, 2002; Yi et al., 2017,), Hippocampus(Dluzniewska et al., 2005), Neuroblastoma(Quesada et al., 2009), Endometrium(Dimitrios S. Milingos et al., 2011), Myocardium(Stavropoulou et al., 2009), Osteosarcoma(Philippou et al., 2011)
IGFR1 dependent	Myoblast(Brisson and Barton, 2012; Yi et al., 2017, p. 12)

Table 1.4: Pathways elucidated for IGF-1Ec

Author	Cancer	Study type and design	Study findings
Armakolas et al. (Armakolas et al., 2010a) (2010)	Prostate cancer	IGF-1Ec expression was assessed with immunohistochemistry and real-time PCR for 10 tissues with prostate cancer, and cell lines PC-3, LNCaP, and HPrEC.	IGF-1Ec RNA expression was demonstrated in the cancerous cell lines PC-3 and LNCaP cell lines and not in the normal prostate epithelial cell line HPrEC. Higher IGF-1Ec peptide expression was demonstrated in prostate cancer and intra-epithelial neoplasia tissues compared to normal prostate tissues. Further studies using exogenous administration of a synthetic Ec peptide stimulated prostate cancer cell line growth and acted via an IGF-1R and Insulin receptor-independent pathway involving ERK1/2 phosphorylation without Akt phosphorylation.
Koczorowska et al. (Koczorowska et al., 2011) (2010)	Cervical cancer	IGF-1 splice variants expression (mRNA) assessed using real-time PCR in 109 pre-cancerous and cancerous cervical tissue samples in HPV infected patients	IGF-1Ea RNA transcript was identified to the predominant isoform in all tissues (85 – 92%), and IGF-1Ec was the lowest expressed at 1% in all tissues (control and diseased). All isoforms were significantly raised in high and low grade squamous intraepithelial neoplasia compared to control and compared to cancer tissue predominantly in class I transcripts. The proportion of IGF-1Eb RNA transcripts was higher in cervical cancer tissues, suggesting a role in cancer progression.
Philippou et al. (Philippou et al., 2011) (2011)	Bone, Osteosarcoma	*In vitro* study using cell lines MG-63. IGF-1EC mRNA expression characterized by using real-time PCR, reverse transcription PCR and western blot analysis. Effect of Dihydrotestosterone (DHT) on IGF splice variants assessed.	IGF-1Ea and IGF-1Ec RNA transcripts demonstrated to be expressed by the MG-63 cell line. IGF-1Eb not expressed. The expression of IGF-1Ea and IGF-1Ec transcripts increased significantly in response to DHT, suggesting hormonal regulation. In addition, exogenous administration of a synthetic Ec peptide stimulated the growth of cells with IGF-1R and INSR silenced cells which were not demonstrated by the exogenous administration of IGF-1 and insulin.
Kasprzak et al. (Kasprzak et al., 2012) (2012)	Colorectal cancer	IGF-1 splice variant RNA expression assessed using quantitative real-time PCR from tissues of 13 patients. Immunocytochemical studies were done for IGF-1 and not for the isoforms.	Class II transcripts were significantly higher than class I in both tumour and normal colonic tissues. In tumour tissues, IGF-1Ea RNA transcripts were the highest expressed, followed by IGF-1Eb and IGF-1Ec. In normal tissues, IGF-1Eb was the highest expressed, followed by IGF-1Ea and IGF-1Ec. Significantly lower expression of IGF-1 isoform RNA transcripts overall in colorectal cancer tissues compared to normal colonic tissue. The expression of IGF-1Ea and IGF-1Eb was significantly higher in colorectal cancer tissues compared to IGF-1Ec. No correlation was identified between IGF-1 RNA expression and tumour location, macroscopic and microscopic type of the tumour or grading.

Author	Cancer	Study type and design	Study findings
Kasprzak et al. (Kasprzak et al., 2013) (2013)	Colorectal cancer	IGF-1 splice variants RNA expression assessed using quantitative real-time PCR and immunocytochemistry for IGF-1 (not isoforms) on tissues from 28 patients	Immunohistochemistry demonstrated cytoplasmic expression of IGF-1 in 50% of tumour tissues and 39% of normal colon tissues. In normal and tumour tissues, no significant differences in mRNA expression with regards to class I and class II transcripts was demonstrated, and significantly higher IGF-1Ea and IGF-1Eb transcripts compared to the IGF-1Ec identified. A higher amount of Class II mRNA for IGF-1 compared to Class I mRNA was demonstrated. The total mRNA levels of all IGF-1 isoforms was significantly lower in the colorectal cancer tissues compared to normal tissues. IGF-1Ea was the predominant isoform identified in colorectal cancer tissues and at significantly higher levels compared to normal colon tissues. IGF-1Eb was significantly higher in normal tissues compared to cancer tissues. IGF-1Ec was expressed at low levels in the different tissue types and was significantly lower in tumour tissue compared to normal tissues.
Zinevich et al. (Zinevich et al., 2013) (2013)	Liver tumours	IGF-1 mRNA expression and isoform mRNA expression studied in mice liver. *Paper not accessed, and in Russian*	IGF-1 mRNA expression in all liver neoplasms (dysplasia, nodular hyperplasia, adenoma, carcinoma) was reduced. The mRNA levels of IGF-1EC and IGF-1Ea was lower in hepatocellular carcinoma, but higher in the normal liver tissue adjacent to the tumour compared to the control group
Savvani et al. (Savvani et al., 2013) (2013)	Prostate cancer	Immunohistochemistry for IGF-1Ec was performed for 83 tissues with prostate cancer	The normal prostate epithelium was negative/mild expression for IGF-1Ec peptide. Prostate cancer tissues demonstrated mild to strong cytoplasmic expression, with higher expression in locally advanced prostate cancer compared to localized cancer. There was a mild positive correlation with the Gleason score (grading score for prostate cancer)
Durzynska et al. (Durzyńska and Barton, 2014a) (2014)	Different cell lines	IGF-1 splice variant expression (mRNA) assessed using real-time PCR in cell lines – HelA (cervical adenocarcinoma transformed with HPV18), U20S (osteosarcoma), HepG2 (hepatocellular carcinoma), K562 (myelogenous leukemia), Immunoblotting using cell lysates, cytoplasmic and nuclear fractions were used to determine the level of distribution of IGF-1 peptides	There was a discordance between RNA and peptide levels. RT-PCT demonstrated IGF-1Ea, and IGF-1Ec mRNA transcripts were significantly higher in the K562 cell line compared to all other cell lines, and IGF-1Eb mRNA transcripts were highest in HepG2 and K562. IGF-1Ea peptide levels were highest in the HeLa cell line, while IGF-1Eb peptide was expressed highest in the K562 cell line.

Author	Cancer	Study type and design	Study findings
Shang et al. (Shang et al., 2015) (2014)	Bone, osteosarcoma	*In vitro* study utilizing cell lines Mhos and MG-63. Quantitative PCR and Western blot analysis used to detect IGF-1Ec mRNA transcripts. Exogenous IGF-1Ec (synthetic Ec peptide) administered to stimulate the cell lines	IGF-1Ec mRNA transcripts demonstrated to be over-expressed in the malignant osteosarcoma cell lines, and not expressed in the least malignant cell lines. Exogenous administration of IGF-1Ec promoted proliferation, migration and invasion of the osteosarcoma cell lines.
Christopoulos et al. (Christopoulos et al., 2015) (2015)	Different human cancer cell lines	Quantitative real-time PCR for mRNA of IGF-1 isoforms in different cancer cell lines	Wide variation in expression of the different IGF-1 isoforms. Class I transcripts was identified to be the predominant variant expressed for all isoforms for most cell lines. MCF7 (oestrogen positive breast adenocarcinoma) demonstrated the lowest expression of all IGF-1 isoforms, particularly IGF-1Ec. IGF-1Ec was found at maximum levels in KLE and LnCap cell lines. The expression of IGF-1Eb was not identified in both breast cancer cell lines. The colon cancer cell line expressed equal amounts of Class I and II variants of all isoforms.
Armakolas et al. (Armakolas et al., 2015) (2015)	Prostate cancer	IGF-1Ec expression in 78 prostate cancer tissues was analyzed with immunohistochemistry. Further experiments performed to elucidate pathway of action and association with the epithelial mesenchymal transition (EMT)	Mean IHC IGF-1Ec peptide expression was significantly lower in stage II and lower (localized cancer) tissues compared to stage III and IV. Endogenous produced E peptide (Pec) of the IGF-1Ec induced cellular proliferation in the PC-3 cell line, via the ERK1/2 pathway (and not involving Akt phosphorylation) in an autocrine/paracrine action and induced EMT via IGF-1R independent pathway. Orthotopic injection of the PEc cells in mice was associated with increased metastatic rate.
Alexandraki et al. (Alexandraki et al., 2017) (2017)	Neuroendocrine tumours	IGF-1Ec peptide expression in 47 neuroendocrine tumours was assessed, and proliferation index Ki-67 MIBI evaluated.	IGF-1Ec staining was more significantly expressed in metastatic tissues (70.6%) compared to primary neuroendocrine tumours (36.7%) with a positive correlation with Ki-67 index. Multiple logistic regression demonstrated age and recurrence to be the best predictors of IGF-1Ec expression.
Christopoulos et al. (Christopoulos et al., 2017) (2017)	Breast cancer	Exogenous administration of IGF-1Ec to MCF-7 and MDA-MB-231, proliferation and migratory capacity assessed using MTT, trypan blue and wound healing/scratch assays	IGF-1Ec administration resulted in the proliferation of the MCF-7 cell line but not the MDA-MB-231 cell line. MCF-7 engineered cells to over-express IGF-1EC demonstrated increased proliferation rate and migration capacity with increased ERK1/2 phosphorylation.
Mourmouras et al. (Mourmouras et al., 2018) (2018)	Bladder cancer	Semiquantitative real-time PCR used to identify the expression of all IGF-1 mRNA isoforms in bladder cancer and adjacent normal urothelium	Significantly reduced expression of IGF-1Ec RNA transcripts demonstrated in bladder cancer tissues compared to the normal uroepithelial tissues with positive correlation for advanced disease. A trend in IGF-1Ea and IGF-1Eb transcripts being marginally increased in bladder cancer was noted without reaching statistical significance.

Table 1.5: Summary of studies investigating IGF-1Ec in different cancers

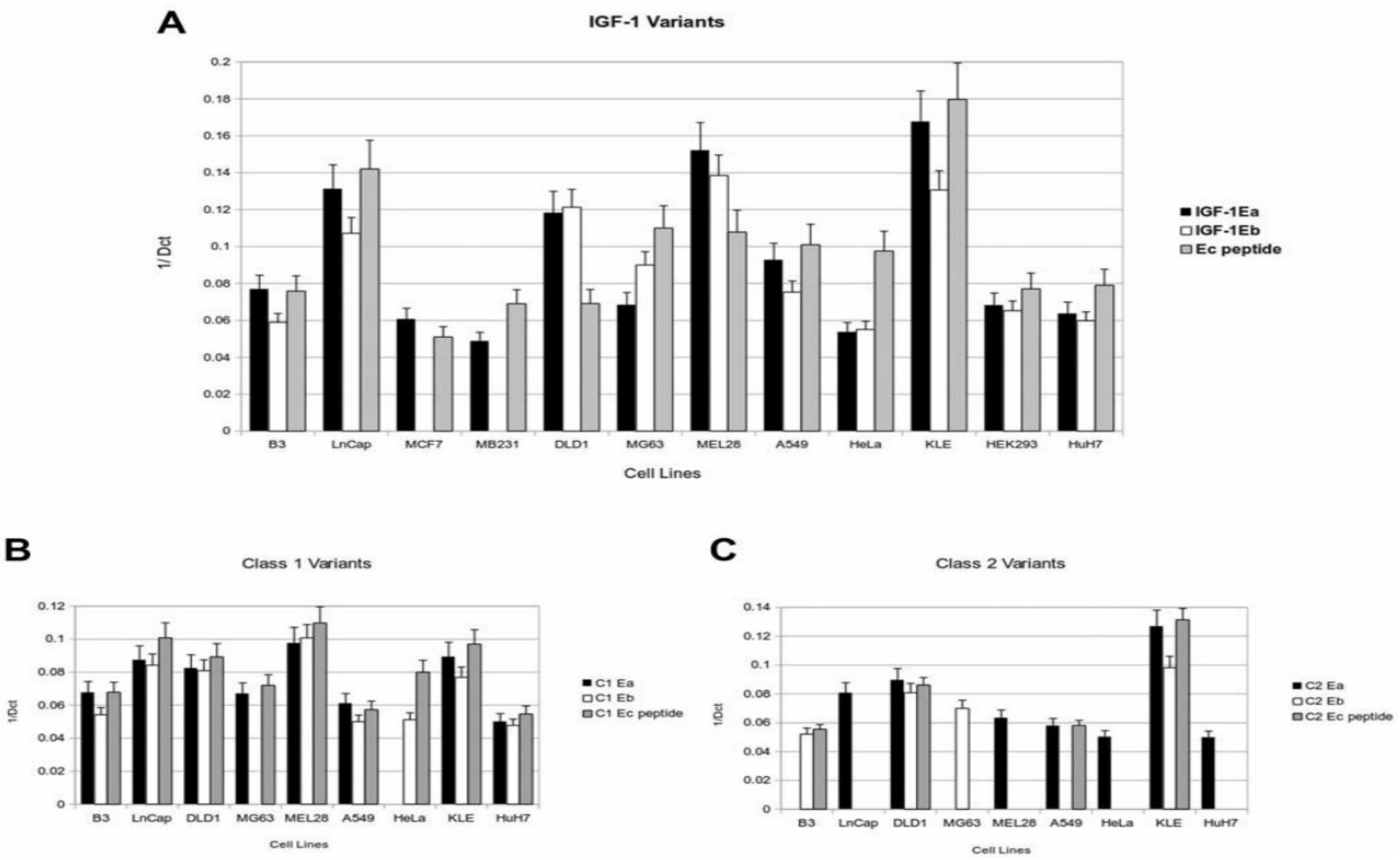

Figure 1.4*:* Graph reproduced from Christopoulous et al. (Christopoulos et al., 2015) demonstrating results from qRT-PCR for IGF-1 isoforms in different normal and cancer human cell lines

1.4 Insulin-like growth factor 1 and its isoforms affecting autophagy in colorectal cancer

1.4.1 Introduction

Autophagy refers to a selection of tightly regulated catabolic processes, involving recycling of cellular macromolecules and organelles, with the delivery of cytoplasmic material to lysosomes for degradation (Lin and Baehrecke, 2015). It is generally accepted that this is an evolutionarily conserved physiological process which assures cellular homeostasis and acts as a survival mechanism to recycle energy and nutrition under specific conditions such as starvation and hypoxia (Burada et al., 2015; Kaur and Debnath, 2015). It involves a bulk process of degrading long-lived proteins and organelles, including endoplasmic reticulum, mitochondria, ribosomes and peroxisomes and promotes the recycling and salvage of cellular nutrients(Kaur and Debnath, 2015). Basal autophagy has been demonstrated to play a vital role in the degradation of damaged organelles preventing the accumulation of misfolded and damaged proteins(Kaur and Debnath, 2015). Three types of autophagy have been described, including macroautophagy, microautophagy and chaperone-mediated autophagy (Maiuri et al., 2007). Macroautophagy involves autophagosomes which are double membraned vesicles which enclose the cytoplasmic material (damaged organelles and unused proteins) and fuses with lysosomes to become autolysosomes in which the lysosome enzymes degrade the cytoplasmic material (Lin and Baehrecke, 2015). Microautophagy involves direct lysosomal engulfment of the cytoplasmic material for degradation, and chaperone-mediated autophagy involves translocation of soluble cytoplasmic proteins via a chaperone-dependent selection across the lysosome membrane (Burada et al., 2015). The genes which regulate this complex process are referred to as the

autophagy-related (*Atg*) genes, initially identified in yeast, and currently, over 30 genes have been implicated (Lin and Baehrecke, 2015). A brief overview of the pathway is outlined in Figure 1.5. Autophagy from this point on will refer to macroautophagy.

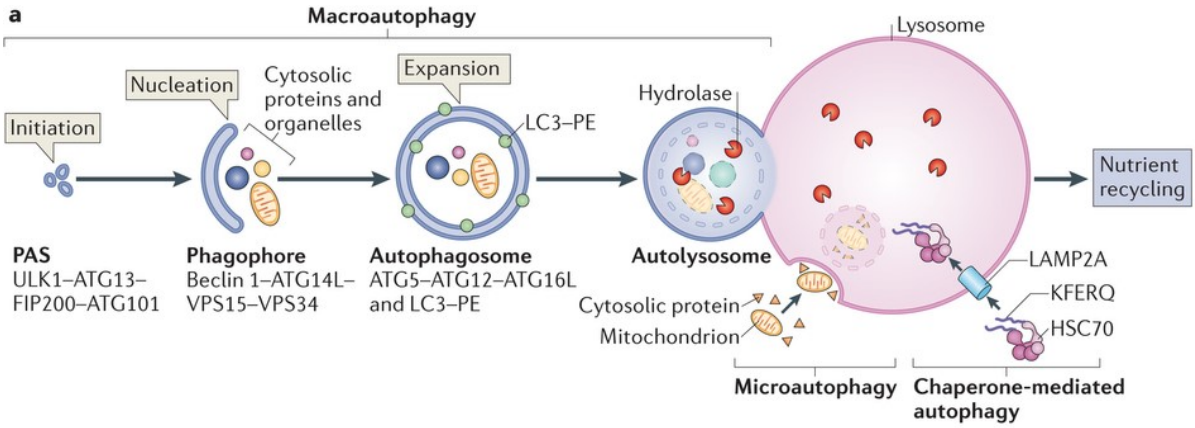

Figure 1.5: Adopted from Kaur et al. (Kaur and Debnath, 2015) Overview of the macroautophagy pathway. The five steps are illustrated. (1) Induction following stress mediated by a complex containing ULK1 protein (2) Nucleation during which phagophore formation is initiated involving predominantly a protein complex with VPS34 (3) Elongation of the phagophore with the ubiquitin like systems including ATG12-ATG12 leading to autophagosome formation (4) Autophagosome fusing with lysosome (5) Degradation of the content of the auophagosome leading to the release of the primary components in the cytosol for recycling

Apoptosis, autophagic cell death and necrosis are three recognised types of programmed cell death during normal development(Lin and Baehrecke, 2015; Schweichel and Merker, 1973). Abnormal regulation of apoptosis has been linked to many human diseases, including cancers, while the role of autophagy is less clear (Lin and Baehrecke, 2015). Apoptosis is currently the most understood pathway, and it can be triggered by cell damage, occur during normal development and morphologically demonstrates chromatin condensation, nuclear fragmentation and membrane blebbing leading to engulfment by phagocytes without invoking a systemic immune response (Swart et al., 2016; Wu et al., 2014). Apoptosis can be triggered by external stimuli such

as the tumour necrosis factor α or intrinsic stimuli via mitochondrial signalling without receptor-mediated stimuli(Swart et al., 2016). Both pathways lead to the activation of caspases which leads to mitochondrial outer membrane permeabilisation (MOMP), activation of effector caspases including caspase 3, caspase 6 and caspase 7 and the release to apoptotic proteins such as cytochrome C, smac and omi causing cell death(Swart et al., 2016). Autophagic cell death refers to lysosomal degradation without the involvement of phagocytes. Necrosis occurs without lysosomal involvement and is associated with organellar swelling, rupture of the plasma membrane and induces of an inflammatory response(Swart et al., 2016). A programmed form of necrosis, referred to as necroptosis, has been described to be elicited in a 'programmed' manner in response to physical trauma, neurodegeneration and cell death due to ischaemia and infection (Nikoletopoulou et al., 2013).

The molecular pathways involved in these three different types of cell death are incredibly complex and associated with considerable overlap with growing evidence demonstrating 'crosstalk' between the pathways in different physiological and pathological situations. Autophagic cell death is characterised by the presence of abundant autophagosomes and the lack of phagocyte participation (Lin and Baehrecke, 2015). This is associated with extensive organelle destruction within the cell, thereby leading it to a state where it cannot function and death of the cell. It, however, remains to be an area of controversy as to whether the autophagy indeed causes cell death, or has been identified as a survival mechanism in a dying cell.

It is not surprising that defects in the autophagy pathway have been associated with a variety of human diseases. A recent review reported defective autophagy to be associated with diseases affecting multiorgan systems including asthma, systemic lupus erythematosus, Crohns disease,

ulcerative colitis, vici syndrome, Parkinson disease, Paget disease of bone, amyotrophic lateral sclerosis, hereditary spastic paraparesis and cancers including breast, ovarian, prostate and colorectal cancers (Jiang and Mizushima, 2014).

1.4.2 Autophagy in colorectal cancer

Autophagy appears to have contradictory dual roles in cancer pathology. In the early stages, it is presumed to have a tumour suppressor role when it protects the cell from transformation to malignancy by removing damaged organelles, thereby reducing DNA damage, reactive oxygen species and mitochondrial abnormalities. However, it has also been identified to be protective to established tumour cells by providing access to nutrients, inhibiting cell death and thereby increasing drug resistance (Burada et al., 2015). Autophagy has also been demonstrated to support metastasis by increasing the survival of detached metastatic cells in the absence of an extracellular matrix, and shifting the cells to a dormant state until appropriate conditions occur (Burada et al., 2015). The expression of the different genes and proteins in the autophagic pathway have been reported to be involved in affecting the prognosis of colorectal cancer. Expression of the LC3B gene and its peptides have been demonstrated to be over-expressed in colorectal cancer tissues and cells with increased aggressiveness of the tumour (Burada et al., 2015; Chen et al., 2013; H. Zheng et al., 2012). Li J et al. (Li et al., 2010) demonstrated the induction of autophagy in colorectal cancers when treated with 5-fluorouracil, which is a standard adjuvant chemotherapy agent in clinical practice. Autophagy was confirmed with immunohistochemistry for LC3B, and the use of 3-Methyladenine, a widely used autophagy inhibitor, along with 5-fu demonstrated increased apoptosis *in-vitro* and significantly increased tumour growth suppression in xenograft models. The expression of the BECN1 gene encoding the

beclin-1 protein, which plays a vital role in autophagy as a component of the autophagy class III PI3K complex, has been investigated in colorectal cancer as well (Burada et al., 2015). Overexpression of BECN1 has been demonstrated in colorectal cancer tissues compared to normal tissues, especially in advanced stages (Burada et al., 2015; Park et al., 2013; Yang et al., 2015). Yang et al. (Yang et al., 2015) demonstrated beclin-1 expression in colorectal cancer tissues to be independently a positive prognostic factor with higher levels associated with increased overall survival and disease-free survival. Park et al. (Park et al., 2013) demonstrated BECN1 expression to be an independent negative prognostic factor in patients with stage II and III colorectal cancer who had received 5-fluorouracil chemotherapy thus suggesting the role of autophagy in promoting drug resistance. Choi et al. (Choi et al., 2014) reported the colorectal cancer tissues with low expression of BECN-1, LC3B and Atg5 are associated with poorer prognosis. However, Han et al. (Y. Han et al., 2014) performed a meta-analysis of six studies which investigated beclin-1 expression in colorectal cancer tissues and concluded that high levels of beclin-1 were associated with a poorer prognosis and increased likelihood of developing distant metastases contradicting the other studies.

Other genes in the autophagy pathway investigated include ATG5 and ATG10, which have demonstrated conflicting results. ATG5 expression has been demonstrated to be down-regulated in colorectal cancer, and its expression associated with lymphovascular invasion (Cho et al., 2012, p.). ATG10 expression was demonstrated to be upregulated in colorectal cancer tissues, and its expression associated with tumour lymph node metastases and invasion with reduced survival (Choi et al., 2013). Apart from the potential use of these markers as prognostic biomarkers, there is some evidence to suggest that the chemotherapy agents used in colorectal cancer, 5-

fluorouracil and cetuximab, induce autophagy (Duffy et al., 2015; Li et al., 2010). Combination therapy with autophagy inhibitors and chemotherapy agents *in-vitro* and *in-vivo* has demonstrated significantly reduced tumour growth compared to the chemotherapy agents alone (Carew et al., 2010; Li et al., 2010, 2009a).

The current literature on autophagy reflects the complexity of this pathway and the conflicting results regarding prognosis and different genes in the process of colorectal cancer. It is important to note that these genes and their relevant expressed peptides are likely to have other roles in the cell metabolism apart from autophagy and therefore confound any conclusions we can reach about the impact of autophagy in colorectal cancer prognosis.

1.5 Autophagy and apoptosis: complex inter-relationship

Autophagy and apoptosis appear to be intricately linked to each other, ensuring cellular homeostasis. The crosstalk between these processes is yet to be clearly defined, owing to the complexity of both pathways. In general, apoptosis and autophagy appear to be mutually inhibitory processes where autophagy precedes apoptosis when a cell is subjected to stresses initially and tends to be anti-apoptotic. As the stresses progress and increase in intensity, apoptosis tends to be induced, and the apoptotic cascade activation degrades the essential autophagic proteins, thereby inhibiting autophagy. Though this would be a convenient means of understanding the two pathways, there are situations where apoptosis can lead to cell death directly without apoptosis, and situations where autophagy can trigger apoptosis and necrotic pathways (Mariño et al., 2014).

Autophagy has been demonstrated to inhibit apoptosis through mitophagy, i.e. removal of mitochondria since damaged mitochondria are more prone towards causing MOMP and the subsequent activation of apoptosis (Mariño et al., 2014; Pattingre et al., 2005). Reduction in cytosolic pro-apoptotic proteins by autophagic processes such as caspase 8 has been identified to be another mechanism by which autophagy inhibits the apoptotic process (Hou et al., 2010). Apoptosis has been demonstrated to inhibit autophagy through the action of caspases which can lead to degradation of essential proteins in the autophagic pathway such as ATG3, Beclin 1 and AMBRA 1(activating molecule in BECN1-regulated autophagy 1)(Mariño et al., 2014; Wirawan et al., 2010). Furthermore, these degraded protein fragments have also been demonstrated to acquire pro-apoptotic functions as demonstrated by the carboxy-terminal of degraded beclin 1 identified to localise in mitochondria in vitro and stimulate the release of cytochrome C (Wirawan et al., 2010). Autophagy has also been demonstrated to mediate cell death either directly by the process referred to as autophagic cell death, or by triggering apoptotic and necrotic pathways. Though these pathways and the stimuli have not been clearly elucidated yet, autophagosome formation has been demonstrated to activate caspase 8 leading to apoptosis, and autophagy has also been demonstrated to deplete the inhibitors of the apoptotic pathway thereby stimulating apoptosis (Mariño et al., 2014; Nezis et al., 2010; Young et al., 2012).

Pathways triggered by intrinsic cell stresses have molecules which have been identified to regulate both autophagy and apoptosis. The tumour suppressor p53 is activated by DNA damage, ischaemic-reperfusion damage and nutrient stress and been demonstrated to suppress autophagy in the cytoplasm by its interactions with FIP200 (Mariño et al., 2014; Tasdemir et al., 2008). In the presence of DNA damage, p53 has been demonstrated to translocate to the nucleus

after phosphorylation by kinases, and the reduction in the cytosolic pool of p53 leads to the induction of autophagy in the cell (Tasdemir et al., 2008). p53 has also been demonstrated to translocate to the mitochondrial matrix and depending on the intensity of binding to cylcophin D, it can promote autophagic removal of the dysfunctional mitochondria or trigger MOMP leading to apoptosis (Galluzzi et al., 2012). In the nucleus, p53 has been demonstrated to bind to promoters of multiple genes which regulate both autophagy (AMPK, ATG5) and apoptosis (PUMA, BAX, BIM) and trigger either pathway (Mariño et al., 2014; Vousden and Lane, 2007). The family of BH3 only proteins has been reported to regulate and activate both pathways (Mariño et al., 2014). Apoptosis induction has been demonstrated via direct interactions and activation of the BCL-2 family, and autophagy induction identified to be caused by interactions of BH3 proteins (BCL-2 antagonist of cell death (BAD), BID, NOXA) with Beclin 1 and releasing it from its inhibitory interactions with BCL-2 or BCL-X (Davids and Letai, 2012; Pattingre et al., 2005). Ser/Thr kinases such as DAPK (Death associated protein kinase) and JNK (Jun N-terminal kinase) have been demonstrated to modulate both autophagy and apoptosis depending on the level of stress on the cell (Mariño et al., 2014). Oncogenes such as MYC and RAS have also been demonstrated to induce either pathway as a response to cellular stress (Mariño et al., 2014).

1.5.1 Insulin-like growth factor and its isoforms in relation to autophagy

The IGF-1 axis has been identified to have a role in regulating autophagy in colorectal cancer (Sipos et al., 2017). mTOR is a major negative regulator of autophagy, and this is activated by class I phosphoinositide 3-kinase (PI3K) and AKT/PKB (Tan et al., 2017). Table 1.6 outlines some of the recent studies demonstrating the involvement of different aspects of the IGF1 signalling axis in controlling autophagy, particularly in times of cellular stress. Most studies (H.-Y. Han et

al., 2014; Liu et al., 2017a; Troncoso et al., 2012; Wang and Gu, 2018; Wang et al., 2014; Yang et al., 2018) demonstrate the suppression of the PI3K/Akt/mTOR pathway is associated with the induction of autophagy, and a couple of studies(Hernández-Breijo et al., 2013; Zeng et al., 2018) have suggested that activation of the ERK pathway is associated with autophagy induction. This suggests that different arms of the downstream signalling pathway of IGF1 have opposing roles in autophagy induction and suppression.

Wang et al. (Wang and Gu, 2018) analysed the autophagy inhibitory effect of IGF-1 treatment on the human colon cancer cell line HCT. They used the HCT-8 cell line and the 5-fluorouracil resistant cell line HCT-8R5-FU. The rationale for this was the known role of autophagy contributing to drug resistance to 5-FU in colon cancer (Wang and Gu, 2018). Treatment with IGF-1 downregulated the mRNA expression levels of the autophagy-associated genes unc-51 like autophagy activating 3-kinase 1 (ULK1), beclin-1 (Becn1) and phosphatidylinositol 3-kinase catalytic subunit type 3 (Vps34) while treatment with IGF-1 and an Akt inhibitor (MK-2206) significantly increased the mRNA expression levels of these genes. Apoptosis assays demonstrated treatment with 5-FU was associated with significantly reduced apoptosis in the HCT-8R5-FU cell line compared to the HCT-8 cell line while co-culture with IGF-1 in the resistant HCT-8R5-FU cells demonstrated increased apoptosis and these effects were negated by the addition of the Akt inhibitor. This study therefore demonstrated the inhibitory effect of IGF-1 on autophagy acting via the Akt pathway and its potential significance in improving efficacy of chemotherapy agents.

Ascenzi et al. (Ascenzi et al., 2019) investigated the effects of the isoforms of IGF-1 in mice on autophagy in skeletal muscle due to the presumed association between autophagy and

sarcopenia (muscle loss) with age. The two isoforms, IGF-1Ea and IGF-1Eb (analogous to IGF-1Ec/MGF in humans) were investigated with the use of transgenic mice lines for each isoform and compared to wild type mice at young (6 months) and old ages (26 months). Interestingly, both IGF-1Ea and IGF-1Eb was associated with significantly upregulated autophagy markers in the aged transgenic mice compared to the aged wild type mice with preserved integrity of the neuromuscular junctions and muscle weight with significantly increased running distance.

The role of the different IGF-1 isoforms and autophagy and cancer has not been investigated. I describe the use of a MAPkinase inhibitor to stimulate autophagy in colorectal cancer cell lines and confirm the relationship between autophagy and apoptosis. This should set a model for work with investigating the relationship between the IGF-1 isoforms, including IGF-1Ec in autophagy in colorectal cancer for potential therapeutic roles in improving the efficacy of chemotherapy agents.

Authors	Study	Findings
Liu et al. (2017) (Liu et al., 2017b)	Mouse embryonic fibroblasts in hypoxic conditions IGF-1 Receptor disruption and over-expressing cells compared	Suppression of PI3k/Akt/mTOR signalling pathway promotes autophagy and cell survival in hypoxic conditions
Yang et al. (2018) (Yang et al., 2018)	Bone marrow mesenchymal stem cells in hypoxic conditions	IGF-1 knockdown reduced Akt/mTOR signalling and increased the level of autophagy in bone marrow mesenchymal stem cells in hypoxic conditions.
Troncoso et al. (2012)(Troncoso et al., 2012)	Neonatal rat cardiomyocytes subjected to nutritional stress	IGF-1 reduced autophagy by activation of the Akt/mTOR signalling pathway.
Hernández-Breijo et al. (2013) (Hernández-Breijo et al., 2013)	Azathioprine treatment of hepatoblastoma and hepatocellular carcinoma cell lines	Treatment of HepG2 cells with azathioprine stimulated the ERK/p70S6K pathway with subsequent activation of autophagy. Prolonged treatment is proposed to have caused resistance to IGF-1, leading to induction of autophagy.
Zeng et al. (2018) (Zeng et al., 2018)	Application of everolimus (mTOR inhibitor) on renal cell carcinoma cells	Everolimus strongly induced autophagy of the cell line in a dose and time-dependent manner. This was demonstrated to be related to the activation of ERK, leading to resistance of the cancer cell line to the treatment.
Han et al. (2014) (H.-Y. Han et al., 2014)	Sulfasalazine applied to oral squamous cell carcinoma cells	Sulfasalazine was identified to induce autophagic cell death with inhibition of the Akt pathway and activation of the ERK pathway
Wang et al. (2014) (Wang et al., 2014)	N-methyl-D-aspartate (NMDA) was used to induce autophagy in hippocampal neuronal cells and effects of IGF-1 treatment assessed	IGF-1 treatment was found to decrease autophagy with upregulation of p-AKT and p-mTOR with these effects blocked by the inclusion of a PI3K inhibitor.
Wang et al. (2018) (Wang and Gu, 2018)	Human colorectal carcinoma cells (HCT cell line) treated with IGF-1	IGF-1 treatment activated the protein kinase B and induced apoptosis while inhibiting autophagy. This was reversed by the application of an Akt inhibitor.

Table 1.6**:** Studies investigating IGF-1 and its pathways in autophagy

2 Chapter 2: Introduction to nanomedicine and review of quantum dots and gold nanoparticle applications in medicine

2.1 Introduction

Cancer is a leading cause of morbidity and mortality worldwide. In 2012, approximately 14.1 million cases of cancer were diagnosed worldwide and accounted for 8.2 million deaths ("Fact Sheets by Cancer," 2016). Early diagnosis offers the best outcomes for patients affected with cancer, and this requires inexpensive, sensitive and specific diagnostic tests which can be used as screening tools. Late presentation in cancer often presents with local and distant spread of cancer and is a leading cause of cancer mortality. In this situation of advanced cancer, curative surgery is less likely to be an option, and the use of other treatment modalities such as chemotherapy and radiotherapy plays an essential role. Chemotherapy agents are cytotoxic in nature, and therefore the use and dosages are limited by the accompanying side effect profiles resulting from nonspecific interactions with healthy tissues.

Nanomedicine is defined by the European Science Foundation as the science and technology of diagnosing, treating and preventing disease and traumatic injury, of relieving pain and of preserving and improving human health using molecular tools and molecular knowledge of the human body("Nanomedicine : European Science Foundation," 2019). It involves the use of materials in size ranges from one nanometer to hundreds of nanometers ("Nanomedicine : European Science Foundation," 2019). These particles exhibit unique and desirable features and are under extensive research for use as diagnostic, therapeutic and drug delivery purposes. Nanoparticles in current clinical practice include liposomes (including liposomal doxorubicin (Doxil®) and liposomal daunorubicin (DaunoXome®) which are being used to improve tumour specific delivery of chemotherapy drugs, thereby reducing the side effect profile of these drugs and magnetic nanoparticles as diagnostic agents. This chapter describes the basic features

common to all nanoparticles and the use of active targeting to improve their performance. Quantum dots and gold nanoparaticles will be further reviewed in more detail with reference to synthesis, conjugation, functionalisation and current active research in this field.

2.2 Nanoparticle biodistribution

The biodistribution of nanoparticles has been demonstrated to be affected by size, shape, surface characteristics and protein corona effects (Auría-Soro et al., 2019). Factors reducing the circulating times of nanoparticles include renal excretion, splenic and hepatic uptake, and breakdown by the reticuloendothelial system(RES) (Petros and DeSimone, 2010). Renal excretion significantly affects nanoparticle circulation times and occurs if the nanoparticle dimensions are less than the fenestration gaps of the endothelial linings in the kidneys, estimated to be between 20 – 30 nm in animal models (Gaumet et al., 2008). Splenic filtration and breakdown of nanoparticles is a further significant factor which can affect bioavailability. Nanoparticles measuring less than 200 nm have been demonstrated to be small enough to avoid the filtration process at the level of the inter-endothelial slits in the walls of the splenic venous sinusoids (Moghimi et al., 2001). Larger fenestration gaps up to 150 nm have been measured in liver and bone marrow tissues, and nanoparticles smaller than these dimensions have reduced circulation times due to uptake by these organs (Gaumet et al., 2008). The ideal size of nanoparticles for clinical use has been estimated to be 100 nm - 200 nm (Gaumet et al., 2008).

Recent evidence suggests that the shape of the nanoparticle may more significantly affect the circulating times compared to size. Champion et al. (Champion and Mitragotri, 2006) demonstrated the shape rather than the size of polystyrene molecules to independently and

more significantly affect the risk of phagocytosis by macrophages. This was supported by a further study which demonstrated significantly increased circulation times of filamentous micelles compared to spherical micelles despite dimensions of the molecules in micrometres (Champion et al., 2007). The optimal parameters for shape have yet to be determined.

Opsonisation is a process which involves adsorption of proteins on the surface of foreign particles in the bloodstream and encourages the breakdown of the foreign body by the RES. Current strategies to reduce uptake by the RES involve rendering the nanoparticle surface more hydrophilic and neutralising the charge (Petros and DeSimone, 2010). This has been successfully achieved with the use of polyethylene glycol (PEG), which has been demonstrated to prevent the opsonisation process transiently and significantly increases circulation times (Petros and DeSimone, 2010).

The protein corona refers to a complex plasma proteins layer around the nanoparticles which takes place when nanoparticles are exposed to physiological fluids including blood (Auría-Soro et al., 2019). This is thought to arise from a competitive dynamic process between the soluble biomolecules and the nanoparticle surface. The significance of the corona is the effect of the protein composition on the nanoparticles physiochemical properties with consequences on the effectiveness of the nanoparticles including uptake by cells (Auría-Soro et al., 2019). The implicated proteins include immunoglobulin G, serum albumin, serum fibrinogen, clusterin and apolipoproteins depending on the biological environment and type of nanoparticle administration (Auría-Soro et al., 2019; Lee et al., 2015). The protein corona is classified into hard and soft layers based on the duration and affinity of the protein exchanges with the hard corona

forming the closest layer to the nanoparticle surface with a high affinity and long exchange times while the soft corona is a low affinity layer of proteins with a fast exchange over time (Auría-Soro et al., 2019). The relationship of different nanoparticles, type of administration, different physiological fluids and interactions with the protein corona remains an area of research to help improve nanoparticle biodistribution.

2.3 Cancer targeting of nanoparticles

2.3.1 2.3.1 Passive targeting

The endothelial barrier is an essential factor affecting the biodistribution of nanoparticles. The anatomical and pathophysiological abnormalities arising from disordered angiogenesis of solid tumours can be utilised to the advantage of nanocarriers. The tumour vascular architecture is often abnormal, with dilated vessels composed of disorganised endothelial layers with large fenestrations (Iyer et al., 2006). Measurements of the fenestration gaps on animal models of tumour tissues have been estimated to be between 200 – 780 nm (Jain, 1994). Appropriately sized nanoparticles can, therefore, penetrate the abnormal endothelial layers in the tumour tissues, whilst being size restricted by normal endothelial layers in the other tissues. The disordered tissue architecture in tumours results in poor lymphatic drainage and venous flow, thereby contributing to inefficient drainage from the tumour bed (Skinner et al., 1990). This leads to high local concentrations of the nanoparticles at the tumour sites in comparison to healthy tissues (Figure 2.1). This passive phenomenon has been referred to as the Enhanced Permeability and Retention effect (EPR) and was initially reported by Matsumara and Maeda in 1998 (Matsumura and Maeda, 1986) when they identified, with the use of radioactively labelled proteins, that there is a tumour specific accumulation of these proteins with a ratio of 5:1 to the

concentration in blood over a period ranging from 19 hours to 72 hours, though this did not apply to proteins less than 20 kDa. Retention times from as long as days to weeks have been demonstrated in animal models (Maeda, 2010). Though passive targeting of tumour cells via the EPR effect is the basis of many current clinically utilised nanocarriers including liposomal doxorubicin (Doxil®) and liposomal daunorubicin (DaunoXome®), there are a few limitations with this approach to tumour targeting. The random approach for nanoparticles to accumulate in the target tumour tissue makes it a complicated process to control. There is some evidence to suggest that this poor control may induce multidrug resistance (Peer et al., 2007). In addition to this, the EPR effect is not demonstrated in all tumour tissues, and variations in tumour architecture in the same tissue can affect the uniform distribution of the nanoparticle and thereby the drug delivered (Peer et al., 2007). Hepatocellular and renal cell carcinoma have been demonstrated to have a higher EPR effect due to the higher vascular density in these tissues compared to prostate and pancreatic cancer which have lower vascular densities (Kalyane et al., 2019; Maeda, 2015; Nagamitsu et al., 2009). Henerweer et al. (Heneweer et al., 2011) ^{90}Zr-labelled mouse albumin to assess the uptake and retention in three human xenograft models of prostate cancer and demonstrated at 20 hours post-administration, just 5% of the injected dose accumulated in the tumour tissues. This has been replicated in other studies with the tumour uptake for pegylated nanoparticles, including ZnSe quantum dots at 8.3% (Yu and Zheng, 2015). The need to improve tumour delivery of nanoparticles has led to the increasing work in active targeting strategies as discussed below.

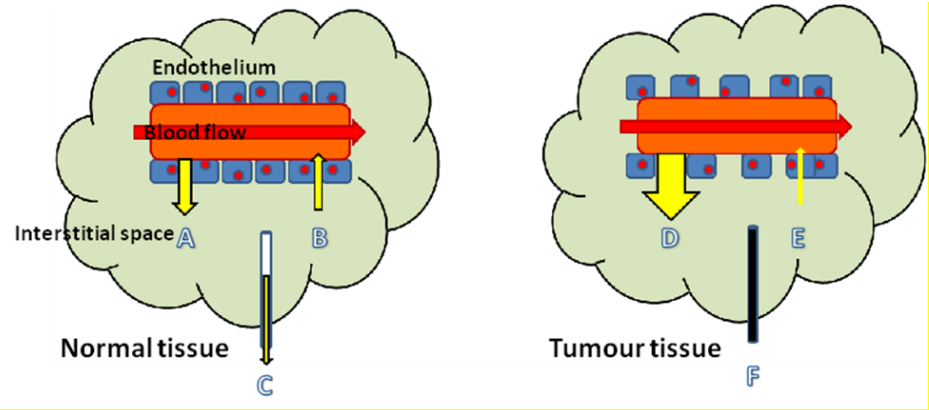

Figure 2.1: Enhanced Permeability and Retention (EPR) effect. Normal tissue on the left. (A) Hydrostatic pressure pushes fluid into in interstitial space (B) Oncotic pressure draws fluid back into the bloodstream (C) Lymphatic drainage of fluid. Tumour tissue on the right. (D) Leaky endothelium leads to a more substantial volume of fluid leaking into the interstitial spaces (E) Low protein leading to low oncotic pressure drawing fluid into the bloodstream (F) Minimal lymphatic drainage due to disordered tissue architecture. Nanoparticles can utilise the combination of D, E and F to accumulate in tumour tissue.

2.3.2 Active targeting

Active targeting relies on targeting receptors overexpressed in tumour tissues and minimally expressed in normal tissues. Active targeting nanocarriers are transported in the same manner as the passively targeted nanocarriers and therefore are subjected to the same factors that affect blood circulation times. The targeting ligands include proteins (monoclonal antibodies or their fragments), nucleic acids (aptamers) or other receptor ligands (peptides, vitamins and carbohydrates) (Peer et al., 2007). Targets currently under research can be broadly classified as cellular targets and tumour endothelial targets (Danhier et al., 2010). Cellular targets (Table 2.1) are utilised for drugs which directly cause cell death. These ligands target receptors which promote cell internalisation, thereby ideal for drugs acting on DNA, RNA and proteins. Receptors that have been targeted for this purpose include the transferrin receptor, the folate receptor, and the epidermal growth factor receptor (EGFR). Targeting the tumour endothelium (Table 2.2)

aims to cause tumour cell death due to hypoxia and the lack of nutrients. The concept was initially suggested in 1971 by Judah Folkman (Folkman, 1971) and targets include vascular endothelial growth factor (VEGF), (alphavbeta3) integrin, vascular cell adhesion molecule-1 (VCAM-1) and the matrix metalloproteinases. Limitations of active targeting nanoparticles include the binding site barrier and non-specific cell binding (Allen et al., 1995; Juweid et al., 1992). The binding site barrier results from nanoparticles with high-affinity ligands binding with perivascular cancer cells (the first cancer cells in contact with the nanoparticle), thereby resulting in poor tumour penetration. Therefore, despite increased tumour accumulation, the efficacy of the delivered drug may not be improved due to non-uniform distribution. The other identified limitation is the presence of the targeted receptor in normal cells, which will result in reduced circulation times and systemic toxicity (Allen et al., 1995).

Receptor	Role	Overexpressed in tumours
Transferrin receptor	Type II transmembrane glycoprotein The binding site for transferrin which transports iron, thereby delivering iron intracellularly.	Breast, bladder (transitional cell), glioma, lung adenocarcinoma, chronic lymphocytic leukaemia, non-Hodgkin's lymphoma, ovarian, prostate, renal (Daniels et al., 2006; Wirth et al., 2006).
Folate receptor	Glycosylphosphatidylinositol-anchored protein Folic acid is required for the synthesis of purines and pyrimidines.	Alpha form - epithelial cancers including ovarian, cervix, endometrium, lung, kidney and brain. beta-form - acute and chronic myeloid leukaemia (Low and Kularatne, 2009).
Epidermal growth factor receptor	tyrosine kinase receptor Mediate a cell signalling pathway for growth and proliferation in response to binding of the growth factor (Byrne et al., 2008).	Breast cancer, colorectal, non-small cell lung cancer, squamous cell carcinoma of the head and neck, ovarian, kidney, pancreatic and prostate (Lurje and Lenz, 2009).

Table 2.1*:* Targets for active targeting nanoparticles: Cell proliferation receptors

Receptor	Role	Overexpressed in tumours
Vascular endothelial growth factor receptor - (VEGFR)	Inducer of tumour angiogenesis. VEGFR-1 and VEGFR-2 receptors targeted. The latter is the most commonly targeted (Byrne et al., 2008).	Breast, colon, pancreatic, non-small cell lung cancer, squamous cell cancer of the head and neck, prostate, bladder (Fischer et al., 2008; Sato et al., 1998).
$\alpha_v\beta_3$ Integrin	Endothelial cell receptor for extracellular matrix proteins. Role in the calcium-dependent signalling pathway leading to endothelial cell migration (Byrne et al., 2008; Danhier et al., 2010).	Lung, breast, colon, melanoma, squamous cell skin carcinoma, Kaposi sarcoma (Byrne et al., 2008; Kessinger et al., 2010).
Vascular cell adhesion molecule (VCAM-1)	Immunoglobulin-like transmembrane glycoprotein Expressed in inflammation and tumours and promotes cell to cell adhesion (Osborn et al., 1989).	Lung, breast, melanoma, renal cell carcinoma, gastric, nephroblastoma, Hodgkins disease, B-cell lymphocytic leukaemia (Dienst et al., 2005).
Matrix metalloproteinases	Zinc-dependent endopeptidases which break down the extracellular matrix. Essential physiological component for tissue repair, morphogenesis and angiogenesis (Vihinen et al., 2005).	Lung, gastric, colon, breast, cervix, glioma, melanoma (Byrne et al., 2008; Sato et al., 2005).

Table 2.2: Targets for active targeting nanoparticles: tumour endothelium receptors

2.4 Fluorescent nanoparticles

2.4.1 Quantum dots

2.4.1.1 Introduction

Quantum dots are classically described as inorganic nanocrystals measuring around 2 – 10 nm with size controllable optical and electrical properties (Volkov, 2015). Since Louis Brus demonstrated the quantum confinement effect of these nanocrystals, these particles have been investigated in different roles in medicine including drug delivery, biomarker detection, sentinel lymph node mapping agents, intraoperative imaging to aid clear margin excisions of tumours and photodynamic therapy (Brus, 1984; Onoshima et al., 2015; Rosenthal et al., 2007; Steigerwald and Brus, 1990). The 'classical' quantum dots related to semiconductors synthesised from groups III-V and II-VI elements of the periodic table. However, in the last decade, an increasing number of nanoparticles based on carbon, noble metals and silicon have been identified to demonstrate the quantum confinement effect, and therefore the definition of quantum dots has to be broadened to encompass this (Volkov, 2015). Semiconductor quantum dots possess a broad excitation spectrum and a narrow, symmetrical and size-controlled emission spectrum. In comparison to organic fluorophores, these quantum dots have been demonstrated to have 100 to 1000 fold greater fluorescent stability against photobleaching with 10 to 100 fold higher intensity in brightness (Onoshima et al., 2015). Table 2.3 summarises the advantages of semiconductor quantum dots compared to organic fluorophores.

Property	Semiconductor quantum dots	Organic fluorophores
Absorption spectrum	Broad	Narrow
Emission spectrum	Narrow, symmetrical with Gaussian profile	Asymmetrical, often tailing to long-wavelength side
Photobleaching threshold	High	Low
Fluorescence lifetimes	10 – 100ns, typically multi-exponential decay	1-10 ns, mono-exponential decay
Quantum yield	High	Low
Saturation intensity	High	Low

Table 2.3*:* Comparison of semiconductor quantum dots as labelling agents and organic dyes (Resch-Genger et al., 2008)

Over the last two decades, the structural evolution of the quantum dots has included the design of 'self-illuminating' quantum dots. Self-illuminating quantum dots absolve the need for external excitation energy to make the quantum dots fluoresce and therefore reduce the background signal and avoid the non-specific tissue damage by the excitation energy (Aswathy et al., 2010). These quantum dots have been constructed with the principle of bioluminescence resonance energy transfer (BRET), where a light-emitting protein nonradiatively transfers energy to the acceptor quantum dot, thereby causing it to fluoresce. To achieve this, So et al. (So et al., 2006) described coupling carboxylate bearing quantum dots with a mutant of the bioluminescent protein *Renilla* luciferase, and upon addition of the substrate coelenterazine, the protein emits blue light which excites the nearby quantum dot causing it to fluoresce (Aswathy et al., 2010; So et al., 2006). The structure, synthesis and functionalisation of 'classical' quantum dots are described below after a brief description of the quantum confinement effect.

2.4.1.2 The quantum confinement effect

2.4.1.2.1 Semiconductor quantum dots

The quantum confinement effect, band gaps and excitons can be better understood after reviewing the basics of semiconductors. Semiconductors are materials with electrical conductivity between an insulator and a conductor. Electrons in materials are described to

have energies with discrete bands which are between the ground state (electrons bound to the nucleus) and free electron energy (electrons are free of the material). Electrons with lower energy tend to lie in the valence band, while those with higher energy lie in the conduction band. Conductors have a predominance of electrons in the conduction band, while insulators have a predominance of electrons in the valence band. Semiconductors have a few electrons in the conduction band, with a majority in the valence band. The energy required to excite electrons from the valence band to the conduction band is referred to as the bandgap, and this increases the conductivity of the material. The bandgap is larger in insulators compared to semiconductors, and arbitrarily a gap of 4eV is the defining line between the two materials. When electrons acquire energy (from an external source), they can 'jump' from the valence band to the conduction band, thereby leaving a positively charged 'hole' in the valence band. The electron and its hole are referred to as an exciton sharing attractive forces between them. The distance in an electron-hole pair is referred to as the exciton bohr radius. When the electron returns from the conduction band to the valence band (after the external energy source is removed), energy is released in the electromagnetic spectrum. In quantum dots, the nanoscale of these particles results with the size of the dot to be of the same order as the exciton bohr radius, thereby 'confining' the electron-hole pair. This effect arising from the quantisation of the energy levels into discrete bands is referred to as the quantum confinement effect. Small alterations in the size of the quantum dot can affect the bandgap and therefore wavelength of the transmitted energy.

2.4.1.3 Semiconductor quantum dot structure

The largest groups of quantum dots in nanomedicine research are the II-VI type of quantum dots, based on the elements of the periodic table. These include CdSe, CdTe, Zn and Hg based quantum dots. Other types of quantum dots include III-V and IV-VI quantum dots. Quantum

dots with two semiconductor materials arranged in a core-shell structure have been demonstrated to better photostability and higher quantum yields (Obonyo et al., 2010). The core quantum dot can develop surface defects which can quench the fluorescent properties of the quantum dot. 'Coating' the quantum dot with a shell limits this by protecting the bare quantum dot from surface oxidation and prevents leaching of metal ions when exposed long term to cellular media and therefore metal toxicity (Karakoti et al., 2015; Singh et al., 2012). The alteration of the constituents of the core and shell material can be used to fine-tune the emission wavelengths. Depending on the band gaps of the core and the shell, quantum dots can be classified as either type I, reverse type 1 or type II (Kim et al., 2003; Ma and Su, 2010). In type I quantum dots, the bandgap of the core is smaller than the shell and a lower conduction band and higher valence band electron energies in the core compared to the shell, thereby confining the electrons and holes to the core of the quantum dots. In reverse type I quantum dots, the bandgap of the core is larger than the shell thereby confining the electrons and holes in the shell. Examples of type I quantum dots include CdSe/CdS (core/shell) and CdSe/ZnS quantum dots. Examples of type I reverse quantum dots include CdS/HgS and CdS/CdSe quantum dots. In type II quantum dots, both the valence and conduction bands are either higher or lower in the core compared to the shell with the result of one carrier confined to the core and the other to the shell. This staggered bandgap alignment leads to increased spatial separation with radiative recombination across the material interface, allowing for emission wavelengths which may not be possible with type I quantum dots. Examples of type II quantum dots include CdTe/CdSe quantum dots where the electron is confined to the CdSe shell and the hole in the CdTe core and CdSe/ZnTe where the electron is confined to the CdSe core and the hole in the ZnTe shell(Kim et al., 2003).

In type I quantum dots, the shell acts as a barrier and protects the core from photobleaching (loss of fluorescence). Reverse type I quantum dots have shells with smaller band gaps compared to the core, and therefore the emission spectrum of the quantum dot is affected by the shell thickness with a significant red-shift with increasing size(Reiss et al., 2009). A further larger bandgap material may be grown over this core/shell structure to protect it from photobleaching. The staggered bandgap alignment in type II quantum dots allows for a more significant red-shift of the emission spectra and allows for alterations of shell thickness to achieve emission wavelengths which are challenging to achieve with other materials particularly in the highly desirable near IR spectrum(Reiss et al., 2009).

2.4.1.4 Quantum dot synthesis and functionalisation

There are increasingly different strategies being reported for the precise production of quantum dots. These include organometallic synthesis, aqueous synthesis and 'green' methods involving biosynthesis.

2.4.1.4.1 Organic synthesis

Synthesis of quantum dots by pyrolysis of organometallic reagents by injection into hot coordinating solvents described initially in 1993, remains to be the most popular method of quantum dot synthesis for making robust and high-quality quantum dots (Murray et al., 1993; Yong et al., 2012). This involved the use of dimethyl cadmium mixed with trioctylphosphine (TOP) and selenium, rapidly injected into hot trioctylphosphine oxide (TOPO) enabling the production of highly monodisperse CdSe (Murray et al., 1993). This method was limited by the drawbacks of dimethyl cadmium being pyrophoric (therefore necessitating airless techniques in handling) and associated with high cost and toxicity. Other precursors are now being used successfully in place of dimethyl cadmium including CdO and cadmium acetate

which are more acceptable for widespread industrial use(Peng and Peng, 2001; Qu et al., 2001; Rosenthal et al., 2007). Quantum dots produced by the organic synthesis routes are insoluble in aqueous solutions, and therefore require further surface modifications prior to use in biological systems.

2.4.1.4.2 Aqueous synthesis

This method of synthesis renders the quantum dot water-soluble thereby removing the need for further modifications of the quantum dot surface which results in significantly decreased photoluminescence (Bruchez et al., 1998; Mattoussi et al., 2000; Mussa Farkhani and Valizadeh, 2014). Aqueous phase synthesis utilizes capping agents such as thiols in alkaline solution with the precursors of the quantum dot constituents such as Cd and Te. The use of short-chain thiols renders the quantum dots dispersible in aqueous media, thereby removing the need for further functionalization and offers reactive groups which can be directly conjugated with biomolecules for targeted delivery (Yong et al., 2011). This method of quantum dot synthesis is of a lower cost compared to the organometallic approach and offers a more environmentally friendly and higher reproducibility option. However, this method does not possess the same degree of crystallinity of the quantum dots, and the organometallic approach tends to produce quantum dots with a narrower particle size distribution(Gaponik et al., 2002; Mussa Farkhani and Valizadeh, 2014).

2.4.1.4.3 Biosynthesis of quantum dots

Biological methods of synthesis of quantum dots involve the use of biological organisms and biomimetic systems for quantum dot synthesis and functionalization of these chemically synthesised quantum dots with biomolecules (Zhou et al., 2015). This method offers milder conditions for quantum dot synthesis and the advantage of synthesized quantum dots with

inherent biostability without the need for further functionalization (Zhou et al., 2015). Organisms successfully used for this purpose include *E.Coli,* yeast cells including *saccharomyces cerevisiae*, the earthworm and *staphylococcus aureus* (Bao et al., 2010; Kang et al., 2008; Luo et al., 2014; Stürzenbaum et al., 2013; Xiong et al., 2014; Zhou et al., 2015). The organisms are incubated with the relevant precursor ions such as cadmium salts, and the organisms produce peptides and enzymes which catalyse the reaction in the intracellular environment to generate the quantum dots. Some groups have reported a relatively high yield of quantum dots (as high as 33%) using these means and report the emission wavelength of the quantum dot can be tuned by adjusting the incubation time of the yeast cells (Bao et al., 2010; Zhou et al., 2015). Biomimetic systems have also been successfully shown to generate biocompatible quantum dots at relatively high yields (Zhou et al., 2015). This has included the use of lipid vesicles, ribonuclease-A and DNA and offers the advantage of monitoring and modulating the physiochemical properties of the quantum dots thereby providing quantum dot production in a large scale (Kong et al., 2010; P. Yang et al., 2009; C. Zhang et al., 2014; Zhou et al., 2015). These 'green' methods of quantum dot synthesis are currently generally inferior to the chemical methods of synthesis with regards to the yield and uniformity of the quantum dots generated.

2.4.1.4.4 Surface modification for solubility in aqueous media

The organic method of quantum dot synthesis results in hydrophobic surfaces, thereby making them insoluble in aqueous media and therefore inadequate for biomedical purposes. Strategies reported in the literature to make these quantum dots soluble in aqueous solutions include ligand exchange, surface silanisation, and coating the quantum dot surface with amphiphilic polymers. Ligand-exchange involves the removal of the hydrophobic ligands on the quantum dot surface (arising from the solvents used in their synthesis) and substituting

them with ligands which have bifunctional groups such as thiols (-SH) to bind onto the ZnS shell of the quantum dot and either carboxyls (-COOH), amines (-NH_2) or hydroxyls (OH) to enable the quantum dot to be water-soluble and attachment of secondary biomolecules for functionalisation (Bruchez et al., 1998; Kang et al., 2004; Karakoti et al., 2015; Obonyo et al., 2010; Thanh and Green, 2010). Though ligand exchange is generally easier to perform compared to other strategies and the resulting size of the quantum dot can be tightly controlled improving its biological applications, it is limited by the consequent reduction in photoluminescence (from a quantum yield of 80% to 30%), the tendency for quantum dots to aggregate and the short-term stability of thiols (Ma and Su, 2010; Obonyo et al., 2010; Yu et al., 2006).

The use amphiphilic polymers involve encapsulating the quantum dot through hydrophobic interactions with the quantum dot surface and thereby leaving exposed hydrophilic ends which result in the solubility in aqueous media. Polymers used for this purpose include phospholipids, and long-chain polymers which include triblock polymers and this method is not limited by reduced quantum yield since there are no changes to the quantum dot surface with the long-chain polymers, and this offers more binding sites for ligands which is useful for biomedical applications (Obonyo et al., 2010). In addition, this method is associated with reduced toxicity of the quantum dot and increased stability(Obonyo et al., 2010; Yang and Zhang, 2004). Silanisation of the surface of the quantum dot involves creating a layer of amorphous silica which renders the quantum dot soluble in aqueous solutions (Karakoti et al., 2015). This process has been demonstrated to be a very stable capping agent with increased photostability and the terminal groups of the silane shell exposed for further processing with thiol, phosphonate or methyl terminal groups (Correa-Duarte et al., 1998; Karakoti et al., 2015; Thanh and Green, 2010).

2.4.1.4.5 Biofunctionalisation

Further modification of the quantum dot surface is required for biomedical applications. The use of active targeting ligands such as proteins, aptamers and antibodies have been successfully used as targeting moieties in nanomedicine. The two main approaches to achieve this is via covalent or non-covalent binding (Bilan et al., 2015). Non-covalent conjugation involves electrostatic bonding, absorption and mercapto-exchange. The large surface area of quantum dots is utilized for non-selecting binding of molecules and is dependent on the type of biomolecules being adsorbed on the surface, the type of solvent, pH and ionic strength (Karakoti et al., 2015).

Covalent binding is more popular due to the stronger bonds achieved with the biomolecules. Amide coupling has been demonstrated to offer high efficiency and yield with stable bonds. The process usually involves the use of carboxyl terminated functional groups on the surface of the quantum dot to be conjugated with the free amines on proteins, peptides or antibodies through the formation of simple amide bonds (Karakoti et al., 2015; Pereira and Lai, 2008). EDC (1-ethyl-3-(3-dimethylaminopropyl) carbodiimide) is commonly used as a coupling agent between amine groups on proteins and the carboxyl groups on the quantum dots(Obonyo et al., 2010). Other examples of the use of covalent binding for biomolecules include the use of thiols to achieve disulfide binding of the quantum dots with the peptides. These quantum dots offer the advantage of bypassing the two-stage process of making the quantum dot soluble and then achieving functionalisation(Karakoti et al., 2015).

2.4.1.5 Review of current studies on the role of quantum dots in cancer diagnosis and treatment

The unique features of quantum dot nanoparticles have led to research to their use in cancer diagnosis and treatment. Areas of focus in cancer diagnosis and treatment include its use in

labelling biomarkers and immunohistochemistry, tumour targeting and therapy and photodynamic therapy.

2.4.1.5.1 Semiconductor quantum dot for immunohistochemistry

Immunohistochemistry is an essential technique in tumour diagnosis, which is used to identify characteristic antigens in tissues. The technique involves the detection of antigens by using specific antibodies, and the extent of the expression of the antigens is traditionally detected by enzyme-substrate based chromogenic markers via light microscopy. Analysis of the extent of binding is semi-quantitative with the use of scoring systems such as the H score and the Allred score. The use of organic fluorophores conjugated to the second antibody is another method of performing immunohistochemistry. Since the labels can be visualized with a fluorescence microscope, the labels are easily visualized. Quantum dots offer many advantages over the use of organic fluorophores (outlined in Table 2.3) including minimal photobleaching, the advantage of the use of multiple quantum dots simultaneously on the same tissue sample which would help outline multiple antigens due to the ability to fine-tune the emission spectrum of the quantum dots using the same excitation energy (Akhtar et al., 2007). Since the initial reports of quantum dot-based immunohistochemistry in 2001, an increasing number of protocols have been reported in the literature (Akhtar et al., 2007; Vu et al., 2015). Recent studies have been outlined in Table 2.4, and overall the efficacy of quantum dot immunohistochemistry has been demonstrated to have equal or superior ability to quantify the expression of single and multiple antigens in different cancer tissues.

Author	Cancer type	Findings
Peng et al. (Peng et al., 2017)	Gastric	CdSe core with ZnS shell quantum dots bound to secondary antibodies for immunohistochemistry. Multiplexed quantum dot-based quantitative immunofluorescence was used for stromal markers such as lysyl oxidase (LOX). Comparison to traditional immunohistochemistry demonstrated superior fluorescence of the quantum dots and resistance to photobleaching. LOX expression was correlated to overall survival and disease-free survival.
Zheng et al. (Zheng et al., 2016)	Breast	Quantum dots bound to the secondary antibody was used to quantitatively assess the expression of Topoisomerase 2 alpha (TOP2A). Quantum dot immunofluorescence was compared to conventional immunohistochemistry with good agreement with both modalities. TOP2A expression was concluded to be an independent prognostic factor.
Wang et al. (S. Wang et al., 2016)	Colorectal	Large External Antigen (LEA) expression with immunohistochemistry via conventional methods and quantum dot immunohistochemistry. Quantum dot immunohistochemistry demonstrated higher sensitivity (89% compared to 70% of conventional immunohistochemistry).
Hu et al. (Hu et al., 2015)	Head and neck	Multiplexed quantum dots conjugated to E-cadherin, vimentin and EGFR used to quantify immunohistochemistry and compared to single/combination biomarker detection using traditional immunohistochemistry. The combination of these three biomarkers in association with age, gender and grade were used to predict lymph node metastases with an 87.5% sensitivity, 97.4% specificity and 92.9% accuracy which was superior to using single or dual biomarkers using traditional immunohistochemistry.
Gonda et al. (Gonda et al., 2015)	Breast	Protease-activated receptor 1 (PAR1) expression in HER2 negative breast cancer patients was quantified using quantum dot-based immunohistochemistry and the strong correlation with PAR1 expression and relapse-free survival time was demonstrated.
Kwon et al. (Kwon et al., 2015)	Breast	Multiplexed quantum dots utilised for the progesterone receptor, oestrogen receptor and human epidermal growth factor receptor expression were designed and compared to conventional immunohistochemistry demonstrating good correlation with pathologists scoring of the three different biomarkers.
Chen et al. (Chen et al., 2014)	Cervical SCC	Quantum dot immunofluorescence staining of 168 cervical cancer tissue specimens for enhancer of zeste homolog 2(EZH2) and p53 expression, and demonstrated the expression of both antigens was associated with more advanced stages of cervical cancer

Table 2.4*:* Recent studies investigating the role of quantum dots in immunohistochemistry of cancer tissues

2.4.1.5.2 Semiconductor quantum dots in sentinel lymph node mapping

The sentinel lymph nodes are the first few nodes which drain lymph from the primary tumour, and therefore in cancers which are known to spread via lymphatics initially, this status of this node (i.e. involved with the tumour or not) has important prognostic and treatment implications. Breast cancer and malignant melanomas are amongst the cancers for which identification of the sentinel node is useful. In breast cancer, the absence of tumour in the sentinel node avoids the patient from undergoing an axillary node clearance which is associated with life-long morbidity such as lymphedema of the ipsilateral arm, and nerve injuries and randomized controlled studies have demonstrated no benefit in axillary node clearance in patients with negative sentinel nodes (Mamounas, 2016). Currently, patients who undergo surgery for breast cancer have dual imaging of the sentinel node by the injection of a radioactive colloid, and blue dye adjacent to the tumour and the sentinel node is localized intraoperatively with the use of a gamma probe and visualization of the blue tainted lymph node. Identification rates with these two modalities have been demonstrated to be as high as 97.2% with a false-negative rate of 9.8% in the NSABP B-32 trial which is one of the largest randomized controlled studies to date investigating the role of the sentinel nodes in breast cancer (Krag et al., 2007).

The use of quantum dots for sentinel node mapping is an attractive alternative as it offers a non-radiation related modality for this purpose with the use of Near-Infrared emitting quantum dots providing the advantage of deep tissue penetration for the identification of the sentinel node and the size of the quantum dots to achieve optimal sentinel node accumulation. The size of the particles used plays an essential role in its suitability for sentinel node mapping, since particles smaller than 10nm will not stay confined to the sentinel lymph nodes and spread to other groups of lymph nodes, and particles larger than 50nm

demonstrate low lymphatic vessel penetration and slow onset of action (Frangioni et al., 2007; Radenkovic et al., 2016; Zimmer et al., 2006). Currently, research in the role of quantum dots for sentinel node identification has been predominantly in animal models with encouraging results demonstrating superiority over the use of blue dyes for lymph node mapping. Wu et al. (Wu and Chu, 2012) demonstrated the use of self-illuminating 3-mercaptopropionic acid capped CdTe/CdS quantum dots in pigs and demonstrated a 20mm penetration of the emission energy from the quantum dots compared to 10mm from the fluorescence of the quantum dots with external energy and strong background energy. Intradermal injection of these self-illuminating quantum dots demonstrated real-time imaging of the sentinel lymph nodes with no background noise (Wu and Chu, 2012). Other recent studies of the use of quantum dots in sentinel node imaging are outlined in Table 2.5.

Author	Cancer type	Findings
Yaghini et al. (Yaghini et al., 2016)	Breast cancer	Indium based quantum dots (InP core, ZnS shell) were used. Cell viability studies demonstrated no cytotoxicity of these nanoparticles. *Ex Vivo* studies involving the subcutaneous injection of these quantum dots in the rat models demonstrated accumulation in local lymph node accumulation with good photoluminescence.
Si C et al. (Si et al., 2014)	Not a cancer model Invivo	Quantum dots were compared to methylene blue in six mice by injecting them into the plantar metatarsal regions and intraoperatively identifying the lymph nodes (previously stained with Indian ink). Both modalities sstained the sentinel lymph nodes quickly, but the methylene blue was not easily identified in the deep tissues, while quantum dots were localized with near-infrared imaging systems, and the fluorescence lasted for a day after injection.
Li P et al. (Li et al., 2012)	Stomach Not a cancer model	Quantum dots were injected into the lesser curvature of the gastric antrum (subserosal), and subsequent drainage was observed with a near-infrared imaging system. Drainage into perigastric lymph nodes was confirmed with maximal fluorescence at 60 – 120 minutes, and at 2 weeks quantum dots were mainly identified in the liver, spleen and kidneys with no apparent toxicity.
Helle et al. (Helle et al., 2012)	Murine model of breast cancer	Indium based quantum dots used initially in healthy mice and in tumour bearing mice. Sentinel lymph nodes identified in both models within a few minutes of administration with maximum fluorescence in 8 hours.
Erogbogbo et al (Erogbogbo et al., 2011)	Not a cancer model	Silicon-based quantum dots were injected in the subcutaneous space of paws of mice, and sentinel node accumulation demonstrated in the axillary lymph nodes.
Pic et al. (Pic et al., 2010)	Not a cancer model	Near infra-red emitting quantum dots were injected subcutaneously in the paws. Quantum dot accumulation in regional lymph nodes was demonstrated within 5 minutes of the injection and a maximum level at 4 hours.

Table 2.5: Recent studies in quantum dots for mapping sentinel lymph nodes

2.4.1.5.3 Quantum dots in drug delivery and tumour imaging

Quantum dots have been investigated *in vivo* for tumour imaging and as drug delivery agents. The passive targeting of tumours has been demonstrated for quantum dots due to the enhanced permeability and retention effect of the nanoparticle size. Guo and colleagues (Guo et al., 2015) demonstrated the use of self-illuminating quantum dots using radioactive (65)Cu into a CuInS/ZnS nanostructure which was PEGylated and demonstrated high tumour uptake in a U87MG mouse xenograft model. Active targeting of tumours using quantum dots conjugated with ligands has also been reported. Yeh et al (Yeh et al., 2016) used quantum dots conjugated to a synthetic peptide, SP204, and injected mice bearing prostate cancer xenografts (PC3 and DU145), and demonstrated significantly higher tumour accumulated (16 and 5 fold respectively) in the conjugated quantum dots compared to non-conjugated quantum dots demonstrating the benefits of active targeting ligands. Other recent studies are outlined in Table 2.6, including using quantum dots as drug delivery agents.

Authors	Quantum Dot	Target	Drug	Outcomes
Zhao et al. (Zhao et al., 2018)	CdSe/ZnS quantum dots modified with β-cyclodextrin and conjugated with l-Arginine (l-Arg) and neutral l-Tryptophan (l-Trp) and loaded with doxorubicin	HepG2, QSG-7701, and HeLa cells *Invitro* Study	Doxorubicin	The Arginine conjugated quantum dots demonstrated selective delivery to cancer cells and demonstrated the induction of apoptosis in these cell lines.
Kwon et al. (Kwon et al., 2013)	CdTe/CdSe conjugated with antiVEGFR2	Xenograft – murine model bearing PC3 prostate cancer		Conjugated quantum dots demonstrated invivo and invitro binding to the tumour cell line and xenograft model
Nurunnabi et al. (Nurunnabi et al., 2010)	CdTe/Cdse Core/shell encapsulated in 10,12-pentacosadiynoic acid (PCDA) conjugated with Herceptin	Epidermal growth factor -2 (EGRF-2) receptor-expressing human breast cancer (SK BR-3 cell line) vs non-EGRF2 expressing human nasopharyngeal (KB cell line) – *in vitro* study MDA-MB-231 murine xenograft	Herceptin	The increased cytotoxic activity demonstrated for EGRF-2 expressing cell line *in vitro* Significant anti-tumour efficacy of conjugated demonstrated *in vivo* compared to control mice injected with saline, and aggregation in the tumour.
Meng et al. (Meng et al., 2011)	CdTe/ZnS quantum dots conjugated with folic acid	FR positive KB cells – Human nasopharyngeal cancer cell line		Good uptake of the folic acid conjugated QD in the FR positive cells demonstrated compared to FR negative cells (293T cell line – embryonic kidney)
Al-Jamal et al. (Al-Jamal et al., 2009)	QD conjugated with a Liposome vesicle (DSPC:Chol:DSPE-PEG2000)	B16F10 melanoma tumour bearing C57BL6 mice		Rapid accumulation and retention demonstrated in the tumour tissue
Zhang et al. (Zhang et al., 2009)	CD/Te QD conjugated with IGF1R-specific antibody, AVE-1642	Xenograft - mouse embryo fibroblasts expressing human IGF1R or MCF-7 human breast cancer cells		Compared the QD to fluorophore – found to be inferior for detection of downregulation of IGF1
Yang et al. (L. Yang et al., 2009)	ScFvEGFR-QD conjugated with A single-chain anti-EGFR antibody (ScFvEGFR	EGFR in vivo pancreatic cancer cell line		Specific tumour accumulation demonstrated. Demonstrating good potential for use for delivery of therapeutic agents

Authors	Quantum Dot	Target	Drug	Outcomes
Walther et al. (Walther et al., 2008)	CdSe QD conjugated with Human Hormone Calcitonin	HEK93 (embryonic kidney) cell line and HeLa cell line	Cy3 labelled RNA	Successful delivery of Cy3 RNA into cells demonstrated
Weng et al. (Weng et al., 2008)	QD conjugated with immunoliposome	HER2 receptor in SKBR3 and MCF-7 cell lines Xenograft models	Doxorubicin	Efficient antitumour efficacy demonstrated with localizations within the tumour sites demonstrated with fluorescence.
Diagaradjane et al (Diagaradjane et al., 2008)	CdSeTe/ZnS (core/shell)	EGFR in HCT116 xenograft and *in-vitro* colorectal cancer cell lines		Good concentrations in the tumour after 4 hours which return to normal in 24 hours.
Chen et al. (L.-D. Chen et al., 2008)	CdSe/ZnS QDs conjugated with AFP monoclonal antibody	HCCLM6 line *In vitro* and *in vivo* hepatocellular carcinoma cell line		Good specificity of uptake into tumour and metastases demonstrated with minimal toxicity
Derfus et al. (Derfus et al., 2007)	QD conjugated with F3 peptide	EGFP (enhanced green fluorescent protein) transfected HeLa cell line, human cervix cancer	SiRNA	Significant reduction in EGFP signal demonstrating good delivery of siRNA and potential for therapeutic action

Table 2.6*:* Recent studies in drug delivery and tumour imaging for quantum dots

2.4.1.5.4 Semiconductor quantum dots in photodynamic therapy

Photodynamic therapy (PDT) is a treatment used to kill diseased cells with a combination of light, photosensitising drugs and molecular oxygen (Kamila et al., 2016). PDT works by a local generation of reactive oxygen species and reactive nitrogen species to cause cell death. It requires a light source to excite electrons in the photosensitising agent from a single basic state to a single excited state which causes energy conversion that can lead to the electron to reach a triplet excited state which causes the generation of the radicals from the tissue environment and oxygen (Oniszczuk et al., 2016). Photofrin® was the first PDT agent to be approved in clinical use and is currently used to treat and palliate symptoms in oesophageal and non-small cell cancer, and for the treatment of Barret's oesophagus ("Photodynamic Therapy for Cancer," 2016.). Its use has been limited to superficial tissues due to the limitation of tissue penetration of the light source required for the photosensitising agent.

Quantum dots conjugated with the photosensitisers, have been demonstrated to be excellent donors in the fluorescence resonance energy transfer (FRET) process to the photosensitising agent with efficient energy transfer (Hong et al., 2016; Martynenko et al., 2015). Hsu et al. (Hsu et al., 2013) reported the use of self-illuminating quantum dots, which were Renilla luciferase conjugated quantum dots, to generate bioluminescence on treatment with coelenterazine and activate the photosensitiser. The photosensitiser was delivered in a micelle formulation, and effective PDT was demonstrated in A549 cell line (Human adenocarcinoma cell line) and in a murine xenograft model without the need for external excitation thereby potentially alleviating the limitations of the limitation of the tissue penetration by the light source.

2.4.1.5.5 Toxicity of semiconductor quantum dots

Currently, no substantial-conclusion about the toxicity of quantum dots have been made in the literature. This is partly due to the wide variety of quantum dots described in the literature varying from the most frequent used heavy metals such as cadmium to reports of using silicon-based quantum dots. The lack of clarity with regards to the toxicity of quantum dots has limited its application in humans thus far. *In vitro* studies have clearly demonstrated the toxicity of non-coated quantum dot cores containing cadmium ions, resulting in cellular toxicity from the direct action of the heavy metal ions and the formation of reactive oxygen species (Derfus et al., 2007; Kirchner et al., 2005; Yong and Swihart, 2012). Cadmium is a known carcinogen and is associated with diseases affecting the respiratory system (risk of adult respiratory distress syndrome), causing renal damage and bone disease (Godt et al., 2006). Coating the core with a shell (e.g., ZnS) has been demonstrated to reduce the toxicity by minimizing the leaching of free cadmium ions and reduce free radical formation (Chan et al., 2006). There is also some evidence from *in-vitro* studies to suggest that quantum dots can accumulate in the cell's nuclear compartment and potentially cause genetic and epigenetic modifications (Choi et al., 2008; Green and Howman, 2005). *Invivo* studies have reported completely contradictory findings (Fitzpatrick et al., 2009; Hauck et al., 2010; Larson et al., 2003). The reticuloendothelial system appears to take up a majority of circulating quantum dots and therefore identified to be primarily in the liver, spleen and lymph nodes. Hauck et al. administered CdSe quantum dots covered by a ZnS shell and did not identify any long term harmful effects to rats after 80 days with no alteration in behaviour, weight and haematological markers (Hauck et al., 2010; Tsoi et al., 2013). However, the excretion of quantum dots from animal studies have to demonstrate some concerning results with Fischer et al. (Fischer et al., 2006) demonstrating no evidence of quantum dots in the urine or faeces

of rats injected with 25nm and 80nm protein-coated ZnS shell CdSe quantum dots after 10 days. Choi et al. demonstrated at least 50% of quantum dots excreted in the urine of rats when the hydrodynamic diameter of the quantum dots was less than 5.5nm (Choi et al., 2007).

2.4.1.5.6 Future perspectives

The toxicity of semiconductor quantum dots limits its use in drug delivery and sentinel node imaging. The use of semiconductor quantum dots in biomarker labelling in tissue samples and immunohistochemistry is most likely to be its avenue into routine clinical practice.

2.4.2 Gold nanoparticles

Fluorescent gold nanoparticles have been identified to demonstrate strong photoluminescence, photostability and good biocompatibility at nanometer dimensions (Xu and Shang, 2018). These nanoparticles have been demonstrated to exhibit stronger emission intensity and photostability compared to fluorescent dyes, and do not have the inherent cytotoxicity of semiconductor quantum dots (Qu et al., 2008; Xu and Shang, 2018).

2.4.2.1 Gold nanoparticle characteristics

2.4.2.1.1 Surface plasmon resonance phenomenon

The unique size of nanoparticles offers the advantage of the surface plasmon resonance phenomenon (SPR). This is the coherent oscillation of metal-free electrons, in resonance with the electromagnetic field, enhancing the ability of the nanoparticle to absorb, scatter and fluoresce light (Huang et al., 2007). The optical resonances can be continuously tuned by varying the dimensions of the nanoparticle, thereby generating and absorbing wavelengths of the NIR which has maximal tissue penetration and minimal absorption by tissues. This has opened the avenue for the use of gold nanoparticles in photothermal therapy. This describes

the phenomenon where energy irradiated onto material from an external source is converted to kinetic energy resulting in local heat production.

2.4.2.1.2 Luminescence

In addition to the surface plasmon resonance effect, photoluminescence from metal nanoparticles such as gold and silver nanoparticles have a different underlying mechanism to the semiconductor nanoparticles since discrete valence and conduction bands with a bandgap are not as evident in conductors. In metals, as particles approach nanometer sizes and the particle approaches its Fermi wavelength, the quantum size effect is predicted to cause discretisation of the energy levels of the conduction electron (Pattabi and Pattabi, 2014). The transition of electrons between the bands has been proposed to be the mechanism through which fluorescence arises (J. Zheng et al., 2012).

Gold nanoparticles have been demonstrated to contribute to photon capture sections four-five fold higher than conventional dyes, and have been demonstrated to be more resistance to photobleaching and biological denaturation (Loo et al., 2005; Singh et al., 2018; X. Yang et al., 2009). Smaller gold nanoparticles are preferred for photothermal therapy due to the increased efficiency of conversion from light to heat, and larger gold nanoparticles are preferred for photoimaging due to higher scattering efficiency (Singh et al., 2018).

An increasing number of nanoparticles based on the phenomenon is being developed, and a majority of them have gold deposited on the nanoparticle surface (X. Yang et al., 2009). Gold surfaces have good biocompatibility with low cytotoxicity to human cells demonstrated *in vitro*, with ease of preparation and modification of its surface with ligands (Connor et al., 2005; Huang et al., 2007).

2.4.2.2 Gold nanoparticle synthesis

Similar to the semiconductor quantum dots, multiple synthesis strategies have been described in the literature. This includes chemical synthesis, biological synthesis measures using plants and micro-organisms, and physical means of using microwave, ultraviolet irradiation and laser ablation (Singh et al., 2018). Two main strategies are utilized for the synthesis of noble metal quantum dots. These are broadly referred to as the bottom-up and the top-down routes. In the bottom-up approach, the metal ions are reduced to metal atoms, and the nanoclusters are formed with the nucleation of the gold atoms. In the top-down approach, large metal nanoparticles are gradually etched to produce the smaller fluorescent nanoparticles (Zheng et al., 2017). Biofunctionalisation of these nanoparticles is then required for biomedical applications. Techniques to achieve this include the use of ligand exchange, bioconjugation and noncovalent interactions (Song et al., 2016; Zheng et al., 2017).

2.4.2.2.1 Bottom-up synthesis

Chemical reduction of gold precursors in the presence of reducing agents is one of the most versatile and straightforward methods for the synthesis of gold nanoparticles (Yu et al., 2017). This includes techniques such as one-pot synthesis where direct mixing results in the continuous reduction of oxidized metal salts by organic ligands, a reducing agent and stabilizing agents (Yu et al., 2017). For the preparation of gold quantum dots, chloroauric acid and chlorotriphenylphosphine gold salt are the usual precursors, with reducing agents such as sodium borohydride, citrate, hydrazine hydrate and ascorbic acid (Hembury et al., 2015; Retnakumari et al., 2010; Zheng et al., 2017). Stabilising agents commonly involve the use of thiol-containing compounds such as glutathione, mercaptopropionic acid, phenylethylthioate, captopril and tiopronin (Zheng et al., 2017). The use of micro-organisms for this purpose has been described with adsorbtion and accumulation of gold nanoparticles

produced by the secretion of enzymes involved in the reduction of gold ions (Singh et al., 2018, 2016, 2015) .

2.4.2.2.2 Top-down synthesis

The ligand exchange approach is the commonest means of achieving fluorescent metal quantum dots from large metal nanoparticles. Methods described include the use of polyethyleneimine to etch colloidal gold nanocrystals and the use of glutathione as a ligand etchant from MSA-protected silver nanoparticles and gold nanoparticles (Duan and Nie, 2007; Guével et al., 2012; Yuan et al., 2011).

2.4.2.3 Gold nanoparticles in drug delivery

There is a growing number of publications demonstrating the use of gold and silver nanoclusters in tumour imaging and drug delivery *in vivo* with low toxicity. Functionalisation and modification of gold nanoparticles are less complicated due to the presence of a negative charge on the surface (Singh et al., 2018). Like most nanoparticles, these metal nanoclusters accumulate in tumours consistent with the enhanced permeability and retention effect. Liu et al. (Liu et al., 2013) demonstrated glutathione conjugated gold nanoparticles preferentially passively accumulated in MCF-7 tumour bearing mice, emitting in the NIR spectrum and undergoing renal excretion with low uptake by the reticuloendothelial system. Similar findings were demonstrated by Wu et al. (Wu et al., 2010) using MDA-MB-45 and Hela xenograft mice models and gold nanoclusters measuring 2.7nm, which passively accumulated in the tumour sites. Gao et al. (Gao et al., 2014) demonstrated the retention of silver nanoclusters stabilised with glutathione in cervical cancer xenograft mice models for several days with no impact of the normal tissues and other viscera. Literature reports of active targeting metal quantum dots include folic acid conjugated gold nanoclusters stabilised by

bovine serum albumin (BSA) which were identified to be internalised by the oral carcinoma KB cell line though folic acid-mediated endocytosis (Habeeb Muhammed et al., 2010). Chen et al. (Chen et al., 2012) described the use of folate conjugated gold nanoclusters stabilised with BSA as drug delivery agents in MCF-7 xenograft mice models. They demonstrated low toxicity of this probe, along with the preferential accumulation of the probe which was conjugated to doxorubicin in the tumour tissue particularly in models with high LAT1 and LAT2 expression (folate). Other similar studies are outlined in Table 2.7.

2.4.2.4 Gold nanoparticles in photothermal therapy and photoimaging

The gold nanoparticles used in photothermal therapy have been mainly the gold nanorods and gold nanoshells. There have been a growing number of studies demonstrating successful functionalisation of these nanoparticles to improve uptake in target tissues (Table 2.8). In addition, metal nanoclusters have been used as photosensitizers which accumulate in tumours and be able to generate reactive oxygen species such as singlet oxygen when irradiated under light source causing tumour cell death (Zheng et al., 2017). Cui et al. (Cui et al., 2017) described the synthesis of glutathione stabilized gold nanoclusters conjugated to indigo cyanine green and injected these probes to a 4T1 xenograft mice model (breast cancer). These probes were irradiated with near infrared (NIR) light causing the release of reactive oxygen species and tumour cell death (Cui et al., 2017). The use of radiosensitizers helps reduce the dose of radiotherapy performed at specific sites, thereby limiting collateral damage of adjacent normal tissues. Zhang et al. (X.-D. Zhang et al., 2015) described the use of glutathione capped gold nanoclusters *invivo* in mice bearing U14 cervical cancer tumours and demonstrated a significant decrease in tumour volume on irradiation compared to radiotherapy without injection of the gold nanoclusters. The gold nanoclusters accumulated predominantly in the tumour and the kidneys were demonstrating evasion of the

reticuloendothelial system. No significant derangement of the renal and liver biochemistry was identified.

2.4.2.5 Gold nanoparticles in clinical trials

Gold nanoparticles have, over the last decade, slowly made the transition from preclinical research into early phase clinical trials. Recent studies are outlined in Table 2.9 and include gold particles as part of composite nanoparticles with silica. The Aurolase® nanoparticle, which is a silica-gold nanoshell coated with PEG is under clinical trials with lung, head and neck and prostate cancers (Singh et al., 2018). These nanoparticles are being used for their photothermal effects to locally ablate a tumour after intravenous injection leading to accumulation in the tumour and external stimulation with a NIR source.

Libutti et al. (Libutti et al., 2010) reported the use of gold nanoparticles as drug delivery agents for Tumour Necrosis α in phase I clinical trials and demonstrated the use of the nanoparticle drug delivery system enabled three times the standard upper limit of dosage tolerated with minimal adverse effects. The use of gold nanoparticles in nanosensor arrays involving breath analysis is being investigated in clinical trials in gastric, head and neck and lung cancers (Singh et al., 2018). Gold nanoparticles are also being investigated for the treatment of atherosclerosis with local ablation of the atheroma on external excitation.

2.4.2.5.1 Toxicity of gold nanoparticles

The literature is currently unclear with regards to the toxicity of gold nanoparticles. Contradictory findings include the debate over the surface charge of the gold nanoparticles influencing its level of toxicity (positively charged particles suggested to be more toxic) (Singh et al., 2018). Ali et al. (Ali et al., 2017) investigated the long term toxicity of gold nanorods on

mice. They demonstrated at 15months following a single injection of intravenous gold nanorods coated with PEG, only a small amount of the gold nanorod had been excreted, and the majority had accumulated in the liver and spleen. However, no clinical or histopathological abnormalities of the kidney , spleen and liver were identified at this time point. Bahamonde et al. (Bahamonde et al., 2018) reported that gold nanoparticle treated mice and rats responded differently with multiple rats dying post administration and no fatalities affecting mice .

The early phase human clinical trials (Table 2.9) has not demonstrated any significant adverse effects of the intravenous injection of gold nanoparticles. This remains an area to be closely monitored the long term effects particularly given the findings of Ali et al. (Ali et al., 2017) who demonstrated that only a small proportion of the nanoparticles are excreted.

Authors	Target	Drug	Outcomes
Ramalingam et a (Ramalingam et al., 2018)	Gold nanoparticles functionalized with polyvinylpyrrolidone and doxorubicin in human lung cancer cell line	Doxorubicin	The conjugated gold nanoparticle demonstrated enhanced inhibition of cell growth compared to free doxorubicin and unconjugated gold nanoparticles. Intracellular delivery of the doxorubicin was demonstrated and increased reactive oxygen species generation identified with the conjugated nanoparticle leading to early and late apoptosis.
Farooq et al. (Farooq et al., 2018)	Gold nanoparticles functionalized with PEG and conjugated to two chemotherapy agents in HeLa cell line	Doxorubicin Bleomycin	Intracellular localization of the gold nanoparticles demonstrated with a significant decrease in the half-maximal drug concentration demonstrated to achieve cytotoxicity.
Chen et al. (Chen et al., 2016)	Active targeting with 2 ligands – cyclic RGD and aptamer AS1411 *Invitro*: U87MG (malignant glioma), MCF-7, LO2 (Hepatic cancer), A549 (alveolar adenocarcinoma) *Invivo*: U87MG mice xenograft model	Doxorubicin	Accumulation of the gold nanocluster conjugated to the 2 active targeting ligands in the tumour tissue was demonstrated with significantly increased efficacy of the doxorubicin-loaded nanoparticle with one or both ligands compared to free doxorubicin and saline. Reduced toxicity was demonstrated on histological examination of the lung, liver, heart, spleen and kidneys.
Chattoraj et al. (Chattoraj et al., 2016)	*Invitro* study using breast cancer MCF7 cells and normal breast cells MCF10A. and lung cancer A549 cell line and WI38 lung fibroblasts	Doxorubicin	Lysozyme capped gold nanoclusters were conjugated to doxorubicin and delivered to MCF7 cells and A549 cells. Selective increase in MCF7 cell death was demonstrated with improved survival of the MCF10A cell line. This was not reproduced in the lung cancer cell lines.
Nair et al. (Nair et al., 2015)	Active targeting with folic acid ligand C6 glial tumour *Invivo*	Protoporphyrin IX (photosensitizer)	Lipoic acid capped gold nanocluster conjugated to folic acid for active targeting and Protoporphyrin IX. Irradiation with a laser at 532nm demonstrated increased tumour death compared to protoporphyrin alone *invivo.*

Table 2.7: Recent studies on gold nanoclusters in cancer imaging and therapy

Authors	Target	Outcomes
Wang et al. (J.-Y. Wang et al., 2016)	Passive targeting U14 cervical cancer *Invivo*	Glutathione capped gold nanoclusters were injected into mice bearing U14 cervical cancer tumour models. The study investigated the effect of the surface charge of the gold nanocluster on tumour accumulation and cell death. The negatively charged gold nanocluster demonstrated significantly higher tumour accumulation and anti-tumour efficacy on irradiation.
Zhang et al. (X.-D. Zhang et al., 2014)	Passive targeting U14 cervical cancer *Invivo*	Glutathione capped gold nanoclusters were used and injected intraperitoneally. There was a significant reduction in tumour volume on irradiation of mice with the injected gold nanoclusters compared to mice without injected nanoclusters. No long-term damage to the liver, spleen and kidney were identified for the mice injected with the nanocluster.
Dickerson et al. (Dickerson et al., 2008)	Pegylated gold nanorods in murine models of squamous cell carcinoma	Significant tumour reduction demonstrated in intravenous and direct injection of the gold nanorods into the tumour following excitation with a small portable near infra-red laser.
Vankayala et al. (Vankayala et al., 2014)	Gold nanoshells *in vitro* and *in vivo* studies using B16F0 melanoma murine model investigating photothermal and photodynamic therapy potential	Photothermal and photodynamic effects can be switched based on the excitation wavelength. This was confirmed *in vivo* with adjustments of the excitation wavelength used to generate both photothermal and photodynamic effects identified to be the most efficacious in destroying the solid tumour.
Ali et al. (Ali et al., 2017)	Gold nanorods functionalized with Bovine Serum Albumin and rifampicin. *In vitro* (5 head and neck squamous cell carcinoma cell lines) and *in vivo* studies on murine models of the oropharyngeal squamous cell carcinoma line MDA686TU	The photothermal effects were elicited by irradiation with an external laser. Significantly reduced cell viability was demonstrated with the induction of autophagy. Significantly reduced tumour growth was demonstrated in the gold nanoparticle treated mice compared to controls. This gold nanoparticle was comparted to similar gold nanoparticles functionalized by PEG instead, and the rifampicin-BSA conjugated gold nanoparticles demonstrated a similar reduction in tumour growth at lower doses. Long term toxicity was assessed by monitoring mice to up to 15 months injected with the PEG functionalized gold nanorods. No clinical and histopathological signs of toxicity were identified at 15 months in the kidney, spleen and liver. Only a small proportion of the gold nanoparticle was excreted with the majority accumulated in the liver and spleen.

Table 2.8**:** Gold nanoparticles in photothermal therapy and photoimaging

Gold nanoparticle	Phase of trial	Clinical use
CYT-6091 PEGylated gold nanoparticle conjugated to TNFα	Phase 1 trials(Libutti et al., 2010) Patients with advanced solid tumour malignancies considered non-responsive to conventional treatments	Drug delivery agent with TNFα. Intravenously injected, greater than 3x the standard upper limit of the dosage of TNFα was tolerated with the conjugated gold nanoparticle with confirmed delivery in tumour tissue.
NCT01270139 Silica-gold nanoparticle targeting atheromatous lesions	Phase 1/2 trial (Kharlamov et al., 2015) Silica-gold nanoparticles investigated regarding effectiveness in reducing atheroma in cardiovascular disease	Two systems were investigated. Direct delivery of the nanoparticle through a mini surgery involving an onlay arterial patch (subsequently excited by an intravascular NIR laser) and delivery of the nanoparticle with iron by using a magnetic navigation system (ex-vivo stimulation with NIR laser). This was compared to conventional stents in targeting atheromatous lesions in the coronary vessels. Significant regression of the atheroma was demonstrated in the first group compared to the other groups at 12 months. No complications were identified.
Gold nanoparticles and single-walled carbon nanotubes NA-NOSE	Clinical trial(Broza et al., 2017) assessing the efficacy of these nanoparticle-based sensors on detecting volatile organic compounds in breath for diagnosis and assessment of disease in Multiple Sclerosis (MS)	The nanoparticle sensors demonstrated 90% accuracy in differentiating between MS and healthy patients. Blinded sets showed 95% positive predictive value (PPV) between MS remission and control, 100% sensitivity with 100% negative predictive value (NPV) between MS not-treated (NT) and control, and 86% NPV between relapse and control.
Gold nanoparticles and single-walled carbon nanotubes NA-NOSE	Clinical trial (Hakim et al., 2011) assessing the efficacy of these gold nanoparticle-based sensors in the differentiation of volatile organic compounds in breath comparing head and neck cancer, lung cancer and healthy controls	Patient numbers – 16 head and neck cancers, 20 lung cancers and 26 healthy controls. The NA-NOSE test demonstrated significantly different results between the head and neck cancers, lung cancers and healthy control patients. This provides a potential non-invasive screening tool.
Gold nanoparticles utilized for analysis of blood	Clinical trial (Xue et al., 2018) assessing the efficacy of gold nanoparticle-based Raman spectroscopy assessment of serum samples from patients with oral squamous cell carcinoma	The accuracy of this model to detect and classify the different stages of oral squamous cell carcinoma was >85% for each category (of T and N stage)
Auroshell® Gold-silica nanoshells	Phase I clinical trial in prostate cancer (Stern et al., 2016)	Twenty-two patients with prostate cancer underwent intravenous infusion of the nanoparticle followed by radical prostatectomy. One patient complained of itching and one patient complaining of abdominal discomfort. No other adverse reactions identified. Well tolerated infusion. Progression to further clinical trials planned (and ongoing)

Table 2.9*:* Gold nanoparticles in clinical trials

2.5 Nanoparticles used as adjuncts to colonoscopy

Few nanoparticles have been investigated for roles in improving colonoscopic detection of colorectal tumours and polyps. Recent studies are summarized in Table 2.10. These nanoparticles have been investigated with intravenous and topical application to the colonic mucosa and in some cases supplemented with fluorescent colonoscopy. Nanobeacon, polystyrene nanoparticles with coumarin 6 dyes encapsulated within the core with a surface of poly(N-vinylaceramide) (PNVA), has been investigated for this purpose. This was predominantly conjugated to peanut agglutin (PNA) targeting Thomsen-Friedenreich (TF) antigen which is expressed in colorectal cancer and not in the normal colon mucosa. Studies have demonstrated no adverse reactions or toxicity with its administration and no evidence of colonic absorption when applied topically to the colonic mucosa (Sakuma et al., 2015). Recent studies regarding the application of nanobeacon are summarized in Table 2.10. Other nanoparticles reported in the literature for this purpose include carbon nanoparticles and charcoal nanoparticles (Table 2.10).

Authors	Nanoparticle used	Findings of the study
Wang et al. (2013)(Wang et al., 2013) Clinical trial	Charcoal nanoparticles injected during colonoscopy submucosally near the tumour prior to laparoscopic resection	Twenty-six patients enrolled in the study. No safety concerns/adverse effects noted. The injected area was easily identified during laparoscopy, and there were no cases of the wrong segment of bowel being removed or remnant tumour at the resection margins.
Lin C et al. (2017) (Lin et al., 2017) Clinical trial	Carbon nanoparticles injected during colonoscopy submucosally near the tumour prior to laparoscopic surgery	Thirty-five patients were enrolled in the study. No adverse reactions were identified. The area of interest was easily identified laparoscopically.
Chen et al. (Chen et al., 2017) *In vitro* and *in vivo* study	Mesoporous silica nanoparticles fluorescently labelled (FITC) using α-L-fucose targeting lectin Ulex Europaeus Agglutinin-1	Significant binding specific of these nanoparticles was demonstrated *in vitro, ex vivo and in vivo* with colonoscopy. The colons were irrigated with a solution containing the nanoparticles, and probe-based laser confocal fluorescence endomicroscopy was performed demonstrating significant binding specific to colorectal polyps.
Zhang et al. (2015) (X. Zhang et al., 2015) Clinical trial	Carbon nanoparticles injected adjacent to the tumour during colonoscopy prior to laparoscopic surgery	Twenty-six patients with colorectal cancer were injected with carbon nanoparticles preoperatively and compared to 27 patients without this. Increase lymph node yield was demonstrated with no statistical difference in lymph node metastatic rates.
Wang et al. (2015) (R. Wang et al., 2016)	Carbon nanoparticles injected adjacent to pre-cancerous or early cancerous lesions	Twenty four patients were divided into 2 groups – 1 injected with carbon nanoparticles and 1 without. No adverse reactions were identified, and after a year, the area of marking was present.
Kolitz-Domb et al. (2014) (Kolitz-Domb et al., 2014)	Near infra-red fluorescent nanoparticles (protein and polymer-based) PLLA conjugated to the antibody to CEA and Indigo Carmine Green	Intravenous injection of this nanoparticle in a mice model was performed, which demonstrated no toxicity and excretion of the nanoparticle within 24 hours. Selective accumulation of the nanoparticle in colorectal cancer was demonstrated in mouse and chicken embryo models.
Kogan-Zviagin et al. (2014) (Kogan-Zviagin et al., 2014)	Near infra-red nanoparticles (polymer-based with near-infrared dyes) N-(2-hydroxypropyl)methacrylamide (HPMA) with fluorescein-isothiocyanate (FITC) or NIR dye IR-783	Intracolonic administrated nanoparticles demonstrated colonic tumour specific binding relative to normal mucosa and improving colonoscopic identification of these lesions.
Nakase et al. (2017) (Nakase et al., 2017)	Nanobeacon comprised of polystyrene nanoparticles with coumarin 6 dyes encapsulated with a surface of poly(N-vinylaceramide) (PNVA).	This was conjugated to peanut agglutin (PNA) targeting Thomsen-Friedenreich (TF) antigen.. This nanobeacon was applied to human colorectal cancer, polyp and normal tissues. This demonstrated the specificity of to colorectal cancer and adenomatous polyps.
Sakuma et al. (2015) (Sakuma et al., 2015)	Nanobeacon targeting TF antigen using fluorescence colonoscopy for early colorectal cancer detection	Nanobeacon was sprayed topically onto the colonic mucosa, and fluorescence colonoscopy was performed. This was not absorbed by colonic mucosa. Fluorescence colonoscopy was able to identify early colorectal tumours, distinguish tumour grade and monitor tumour response to chemotherapy.

Table 2.10: Recent studies investigating nanoparticles used as adjuncts to colonoscopy

3 Chapter 3 – General methods and materials

3.1 Materials

Material	Source
1-Ethyl-3-(3-dimethylaminopropyl)carbodiimide (EDC)	Sigma-Aldrich
2x SDS-PAGE loading buffer	ThermoFisher scientific
1x SDS-PAGE running buffer	ThermoFisher scientific
Cadmium chloride ($CdCl_2$) 99.99%	Sigma-Aldrich
CellTiter-Blue®	Promega
Dimethyl sulfoxide (DMSO)	Sigma-Aldrich
Dimethylformamide (DMF)	Sigma-Aldrich
Dulbecco's modified eagle medium (DMEM)	Sigma-Aldrich
Foetal Bovine Serum (FBS)	ThermoFisher scientific
Goat anti-Rabbit IgG secondary antibody, biotin conjugate	ThermoFisher scientific
Gold (III) chloride trihydrate ($HAuCl_4.\ 3H_2O$)	Sigma-Aldrich
Mercaptosuccinic acid MSA (98%)	Sigma-Aldrich
MGF antibody for immunohistochemistry	Phoenix Pharmaceuticals INC
NuPAGE gel	ThermoFisher scientific
PBS/Tween 20	Sigma-Aldrich
Pierce™ BCA protein assay kit	ThermoFisher scientific
Phosphate buffered saline	Sigma-Aldrich
Prostate adenocarcinoma – tissue sections	Invitrogen
PVDF pre-cut blotting membranes, 0.2µM pore size (Check with Dr Yang)	ThermoFisher scientific
Penicillin-Streptomycin 10,000 units penicillin and 10mg Streptomycin/ml	ThermoFisher scientific
RIPA lysis and extraction buffer	ThermoFisher scientific
ROCHE inhibitor	Sigma-Aldrich
Trypsin-EDTA	ThermoFisher scientific
VECTASTAIN ABC Kit	Vector Laboratories Ltd

3.2 Analytical techniques and instruments

3.2.1 Atomic force microscopy

Atomic force microscopy (AFM) offers high sensitivity to the nanometer scale and allows for monitoring of the dynamics of bioconjugates at a molecular level (Jin et al., 2010; Tessmer et al., 2013; Wolcott et al., 2006). AFM offers a near-field approach where the sample is directly probed with the AFM tip and achieves very high-resolution images at a molecular level which is comparable to electron microscopy and superior to conventional optical approaches (Tessmer et al., 2013). The tapping mode was used as described in other studies for characterisation of the quantum dots (B. Chen et al., 2008; Jin et al., 2010; Wolcott et al., 2006; Zeng et al., 2009).

3.2.2 V-Vis-NIR spectroscopy

The emission wavelength of synthesised quantum dots and the conjugates were measured using the USB 2000+ Ocean Optics spectroscopy. This portable system offers rapid evaluation which covers broad wavelengths from 350nm to 1000nm and has been described in the literature for this purpose for fluorescent nanoparticles (Ghaderi et al., 2012; Jiang et al., 2016; Ramesh et al., 2016).

3.2.3 Confocal fluorescence microscopy

Confocal fluorescence microscopy overcomes the limitations of traditional wide-field fluorescence microscopes by utilising point illumination and a pinhole in an optically conjugate plane in front of the detector, thereby eliminating the out-of-focus signal. I used the Nikon Eclipse TE300 to assess the fluorescence from the cell studies involving the CdTe quantum dots. For the gold quantum dots, images were acquired by the Olympus BX 63. which can operate in fluorescence, reflection and phase contrast modes, and it was provided

with high transmission objectives with reduced autofluorescence. Fluorescent image acquisition was conducted via LED light source excitation at 620 nm with emission long-pass filter at 700 nm with image processing with Olympus cellSens software. All the near-infrared images acquired are displayed in the pseudocolour (red) format.

3.2.4 Transmission electron microscopy (TEM)

The Phillips CM 201 microscope was used in the experiments to confirm autophagy and characterize the size of the gold quantum dots. TEM offers significantly higher resolutions compared to light microscopes but are limited by the high costs and complex sample preparation.

3.2.5 Fluorescence spectrometry

The JASCO FP-8000 fluorescence spectrometer was used to measure the fluorescence intensity of the quantum dots. This instrument uses separate monochromators for excitation and emission lights and was used to measure the fluorescence intensity at an excitation wavelength of 355nm.

3.3 Methods

3.3.1 Cell culture types

The following cell lines were cultured and were purchased from the European Collection of Cell Cultures (ECACC). All experiments were at 3-12 passages after receipt from the supplier.

- HT29 cell line which is derived from a human primary colonic adenocarcinoma tumour from a 44-year-old female patient ("HT-29 ATCC ® HTB-38™" 2019)

- SW620 cell line derived from a human metastatic colorectal lymph node of a Dukes C adenocarcinoma in a 51-year-old male patient ("SW620 [SW-620] ATCC ® CCL-227™ " 2019)
- HUVEC cell line is an umbilical vein derived endothelial cell line ("HUV-EC-C [HUVEC] ATCC ® CRL-1730™" 2019)
- The PC3 cell line is a prostate cancer cell line ("PC-3 ATCC ® CRL-1435™," 2019)

I used both HT29 and SW620 since these cell lines have been extensively used to investigate the biologics of colorectal cancer. HT29 provides information from primary colon tumour, and SW620 provides information for the metastatic tumour in pericolic lymph nodes. I used the HUVEC cell line as a negative control since it has not been demonstrated to express IGF-1 and I used the PC-3 cell line as a positive control for my MGF experiments since this cell line has been previously demonstrated to express MGF (Armakolas et al., 2010a).

3.3.2 Thawing from frozen

The cell lines were stored in a cell storage bank in liquid nitrogen. The vial containing the cell line was removed from the liquid nitrogen bank and warmed to room temperature rapidly. The ampoule of cells was wiped with 70% ethanol, and placed in the laminar flow hood, and was pipetted into a 20ml centrifuge tube. 10mls of the culture medium (DMEM+10%FBS+1%antibioitic) were slowly introduced to the centrifuge tube, with gentle rocking movements to ensure adequate mixing. The cells with the culture medium were then pipetted into a culture flask, and left overnight in an incubator at 37^{o}C with 5% CO_2. The medium was changed the next day to fully remove any DMSO traces.

3.3.3 Subculturing cells

The cell culture medium was aseptically removed from the flask, and the flask rinsed with 3 washes of 5mls PBS solution. 3mls of Trypsin were then added to the flask, and this was placed in the incubator at 37°C with 5% CO_2 for 5 minutes. After confirming detachment of the cells under light microscopy, 10mls of the cell culture medium was added to deactivate the trypsin, and the cells and medium aspirated and pipetted into a centrifuge tube. The tube was centrifuged at 400g for 5 minutes, and the supernatant discarded. 5mls of cell culture medium was added to the pellet and mixed. 1 ml of this cell suspension was pipetted for total cell count and viability. Depending on the cell count, adequate volumes of the cell suspension and culture medium were added to a new culture flask at an estimated cell density of 1 x 10^6 cells in 15mls of culture medium.

Cell lines were used for the experiments after a minimum of 2 subcultivations (passage) procedures from frozen.

3.3.4 Immunohistochemistry

The protocol was derived from the Department of Experimental Physiology at the University of Athens and outlined here. Formaldehyde-fixed (4%) tissue samples were paraffin wax embedded and processed for paraffin sections. Microtome sections of 3µm were prepared from the paraffin-fixed samples, allowed to adhere to glass slides, dried at 37° C overnight, dewaxed in xylene and rehydrated in serial dilutions of ethanol. Endogenous peroxidase activity was quenched with 1% hydrogen peroxide in distilled water for 15 minutes. After two serial washings in distilled water and PBS buffer, the sections were then incubated with the polyclonal anti-MGF antiserum at a dilution of 1: 1,000 in PBS overnight at 4° C. After repeated PBS buffer washing, secondary biotinylated goat anti-rabbit IgG was added for 25 minutes at

room temperature, followed again by repeated PBS buffer washes. Visualization of the immunocomplex was obtained by incubating the sections in a solution of 3,3-diaminobenzidine in PBS for 10 minutes. Sections were counterstained in haematoxylin for 5 minutes, washed in distilled water, dehydrated in serial dilutions of ethanol and xylene and finally mounted in dibutyl phthalate xylene. Tissue sections were visualized under light microscopy. Positive controls for the specificity of the reactions obtained by analysing prostate adenocarcinoma FFPE (Formaldehyde-fixed paraffin-embedded) tissue obtained from Invitrogen UK, and negative control by substituting the primary anti-MGF antiserum with the antibody diluent (PBS) minus the primary anti-MGF antiserum.

3.3.5 Colorectal cancer tissues

Ethics approval was obtained from the National Research Ethics Service committee in West London (reference 11/LO/1521) for the use of colorectal cancer tissues from tumours resected from patients who had undergone surgery at the Royal Free Hampstead Hospital. Tissue blocks were identified retrospectively, and slides cut and confirmed by a consultant Histopathologist. The hospital database was utilised to obtain tissues based on the TNM staging and polyps excised.

Basic demographics of the patients such as age and gender were collected from the hospital database and follow up where available was reviewed by looking at clinic letters and investigations from the hospital database with an emphasis on evidence of recurrent cancer.

3.3.6 Control tissues

Formalin fixed paraffin embedded tissue slides of prostate cancer and normal colon tissues were obtained from AMS Biotechnology Europe Ltd.

4 Chapter 4: MGF expression in colorectal cancer

Manuscript being submitted to Growth hormone and IGF research:

Increased expression of IGF-1Ec with increasing colonic polyp dysplasia and colorectal cancer
S Alagaratnam, S Yang, B Ramesh, TV Luong, M Loizidou, B Fuller

4.1 Introduction

The Mechanogrowth factor is an isoform of the insulin-like growth factor-1 (IGF-1) which is generated from the splicing of exons 4,5 and 6 of the IGF-1 gene (Matheny et al., 2010). It was initially demonstrated to be upregulated in skeletal muscle after exercise and injury, and subsequently been identified to have other physiological roles in neuroprotection in the setting of brain ischaemia, promoting cartilage regeneration at sites of damaged cartilage and protection of cardiac tissues in ischaemia (Dluzniewska et al., 2005; Z. Luo et al., 2015; Stavropoulou et al., 2009; Zanou and Gailly, 2013). Its role in cancer pathogenesis has been recently investigated and initially confirmed in prostate cancer by work performed by the Department of Experimental Physiology at the University of Athens confirming prostatic adenocarcinoma tissues to demonstrate higher expression of MGF compared to normal prostate tissues and intraepithelial neoplasia (Savvani et al., 2013). Research into MGF expression has centred around the expression of the isoforms of IGF-1 mRNA and the peptide in different cancers with conflicting results. Upregulation of MGF expression has been demonstrated in prostate adenocarcinoma, osteosarcoma cell lines (Shang et al., 2015) and in gut neuroendocrine tumours (Alexandraki et al., 2017), however the expression of the MGF mRNA was lower in hepatocellular carcinoma compared to surrounding normal liver tissue (Zinevich et al., 2013). Durznyska et al. (Durzyńska and Barton, 2014b) used real-time PCR to assess the mRNA expression of IGF1 splice variants and immunoblotting of cell lysates to assess the protein expression of IGF1Ea, IGF1Eb and MGF in cervical adenocarcinoma, osteosarcoma, hepatocellular carcinoma, myelogenous leukaemia cell lines and demonstrated a discordance between the mRNA expression and peptides in the different cell lines reflecting the impact of post translational modification of the mRNA. Kasprzak et al(Kasprzak et al., 2015, 2012) published their work in colorectal cancer tissues by performing

real-time PCR for MGF mRNA and demonstrated significantly lower expression of MGF mRNA in colorectal cancer tissues compared to normal colonic tissue. Their work did not extend to investigating the expression of the IGF-1 peptides and did not investigate MGF peptide expression in colorectal polyps which are known precursors for colorectal cancers.

This chapter describes the use of immunohistochemistry to identify the expression of MGF in normal colon tissues, colonic polyps and colorectal adenocarcinoma. The prognostic significance of MGF expression is then investigated with the use of quantitative immunohistochemistry and follow up data for 16 patients with an emphasis on recurrence. The expression of MGF peptide in these tissues was also compared to MGF expression in colonic polyps (11), staging from a TNM perspective, including lymph node involvement. The results are described below.

4.2 Aims

- Compare expression of MGF peptide, using quantitative immunohistochemistry, between normal colon, colon polyp and colon cancer tissues
- Assess the potential for MGF peptide expression to be a prognostic factor in colon cancer

4.3 Supplementary materials and methods

4.3.1 Immunohistochemistry quantification

The slides were captured with a Leica SCN400F and scanned at 20x magnification. Semi-quantitative image analysis was performed with the open-source software ImageJ, and the IHC profiler plug-in developed by Varghese et al. (Varghese et al., 2014). This software performs quantitative antibody staining intensity measurements for DAB/haematoxylin

stained tissues with pixel-by-pixel analysis and assigns a score to a four-tier system. The score included high positive (pixel intensity 0-60), positive (pixel intensity 61-120), low positive (pixel intensity 121-180), negative (pixel intensity 181-235), while pixels from 236-255 were excluded due to it representing fatty tissues which were not relevant to the score. The final score was calculated by the simple algebraic formula:

Score = ((number of pixels in a zone) x (each score of the zone))/total number of pixels in the image

The score of the zone was 4 for high positive, 3 for positive, 2 for low positive and 1 for negative. Varghese et al. (Varghese et al., 2014) validated this software by analysing 1703 DAB stained IHC images and demonstrated an 88.6% concordance in a comparison study with manual pathological scoring. Few recent studies utilising Image J and the IHC profiler are outlined in Table 4.1.

Images were magnified to x40 and analysed using the IHC profiler plug-in. 3 slides for each tumour section was utilised, and 4 random areas captured for analysis. The software produces results as an overall outcome of 'High positive/positive/low positive/negative' and simultaneously provides the pixel count for each intensity. The pixel counts for each intensity was utilised and the score calculated using Microsoft Excel using the simple algebraic equation outlined above. Statistical analysis was performed using IBM® SPSS® v22. Comparisons between 2 groups were performed with the Mann-Whitney test and between multiple groups (more than 2) with the Kruskal-Wallis test. A $p<0.05$ was regarded as statistical significance and denoted with * while $p<0.01$ was regarded as highly significant and denoted with ** on the graphs, and the medians of the samples collected were plotted with 95% confidence interval bars.

Author and year	Study
Alrashdan et al. 2016 (Alrashdan et al., 2016)	IHC profiler used to quantify immunohistochemistry for expression of CD3, CD4, CD8, CD68 and CD1a and compare between smokers and non-smokers for oral lichenoid lesions
Ke et al. 2016 (Ke et al., 2016)	Effect of Vitamin D3 on tissue damage and oxidative stress following exhaustive exercise investigated in mice. IHC profiler used to quantify oxidative product 4-hydroxynonenal in lung and kidney tissues.
Rotoli et al. 2016 (Rotoli et al., 2016)	The effect of oxaliplatin-based chemotherapy on the expression of immunophilin FK506-binding protein 5 (FKBP51) in colorectal liver metastases was quantified using the IHC profiler.
Zhang et al. 2016 (C. Zhang et al., 2016)	Immunochemistry and expression of protein cytokeratin 5 in vulval squamous cell carcinoma compared to intraepithelial neoplasia and normal vulval tissue using IHC profiler
Fathollah et al. 2016 (Fathollah et al., 2016)	Expression of transforming growth factor cytokine was quantified using the IHC profiler and compared in diabetic wounds subjected to non-thermal atmospheric plasma treatment
Nanda et al. 2016 (Nanda et al., 2016)	Inflammatory and anti-apoptotic markers in rat models of colorectal cancer were quantified using IHC profiler, and the effects of doxycycline administration studied.
Dequanter et al. 2016 (Dequanter et al., 2016)	IHC profiler was used to quantify the expression of glutamate=cysteine ligase in head and neck squamous cell carcinoma
Kumar et al. 2014 (Kumar et al., 2014)	Dietary effects of curcumin on the levels of benzopyrene induced DNA adducts in mice investigated with quantitative comparisons of BPDE-DNA nuclear adducts in lung and liver sections using IHC profiler.

Table 4.1*: Recent studies utilising the IHC profiler plug-in for quantifying immunohistochemistry with the ImageJ software*

4.3.2 Tissues collected

Following ethics approval (National Research Ethics Service committee in West London (reference 11/LO/1521)), cancer tissues were obtained for 16 patients, and 11 polyps. This included 7 patients with cancers without lymph node involvement and 9 patients with lymph node involvement, including 3 patients with metastatic disease on presentation. The median age for this patient group was 79 (range 67 – 92) with a 10:6 male: female ratio (Table 4.2). The polyps examined included adenomas with low to moderate dysplasia (4) and high-grade dysplasia (3) and serrated adenomas (3). Tumour cells demonstrated predominantly cytoplasmic staining. The positive control tissues used were prostate adenocarcinoma tissues after reviewing the work done by Armakolas et al. (Armakolas et al., 2010a). Figure 4.1

demonstrates the images captured from the slides, including the positive and negative control tissues, normal colon and colon cancer tissues and colonic polyps.

4.3.3 Acknowledgement of work done by others

The immunohistochemistry staining was done by Dr Jessica Broni and Dr Francesca Launchbury at the UCL Queen Square Institute of Neurology. Specimen procurement, quantification and analysis of the immunohistochemistry work and data collection for the patients was performed by me.

4.4 Results

4.4.1 Immunohistochemistry

The staining intensity on the IHC profiler for the positive control prostate cancer tissues was a median of 1.95 (range 1.4 – 2.3), while the intensity for the negative control (colorectal) tissues was a median of 0.4 (range 0.1 – 0.6). There was a significantly reduced expression of IGF-1Ec in normal colon tissues with a median expression of 1.2 (range 1.1 – 1.4) compared to colonic polyps ($p<0.001$) with a median expression of 1.7 (range 0.7 – 2.4) and colon cancer tissues ($p<0.001$) with a median expression of 1.7 (range 0.7 – 2.6). There were no differences in the expression of IGF-1Ec between colonic polyps and colonic cancer tissues ($p=1$). There was a significant increase in expression of IGF-1Ec ($p=0.001$) in high-grade dysplastic adenomas (median 2, range 0.8 – 2.4) compared to low and moderate grade dysplastic adenomas (median 1.6, range 1 – 2.2). Compared to normal colon tissues, a significantly higher expression of IGF-1Ec was identified in low/moderate grade dysplastic adenomas ($p=0.001$), high grade dysplastic adenomas ($p<0.001$) and serrated adenomas ($p=0.001$) (Figure 4.3). Lymph node-negative tumours demonstrated a significantly higher expression of IGF-1Ec (median 1.9, range 1 – 2.6) compared to lymph node-positive tumours (median 1.6,

range 0.7 – 2.2) as illustrated in Figure 4.4 (p=0.008). Comparison of the scores for the primary colon tumours with different T stages and M stages (metastatic disease at the time of presentation) did not demonstrate any difference in IGF-1Ec expression (Figure 4.5 and Figure 4.6). Similarly, for patients who presented with stage II disease, comparison between recurrent disease and no evidence of recurrence on follow up did not demonstrate any differences in IGF-1Ec expression (Figure 4.7) though this was limited to just 2 patients.

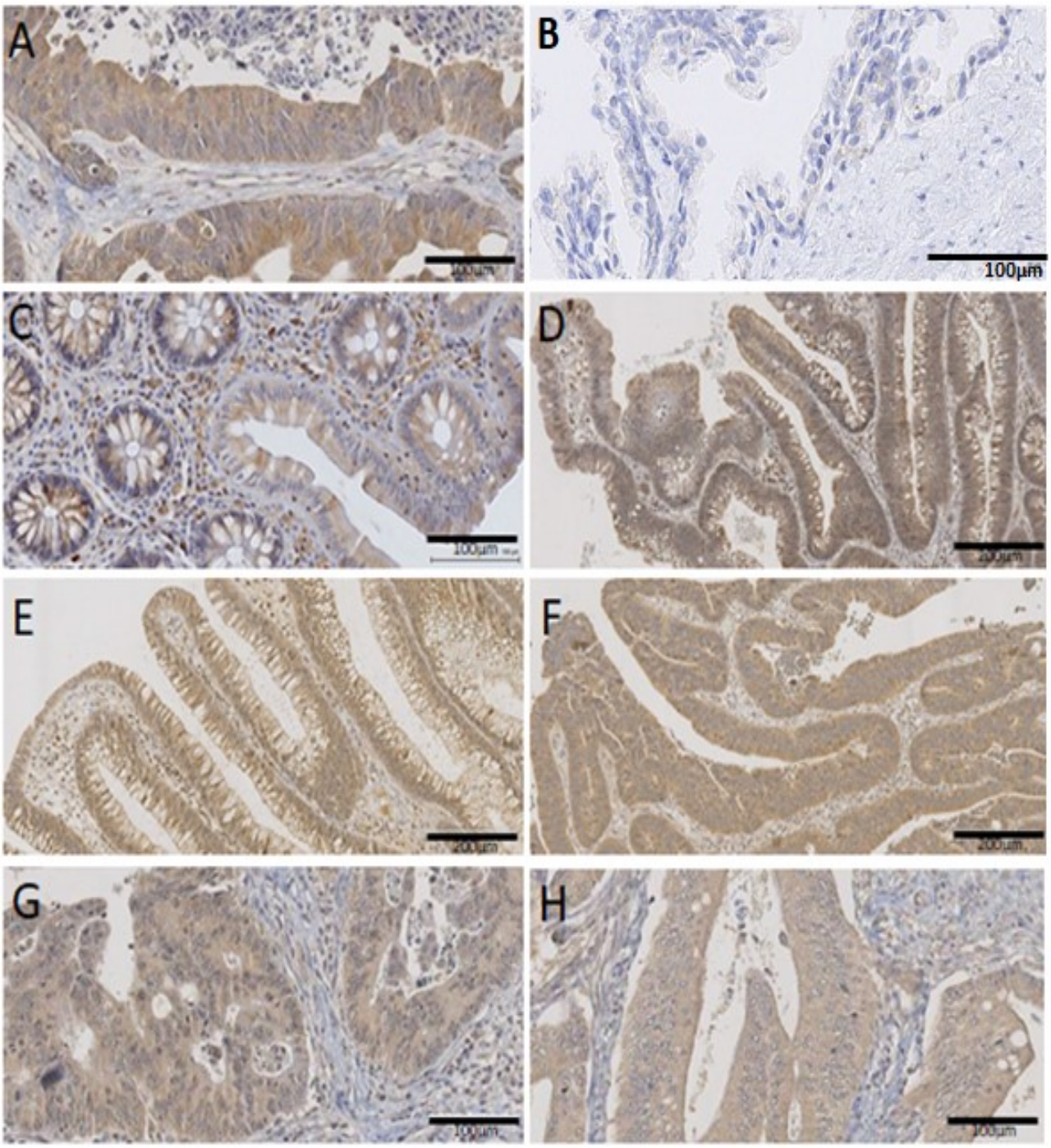

Figure 4.1*:* Immunohistochemistry for MGF expression. **A** – Positive control – Prostate cancer **B** – Negative control – Prostate cancer without primary MGF antibody **C** – Normal colon tissue **D** – colon cancer tissue **E** – Low grade dysplastic adenomatous polyp **F** – high grade dysplastic adenomatous polyp **G** – colon cancer tissue with lymph node-negative disease **H –** colon cancer with lymph node-positive disease

Category	Numbers
Patients – cancer tissues	16
Age	67 – 92 years (Median 79 years)
Gender – M:F	10:6
Patients with follow up	12
Length of follow up	4 days – 132 months (Median 30 months)
Cancer tissues	
T stage s	T1 (3), T2 (3), T3 (4), T4 (6)
N stage	Node positive (9), Node negative (7)
M stage	Metastasis (3), No metastasis (13)
Polyps	
Low and moderate dysplasia – adenoma	5
Severe dysplasia – adenoma	3
Serrated adenoma	3

Table 4.2*:* Patient demographics and cancer tissues

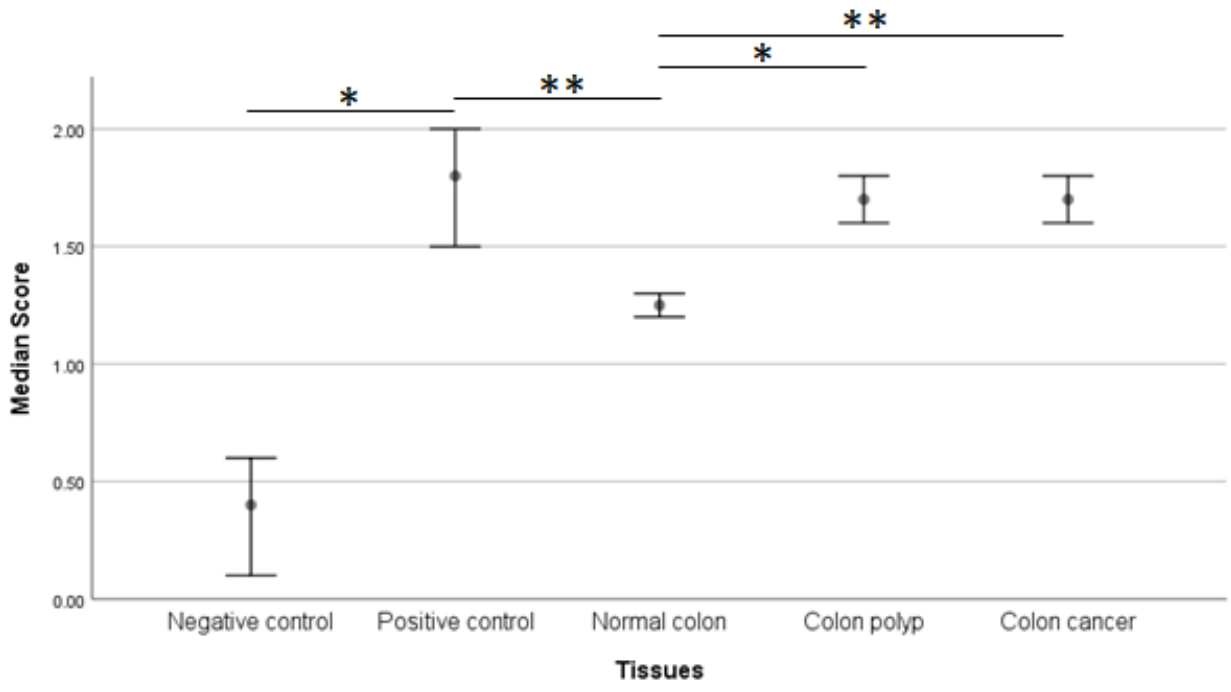

Figure 4.2*:* Median immunohistochemistry scores (IHC profiler) with 95% confidence interval bars for different tissues. Positive control – prostate cancer tissues (n=5). Negative control – prostate cancer tissues with the primary IGF-1Ec antibody substituted with PBS (n=3). Significant differences between the negative and positive control as illustrated. Normal colon tissues expression (n=3) of IGF-1Ec was significantly lower than colon polyp (n=11) and colon cancer tissues (n=16). $p<0.05$ was considered as significant and denoted as * and $p<0.01$ was considered as highly significant and denoted as **.

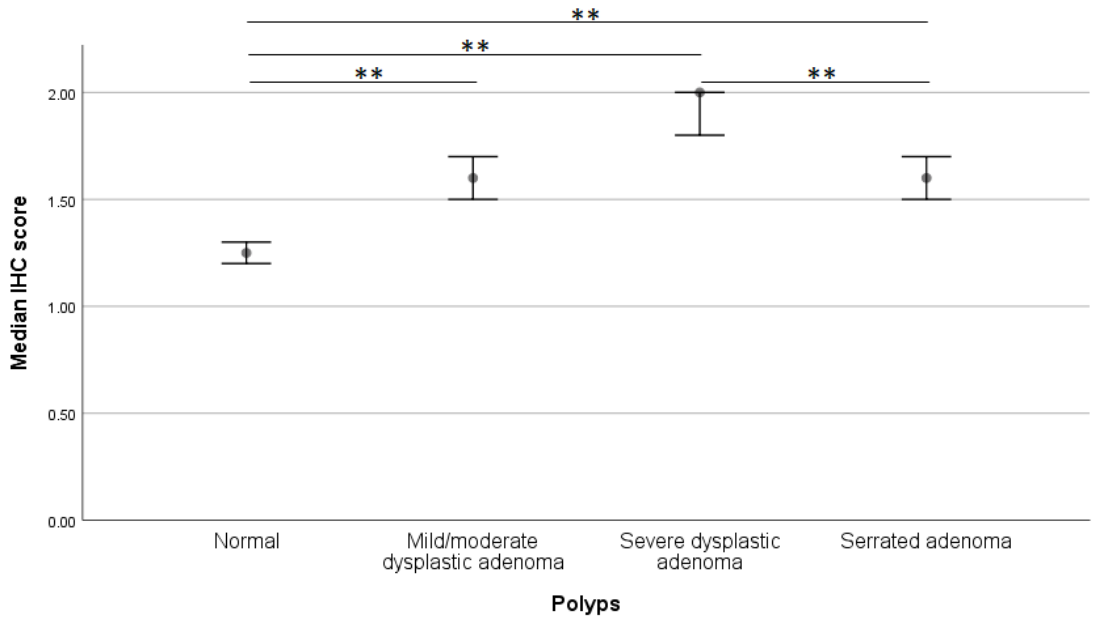

Figure 4.3: Median immunohistochemistry scores (IHC profiler) with 95% confidence interval bars for the expression of IGF-1Ec peptide in the different colonic polyp tissues. Significantly higher expression of IGF-1Ec in high grade dysplastic tubular adenomas (n=3) compared to low grade dysplastic polyps (n=5), serrated adenomas (n=3) and normal colon tissues (n=3) . p<0.05 was considered as significant and denoted as * and p<0.01 was considered as highly significant and denoted as **

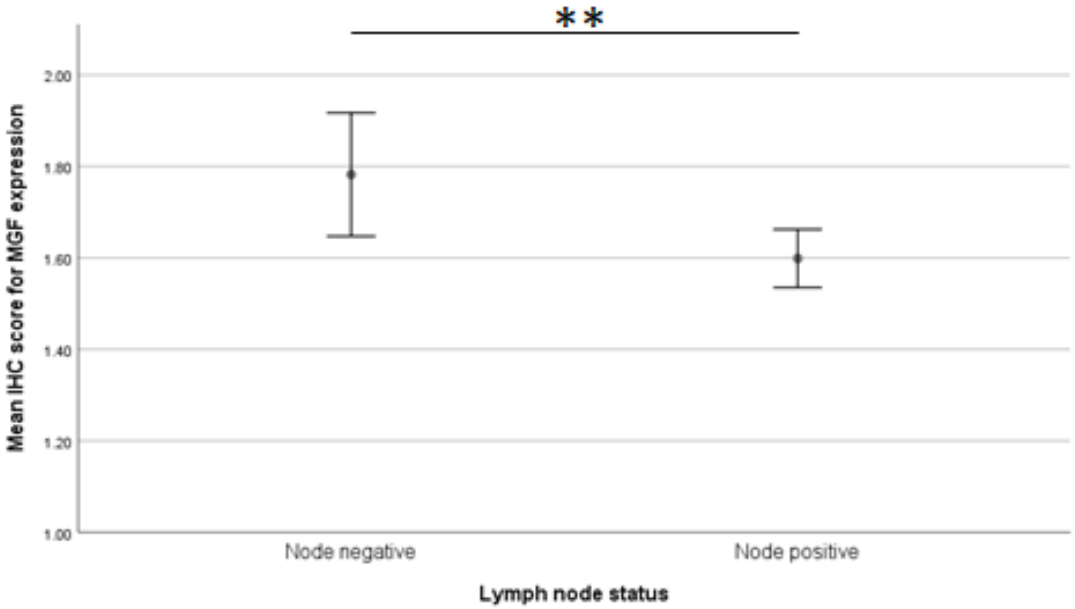

Figure 4.4*:* Median immunohistochemistry scores (IHC profiler) with 95% confidence interval bars for primary colon cancer tissues with lymph node status. A higher level of expression of IGF-1Ec in node-negative disease (n=7) compared to lymph node involvement (n=9) p=0.008

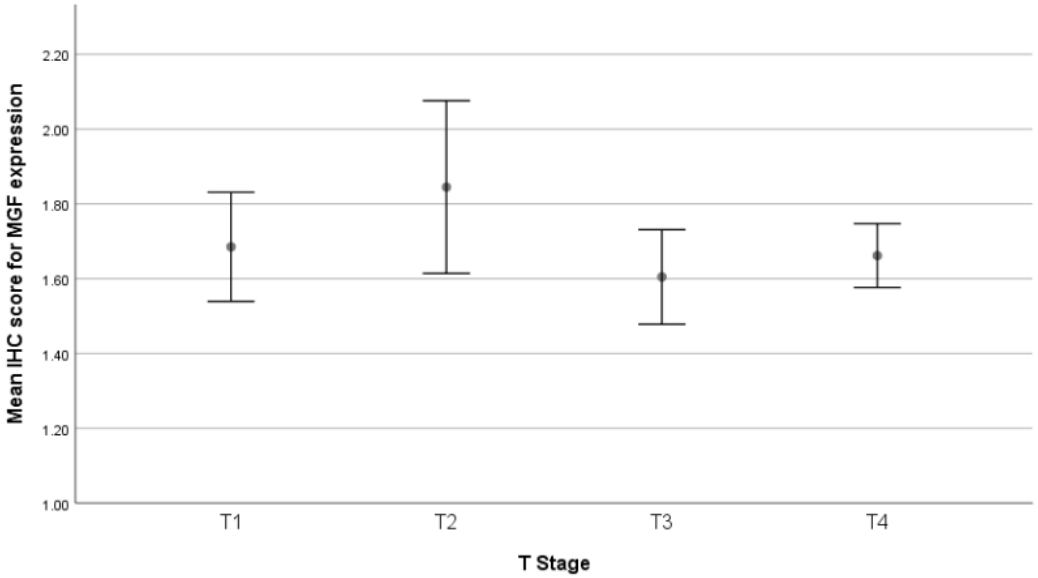

Figure 4.5*:* Median immunohistochemistry scores (IHC profiler) with 95% confidence interval bars for the expression of IGF-1Ec peptide in different T stages of the primary colon cancer tissues (n=3(T1), 3(T2), 4(T3), 6(T4)). No significant differences for the expression of IGF-1Ec identified between the T stages p=0.15.

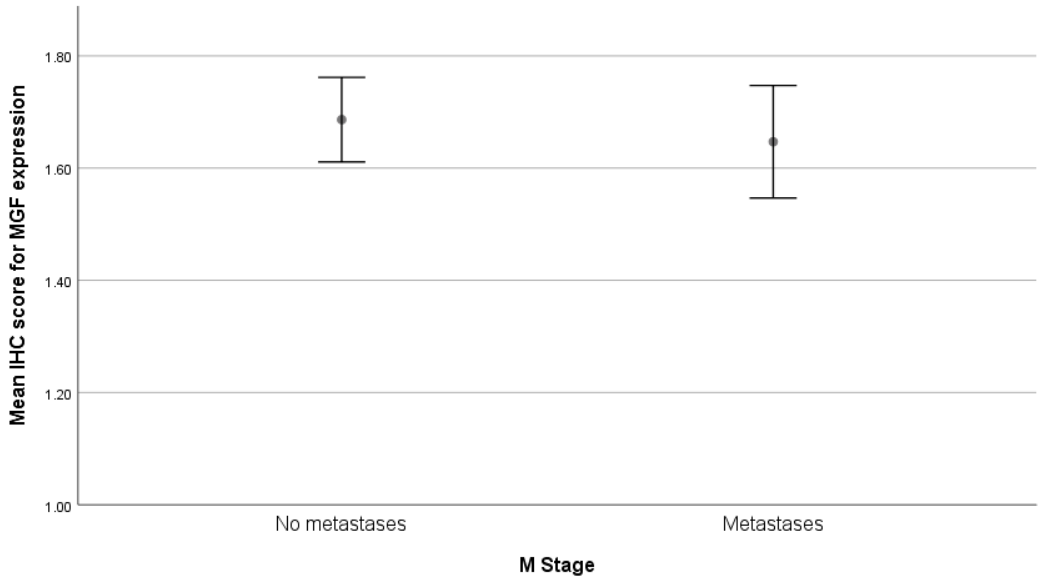

Figure 4.6*:* Median immunohistochemistry scores (IHC profiler) with 95% confidence interval bars for primary colon cancer tissues with (n=3) and without (n=13) metastatic disease at the time of presentation. No difference between the two groups identified p=0.53.

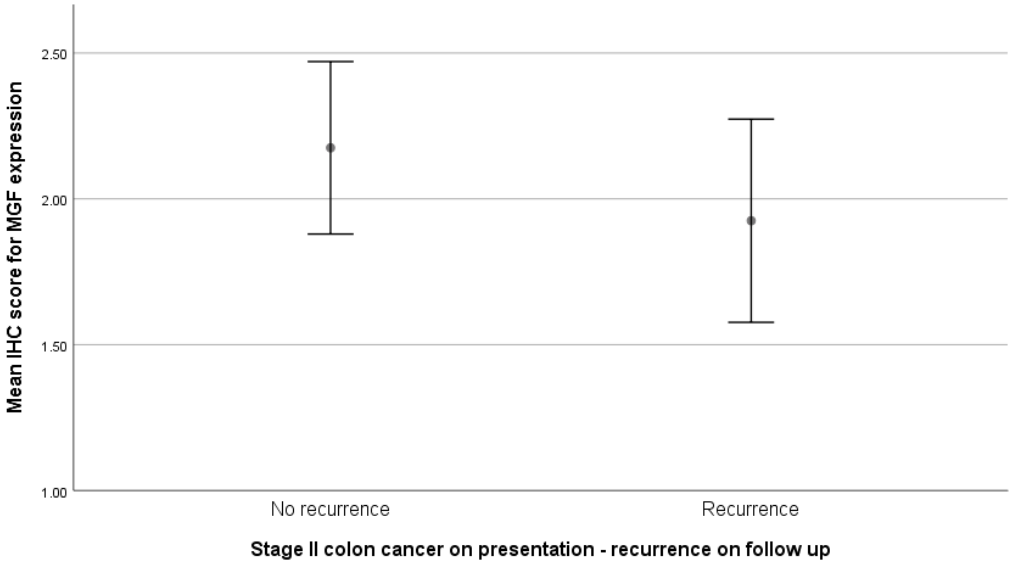

Figure 4.7*:* Stage II colon cancer. Results from 2 patients (1 recurrent disease within 17 months and 1 with no recurrent disease for 48 months). Assessing if MGF expression in the primary colon cancer tissue is predictive of risk of recurrence. No difference was seen though these are low numbers. p=0.19

4.5 Discussion

The findings of the immunohistochemistry suggest that MGF is overexpressed in colon polyps and cancer tissues at significantly higher levels than normal colon tissues. There appears to be some baseline expression of MGF in the normal colon tissues as evidenced by significantly higher levels than the negative controls. However, MGF expression was not affected by advancing stages of cancer with similar levels of expression in patients presenting with metastatic disease compared to patients presenting without metastatic disease. Interestingly, there appears to be a higher expression of MGF in lymph node-negative disease at presentation compared to lymph node-positive disease. Generally, lymph node involvement is regarded to be associated with increased risk of recurrent disease and is a rationale for offering postoperative chemotherapy in patients with colorectal cancer to reduce this risk ("Colorectal cancer," n.d.). However, there is an area of uncertainty with stage 2 colorectal cancer where the incidence of recurrent disease in these patients has been demonstrated to

be approximately 20%-25% within five years with outcomes for these patients similar to those with stage III disease where lymph nodes are involved (Chen and Bilchik, 2006; Davies et al., 2008). The use of chemotherapy in all patients with stage II colorectal cancer has not been demonstrated to be beneficial, and therefore arises the need to identify the subgroup of patients with stage II cancer who would benefit from chemotherapy thereby avoiding over or undertreating patients with adjuvant therapies and their associated side effects and complications. In the small numbers in my cohort (3 patients), no significant differences were identified in the expression of MGF affecting the risk of recurrent disease. This certainly would benefit from further work with larger numbers of patients.

I investigated the expression of MGF in colonic polyps which are known precursor lesions for colorectal cancer. The 'adenoma-carcinoma' sequence is an accepted concept in the pathogenesis of colorectal cancer, and most cancers are thought to arise from polyps. This hypothesis is supported by the epidemiological evidence that the prevalence of adenomas and carcinomas both increases with age, with adenomas peaking 5 years prior to carcinomas and the geographical variations in prevalence of both adenomas and carcinomas are very similar (Leslie et al., 2002). In addition, the distribution of adenomas and carcinomas are very similar in the colon, and removal of the adenomas have been demonstrated to reduce the long term incidence of colorectal cancers (Atkin et al., 1992; Leslie et al., 2002; Winawer et al., 1993). I looked at the expression of MGF in the polyps of different grades of dysplasia (mild/moderate and severe dysplasia) and compared adenomatous polyps to normal colon tissues. The expression of MGF was identified to be significantly higher in colonic polyps compared to normal colon tissues with increased expression with a worsening degree of dysplasia. This suggests that MGF is involved in the early stages of cancer pathogenesis in colon cancer.

Within the limits of my small study, MGF expression was identified to occur at a low level in normal colon tissues with significantly higher expression in colonic polyps, particularly with worsening dysplasia. Significantly higher expression of MGF was identified in colon cancer compared to normal colon tissues though this was identified to be at similar levels to colonic polyps. Further work would include reviewing MGF as a prognostic factor in stage II colorectal cancer. Based on current data, MGF offers a potential target for fluoroscopic agents to improve colonoscopic visualization of polyps and tumours, thereby reducing missed lesions which have been reported as high as 25%(Zhao et al., 2019). Additionally, there is a potential for targeting MGF with drug delivery agents and fluoroscopic agents for intraoperative visualization of the tumour.

5 Chapter 5: Synthesis, characterisation and conjugation of fluorescent nanoparticles to MGF antibody

Manuscript publication:

Mechano-growth factor expression in colorectal cancer investigated with fluorescent gold nanoparticles. *Alagaratnam s, Yang SY, Loizidou M, Fuller B, Ramesh B.* Anticancer Research. 2019 April;39(4):1705-1710

Presented in the annual British Society of Surgical Oncology meeting – Association of Cancer Surgery in 2012. Abstract published:

P59. The mechanogrowth factor expression in colorectal cancer: a potential new target for nanoparticles. *Swethan Alagaratnam, Ajit Johnson, Jonny Coppel, Bala Ramesh, Shi-Yu Yang, Marc Winslet, Alexander Seifalian*. European Journal of Surgical Oncology 38(11):1122 · November 2012

5.1 Introduction

The application of fluorescent nanoparticles in oncological medicine offers exciting avenues in diagnosis and treatment. The potential role of fluorescent nanoparticles in colorectal cancers includes delineating the resection margins of tumours during surgery, improving the accuracy and efficiency of histological assessment of tumour biopsies and improving the diagnostic accuracy of colonoscopy by reducing the rates of missed lesions.

Semiconductor quantum dots, despite promising preclinical results, have not reached the phase of clinical trials because of potential toxicity. Their unique fluorescent ability and intensity, along with reduced photobleaching, offers an enticing alternative to conventional immunohistochemistry. The ability to simultaneously use quantum dots with different emission spectra with ligands targeting different receptors/proteins offers advantages over conventional immunohistochemistry techniques to identify multiple targets with the same and small tissue samples and potentially automated quantification. Since this work is ex-vivo, the toxicity of the quantum dots does not limit application in immunohistochemistry work.

I describe experiments involving the synthesis of CdTe quantum dots functionalized with MSA and conjugated to the MGF antibody and peptide and the application of these quantum dots to colorectal cancer cell lines HT29 and SW620. I did not achieve the expected results with the application of these quantum dots and discuss the flaws and limitations of my methodology below. Using the lessons learnt from this work, I proceeded to experiments with gold nanoparticles.

Gold nanoparticles have been under research for applications in biomedicine due to strong photoluminescence, photostability, biocompatibility and nanometer dimensions (Xu and Shang, 2018). The fluorescence quantum yield of gold nanoparticles is lower than

semiconductor quantum dots, thereby limiting its use in quantitative immunofluorescent techniques. Gold nanoparticles are currently undergoing early phase clinical trials, and preliminary results suggest that these nanoparticles are tolerated in human subjects without significant adverse effects as described in chapter 2 (2.10). My work in chapter 4 demonstrating MGF expression in colon cancer and tissues with its absence in normal colon tissues offers two avenues for the application of gold nanoparticles to improve the management of colorectal cancers. Endoscopically, the use of an intravenously administered fluorescent nanoparticle conjugated with MGF antibody could potentially improve the identification of colonic polyps and cancers. Surgically, the intravenous injection of the nanoparticle conjugated to the MGF antibody could help delineate the margins of the tumour thereby helping with localisation of the malignancy in minimally invasive surgical procedures alleviating the need for endoscopically administered tattooing of the bowel. We, therefore, decided to use fluorescent gold nanoparticles with this aim in mind. I describe experiments including the synthesis, functionalization and characterisation of the gold nanoparticles conjugated with the MGF antibody. Learning from the flaws in the methodology of my work with the semiconductor quantum dots, the characterisation experiments included dot blot techniques to ensure that the MGF conjugated gold nanoparticle binds to our target of interest. Following confirmation of this, I describe experiments administering this gold nanoparticle to the colorectal cancer cell lines HT29 and SW620 using prostate cancer cell line PC3 as a positive control and the HUVEC cell line as a negative control. Further work is des using colorectal cancer tissues, polyp tissues and prostate adenocarcinoma tissues (positive control) is described.

5.2 Aims

- Develop semiconductor quantum dots conjugated to MGF antibody
- Develop gold nanoparticles conjugated to MGF antibody

5.3 Supplementary methods and materials

5.3.1 Semiconductor quantum dots

5.3.1.1 Quantum dot synthesis

CdTe QDs were synthesized by a one-pot procedure. All the starting materials were obtained from commercial suppliers (as outlined in chapter 3.1) and were used without further purification. All reactions were carried out in a buffer solution composed of 15mM $Na_2B_4O_7$ and 15mM citrate acid, pH adjusted to 7.0 with 1M HCL. The precursor material included solutions of $CdCl_2$ (2mM), Na_2TeO_3 (0.5mM), MSA (4mM) and in 50ml of the above buffer solution in a one-neck flask immersed in ice. The above mixture was subjected to vigorous mixing using a magnetic stirrer for 5 minutes. At 5 minutes, solid $NaBH_4$ (15mg) was added rapidly and mixed for a further 5 minutes. Finally, the flask was connected to a condenser and refluxed with mixing at 100^oC under aerobic conditions for 12 h.

5.3.1.2 CdTe Quantum dot conjugation to MGF peptide and MGF antibody

Fluorescent CdTe/MSA QD solution was diluted with an equal volume of cold 70% ethanol and centrifuged at 4000 rpm for 20 minutes. The precipitated CdTe/MSA QD was vacuum dried to obtain as a powder. The precipitated dried QDs (Approximately, 1 mg) were re-suspended in 1 mL phosphate buffer saline/tetrahydrofuran (PBS/THF) (1:1 v/v) and centrifuged at 4000rpm for approximately 10 to 15 minutes. The obtained coated QD (1 mL) solution was conjugated to the MGF peptide/antibody using 1-Ethyl-3-(3-dimethyl aminopropyl carbodiimide) hydrochloride (EDC) as an acylating agent (Figure 5.1). This

involved 200 µL QD/MSA solution (1 mg/mL) mixed with 200 µL EDC (1 mg/mL) for 30 minutes at room temperature. 100 µL of the MGF peptide/quantum dot solution (5 mg/mL) was added to the mixture and mixed for 2 h in ice. To separate the reagent and unconjugated CdTe/MSA QDs, centrifugal membrane columns (centricon) with a cut off of 100 kDa with UV monitoring at 280 nm of the retained samples was used. The purified CdTe/MSA conjugated to MGF peptide/antibody were collected and stored at +4 ºC until further use.

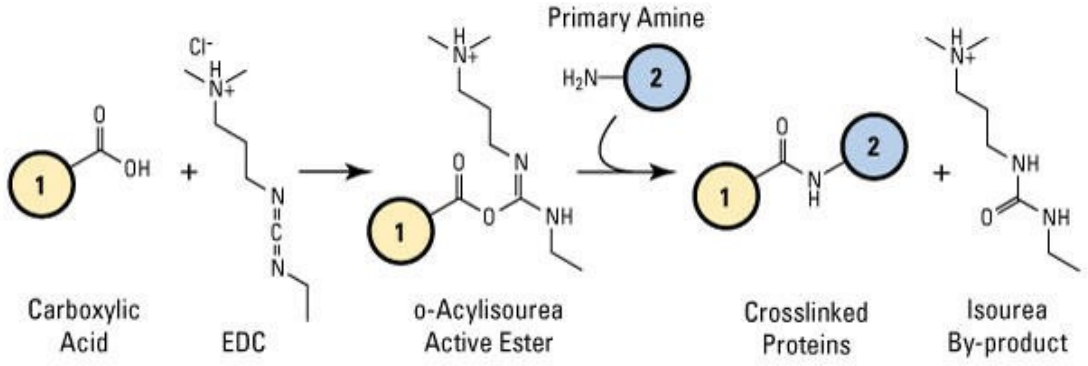

Figure 5.1*: 1-Ethyl-3-[3-dimethylaminopropylcarbodiimide] hydrochloride (EDC) action("EDC (1-ethyl-3-(3-dimethylaminopropyl)carbodiimide hydrochloride) - Thermo Fisher Scientific," n.d.). EDC reacts with carboxylic acid groups to form an active* O*-acylisourea intermediate that is easily displaced by nucleophilic attack from primary amino groups in the reaction mixture. The primary amine forms an amide bond with the original carboxyl group, and an EDC by-product is released as a soluble urea derivative. The by-product can be easily filtered by dialysis or gel filtration(Elzahhar et al., 2019)*

5.3.1.3 Quantum dot characterisation

5.3.1.3.1 Emission spectrum spectroscopy

The USB 2000+ Ocean Optics spectroscopy was used to measure the emission wavelength of the conjugated and unconjugated quantum dots at room temperature. The samples were placed in a 1cm path quartz cuvette. Using an excitation wavelength of 375 nm with a slit width of 5.0 nm, spectra were recorded from 400nm to 800nm regions. This was performed in a single run for both conjugated and unconjugated quantum dots.

5.3.1.3.2 Atomic force microscopy

20µL of the quantum dots (conjugated and unconjugated) were placed on the freshly cleaved and modified mica substrates and allowed to dry over 20 – 30 minutes with N_2 gas. The samples were subsequently dried in air and imaged with a Bruker Multimode 8 atomic force microscopy. Measurements were performed in the tapping mode with amplitude and phase images were simultaneously collected at a scan rate of 1Hz, initially at a scan area of $1\mu m^2$, and further zoomed in to a scan area of $500nm^2$ at room temperature. Analysis of the scanned images was performed using Nanoscope Analysis v1.4 (Bruker corporation).

5.3.1.4 In vitro studies

The colorectal cancer cell lines SW620 and HT29 were used. Cell culture techniques have been previously described (chapter 3). The cells were seeded at a concentration of 100,000 cells/cm^2 per well in 18 wells of two 24 wells plate, and the following experiments were conducted for both cell lines. After 48 hours of incubation at 37°C, the cells were viewed under light microscopy to confirm adherence to the well surface. The 18 wells were divided into 6 groups of 3 wells. Quantum dot conjugated with the MGF antibody (concentration of 1/500 in growth culture medium) was added to group 1, quantum dot conjugated with MGF peptide (concentration of 1/500 in growth culture medium) was added to group 2, MGF antibody (concentration of 1/500 in growth culture medium) was added to group 3, MGF peptide (concentration of 1/500 in growth culture medium) was added to group 4, unconjugated quantum dots (concentration of 1/500 in growth culture medium) were added to group 5 and growth culture medium was added to group 6 (Table 4.2). Following 48 hours of incubation at 37°C with 5% CO_2, the wells were rinsed with 2mls of PBS and 1ml of 10% Formaldehyde was instilled in each well for 15 minutes. The wells were then rinsed with 2mls of PBS, and each well was blocked with 1% Bovine Serum Albumin/0.1% Tween 20 for 30

minutes. After a further rinse with PBS, the wells were viewed under the Nikon laser scanning confocal microscope at 4x magnification.

Due to the absence of binding of the quantum dot conjugated with the MGF antibody to the cell lines, this experiment was repeated with group 1 initially incubated with MGF peptide for 24 hours, and after aspirating the well and washing it with PBS followed by addition of the quantum dot conjugated with MGF antibody, and this was incubated for a further 48 hours prior to being fixed and blocked as described previously.

5.3.1.5 Laser scanning confocal fluorescent microscopy (LSCM)

LSCM (Nikon Eclipse TE 300, Nikon, Chiyoda, Tokyo City, Tokyo, Japan) was used to scan the slides which were illuminated at 488nm and filtered with 630 LP (Long pass) barriers. The PCM scanning head was mounted on an inverted optical microscope (Nikon Eclipse TE 300), which can operate in fluorescence, reflection and phase contrast modes (Ramesh et al., 2016).

5.3.2 Gold nanoparticles

5.3.2.1 Synthesis of MSA-stabilized gold nanoparticles (MSA-AuNPs)

The method used in this study involved a one-pot method to obtain visible fluorescent gold nanoparticles. Purified deionized water adjusted at pH 6.5 was used as the major solvent. 500μl of the polar solvent, dimethylformamide (DMF) was added as a reductant into the aqueous mixture whilst mixing vigorously using a homogenizer at its maximum speed. This mixture was then heated by hydrothermal treatment (autoclave) at 121^{o}C for 25 minutes to give quantum-confined AuNPs with near-infrared (NIR) emission at ≥ 800 nm on cooling to room temperature. The final product could be excited at a range from 375 nm to 630nm to obtain a fluorescent emission peak at 800 nm.

5.3.2.2 Preparation of anti-MGF conjugation to AuNP/MSA (anti-MGF-AuNPs)

Fluorescent MSA-AuNPs solution was diluted with an equal volume of cold ethanol and centrifuged at 10,000g for 30 minutes. The precipitated MSA-AuNPs was vacuum dried to obtain as a powder. The precipitated dried MSA-AuNPs (approximately 1 mg) were re-suspended in 1 ml phosphate buffer saline (PBS). The obtained coated MSA-AuNPs (1 ml) solution was conjugated to the Anti-MGF using EDC as an acylating agent. This was done using 200 μL MSA-AuNPs solution (1 mg/ml) mixed with 200 μL EDC (1 mg/ml) in water for 30 minutes at room temperature. 100 μl of Anti-MGF solution (5 mg/ml) in PBS was added to the activated mixture and agitated gently for 1 hour at room temperature. Membrane centrifugal columns (Centricon) were used with a cut off 100 kDa with UV monitoring at 280 nm of the retained samples to separate the reagent and unconjugated MSA-AuNPs. Further validation of conjugation of the AuNP-anti-MGF was carried out using immunochemistry against the synthetic peptide via immunodots. The purified bio-conjugated nanoparticles defined as anti-MGF-AuNPs were collected and stored at +4^{o}C until further use.

5.3.2.3 Gold nanoparticle characterization

The fluorescence spectra of the AuNPs and its conjugations were recorded to ensure that the emission fluorescence was not quenched to use them for different biomedical applications. Fluorescence spectra were taken by a spectrofluorometer with an excitation source at 375nm in a single run.

TEM (Phillips CM 120) was used previously for visualisation and to obtain the size of the unconjugated gold nanoparticles. To determine the size and shape of the MSA coated QDs, a set of 1:100 serial dilutions were made of coated QD with PBS, and the optimum dilution was chosen. A drop of the samples was mounted on to a Piloform (TAAB) coated G300HS copper

electron microscopy grid (Gilder) and allowed to air dry. The grids were examined with a CM120 (Philips) TEM at 3.0 x 10^5 magnification (Ramesh et al., 2016).

Dot blot confirmation of the functioning MGF antibody bound to the gold nanoparticle was performed as follows. 5µl of 1: 1000 dilution of the anti-MGF-AuNCs and synthetic MGF peptide (1mg/ml) in Phosphate buffered saline (PBS) were spotted separately onto aqueous equilibrated PVDF membrane and allowed to dry at room temperature. A scrambled peptide sequence was used a control. On drying, the membrane was rinsed briefly in PBS with 0.05% Tween 20 (PBS/T; pH 7.4) and was incubated overnight at room temperature in 2% BSA with 0.005% sodium azide to block any residual binding sites on the membrane. After blocking incubation, the membrane strip was rinsed in PBS/T (5x 1 min washes). The second incubation was carried out in the presence of anti-MGF conjugated to gold NCs at 1: 1000 (anti-MGF-AuNPs) for 1 h at room temperature with gentle shaking. The membrane strip was rinsed in PBS/T (5x 1 min washes). The third incubation was with anti-rabbit antibodies conjugated to horseradish peroxidase (anti-rabbit-IgG (1:5000) for 1 h with gentle shaking. This third incubation is to confirm conjugation (anti-MGF-AuNPs) and simultaneously the specificity to the peptide antigen (MGF). The strip was finally washed in PBS/T (5x 5 min washes). The membrane was then used for chemiluminescence to detect the presence of the conjugated anti-MGF to gold.

5.3.2.4 In vitro studies

All cell cultures were routinely propagated in standard growth conditions (37^{o}C, 5% CO_2) and were between 3-12 passages after receipt from the supplier. 75 cm^2 flasks were used to grow the cells, and >80% confluence was avoided. Cancer cell lines SW 620 (“metastatic” colon cancer), HT-29 (colon cancer) and PC3 (prostate cancer) were all maintained in D-MEM (with

1mM pyruvate, 2mM glutamine and 10mM HEPES) supplemented with 10% foetal bovine serum (FBS), 100 IU penicillin and 100mg/ml streptomycin. Human umbilical vein endothelial cells HUVECS were maintained in PromoCell endothelial cell growth medium with supplement mix (PromoCell GmbH) and 5% FBS with growth factors. After 24 hours of incubation at 37^{o}C in 5% CO_2, the cells were washed with PBS and fixed with 4% paraformaldehyde solution for 1 hour at room temperature. These were then washed three times with PBS and incubated with the MGF antibody conjugated AuQDs in PBS with 0.6% bovine serum albumin for 1 hour and then washed three times with PBS. Additional negative control was performed by using unconjugated AuQDs in exchange for the MGF antibody-conjugated quantum dots.

5.3.2.5 Tissues

Frozen sections of colorectal cancer tissues, normal colon tissues and prostate cancer tissues fixed in cold acetone were purchased from Ambsio (AMS Biotechnology (Europe) Limited). Prostate cancer tissues were chosen as positive controls due to established findings in the literature for the over-expression of MGF in prostate cancer compared to normal prostate tissues (Armakolas et al., 2010b). These tissues were incubated with the MGF antibody conjugated AuQDs in PBS with 0.6% bovine serum albumin for 1 hour and then washed three times with PBS. Negative control was performed by using unconjugated AuQDs in exchange for the MGF antibody-conjugated quantum dots. These experiments were performed three times to confirm the findings.

5.3.2.6 Laser scanning confocal fluorescent microscopy (LSCM)

Images were acquired by the Olympus BX 63. which can operate in fluorescence, reflection and phase contrast modes, and it was provided with high transmission objectives with reduced autofluorescence. Fluorescent image acquisition was conducted via LED light source excitation at 620 nm with emission long-pass filter at 700 nm with image processing with

Olympus cellSens software. All the near-infrared images acquired are displayed in the pseudocolour (red) format.

5.3.2.7 Statistical analysis

All data have been examined and demonstrated a normal distribution. All results were expressed as mean±SEM. One-way ANOVA (IBM® SPSS® Statistics Version 25) with multiple comparison tests were used, and independent T-test performed when comparing two groups. Statistical analysis was performed on samples (n=3-6). Microsoft Excel 2016® was used to generate descriptive statistics including mean, standard deviation and illustrate results with graphs.

5.3.3 Acknowledgement of work done by others

The synthesis, conjugation and dot blot characterization experiments were done with the help of Dr Bala Ramesh at the Royal Free Campus. Atomic force microscopy characterization work was done with the assistance of Dr Richard Thorogate based at the London Centre of Nanotechnology. Analysis of the results from atomic force microscopy was performed by me.

5.4 Results

5.4.1 Semiconductor quantum dots

5.4.1.1 Quantum dot characterization

5.4.1.1.1 Emission spectrum spectroscopy

Optical characterisation of the synthesised unconjugated CdTe/MSA quantum dot, the MGF peptide conjugated CdTe quantum dot and MGF antibody conjugated CdTe quantum dots using spectroscopy demonstrated a narrow emission spectrum of the quantum dots with the maximum intensity of the emission at 569.9nm, 595.5nm and 593.7nm for the unconjugated

CdTe/MSA quantum dot, and MGF peptide conjugated quantum dot and the MGF antibody-conjugated quantum dot respectively (Figure 5.2). The impact of conjugation shifted the emission wavelength by approximately 25nm towards the near infra-red spectrum.

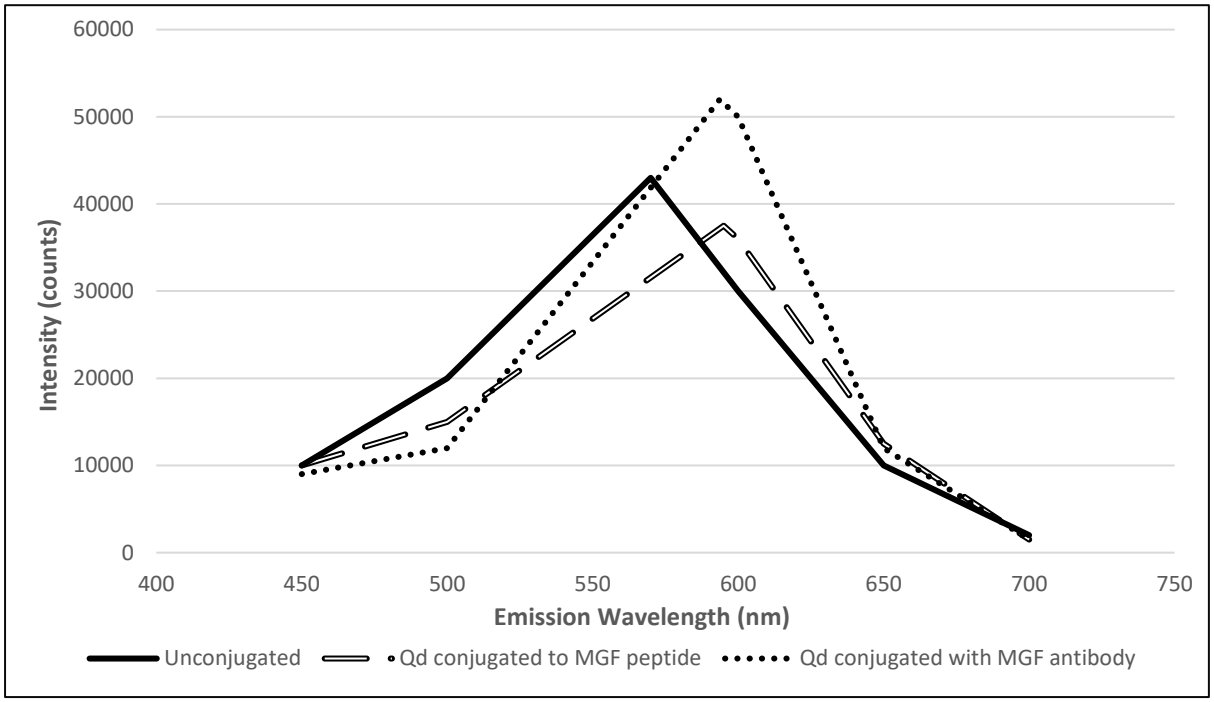

Figure 5.2*:* Emission spectrum of the unconjugated quantum dot, the quantum dot conjugated to the MGF antibody and the quantum dot conjugated to the MGF peptide (n=3). Excitation wavelength at 375nm and emission spectrum recorded between 400nm to 800nm.

5.4.1.1.2 Atomic force microscopy

Direct visualisation of the individual quantum dots with atomic force microscopy demonstrated evidence of conjugation with the peptide and antibody as illustrated in Figure 5.3. The tall spikes were presumed to be representative of the quantum dots and the smaller adjacent spikes in Figure 5.3 identifying the conjugated peptide and antibody, respectively. This contrasted with the single spikes in Figure 5.3 for the unconjugated quantum dots. Table 5.1 summarises the quantitative results for the measurements of the quantum dots. The combined dimensions of the unconjugated CdTe/MSA quantum dot was 318.8 $nm^{3,}$ and the

MGF antibody-conjugated quantum dot was 341.7 nm^3 (p=0.79). The MGF peptide conjugated quantum dot had a mean combined dimension of 1414nm^3 (p=0.02). Therefore, despite the direct visualization of apparent conjugation of the MGF antibody to the quantum dot, the dimensions of the presumed MGF antibody-conjugated quantum dots were not significantly increased compared to the unconjugated quantum dot while there was a shift in the emission spectrum of the conjugated quantum dot to the right.

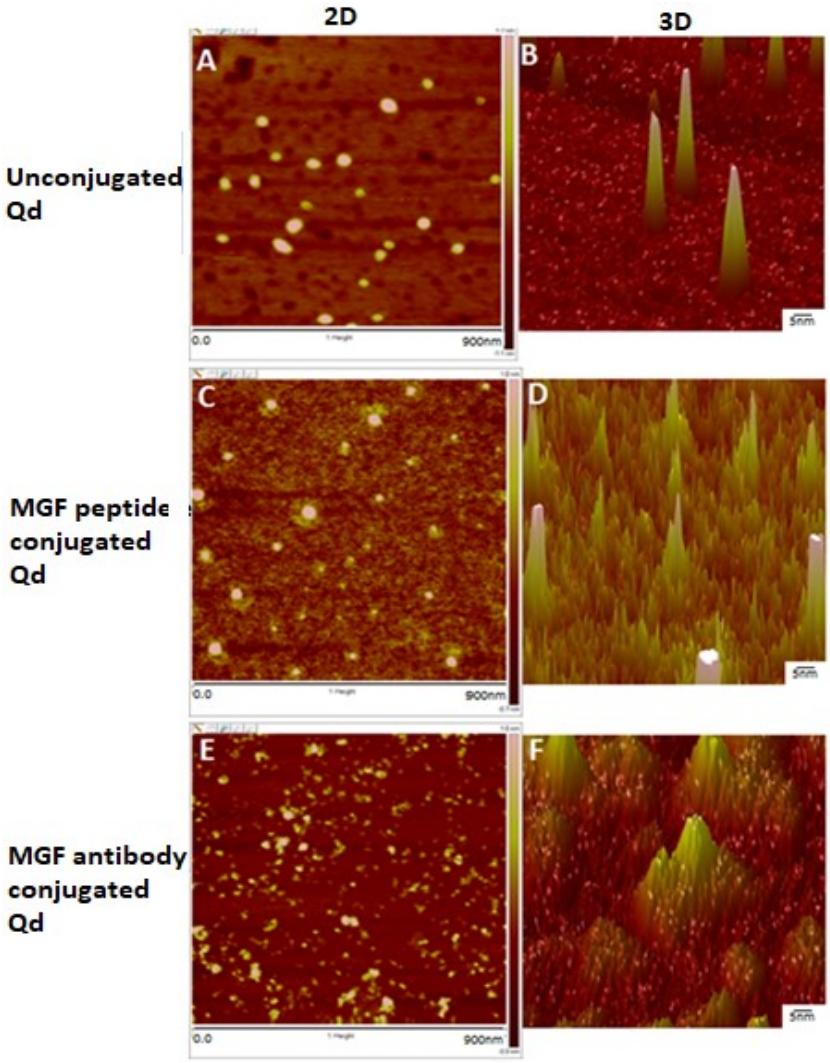

Figure 5.3*:* Atomic Force Microscopy: Unconjugated quantum dots A 2D B 3D, quantum dots conjugated with MGF peptide C 2D D 3D, quantum dots conjugated with MGF antibody E 2D F 3D

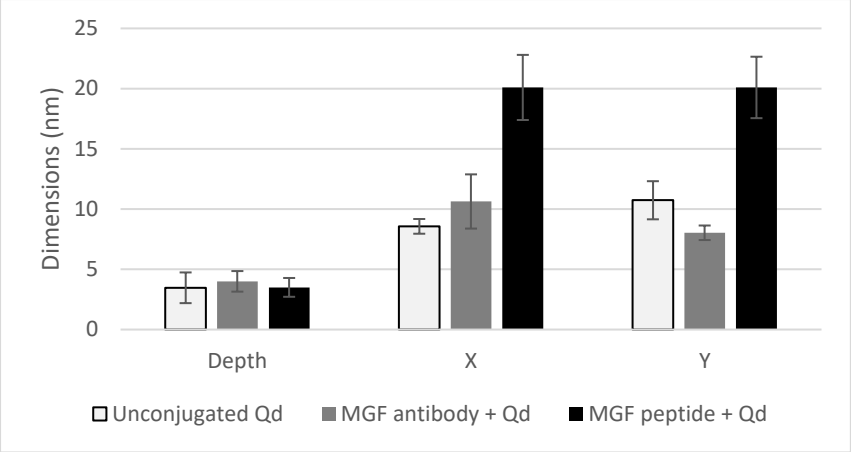

Figure 5.4: Atomic force microscopy measurements were done using Nanoscope Analysis®. Dimensions in depth, transverse (x) and longitudinal (y). SD error bars.

	Depth (nm)	X (nm)	Y (nm)	Combined nm^3 (SD*)
Unconjugated Qd	3.5	8.6	10.7	318.8 (107.80)
MGF Antibody conjugated Qd	4	10.6	8	341.7 (47.1)
MGF peptide conjugated Qd	3.5	20.1	20.1	1414 (158.2)

Table 5.1*:* Average dimensions of the samples of the different groups of quantum dots structurally characterised by AFM (n=3 for each group). t-test for comparison between unconjugated quantum dot s and MGF antibody quantum dots (p=0.79) and comparison between unconjugated quantum dots and MGF peptide quantum dots (p=0.02). *SD – Standard Deviation for combined dimensions of the nanoparticles (Depth multiplied by X and Y)

5.4.1.2 In vitro study

On viewing the cells under confocal microscopy, the Qd-MGF peptide conjugate group was the only group which demonstrated fluorescence. Groups 1 (Qd-MGF antibody conjugate), 3 (MGF antibody only), 4 (MGF peptide only), 5 (unconjugated Qd) and 6 (Growth medium only) did not fluoresce (Table 5.2). The repeat experiments with Group 1 cells initially incubated with MGF peptide for 24 hours, and then subjected to Qd-MGF antibody conjugate yielded the same results of no fluorescence. Figure 5.5 demonstrates the images for the Qd-MGF peptide incubated with the cell lines. Cells in the fixed group were stored in 4^{o}c and reimaged with confocal microscopy one week later, and the fluorescence of the quantum dots remained as demonstrated in Figure 5.5.

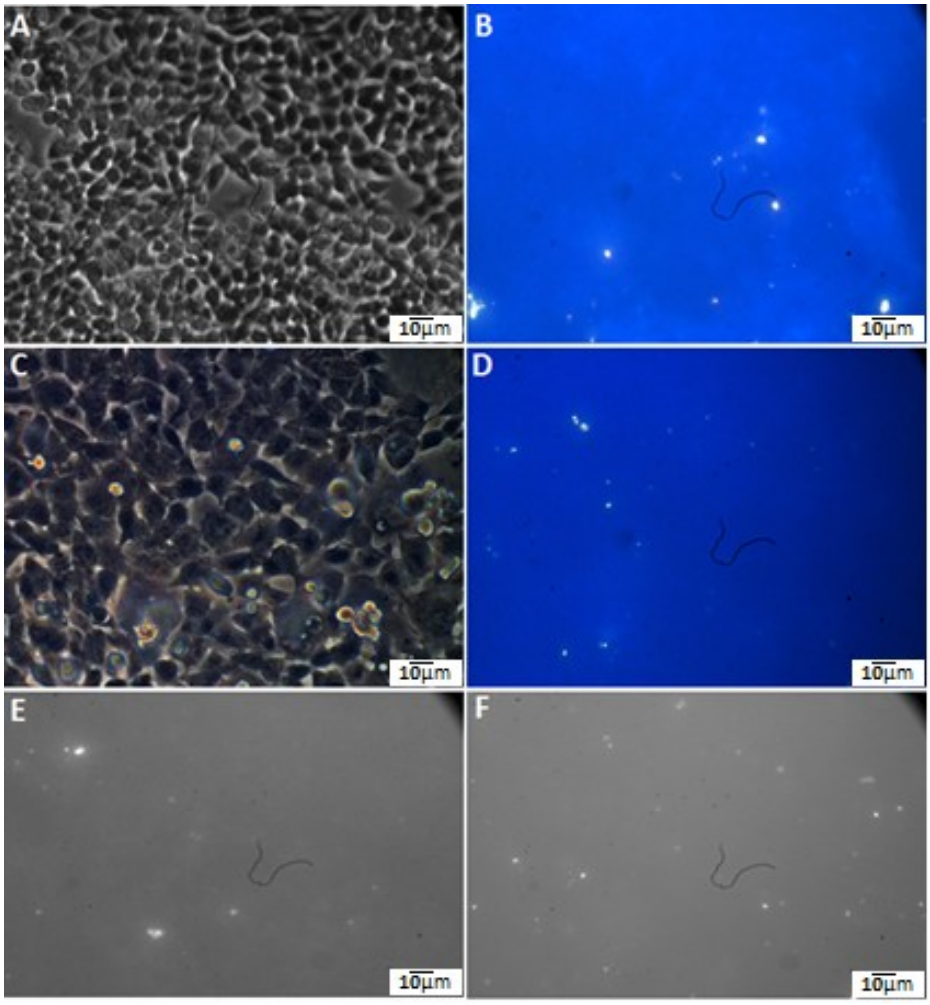

Figure 5.5: *Confocal microscopy images A and B Images from Qd-MGF peptide incubation for 72 hours with HT29 cells, C and D Images from Qd-MGF peptide incubation for 72 hours with SW620 cells E and F Same plates re-imaged after 1 week demonstrating quantum dots fluorescing without photobleaching. E HT29 F SW620*

	Contents	Outcome
Group 1	Qd-MGF antibody conjugate	No fluorescence for both live and fixed cell plates in both cell lines* Repeat experiment with incubation of this group with MGF peptide for 24 hours, followed by incubation of the Qd-MGF antibody did not demonstrate any fluorescence.
Group 2	Qd-MGF peptide conjugate	Fluorescence in both live and fixed cell plates and in both cell lines*
Group 3	MGF antibody	No fluorescence for both live and fixed cell plates in both cell lines*
Group 4	MGF peptide	No fluorescence for both live and fixed cell plates in both cell lines*
Group 5	Unconjugated CdTe/MSA QD	No fluorescence for both live and fixed cell plates in both cell lines*
Group 6	DMEM culture medium	No fluorescence for both live and fixed cell plates in both cell lines*

Table 5.2*:* Invitro study investigating the application of the CdTe/MSA quantum dot conjugated to the MGF-peptide and MGF-peptide to cell lines* (HT29 and SW620). Each group had 3 wells allocated in a 18 wells plate.

5.4.2 Gold nanoparticles

5.4.2.1 Quantum dot characterisation

Optical characterisation of the synthesised unconjugated MSA gold quantum dot and the MGF antibody conjugated gold quantum dot using spectroscopy demonstrated a reduction in the intensity of the emission wavelength of the conjugated gold nanoparticle (Figure 5.6).

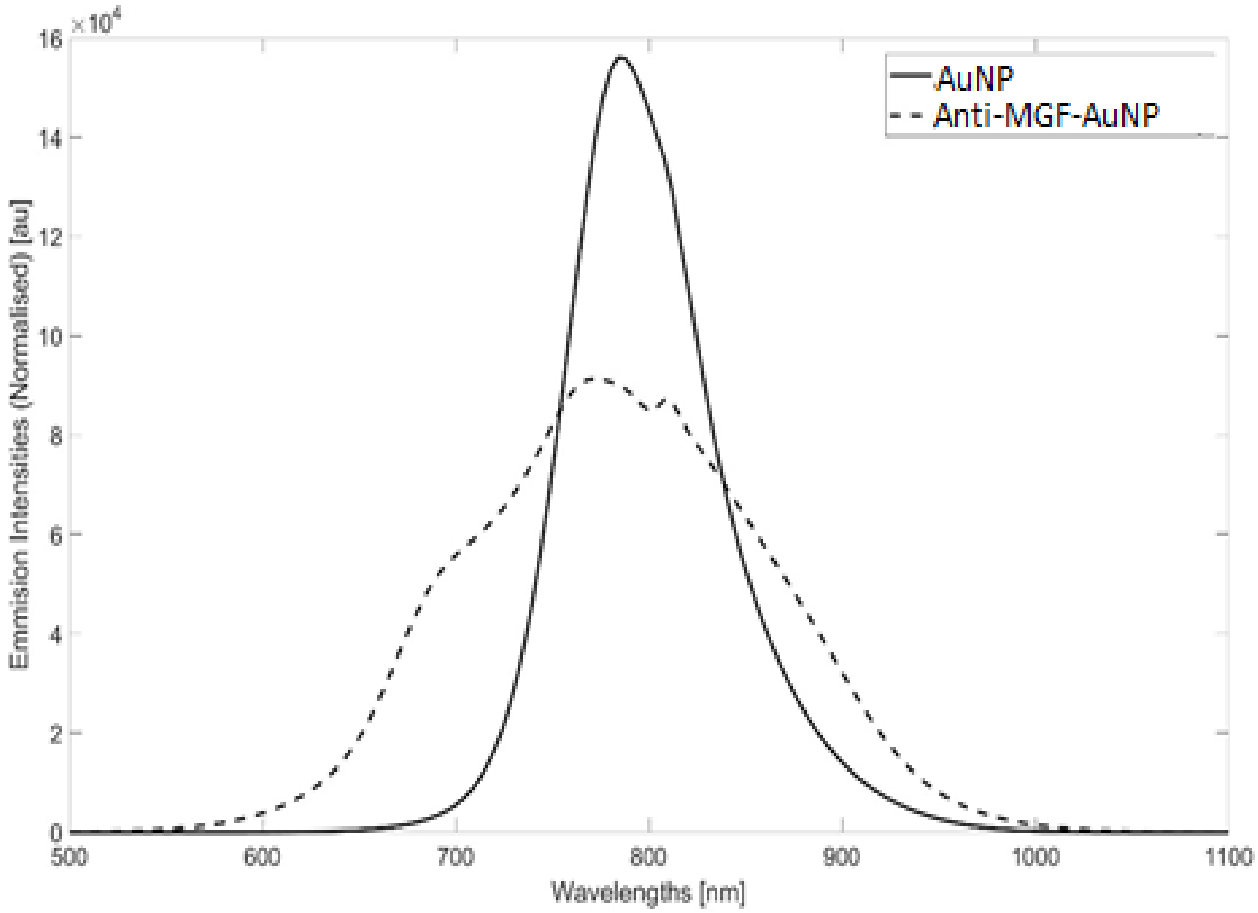

Figure 5.6: Peak photoluminescence of MSA-coated gold nanoparticles and the MGF conjugated MSA-coated gold nanoparticles were at 800nm excited at 488nm (n=3).

5.4.2.2 Transmission Electron Microscopy

The findings from the TEM for the unconjugated MSA-coated gold nanoparticles is illustrated below in Figure 5.7(Ramesh et al., 2016). The mean size of these nanoparticles was 2.4nm (standard deviation 0.6nm).

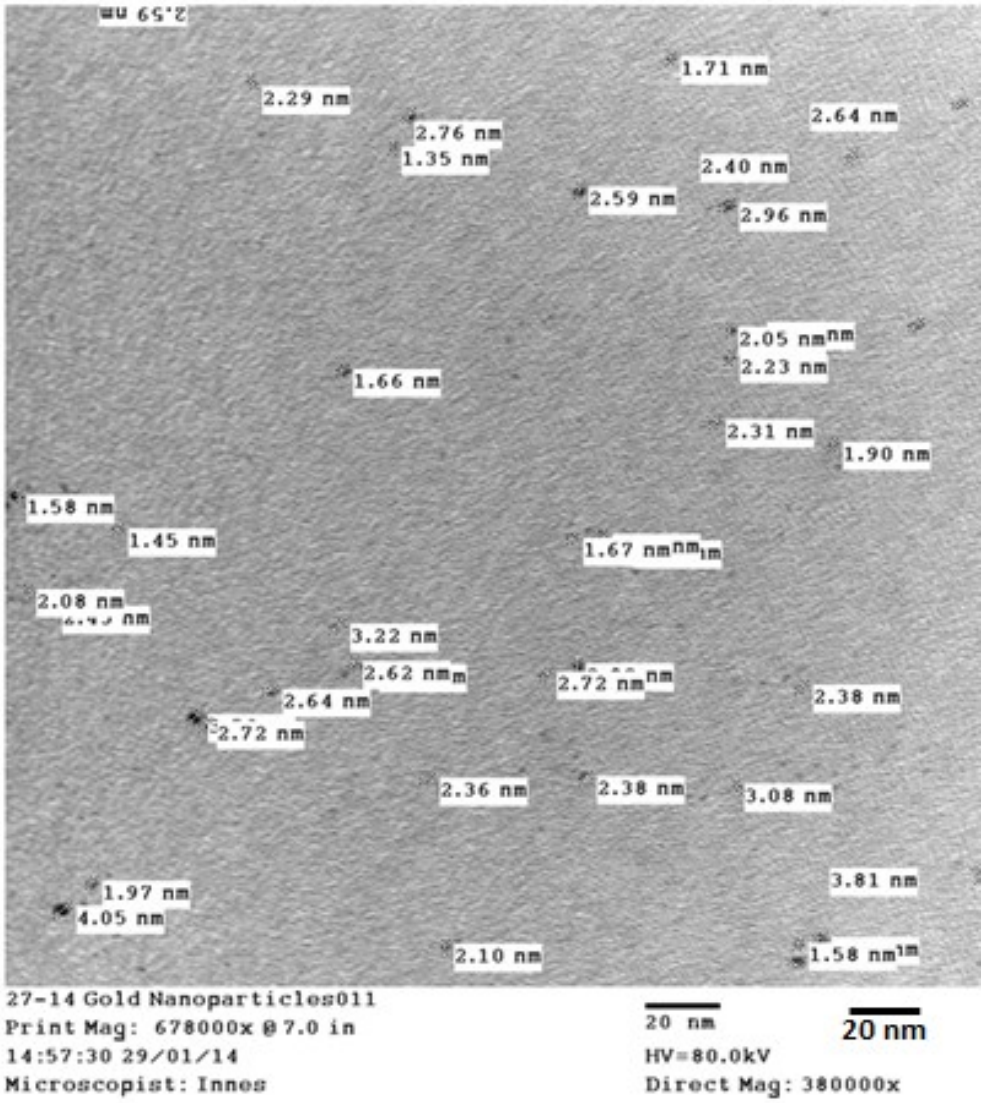

Figure 5.7*:* TEM images of the MSA-gold nanoparticle. Mean size of the 33 particles measured was 2.4nm (Range 1.35nm – 4.01nm, Standard deviation 0.6nm)(Ramesh et al., 2016)

5.4.2.3 Dot blot

The findings from the dot blot experiment are demonstrated in Figure 5.8. The three dots from left to right demonstrated serial dilutions of the MGF peptide, (1mg/l on the left with serial dilutions by x10) and the fourth dot was a scrambled sequence peptide. The findings confirmed binding of the MGF conjugated gold nanoparticles to the MGF peptide.

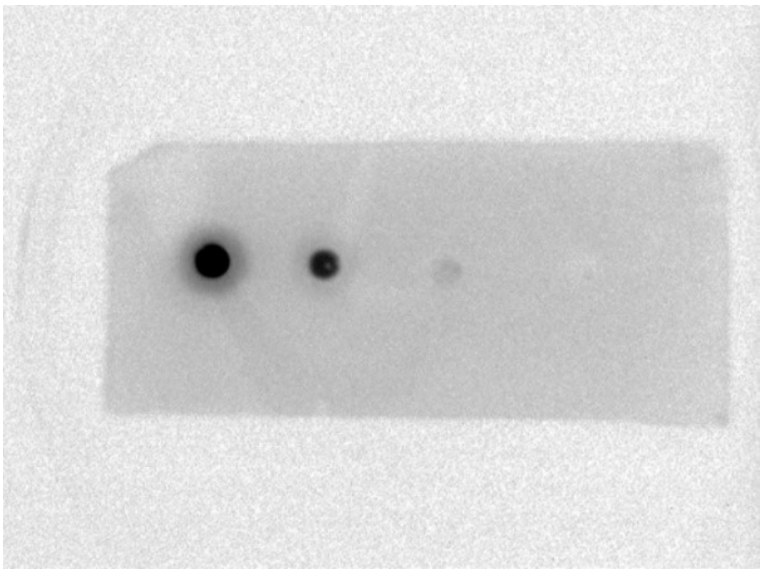

Figure 5.8*:* Dot blot at the left represent a dilution series of MGF peptides the third lighter dot corresponding to the lower concentration (1mg/l on the left with serial dilutions by x10). The fourth dot represents a control peptide (scrambled sequence)

5.4.2.4 MGF conjugated gold nanoparticles demonstrated binding to colon cancer cell lines

On viewing the cells under confocal microscopy, the positive control PC3 cell line demonstrated uniform binding of the anti-MGF-AuNP (Figure 5.9) while the negative control HUVEC cell line did not demonstrate evidence of binding of the MGF conjugated gold nanoparticles (Figure 5.9). Both colorectal cancer cell lines SW620 and HT29 demonstrated uniform fluorescence confirming binding to the MGF conjugated gold nanoparticles as illustrated in Figure 5.9. The application of the unconjugated gold nanoparticles did not demonstrate evidence of binding as demonstrated by the absence of fluorescence.

5.4.2.5 MGF conjugated gold nanoparticles demonstrated binding to colon cancer tissues

The MGF conjugated gold nanoparticles were identified by localising to the epithelial cell lining of my positive control of prostate cancer tissues (Figure 5.10). The normal colon tissues did not demonstrate evidence of binding to the MGF conjugated gold nanoparticles in three different sections (Figure 5.10), while the colon cancer tissues and polyp tissues demonstrated epithelial localisation of the MGF conjugated gold nanoparticles as illustrated in Figure 5.10. Unconjugated gold nanoparticles did not result in any fluorescence in three different sections of tissues, suggesting there was no binding.

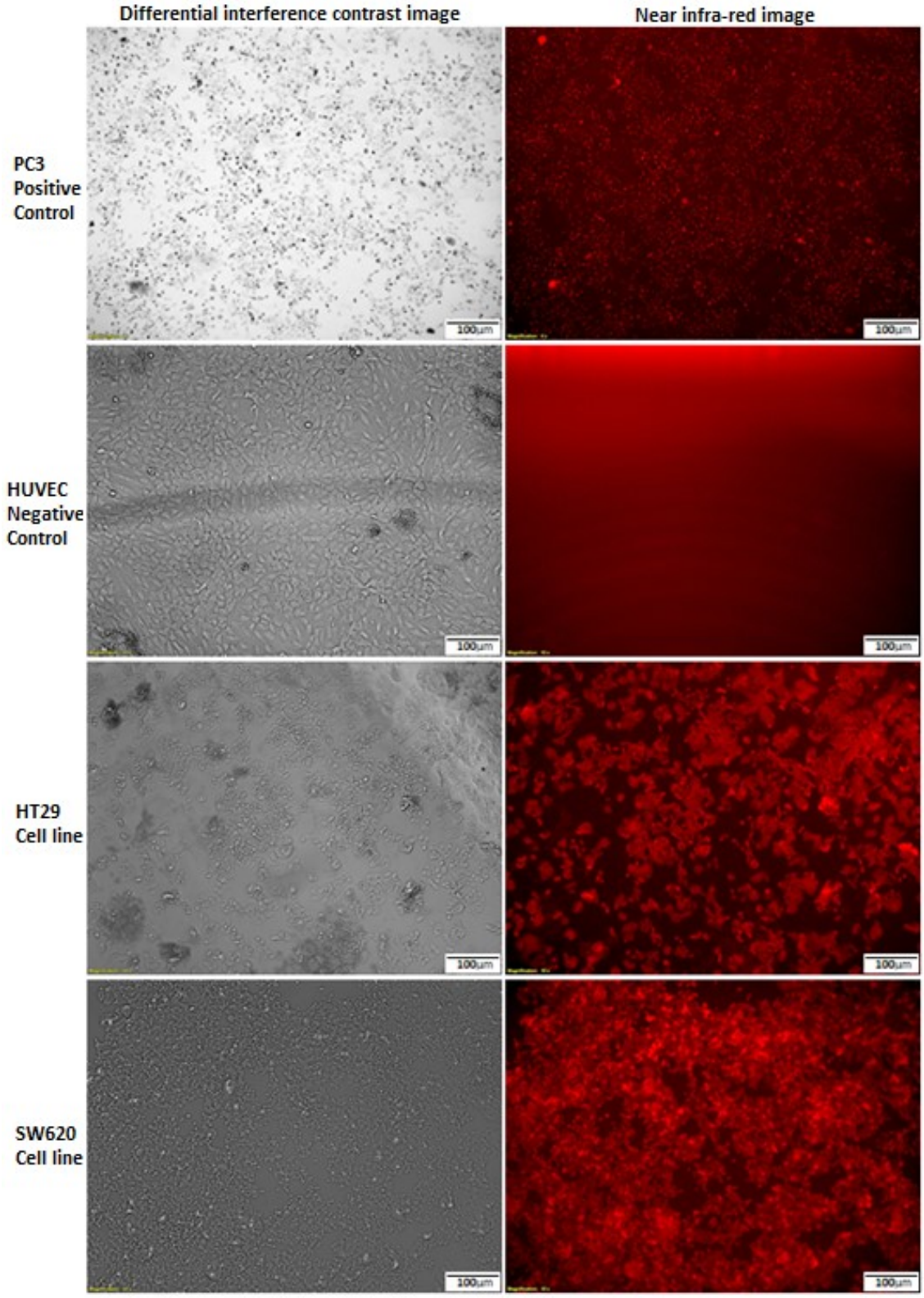

Figure 5.9: A – PC3 cell line (positive control), B - HUVEC cell line (Negative control), C – HT29 cell line, D – SW620 cell line. Magnification 4x. Fluorescence of the gold nanoparticles was identified in the positive control PC3 cell line and the colorectal cancer cell lines HT29 and SW620 while this was absent in the negative control HUVEC line.

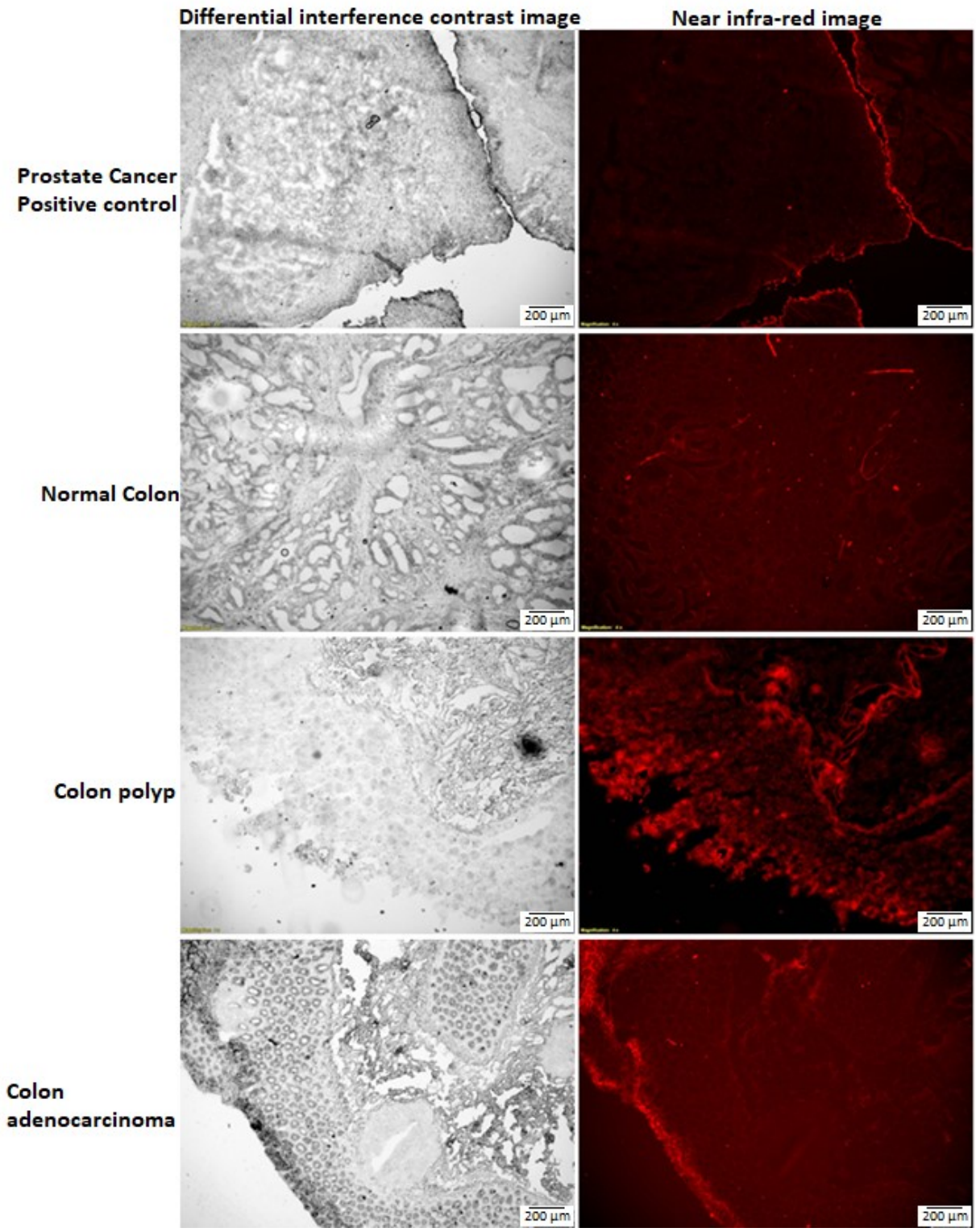

Figure 5.10: A – Prostate cancer tissues (positive control) B - Normal colon tissue C – Colon polyp D – Colon adenocarcinoma Magnification 20x. Fluorescence identified in the positive control of prostate cancer tissues, colonic polyp tissues and colonic adenocarcinoma tissues while this was absent in the normal colon tissues.

5.5 Discussion

5.5.1 Semiconductor quantum dot

CdTe quantum dots were produced via an aqueous synthesis route with a MSA coating rendering it water-soluble. This was synthesised via a one-pot synthesis route as recently described in the literature from our institution and others (Ghaderi et al., 2012; Wang et al., 2008; Ying et al., 2008). The advantages of this approach include the use the air-stable sodium tellurite, high yield and these quantum dots have demonstrated to be stable for many months when stored at 4^{o}C (Ying et al., 2008). The carbodiimide, 1-Ethyl-3-(3-dimethylamino propyl carbodiimide) hydrochloride (EDC) was used as an acylating agent to form covalent bonds between the MGF peptide and MGF antibody with the quantum dot. Carbidiimides are used to mediate the formation of amide linkages between the carboxylates and amines, and they are probably the most popular type of zero-length crosslinker in use for this purpose (Elzahhar et al., 2019; Kirchner et al., 2005). EDC was used to activate the carboxyl group in the MSA coating of the quantum dots, and thereafter conjugate to the amine groups on the MGF peptide and MGF antibody (Figure 5.1). Confirmation of this binding was performed with the use of atomic force microscopy to directly view the individual molecules and measure the size of the nanoparticles. Images of the Qd-MGF peptide and Qd-MGF antibody conjugates demonstrate two peaks adjacent to each other with the Qd peak likely to be the taller peak, and the peptide/antibody is the second peak. Compared to unconjugated quantum dots, there was a significant increase in the size of the quantum dot conjugated with the MGF peptide, though this was not demonstrated in the MGF antibody conjugated with the quantum dots (Table 5.1). Optical characterization of the quantum dots demonstrated a narrow emission spectrum of the conjugated and unconjugated quantum dots and a shift in the peak intensity of emission to the right (towards the NIR spectrum) for the conjugated

quantum dots compared to the unconjugated quantum dots. This is likely to be partly because of modifications to the quantum dot surface and increasing size. Since this shift was demonstrated, despite the unclear structural findings on atomic force microscopy, we proceeded to *in vitro* studies with these quantum dots.

The *in vitro* study demonstrated that the unconjugated quantum dots did not demonstrate any binding to the colon cancer cell lines. The quantum dot conjugated with the MGF peptide bound to both cell lines and the fluorescence was maintained a week later after the cell plates were stored at 4^{o}C. This demonstrated the excellent photobleaching threshold of the CdTe/MSA quantum dot despite undergoing the conjugation reaction. The quantum dot conjugate with the MGF antibody did not demonstrate binding to either of the colorectal cancer cell lines HT29 and SW620.. This was unexpected since the immunohistochemistry for MGF in the previous chapter clearly demonstrates MGF expression in colorectal cancer. In addition, preliminary western blot work (Appendix 8.1) suggested the expression of the MGF peptide in the HT29 and SW620 cell lines. The absence of binding of our MGF antibody-conjugated quantum dots may be due to the failure of this complex to enter the cytoplasm of the cells where MGF is known to be expressed (from our work and confirmed in prostate cancer cells by Savvani et al. (Savvani et al., 2013)) or the possibility that the antibody may have undergone a conformational change during the conjugation process. The latter hypothesis is supported by my second experiment when I incubated the cells with MGF peptide for 24 hours which should have bound to the same receptors as our Qd-MGF peptide conjugate, and the subsequent addition of the Qd-MGF antibody should have bound to the peptide unless it was internalised. Though EDC is the most popular method to conjugate these nanoparticles, there is a potential for side reactions to occur through the routes illustrated in

Figure 5.11 which has been identified to be potentially the reason for variability of using this for particular conjugation reactions (Elzahhar et al., 2019).

Overall, my work with the CdTe quantum dots had many limitations due to methodological issues. With the uncertainty of the characterization of the MGF antibody-conjugated quantum dots based on atomic force microscopy, further characterization using techniques such as dot blot to identify if this quantum dot would bind to MGF peptide would have been useful. The other significant limitation is the absence of the use of a positive control in the *in vitro* studies. Though the MGF peptide conjugated quantum dots demonstrated binding to the cell lines, my focus was for the MGF antibody conjugated nanoparticles since it is unclear as to whether MGF peptide has a unique receptor or binds to IGF1R as discussed in chapter 1.3.3, limiting its use. These issues were addressed in my work with gold nanoparticles, where I focused on MGF antibody conjugated gold nanoparticles as discussed below.

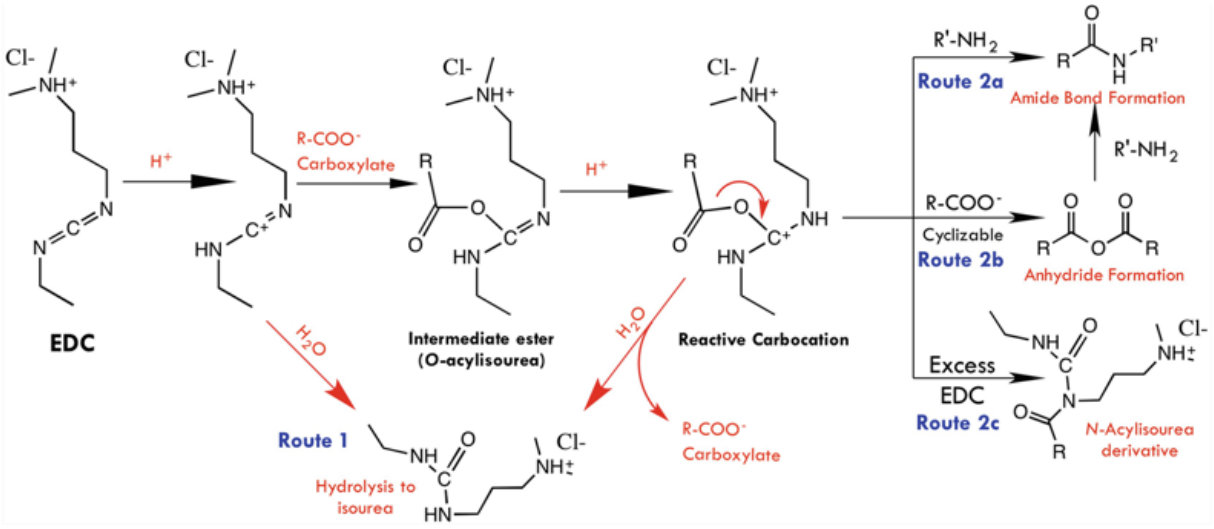

Figure 5.11*: EDC potential side reactions and their possible route(Elzahhar et al., 2019)*

5.5.2 Gold nanoparticles

We successfully designed gold quantum dots via an aqueous synthesis route by reducing gold salts with DMF and MSA rendering it water-soluble. This was synthesised with a one-pot synthesis route, and EDC was used as an acylating agent to form covalent bonds between the MGF antibody with the gold nanoparticles. EDC was used to activate the carboxyl group in the MSA and thereafter conjugate to the amine groups on the MGF antibody. Confirmation of this conjugation process was demonstrated with the use of dot blots. The absorbance spectrum of the MGF conjugated MSA-AuNPs was 375 nm to 630nm with a fluorescent emission peak at 800 nm in the near infra-red region which is vital for deep tissue penetration and is beyond the emission peak of the auto-fluorescence of epithelial tissues which has been demonstrated to be around 550nm (Wu and Qu, 2006).

Prostate cancer tissues and the PC3 cell line were used as a positive control following the work by the Department of Experimental Physiology at the University of Athens for the past few years which demonstrated the overexpression of MGF in both. (Armakolas et al., 2015, 2010; Philippou et al., 2013; Savvani et al., 2013). The MGF antibody conjugated gold quantum dots demonstrated uniform binding to the PC3 cell line, with no fluorescence demonstrated in the HUVEC endothelial cell line, which was used as a negative control. I used HUVEC as a negative control since previous literature had identified that endothelial cells including the HUVEC cell line, not stimulated by external growth factors, expressed minimal IGF-1 (Glazebrook et al., 1998; Hansson et al., 1987). Following this, I applied the MGF antibody conjugated gold nanoparticles to fixed HT29 and SW620 cells, with both cell lines demonstrating good fluorescence suggesting binding. No fluorescence was seen following application of unconjugated gold quantum dots.

The MGF antibody-conjugated quantum dots bound to the prostate cancer tissues in the epithelial lining as illustrated in Figure 5.10, while unconjugated gold quantum dots did not demonstrate any signals. This was similar to the immunohistochemistry images demonstrating MGF expression in prostate cancer tissues by Savvani et al. (Savvani et al., 2013). Colon cancer tissues demonstrated the MGF conjugated gold quantum dots bound to the epithelial layer of the tissues used here, while normal colon tissues did not show any fluorescence after being incubated with the MGF conjugated gold quantum dots. Colonic polyp tissues demonstrated similar findings to the colon cancer tissues with the MGF conjugated quantum dots binding to the epithelial layer of the polyp tissues. My findings suggest that MGF is expressed by colon cancer and colonic polyps and not by normal colon tissues. Colonic polyps are known precursor lesions for colon cancer via the 'adenoma-carcinoma' sequence, and the expression of MGF peptide in these lesions indicates that expression of MGF could be an early event in carcinogenesis.

My findings suggesting MGF expression in colon cancer is in contrast to Kasprzak et al. (Kasprzak et al., 2013, 2012) who published two reports in 2012 and 2013 on the expression of IGF-1 mRNA isoforms in colorectal cancers. Both papers reported findings of quantitative PCR for IGF-1 isoforms' mRNA and immunohistochemistry expression of IGF-1 peptide though not the IGF-1 isoforms. The first paper involved 13 tissue pairs of colorectal cancer and normal adjacent colon tissue with immunocytochemical studies demonstrating cellular expression of IGF-1 in 69% of patients, while control tissues did not demonstrate any significant expression. Expression of the IGF-1Ea isoform mRNA was the most prevalent, followed by IGF-1Eb mRNA and then IGF-1Ec (MGF). The overall expression of IGF-1 mRNA was significantly lower in the colorectal cancer tissues compared to control tissues; however the expression of IGF-1Ea mRNA was significantly higher in the cancer tissues compared to control. IGF-1Eb mRNA was

significantly lower in colorectal cancer tissues, and no significant differences were identified for IGF-1Ec mRNA compared to normal colon tissues. The second report by Kasprzak et al. (Kasprzak et al., 2013) investigatedtissue samples from 28 patients which included paired tumour and normal colorectal tissues. The immunocytochemical analysis of these tissues demonstrated IGF-1 protein expression in 50% of colorectal cancer tissues and 39% of control tissues with cytoplasmic expression. The intensity of the stain was of moderate density with no quantitative differences between the control tissues and cancer tissues. Expression of the different mRNA IGF-1 isoforms demonstrated significantly higher IGF-1Ea and IGF-1Eb compared to IGF-1Ec in both normal and tumour tissues. Comparison of colorectal cancer tissues and control tissues demonstrated significantly higher IGF-1Ea levels and significantly lower IGF-1eb levels in cancer tissues. IGF-1Ec mRNA levels were low for both cancer and control tissues and were significantly lower in cancer tissues. The inference from this work is that MGF does not appear to be overexpressed at the mRNA level in colorectal cancer tissues. However, the levels of IGF-1 isoforms peptide expression was not assessed in this work which could be a significant limitation of this study given the findings of Durzynskat et al. (Durzyńska and Barton, 2014a) who demonstrate a complete discordance between mRNA expression of IGF-1 isoforms and expression of the IGF-1 isoform peptides in cell lines. Durzynksa et al (Durzyńska and Barton, 2014a) published interesting data for the expression of IGF-1 isoforms in the mRNA level using quantitative real-time PCR (qRT-PCR) and expression at the protein level of each isoform using immunoblotting for four cell lines including HeLa (cervical adenocarcinoma), U20S (osteosarcoma), HepG2 (Hepatocellular adenocarcinoma) and K562 (human myelogenous leukaemia). There was a complete discordance between the RNA and protein expression for the isoforms. IGF-1Ea, in its transcript form, was expressed significantly higher in the K562 cell line compared to other cell lines, while IGF-1Ea protein was highest in

the HeLa cells in which its transcript expression was significantly lower. Similarly, IGF-1Eb expression in HepG2 and K562 cells were reversed with regards to transcript and protein levels. IGF-1Ec protein expression was not achieved due to very low expression in all the cell lines utilised. This study reflected the likely crucial role for post translational processing of mRNA affecting peptide production and confirms the limitations of using transcript levels as a surrogate measure of gene expression. Control of translation has a physiological role in cells to enable the cell to adapt swiftly to stress conditions by controlling protein synthesis from an existing pool of mRNAs (Vaklavas et al., 2017). Dysregulation of translation has been confirmed to be a critical nexus for cancer cells to enable cancer cells to overcome the array of stress conditions including that of the tumor microenvironment, immune recognition and anti-tumor therapies (Vaklavas et al., 2017).

In summary, I describe the synthesis, functionalization and characterization of MGF antibody conjugated gold nanoparticles. My findings suggest that MGF peptide is expressed by colon cancer cells, tissues and colonic polyps, and not expressed by normal colon tissues. The potential role for these gold nanoparticles would be in improving the endoscopic visualisation of colonic polyps and tumours (following intravenous administration of the gold nanoparticle), an alternative to tattooing malignant colorectal tumours (following local injection of the gold nanoparticle during the endoscopic procedure) and intraoperative delineation of the edges of the tumour to aid with determining the margins of resection.

Further work would require animal models of colorectal cancers and polyps, and investigating the use of intravenous injection of the MGF antibody conjugated gold nanoparticles. This model will then require to be tested with endoscopy and laparoscopy to identify the validity of the use of the gold nanoparticles for this purpose.

6 Chapter 6: The relationship between autophagy and apoptosis in colon cancer cells

Presented in the annual British Society of Surgical Oncology – Association of Cancer Surgery meeting in 2012. Abstract published:

P52. The role of autophagy in colorectal cancer cells: A pro-survival mechanism. Swethan Alagaratnam, Ajit Johnson, Marc Winslet, Alexander Seifalian, Barry Fuller, Shi-yu Yang

6.1 Introduction

Autophagy appears to have a contradictory dual role in cancer pathogenesis with a tumour suppressor role in its early stages by minimising DNA damage and promotes the survival of established tumour cells in situations of starvation. Chemotherapy agents used in colorectal cancer, including 5-FU, have been demonstrated to induce autophagy in colorectal cancer tissues, and this has been postulated to contribute towards increased drug resistance. IGF-1 has been demonstrated *in vitro* in colon cancer to inhibit autophagy and therefore improve the efficacy of 5-FU (Wang and Gu, 2018). The IGF-1 axis overall has, however, been identified to have a Janus-faced role with induction autophagy via the ERK pathway and inhibition autophagy via the Akt pathway (Table 1.6). Also, the role of the different isoforms of IGF-1 has not been clarified with regards to autophagy and cancer. To investigate this further, I describe preliminary in-vitro studies by inducing and confirming autophagy in a primary colorectal adenocarcinoma cell line (HT29) and a metastatic colorectal cell line (SW620). Following this, I investigated the effect of inhibiting autophagy with known autophagy inhibitors and assess its consequence on cell viability and apoptosis by assessing caspase. I used the p38 MAPK inhibitor SB203580 to induce autophagy and inhibited autophagy with Bafilomycin and 3-MA with the rationale for these agents explained in the discussion. This work has laid a platform for future work with treatment with the different isoforms of IGF-1 and assessing its effect on autophagy.

6.2 Aims

- Demonstrate a model of autophagy induction and inhibition in colorectal cancer cells and investigate its effects on apoptosis

6.3 Supplementary Methods

6.3.1 Cell viability assessment

Cell viability was measured by the addition of 20µl of CellTiter-Blue® dye to each well followed by incubation for 4 hours. The fluorescence was measured at 530nm with excitation at 620nm with 20ms integration time using a Thermo Labsystem Fluoroskan Ascent FL plate reader. SW620 cells at reducing known concentrations were used to standardize this test as outlined in Appendix 8.3.

6.3.2 Induction of autophagy in colorectal cancer cells by inhibition of p38 MAPK

HT29, SW620 colorectal cancer cells were seeded in chamber slides with a density of $1X10^5$ cells/cm^2 in DMEM containing 10% FBS and 1% PenStrep at 37^oC with 5% CO_2/ 95% air for 24 hours. After seeding, the medium was removed, followed by washing the cells three times with PBS and then exposed to the p38 MAPK inhibitor, SB203580 at 5, 10, 15 µM in DMEM containing 10% FBS and 1% PenStrep for 6, 12 24 and 48 hours at 37^oC with 5% CO_2/ 95% air respectively. Following the exposure, live images of autophagic cells were captured and stored using infinity capture software (Lumenera, Ottawa ON) under normal light microscopy.

6.3.3 Immunocyctochemistry

The cells were fixed with 4% paraformaldehyde at 4^oC for 10 minutes and blocked with 1% Bovine Serum Albumin/0.1% Tween 20 for 2 hours at room temperature. Cells were then incubated with polyclonal rabbit anti-human LC3B antibody (Abcam) at a 1:3000 dilution at 4 oC overnight. Following the incubation, cells were washed three times with PBS and the bonded primary antibodies were visualised with goat anti-rabbit horseradish peroxidase secondary antibody and VECTASTAIN ABC Kit. Immune staining images were captured and

stored using infinity capture software (Lumenera, Ottawa ON) under normal light microscopy with 20 (X) magnification.

6.3.4 Caspase activity assay

HT29, SW620 colorectal cancer cells were seeded in 96 well plates with a density of 20,000 cells/well in DMEM containing 10% FBS and 1% PenStrep at 37^{o}C with 5% CO_2/ 95% air for 24 hours. Following the seeding the medium was removed, cells were washed three times with PBS and then exposed to p38 MAPK inhibitors, (SB203580) with or without autophagy inhibitor (Bafilomycin A1) in DMEM containing 10% FBS and 1% PenStrep for 24 and 48 hours at 37^{o}C with 5% CO_2/ 95% air respectively. One group of cells was maintained in DMEM containing 10% FBS and 1% PenStrep without any addition as the control group. After treatment, caspase 3/7 activities measurement was performed with the Caspase-Glo assay kit (Promega, Madison USA). Briefly, the plates containing cells were removed from the incubator and allowed to equilibrate to room temperature for 1 hour. 100 µl of Caspase-Glo reagent was added to each well, and the contents of the wells were gently mixed with a plate shaker at 50g for 30 seconds. The plate was then incubated at room temperature for 40 minutes. The luminescence of each sample was measured in a plate-reading luminometer (Thermo Labsystems) with parameters of 1-minute lag time and 0.5 seconds/well read-time. The experiments were performed in triplicate and repeated on two separately-initiated cultures.

6.3.5 TEM

The HT29 cells were fixed in a solution containing 1.5% glutaraldehyde and 2% paraformaldehyde in PBS overnight. An automated tissue processor (Leica EM TP) was utilised to process the samples, culminating in each sample being embedded in Lemix (TAAB

Laboratories) epoxy resin. Semi-thin (1µm) sections were then cut and stained with 1% Toluidine Blue/1% borax and examined under light microscopy to determine the areas to be cut and processed for TEM. Ultrathin (70 nm) sections were stained with 2% aqueous uranyl acetate followed by Reynold's lead citrate and viewed using a Philips 201 TEM. Representative areas were photographed.

6.3.6 Statistical analysis

The data for the cell viability studies were examined and demonstrated a normal distribution. The results were expressed as mean±SEM with One-way ANOVA (Prism version 4 2004 edition, USA) with multiple comparison tests were used. Statistical analysis was performed on samples (n=4-6), and Bonferroni's Multiple Comparison Test was used post-hoc. $P < 0.05$ was considered as significant and indicated as *. Where $P < 0.01$ was considered as the higher significance and indicated as **. $P > 0.05$ is considered as not significant and marked as NS. Caspase assay results were assessed

6.3.7 Acknowledgement of work done by others

All experimental work in this chapter was done along with Ajit Johnson who was Professor Fuller's MSc student and Dr Shi-yu Yang.

6.4 Results

6.4.1 Induction of autophagy

Induction of autophagy in the HT29 cell line was initially confirmed by identifying the presence of the autophagic vacuoles with light microscopy. Induction of autophagy was noted to occur in a time and dose-depended manner by p38 MAPK inhibitors. After 6 hours treatment, minimal autophagic vacuoles were identified in the group which received lowest concentration (5µM) of SB203580 while small numbers of autophagic vacuoles appeared in

the cells exposed to the higher concentrations (10µM and 15µM) of SB203580. After 12 hours of treatment, smaller autophagic vacuoles appear in all treatments and following 24 and 48 hours of treatment, both the numbers and volumes of the autophagic vacuoles markedly increased in all treatments. The induction of autophagy by the P38 MAPK appeared to be an ongoing process demonstrated by the presence of co-existing small and large vacuoles in all the cell colonies (Figure 6.2).

To confirm autophagy was indeed undergoing in the cells following inhibition of p38 MAPK, the treated cells were subjected to the immunostaining with the anti-human LC3B antibody. LC3B is an autophagic marker used for monitoring autophagy in cancer cells [14]. The result of immunostaining (Figure 6.3) confirmed the induction of autophagy in the cells exposed to SB203580 in a time and dose-dependent manner. TEM was used to confirm the presence of autophagosomes to further validate the presence of autophagy in these cells (Figure 6.4).

Interestingly the use of the same concentrations of the P38 MAPK inhibitor did not demonstrate any observable induction of autophagy in the SW620 cell line over the same duration of incubation as the HT29 cells. Much higher doses of SB203580 (25µM) were required before much smaller presumed autophagic vacuoles were identified (Figure 6.5).

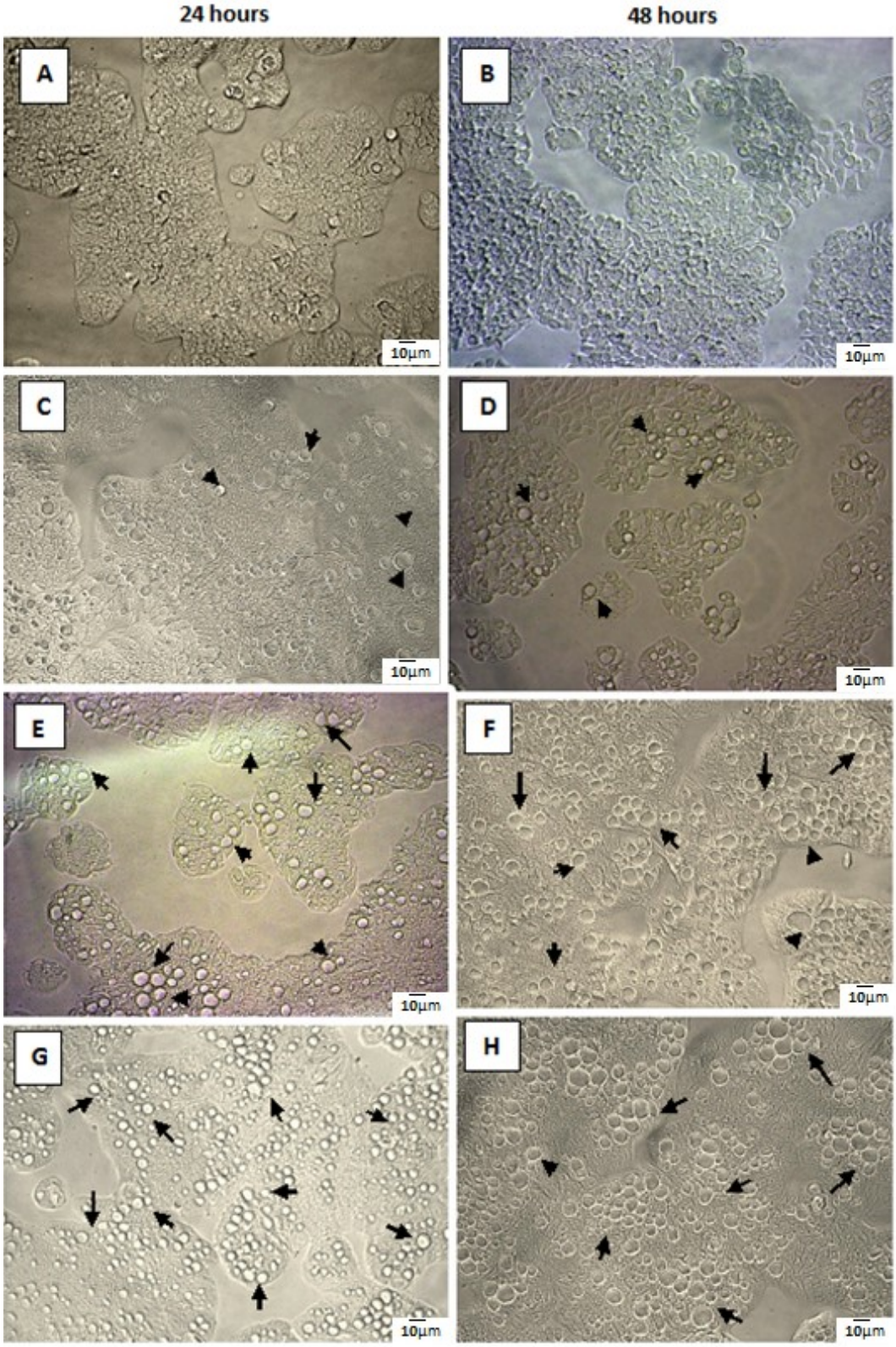

Figure 6.1*:* Light microscopy images of HT29 cells after induction of autophagy following treatment with SB203580 at 24 and 48 hours. A,B-control; C,D - 5µM SB203580; E,F - 10µM SB203580, GH - 15µM SB203580. Magnification 20x. Arrows indicating the autophagic vacuoles

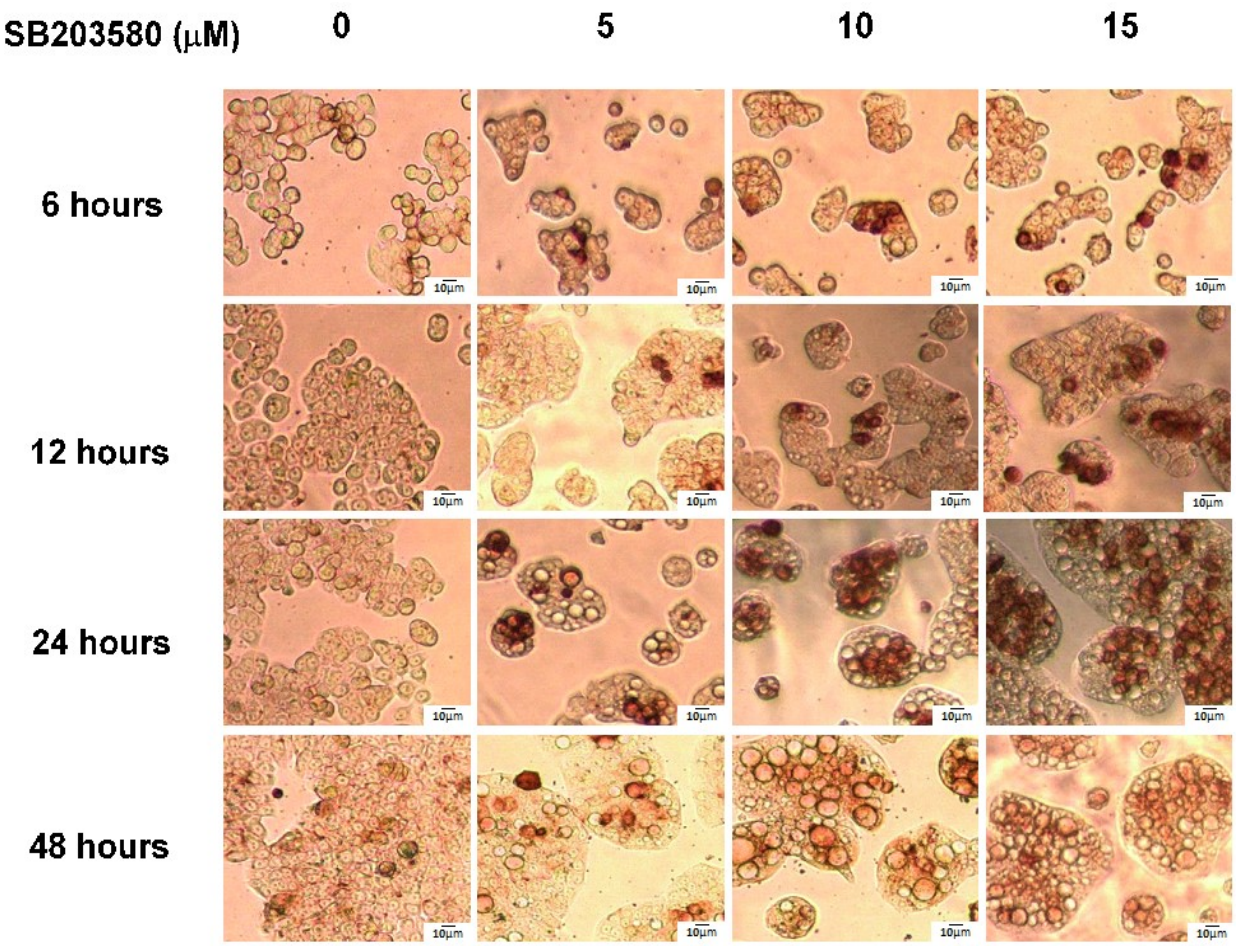

Figure 6.2*:* Immunocytochemistry for LC3B of induced autophagy in HT29 cells. Significant levels of Autophagy are observed in all treatment concentration using SB203580 after 24 hours. Magnification: 20x. Brown staining indicates positive autophagy vacuoles

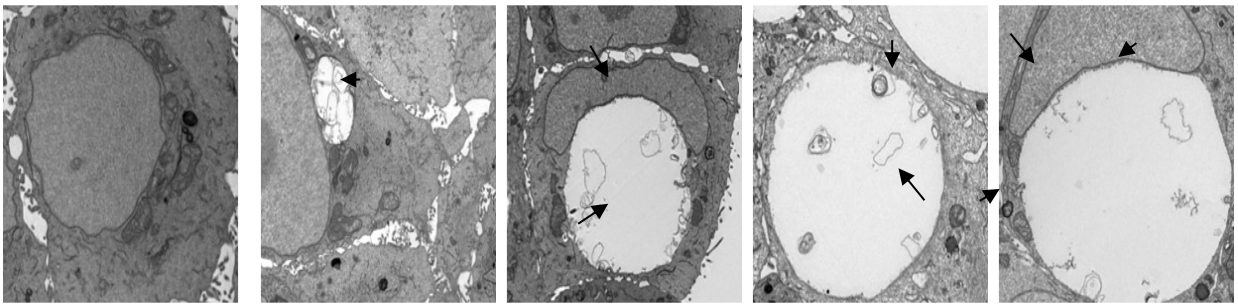

Figure 6.3*:* Electron Microscopy images showing the morphology of induced Autophagy. Arrow indicates autophagy vacuoles which appear to encompass the major part of the intracellular cell volume

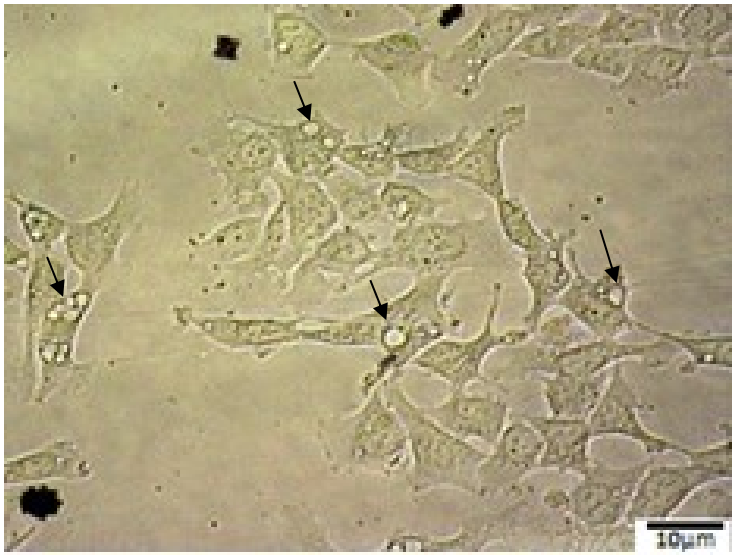

Figure 6.4*:* Autophagy induction and inhibition in SW620 cells: SB203580 (25µM) inducing autophagy; Arrow indicates positive autophagy vacuoles. Magnification x40

6.4.2 Effect of autophagy induction and inhibition on cell viability

The effect of autophagy and its inhibition on cell viability was assessed using the autophagy inducers (SB203580), and inhibitor (Bafilomycin A1 and 3-Methyladenine). In the HT29 cell line, induction of autophagy with SB203580 led to a significant increase in cell viability at 24 and 48 hours compared to the control cell group. The addition of Bafilomycin (5nM) to inhibit autophagy led to a significant decrease in the cell viability at 24 hours for the groups treated with 2.5µM, 5µM and 10µM of SB2030580 compared to groups only treated with SB2030580 at the same concentrations. At 48 hours, though the numbers of viable cells were lower in the autophagy inhibited group (with 5nM Bafilomycin), this difference was not significant in the lower concentrations of SB2030580. There remained a significant decrease in cell viability in the cells treated with higher concentrations of SB203580 (10 µM and 15 µM) (Figure 6.6). Figure 6.7 demonstrates the light microscopy images for the HT29 cells confirming the induction of autophagy with SB2030580, and inhibition of autophagy with the Bafilomycin A1. The incubation of HT29 cells with the autophagy inhibitors alone (Bafilomycin A1 and 3-

Methyladenine) did not lead to any significant differences in cell viability, thereby demonstrating no independent toxicity of these agents to the cell line. Overall, the findings suggest that the induction of autophagy led to increased cell viability, and its inhibition led to increased cell death in the HT29 cell line.

Induction of autophagy in the SW620 cell line using the same concentrations for the HT29 cell line (2.5µM, 5µM, 10µM and 15µM) did not demonstrate any differences in cell viability compared to control. Light microscopy did not demonstrate evidence of induction of autophagy at these concentrations. The addition of Bafilomycin A1 to these groups was mostly unremarkable apart from a significant increase in cell viability at the lowest dose of SB203580 (2.5µM) at 24 hours and a significant decrease in cell viability at 48 hours for the group treated with 10µM SB203580. The effect of treating the cells with autophagy inhibitors alone identified a significant increase in cell viability after 48 hours of incubation with Bafilomycin A1. This was not reproduced with the 3-Methyladenine group where no significant difference in cell viability was identified (Figure 6.8).

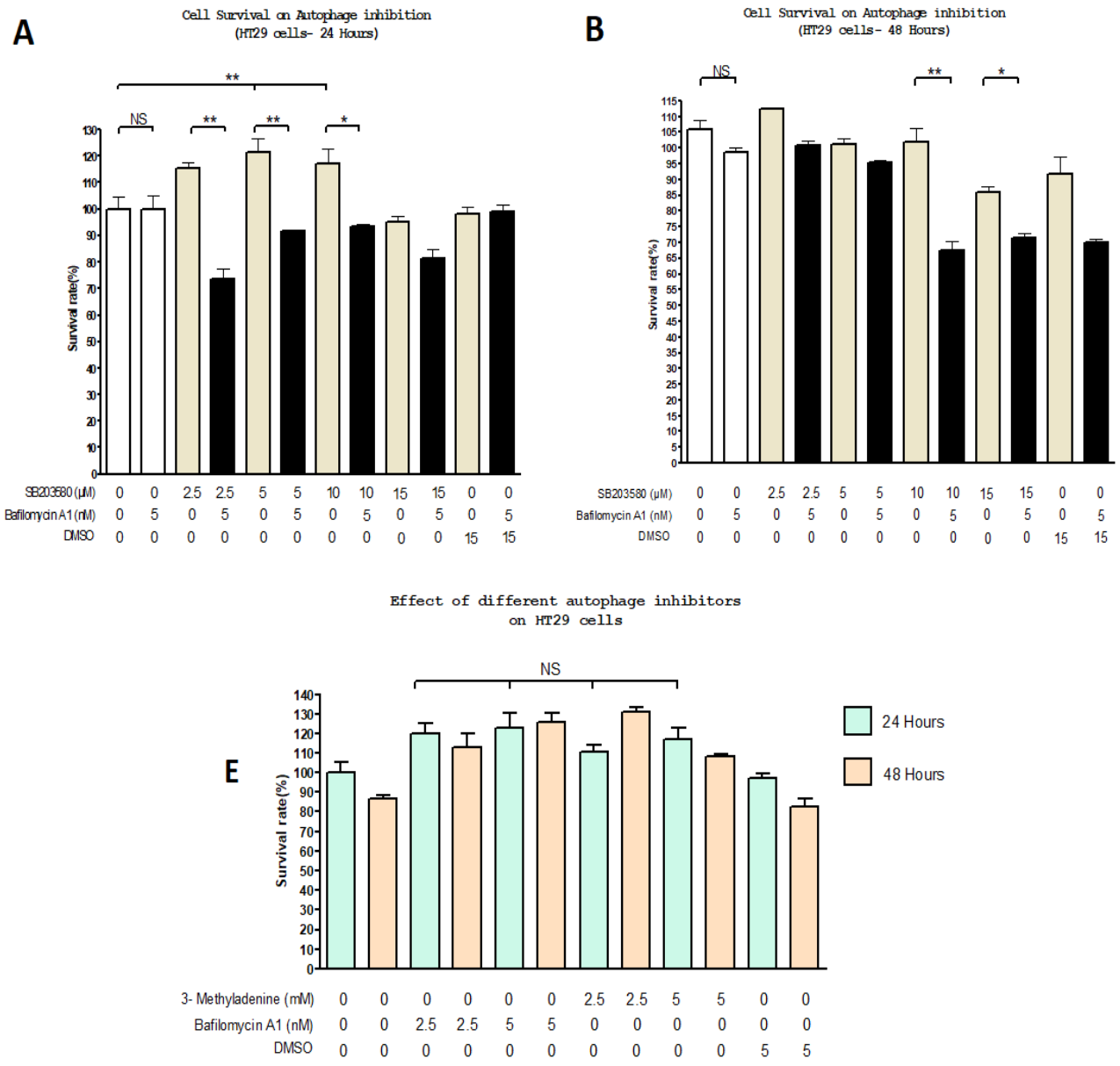

Figure 6.5*:* Effect of autophagy induction and inhibition on cell viability in HT29 cells at 24 and 48 hours: Cell viability was measured and is presented in relative percentage of viability to untreated cells (Y-axis). Measurements are depicted as means± SD- control and treated. ** represents P<0.01 and * represents P<0.05. NS represents Not-significant. A- HT29 cells, autophagy induced by SB203580 (Diff conc.); autophagy inhibited by Bafilomycin A1 (5nm) and cell viability measured at 24hrs. B- HT29 cells, autophagy induced by SB203580 (Diff conc.); autophagy inhibited by Bafilomycin A1 (5nm) and cell viability measured at 48hrs.C- HT29 cells, Different concentrations of two different inhibitors (Bafilomycin A1 and 3- Methyladenine) are used, and results are depicted for both 24 and 48hours. Both inhibitors have the same effect.

Incubation duration	24 hours	24 hours	48 hours	48 hours
Autophagy inhibitor (Bafilomycin)	0 nm	5 nm	0 nm	5 nm

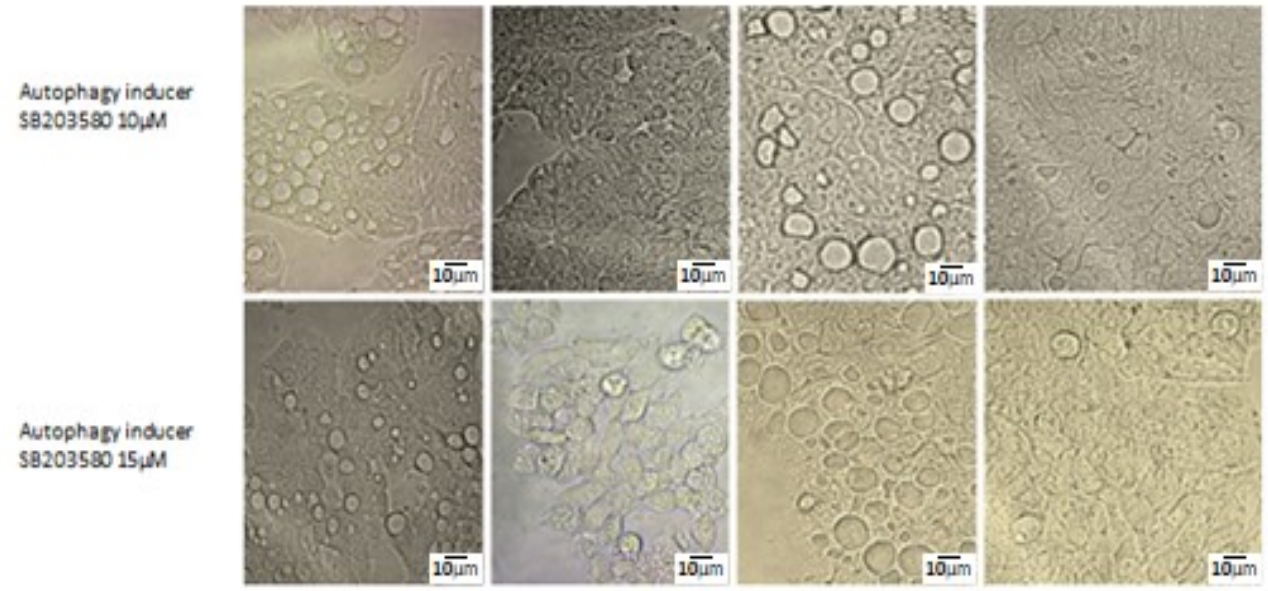

Figure 6.6*:* Light microscopy images for HT29 cells treated with the autophagy inducers, and with and without the addition of the autophagy inhibitor. Magnification 20x

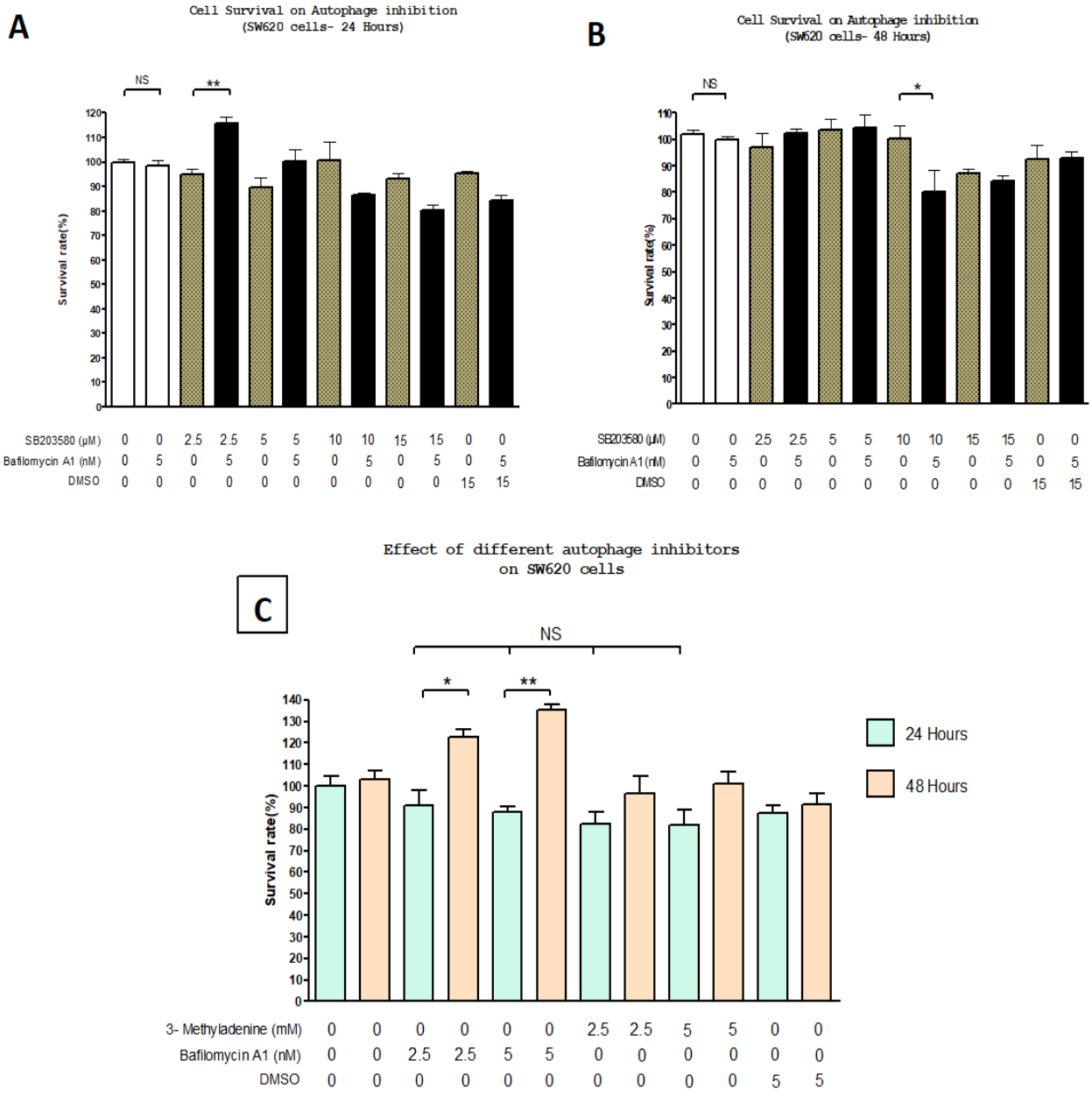

Figure 6.7*:* Effect of autophagy induction and inhibition on cell viability in SW620 cells at 24 and 48 hours: Cell viability was measured and is presented in relative percentage of viability to untreated cells (Y-axis). Measurements are depicted as means± SD- control and treated. ** represents P<0.01 and * represents P<0.05. NS represents Not-significant. A- SW620 cells, autophagy induced by SB203580 (Diff conc.); autophagy inhibited by Bafilomycin A1 (5nm) and cell viability measured at 24hrs. B- SW620 cells, autophagy induced by SB203580 (Diff conc.); autophagy inhibited by Bafilomycin A1 (5nm) and cell viability measured at 48hrs.C- SW620 cells, Different concentrations of two different inhibitors (Bafilomycin A1 and 3- Methyladenine) are used, and results are depicted for both 24 and 48hours. Both inhibitors have the same effect.

6.4.3 Effect of autophagy induction and inhibition of caspase 3 levels

The results from the caspase 3 assay of the HT29 cells treated with SB203580 compared to control cells and in combination with the autophagy inhibitors is illustrated in Figure 6.9 and Figure 6.10. At 24 hours, the levels appeared to be generally similar through the groups apart from slightly elevated caspase 3 activity in the Bafilomycin A1 only group. At 48 hours, the results were very different. The caspase 3 activity of the SB203580 only group were much lower than the control, and there was a fourfold higher level of caspase 3 activity in the group treated with SB203580 and Bafilomycin (autophagy inhibited) compared to the SB203580 (autophagy induced) group. Similarly, the levels were twice as high in the SB203580 + 3-Methyladenine (autophagy inhibited) group compared to SB203580 (autophagy induced group) only. The groups treated with just the autophagy inhibitors alone demonstrated very low levels of caspase 3 activity compared to the other groups.

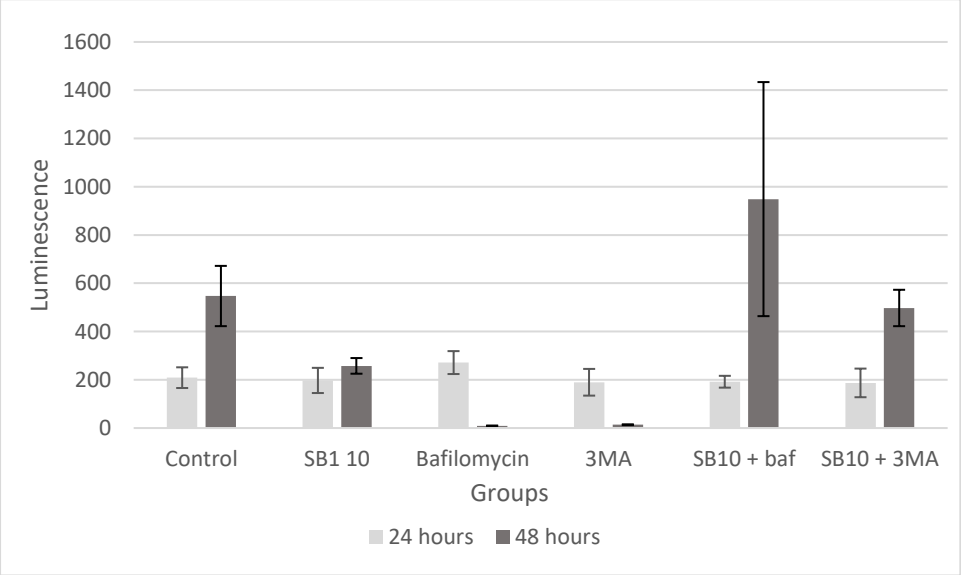

Figure 6.8*:* Caspase 3 activity. Significantly higher caspase activity at 48 hours identified in the autophagy inhibited groups (SB10+bafilomycin and SB10+3MA) compared to the control group. Very low levels of caspase 3 activity identified in the autophagy inhibitor only groups. ANOVA one way analysis between groups p=0.001 at 48 hours p=0.04 at 24 hours.

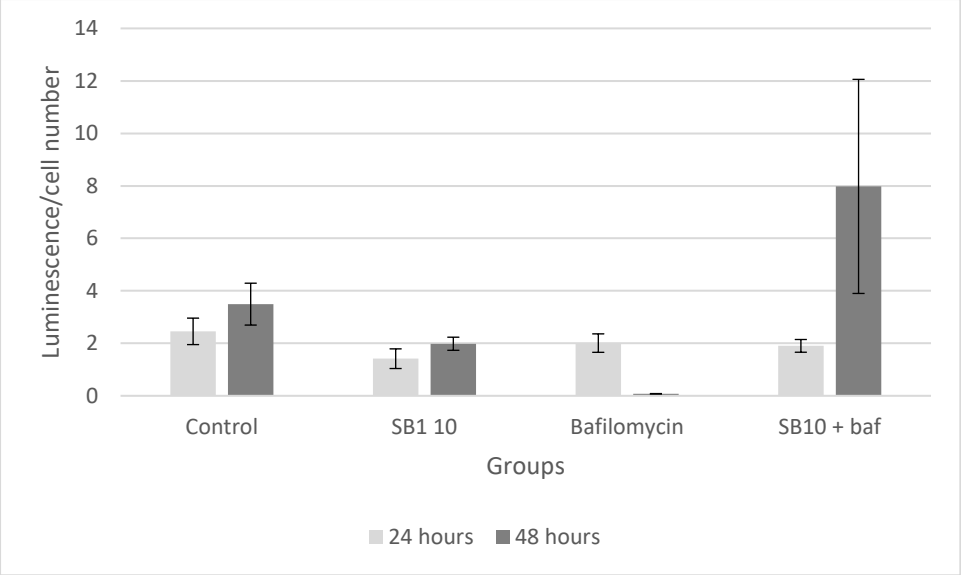

Figure 6.9*:* Caspase 3 activity standardised to cell numbers. Cell numbers data not available for 3MA. ANOVA one way analysis. 24 hours – p=0.001, 48 hours – p<0.001

6.5 Discussion

Induction of autophagy in the primary colon cancer cell line HT29 was achieved with SB203580. This was confirmed morphologically with light, and transmission electron microscopy and immunohistochemistry confirmed the presence of microtubule-associated protein light chain 3 (LC3). Autophagy was initially detected in 1950 using transmission electron microscopy, and the 3rd edition of the guidelines for the use and interpretation of assays for monitoring autophagy have reported this to be the only technique that shows autophagy in its complex cellular environment with subcellular resolution (Klionsky et al., 2016). In addition, this guideline promoted the use of immunohistochemistry for LC3B with TEM since LC3 can be localized in cellular structures other than autophagosomes (Klionsky et al., 2016). Following the demonstration of the autophagic vacuoles in the HT29 cell line, immunohistochemistry for LC3B confirmed its localization in the autophagic vacuoles. Autophagy induction was achieved with the use of SB203580, which is a p38 MAPK inhibitor used in other studies previously (Keil et al., 2013). We were unable to reproduce autophagy in the SW620 cell line at the same doses of SB203580. Almost double the concentration of

SB203580 was required to induce possible autophagy vacuoles in the SW620 cell line. The SW620 cell line is a metastatic colorectal lymph node derived cell line compared to HT29 which is a primary colonic tumour cell line, and it is possible that the metastatic cell line is more resistant to induction of autophagy or may undergo autophagy via other pathways.

Bafilomycin A1(predominantly) and 3-methyladenine were used as the autophagy inhibitors. Bafilomycin A1 is a macrolide antibiotic which specifically inhibits vacuolar H^+ATPase and therefore inhibits the fusion between the autophagosomes and the lysosomes inhibiting autophagy (Kanzawa et al., 2004). 3-Methyladenine is a Phosphoinositide 3-kinase inhibitor (Pi3K) which is has been widely used as an autophagy inhibitor but has been demonstrated to promote autophagy with prolonged treatment in nutrient-rich conditions (Yang et al., 2013). My work was focused predominantly on the HT29 cell line since the induction of autophagy with the SB203580 administration was confirmed in this cell line with TEM and immunohistochemistry. Cell viability assays demonstrated increased cell viability when autophagy was induced with SB203580 compared to the control cells in the HT29 cell line. The cells treated with SB203580 and Bafilomycin A1 demonstrated significantly reduced cell viability in 24 hours and 48 hours, suggesting that the inhibition of autophagy led to increased cell death. The administration of Bafilomycin A1 alone did not demonstrate any differences in cell viability compared to control groups. The absence of autophagosomes in the Bafilomycin group was confirmed with light microscopy. To further elucidate the underlying process causing reduced cell viability in the cells treated with SB203580 and Bafilomycin A1, I performed caspase 3 assays which demonstrated levels of caspase 3 activity to be almost 4 fold higher in the autophagy inhibited group compared to the autophagy induced group. This strongly suggests that inhibition of autophagy resulted in induction of apoptosis, leading to the increased cell death. We have demonstrated the pro-survival role of autophagy in the

primary colon cancer cell line HT29, and its inhibition leading to apoptosis, causing increased cell death. The clinical relevance to these findings is the previous identification of the induction of autophagy by 5-fluorouracil, which is a standard chemotherapy agent used in adjunctive therapy to reduce the risk of recurrence following surgery for colorectal cancer. Inhibition of autophagy, in what type of model? In vitro? has been demonstrated to improve the efficacy of 5-FU (Tang et al., 2016).

Interestingly, the cells treated with Bafilomycin A1 or 3-Methyladenine alone demonstrated very low caspase activity, though when used along with SB203580, there was an increase in the levels of caspase 3 activity compared to the control group. Both inhibitors work at different points on the autophagy pathway. Bafilomycin A1 is a late inhibitor preventing the binding of the lysosome to the autophagosome and inhibits lysosomal degradation. Yuan et al. (Yuan et al., 2015) investigated the effects of Bafilomycin A1 in B-cell acute lymphoblastic leukaemia and demonstrated Bafilomycin A1 induced apoptosis in a caspase-independent pathway. Similar findings were demonstrated by Yan et al. (Yan et al., 2016) in hepatocellular cancer cells where Bafilomycin A1 administration led to increased cell death via a non-caspase dependent apoptotic pathway. Both studies demonstrated a direct inhibition of growth with Bafilomycin A1 at concentrations that were similar to this study. Interestingly, I did not identify any direct cytotoxic effect of Bafilomycin A1 when used without the autophagy inhibitor leading us to hypothesise that colorectal cancer cells are more resistant to direct autophagic inhibition by Bafilomycin A1. The findings of independent administration 3-Methyladenine, causing a decrease in caspase 3 activity have not been described before. Li et al. (Li et al., 2009b) assessed the efficacy of 5-FU with and without 3-MA in HT29 cells and demonstrated increased cell death with dual therapy. They performed immunoblotting with antibodies to caspase 3 and demonstrated a slight increase in caspase 3 in the 3-MA only

treated cells compared to control cells and this finding was reproduced by Miki et al. (Miki et al., 2012) who detected cleaved caspase 3 levels by immunoblotting while investigating the effect of resveratrol in HT29 cells. This would be in sharp contrast to my findings in the HT29 cell line, where I identified caspase 3 activity to be much lower. Though the modality used to detect caspase 3 is very different from the other studies, this would require further studies to investigate this effect.

Overall, the findings have confirmed that autophagy induction in the primary colon cancer cell line HT29 acts as a pro-survival mechanism, and its inhibition results in increased cell death as a result of apoptosis. This is consistent with the recent literature in autophagy and provides the model for further work with the different isoforms of IGF-1, including MGF and investigating its effect on autophagy and cell viability.

7 Chapter 7: Summary of results

The primary objectives of this thesis were to investigate the expression of MGF, an isoform of IGF-1, and investigate the use of fluorescent nanoparticles in colorectal cancer. Further work in investigating autophagy and apoptosis in colorectal cancer was performed with a view towards further work investigating the role of MGF in inducing autophagy. The studies which were undertaken to achieve these objectives included:

- Quantitative immunohistochemistry of MGF expression in colon tissues including normal colon, colonic polyps and colon cancer and investigating its effect on recurrence.
- Synthesis, functionalization and conjugation of CdTe quantum dots to MGF antibody and peptide with application to colon cancer cell lines
- Synthesis, functionalization, conjugation and characterization of gold nanoparticles conjugated to MGF antibody with application to colon cancer cell lines and tissues to investigate the expression of MGF
- Developing a model for investigating the role of MGF in autophagy in colorectal cancer

Chapter 4:

Immunohistochemistry was performed on colorectal cancer tissues, colon polyp tissues and normal colon tissues after obtaining ethics approval from a regional (national run) ethics committee. The strength of the immunohistochemistry stain was quantified using Image J software with the IHC profiler plug-in. This plug-in was developed to semi quantify DAB/Haematoxylin stained tissues for immunohistochemistry and has been validated by other studies in the literature to be comparable to manual semi-quantitative measures such as using the H-score (Alrashdan et al., 2016; Ke et al., 2016; Rotoli et al., 2016; S. Zhang et al.,

2015). Immunohistochemistry was performed for MGF peptide in 16 patients with colorectal cancers including 9 patients affected by lymph node metastases at the time of presentation, 7 patients affected by lymph node-negative disease. Three patients in this cohort had distant metastases. In addition, I performed immunohistochemistry for MGF in 11 polyps, including those with high-grade dysplastic tubular adenomas (3), low/moderate-grade dysplastic tubular adenomas (5) and serrated adenomas (3). I found that MGF was overexpressed in colon cancer and colonic polyp tissues compared to normal colon tissues. The expression of MGF in high-grade dysplastic polyps was significantly higher than compared to low-grade dysplastic polyps and serrated adenomas. However, there were no differences in the expression between colon polyps and colon cancer tissues. At the time of presentation, lymph node-negative disease was associated with significantly higher expression of MGF peptide compared to lymph node-positive disease in the primary colon cancer tissues. MGF expression was not affected by the T stage or the M stage of the disease, and within the limits of the small numbers, MGF expression does not appear to be a prognostic factor for colon cancer with regards to recurrence.

Chapter 5:

Aqueous synthesis of a semiconductor quantum dot was achieved with a one-pot synthesis technique was performed, with an MSA coat to make these quantum dots water-soluble. EDC was used to conjugate the Mechanogrowth factor antibody and peptide to the quantum dots, and these quantum dots were characterized with the help of a NIR spectrometer, and morphologically with atomic force microscopy. Conjugation for the MGF peptide conjugated quantum dot was confirmed with AFM, but the MGF antibody-conjugated quantum appeared less likely to have been successfully conjugated with no significant increase in the dimensions

of the MGF-antibody conjugated quantum dot compared to the unconjugated quantum dots. The MGF peptide conjugated quantum dots demonstrated evidence of binding to the colon cancer cell lines, and the MGF antibody-conjugated quantum dots did not. The MGF antibody-conjugated quantum dots did not bind to the colon cancer cell lines despite the exogenous addition of the MGF peptide, leading us to suspect that the conjugation process is likely to have failed.

Following the issues with my MGF antibody conjugated CdTe quantum dots, I used gold nanoparticles to help elucidate and confirm the relationship between MGF expression and colon cancer. Aqueous synthesis of gold nanoparticles was performed with a one-pot technique, and these were capped with MSA and conjugated to the MGF antibody using EDC. Optical characterization with NIR spectroscopy demonstrated an emission peak at 800nm, and TEMs of these nanoparticles measured the size at 2nm. Given the issues with the CdTe quantum dots, dot blot experiments were used to confirm the ability of the anti-MGF-AuNP to bind to the MGF peptide. The anti-MGF-AuNP was applied to colon cancer cell lines using prostate cancer PC3 cell lines as a positive control since Armakolas et al. (Armakolas et al., 2010b) demonstrated MGF expression in this cell line. Uniform binding of the PC3 cell line was demonstrated with the anti-MGF-AuNP, with similar findings in the colon cancer cell lines HT29 and SW620, while no fluorescence was demonstrated in the negative control HUVEC cell line which has known low IGF1 expression (Glazebrook et al., 1998; Hansson et al., 1987). The anti-MGF-AuNP was then applied to colonic tissues including normal colon, colonic polyp and colon adenocarcinoma tissues with the use of prostate cancer tissues as a positive control. This demonstrated fluorescence in the colonic polyp and adenocarcinoma tissues (similar to the positive control) with no fluorescence identified in the normal colon tissues. This study confirmed the findings of the immunohistochemistry work and the absence of

binding of the MGF antibody conjugated gold nanoparticles to normal colon tissues confirmed the deficient level of expression of MGF in these tissues. These gold nanoparticles can now be applied in-vivo studies and particularly with a view to improving the detection rates of polyps and cancers during colonoscopy.

Chapter 6:

Autophagy is a complex cellular mechanism with contradictory roles in carcinogenesis since it is presumed tumour suppressor role at the early stages, and then promotes tumour cell survival at the later stages. IGF-1 appears to induce autophagy via the ERK pathway and inhibit autophagy via the Akt/PI3K pathway. We investigated the relationship between autophagy and apoptosis in the HT29 cell line and demonstrated that induction of autophagy increased cell viability, and its inhibition led to increased cell death due to apoptosis confirmed with caspase 3 assays. This has provided us with a model to perform further work with the isoforms of IGF-1 including MGF to investigate a potential therapeutic role towards improving the efficacy of chemotherapy agents such as 5-Flououracil for which autophagy has been implicated in drug resistance.

8 Discussion and future directions

The increased expression of MGF in colonic polyps and cancer compared to normal colon tissues offers a target tissue accumulation by drug delivery agents and diagnostic agents. Based on my results, there does not appear to be a role for MGF to be a prognostic biomarker in colorectal cancer with no correlation between recurrent disease and metastatic disease and level of MGF expression. The similar levels of expression of MGF in colonic polyps, the precursor lesions for malignancy, and colonic cancer tissues implies that MGF overexpression is an early process in the cancer pathway. This provides a novel target for identification of polyps along with early and late stage malignancies. An area where this could be used effectively would be in improving colonoscopic identification of polyps and malignancies. Though colonoscopy remains the gold standard for identification of colorectal polyps and cancers, the current estimated missed rate of lesions has been estimated as high as 25% (Zhao et al., 2019). This has a significant consequence to patient care due to the subsequent risk of developing cancers and missed opportunities to resect lesions at an early stage with better outcomes for the patient. Work into adjuncts to help colonoscopic identification of lesions has been ongoing for many years and more recently nanoparticles such as a carbon and charcoal based nanoparticles have been investigated for their use to help improving colonoscopic outcomes targeting antigens such as the Thomsen-Friedenreich antigen as outlined in Table 2.10. Though the results are promising, they are yet to be used in routine clinical practice.

The use of fluorescent nanoparticles can help improve our ability for cancer diagnosis and treatments. Semiconductor quantum dots may be limited by their inherent cytotoxicity, however this does not preclude from their use in *ex-vivo* particularly in the assessment of tissue biopsies. Currently, immunohistochemical assessment of colorectal cancer tissues provide vital information with regards to the risks of recurrent cancer and the efficacy of

chemotherapy drugs. Quantum dot-based immunohistochemistry can provide the ability for multiple antigens to be assessed simultaneously using tissue biopsies thereby improving the efficiency of assessments and reducing the volume of tissue required. The possibility of quantifying the fluorescence generated by the quantum dots, given their superior fluorescence ability to organic dyes, will further improve the speed and efficacy of our immunohistological assessments. My work was unfortunately limited by inadequate characterization studies to confirm the successful conjugation of the MGF antibody to the CdTe quantum dot, but I was able to measure fluorescence using a spectrofluorometer and identify the level of fluorescence to correlate to the concentration of quantum dots present thereby offering an avenue for quantification.

Gold has been a treatment for inflammatory arthropathies for many decades with known self-limiting toxicity to the liver, and other side effects including pruritis ("Gold Preparations," 2012). Gold nanoparticles have been demonstrated to be safe to use in early phase clinical studies. The potential roles for the MGF conjugated gold nanoparticles are in improving the sensitivity of colonoscopy in colorectal polyps and cancer, and potentially aiding in the intraoperative identification of the colorectal tumour. The presumed role, which requires further work, will either via a solution to irrigate the colonic mucosa (similar to work done by Chen et al with silica nanoparticles (Chen et al., 2017)) or by an intravenous injection of the gold nanoparticles to enable them to preferentially accumulate in the colonic lesions (Similar to work done by Kolitz-Domb et al with polymer based nanoparticles (Kolitz-Domb et al., 2014)). The potential use for identification of a colonic tumour for minimally invasive surgical techniques with intravenous injection of the MGF conjugated gold nanoparticles will alleviate the need for the injection of 'tattoos' thereby avoiding its limitations such as inadvertent intraperitoneal injections affecting tissue planes, incorrect placement proximal to the tumour

and avoidance in rectal tumours. *Invivo* mice xenograft models would be the likely best next step to investigate the utility of the MGF conjugated gold nanoparticles for this role.

Finally, the effect of autophagy promoting resistance to chemotherapy agents makes this an importance cell process to target. IGF-1 has been demonstrated to both promote and inhibit autophagy via different pathways (Chapter 1.5.1). Therefore, it would be useful to identify the effect of MGF on autophagy to assess it if may have a potential therapeutic role in the improving chemotherapy efficacy. My work with HT29 cells has provided a model for this to be investigated. By using p38 kinase inhibitors, autophagy was induced and confirmed with TEM and immunohistochemistry for LC3B. Inhibition of autophagy with Bafilomycin and 3MA demonstrated an increase in caspase activity and reduced cell viability suggesting that inhibition of autophagy was associated with increased apoptosis. Further work would involve the administration of IGF-1Ec to the HT29 cell line in autophagy and assessing its effect on autophagy.

References

Adamo, M.L., Ben-Hur, H., LeRoith, D., Roberts, C.T., 1991. Transcription initiation in the two leader exons of the rat IGF-I gene occurs from disperse versus localized sites. Biochem. Biophys. Res. Commun. 176, 887–893.

Aebi, S., Kurdi-Haidar, B., Gordon, R., Cenni, B., Zheng, H., Fink, D., Christen, R.D., Boland, C.R., Koi, M., Fishel, R., Howell, S.B., 1996. Loss of DNA mismatch repair in acquired resistance to cisplatin. Cancer Res. 56, 3087–3090.

Akhtar, RizwanS., Latham, CeceliaB., Siniscalco, D., Fuccio, C., Roth, KevinA., 2007. Immunohistochemical Detection With Quantum Dots, in: Bruchez, MarcelP., Hotz, CharlesZ. (Eds.), Quantum Dots, Methods in Molecular Biology. Humana Press, pp. 11–28. https://doi.org/10.1385/1-59745-369-2:11

Alcaide, J., Funez, R., Rueda, A., Perez-Ruiz, E., Pereda, T., Rodrigo, I., Coveñas, R., Muñoz, M., Redondo, M., 2013. The role and prognostic value of apoptosis in colorectal carcinoma. BMC Clin. Pathol. 13, 24. https://doi.org/10.1186/1472-6890-13-24

Alexandraki, K.I., Philippou, A., Boutzios, G., Theohari, I., Koutsilieris, M., Delladetsima, I.K., Kaltsas, G.A., 2017. IGF-IEc expression is increased in secondary compared to primary foci in neuroendocrine neoplasms. Oncotarget 8, 79003–79011. https://doi.org/10.18632/oncotarget.20743

Ali, M.R.K., Rahman, M.A., Wu, Y., Han, T., Peng, X., Mackey, M.A., Wang, D., Shin, H.J., Chen, Z.G., Xiao, H., Wu, R., Tang, Y., Shin, D.M., El-Sayed, M.A., 2017. Efficacy, long-term toxicity, and mechanistic studies of gold nanorods photothermal therapy of cancer in xenograft mice. Proc. Natl. Acad. Sci. U. S. A. 114, E3110–E3118. https://doi.org/10.1073/pnas.1619302114

Al-Jamal, W.T., Al-Jamal, K.T., Tian, B., Cakebread, A., Halket, J.M., Kostarelos, K., 2009. Tumor targeting of functionalized quantum dot-liposome hybrids by intravenous administration. Mol. Pharm. 6, 520–530. https://doi.org/10.1021/mp800187d

Allegra, C.J., Jessup, J.M., Somerfield, M.R., Hamilton, S.R., Hammond, E.H., Hayes, D.F., McAllister, P.K., Morton, R.F., Schilsky, R.L., 2009. American Society of Clinical Oncology provisional clinical opinion: testing for KRAS gene mutations in patients with metastatic colorectal carcinoma to predict response to anti-epidermal growth factor receptor monoclonal antibody therapy. J. Clin. Oncol. Off. J. Am. Soc. Clin. Oncol. 27, 2091–2096. https://doi.org/10.1200/JCO.2009.21.9170

Allen, T.M., Brandeis, E., Hansen, C.B., Kao, G.Y., Zalipsky, S., 1995. A new strategy for attachment of antibodies to sterically stabilized liposomes resulting in efficient targeting to cancer cells. Biochim. Biophys. Acta 1237, 99–108.

Allison, J.E., Sakoda, L.C., Levin, T.R., Tucker, J.P., Tekawa, I.S., Cuff, T., Pauly, M.P., Shlager, L., Palitz, A.M., Zhao, W.K., Schwartz, J.S., Ransohoff, D.F., Selby, J.V., 2007. Screening for colorectal neoplasms with new fecal occult blood tests: update on performance characteristics. J. Natl. Cancer Inst. 99, 1462–1470. https://doi.org/10.1093/jnci/djm150

Alrashdan, M.S., Angel, C., Cirillo, N., McCullough, M., 2016. Smoking habits and clinical patterns can alter the inflammatory infiltrate in oral lichenoid lesions. Oral Surg. Oral Med. Oral Pathol. Oral Radiol. 121, 49–57. https://doi.org/10.1016/j.oooo.2015.08.020

Al-Sohaily, S., Biankin, A., Leong, R., Kohonen-Corish, M., Warusavitarne, J., 2012. Molecular pathways in colorectal cancer. J. Gastroenterol. Hepatol. 27, 1423–1431. https://doi.org/10.1111/j.1440-1746.2012.07200.x

Armakolas, A., Dimakakos, A., Loukogiannaki, C., Armakolas, N., Antonopoulos, A., Florou, C., Tsioli, P., Papageorgiou, E., Alexandrou, T.P., Stathaki, M., Spinos, D., Pektasides, D., Patsouris, E., Koutsilieris, M., 2018. IL-6 is associated to IGF-1Ec upregulation and Ec peptide secretion, from prostate tumors. Mol. Med. Camb. Mass 24, 6. https://doi.org/10.1186/s10020-018-0003-z

Armakolas, A., Kaparelou, M., Dimakakos, A., Papageorgiou, E., Armakolas, N., Antonopoulos, A., Petraki, C., Lekarakou, M., Lelovas, P., Stathaki, M., Psarros, C., Donta, I., Galanos, P.S., Msaouel, P., Gorgoulis, V.G., Koutsilieris, M., 2015. Oncogenic Role of the Ec Peptide of the IGF-1Ec Isoform in Prostate Cancer. Mol. Med. 21, 167–179. https://doi.org/10.2119/molmed.2014.00222

Armakolas, A., Philippou, A., Panteleakou, Z., Nezos, A., Sourla, A., Petraki, C., Koutsilieris, M., 2010a. Preferential expression of IGF-1Ec (MGF) transcript in cancerous tissues of human prostate: evidence for a novel and autonomous growth factor activity of MGF E peptide in human prostate cancer cells. The Prostate 70, 1233–1242. https://doi.org/10.1002/pros.21158

Armakolas, A., Philippou, A., Panteleakou, Z., Nezos, A., Sourla, A., Petraki, C., Koutsilieris, M., 2010b. Preferential expression of IGF-1Ec (MGF) transcript in cancerous tissues of human prostate: evidence for a novel and autonomous growth factor activity of MGF E peptide in human prostate cancer cells. The Prostate 70, 1233–1242. https://doi.org/10.1002/pros.21158

Ascenzi, F., Barberi, L., Dobrowolny, G., Bacurau, A.V.N., Nicoletti, C., Rizzuto, E., Rosenthal, N., Scicchitano, B.M., Musarò, A., 2019. Effects of IGF-1 isoforms on muscle growth and sarcopenia [WWW Document]. Aging Cell. https://doi.org/10.1111/acel.12954

Aswathy, R.G., Yoshida, Y., Maekawa, T., Kumar, D.S., 2010. Near-infrared quantum dots for deep tissue imaging. Anal. Bioanal. Chem. 397, 1417–1435. https://doi.org/10.1007/s00216-010-3643-6

Ates, K., Yang, S.Y., Orrell, R.W., Sinanan, A.C.M., Simons, P., Solomon, A., Beech, S., Goldspink, G., Lewis, M.P., 2007. The IGF-I splice variant MGF increases progenitor cells in ALS, dystrophic, and normal muscle. FEBS Lett. 581, 2727–2732. https://doi.org/10.1016/j.febslet.2007.05.030

Atkin, W.S., Morson, B.C., Cuzick, J., 1992. Long-term risk of colorectal cancer after excision of rectosigmoid adenomas. N. Engl. J. Med. 326, 658–662. https://doi.org/10.1056/NEJM199203053261002

Auría-Soro, C., Nesma, T., Juanes-Velasco, P., Landeira-Viñuela, A., Fidalgo-Gomez, H., Acebes-Fernandez, V., Gongora, R., Almendral Parra, M.J., Manzano-Roman, R., Fuentes, M., 2019. Interactions of Nanoparticles and Biosystems: Microenvironment of Nanoparticles and Biomolecules in Nanomedicine. Nanomater. Basel Switz. 9. https://doi.org/10.3390/nano9101365

Bahamonde, J., Brenseke, B., Chan, M.Y., Kent, R.D., Vikesland, P.J., Prater, M.R., 2018. Gold Nanoparticle Toxicity in Mice and Rats: Species Differences. Toxicol. Pathol. 46, 431–443. https://doi.org/10.1177/0192623318770608

Baker, J., Liu, J.P., Robertson, E.J., Efstratiadis, A., 1993. Role of insulin-like growth factors in embryonic and postnatal growth. Cell 75, 73–82.

Bao, H., Hao, N., Yang, Y., Zhao, D., 2010. Biosynthesis of biocompatible cadmium telluride quantum dots using yeast cells. Nano Res. 3, 481–489. https://doi.org/10.1007/s12274-010-0008-6

Beckwith, H., Yee, D., 2015. Minireview: Were the IGF Signaling Inhibitors All Bad? Mol. Endocrinol. 29, 1549–1557. https://doi.org/10.1210/me.2015-1157

Bendardaf, R., Lamlum, H., Pyrhönen, S., 2004. Prognostic and predictive molecular markers in colorectal carcinoma. Anticancer Res. 24, 2519–2530.

Bertero, L., Massa, F., Metovic, J., Zanetti, R., Castellano, I., Ricardi, U., Papotti, M., Cassoni, P., 2018. Eighth Edition of the UICC Classification of Malignant Tumours: an overview of the changes in the pathological TNM classification criteria-What has changed and why? Virchows Arch. Int. J. Pathol. 472, 519–531. https://doi.org/10.1007/s00428-017-2276-y

Beştaş, R., Kaplan, M.A., Işikdoğan, A., 2014. The correlation between serum VEGF levels and known prognostic risk factors in colorectal carcinoma. Hepatogastroenterology. 61, 267–271.

Bilan, R., Fleury, F., Nabiev, I., Sukhanova, A., 2015. Quantum dot surface chemistry and functionalization for cell targeting and imaging. Bioconjug. Chem. 26, 609–624. https://doi.org/10.1021/acs.bioconjchem.5b00069

Biomarkers Definitions Working Group., 2001. Biomarkers and surrogate endpoints: preferred definitions and conceptual framework. Clin. Pharmacol. Ther. 69, 89–95. https://doi.org/10.1067/mcp.2001.113989

Blum-Guzman, J.P., Wanderley de Melo, S., 2017. Location of colorectal cancer: colonoscopy versus surgery. Yield of colonoscopy in predicting actual location. Endosc. Int. Open 5, E642–E645. https://doi.org/10.1055/s-0043-110564

Bokemeyer, C., Bondarenko, I., Makhson, A., Hartmann, J.T., Aparicio, J., de Braud, F., Donea, S., Ludwig, H., Schuch, G., Stroh, C., Loos, A.H., Zubel, A., Koralewski, P., 2009. Fluorouracil, leucovorin, and oxaliplatin with and without cetuximab in the first-line treatment of metastatic colorectal cancer. J. Clin. Oncol. Off. J. Am. Soc. Clin. Oncol. 27, 663–671. https://doi.org/10.1200/JCO.2008.20.8397

Bokemeyer, C., Van Cutsem, E., Rougier, P., Ciardiello, F., Heeger, S., Schlichting, M., Celik, I., Köhne, C.-H., 2012. Addition of cetuximab to chemotherapy as first-line treatment for KRAS wild-type metastatic colorectal cancer: pooled analysis of the CRYSTAL and OPUS randomised clinical trials. Eur. J. Cancer Oxf. Engl. 1990 48, 1466–1475. https://doi.org/10.1016/j.ejca.2012.02.057

Boland, C.R., Goel, A., 2010. Microsatellite instability in colorectal cancer. Gastroenterology 138, 2073-2087.e3. https://doi.org/10.1053/j.gastro.2009.12.064

Bolocan, A., Ion, D., Ciocan, D.N., Paduraru, D.N., 2012. Prognostic and predictive factors in colorectal cancer. Chir. Buchar. Rom. 1990 107, 555–563.

Bowel cancer statistics [WWW Document], 2015. . Cancer Res. UK. URL http://www.cancerresearchuk.org/health-professional/cancer-statistics/statistics-by-cancer-type/bowel-cancer (accessed 9.29.16).

Bowers, L.W., Rossi, E.L., O'Flanagan, C.H., deGraffenried, L.A., Hursting, S.D., 2015. The Role of the Insulin/IGF System in Cancer: Lessons Learned from Clinical Trials and the Energy Balance-Cancer Link. Front. Endocrinol. 6, 77. https://doi.org/10.3389/fendo.2015.00077

Brisson, B.K., Barton, E.R., 2013. New Modulators for IGF-I Activity within IGF-I Processing Products. Front. Endocrinol. 4. https://doi.org/10.3389/fendo.2013.00042

Brisson, B.K., Barton, E.R., 2012. Insulin-like growth factor-I E-peptide activity is dependent on the IGF-I receptor. PloS One 7, e45588. https://doi.org/10.1371/journal.pone.0045588

Broll, R., Duchrow, M., Oevermann, E., Wellm, C., Schwandner, O., Schimmelpenning, H., Roblick, U.J., Bruch, H.P., Windhövel, U., 2001. p53 autoantibodies in sera of patients with a colorectal cancer and their association to p53 protein concentration and p53 immunohistochemistry in tumor tissue. Int. J. Colorectal Dis. 16, 22–27.

Brown, S.R., Baraza, W., Din, S., Riley, S., 2016. Chromoscopy versus conventional endoscopy for the detection of polyps in the colon and rectum. Cochrane Database Syst. Rev. 4, CD006439. https://doi.org/10.1002/14651858.CD006439.pub4

Broza, Y.Y., Har-Shai, L., Jeries, R., Cancilla, J.C., Glass-Marmor, L., Lejbkowicz, I., Torrecilla, J.S., Yao, X., Feng, X., Narita, A., Müllen, K., Miller, A., Haick, H., 2017. Exhaled Breath Markers for Nonimaging and Noninvasive Measures for Detection of Multiple Sclerosis. ACS Chem. Neurosci. 8, 2402–2413. https://doi.org/10.1021/acschemneuro.7b00181

Bruchez, M., Moronne, M., Gin, P., Weiss, S., Alivisatos, A.P., 1998. Semiconductor nanocrystals as fluorescent biological labels. Science 281, 2013–2016.

Brus, L.E., 1984. Electron–electron and electron-hole interactions in small semiconductor crystallites: The size dependence of the lowest excited electronic state. J. Chem. Phys. 80, 4403–4409. https://doi.org/10.1063/1.447218

Bui, M.H.T., Visapaa, H., Seligson, D., Kim, H., Han, K.-R., Huang, Y., Horvath, S., Stanbridge, E.J., Palotie, A., Figlin, R.A., Belldegrun, A.S., 2004. Prognostic value of carbonic anhydrase IX and KI67 as predictors of survival for renal clear cell carcinoma. J. Urol. 171, 2461–2466.

Burada, F., Nicoli, E.R., Ciurea, M.E., Uscatu, D.C., Ioana, M., Gheonea, D.I., 2015. Autophagy in colorectal cancer: An important switch from physiology to pathology. World J. Gastrointest. Oncol. 7, 271–284. https://doi.org/10.4251/wjgo.v7.i11.271

Byrne, J.D., Betancourt, T., Brannon-Peppas, L., 2008. Active targeting schemes for nanoparticle systems in cancer therapeutics. Adv. Drug Deliv. Rev. 60, 1615–1626. https://doi.org/10.1016/j.addr.2008.08.005

Cancer survival in England - Office for National Statistics [WWW Document], 2016. URL http://www.ons.gov.uk/peoplepopulationandcommunity/healthandsocialcare/conditionsanddiseases/bulletins/cancersurvivalinenglandadultsdiagnosed/2010and2014andfollowedupto2015#5-year-survival (accessed 9.29.16).

Carew, J.S., Medina, E.C., Esquivel, J.A., Mahalingam, D., Swords, R., Kelly, K., Zhang, H., Huang, P., Mita, A.C., Mita, M.M., Giles, F.J., Nawrocki, S.T., 2010. Autophagy inhibition enhances vorinostat-induced apoptosis via ubiquitinated protein accumulation. J. Cell. Mol. Med. 14, 2448–2459. https://doi.org/10.1111/j.1582-4934.2009.00832.x

Cargnello, M., Roux, P.P., 2011. Activation and Function of the MAPKs and Their Substrates, the MAPK-Activated Protein Kinases. Microbiol. Mol. Biol. Rev. MMBR 75, 50–83. https://doi.org/10.1128/MMBR.00031-10

Carpenter, V., Matthews, K., Devlin, G., Stuart, S., Jensen, J., Conaglen, J., Jeanplong, F., Goldspink, P., Yang, S.-Y., Goldspink, G., Bass, J., McMahon, C., 2008. Mechano-growth factor reduces loss of cardiac function in acute myocardial infarction. Heart Lung Circ. 17, 33–39. https://doi.org/10.1016/j.hlc.2007.04.013

Carro, E., Trejo, J.L., Núñez, A., Torres-Aleman, I., 2003. Brain repair and neuroprotection by serum insulin-like growth factor I. Mol. Neurobiol. 27, 153–162. https://doi.org/10.1385/MN:27:2:153

Cathomas, G., 2014. PIK3CA in Colorectal Cancer. Front. Oncol. 4. https://doi.org/10.3389/fonc.2014.00035

Champion, J.A., Katare, Y.K., Mitragotri, S., 2007. Particle shape: a new design parameter for micro- and nanoscale drug delivery carriers. J. Control. Release Off. J. Control. Release Soc. 121, 3–9. https://doi.org/10.1016/j.jconrel.2007.03.022

Champion, J.A., Mitragotri, S., 2006. Role of target geometry in phagocytosis. Proc. Natl. Acad. Sci. U. S. A. 103, 4930–4934. https://doi.org/10.1073/pnas.0600997103

Chan, W.-H., Shiao, N.-H., Lu, P.-Z., 2006. CdSe quantum dots induce apoptosis in human neuroblastoma cells via mitochondrial-dependent pathways and inhibition of survival signals. Toxicol. Lett. 167, 191–200. https://doi.org/10.1016/j.toxlet.2006.09.007

Chang, S.-C., Lin, J.-K., Lin, T.-C., Liang, W.-Y., 2005. Genetic alteration of p53, but not overexpression of intratumoral p53 protein, or serum p53 antibody is a prognostic factor in sporadic colorectal adenocarcinoma. Int. J. Oncol. 26, 65–75.

Chattoraj, S., Amin, A., Jana, B., Mohapatra, S., Ghosh, S., Bhattacharyya, K., 2016. Selective Killing of Breast Cancer Cells by Doxorubicin-Loaded Fluorescent Gold Nanoclusters: Confocal Microscopy and FRET. Chemphyschem Eur. J. Chem. Phys. Phys. Chem. 17, 253–259. https://doi.org/10.1002/cphc.201500982

Cheema, U., Brown, R., Mudera, V., Yang, S.Y., McGrouther, G., Goldspink, G., 2005. Mechanical signals and IGF-I gene splicing in vitro in relation to development of skeletal muscle. J. Cell. Physiol. 202, 67–75. https://doi.org/10.1002/jcp.20107

Chen, B., Liu, Q., Zhang, Y., Xu, L., Fang, X., 2008. Transmembrane delivery of the cell-penetrating peptide conjugated semiconductor quantum dots. Langmuir ACS J. Surf. Colloids 24, 11866–11871. https://doi.org/10.1021/la802048s

Chen, D., Li, B., Cai, S., Wang, P., Peng, S., Sheng, Y., He, Y., Gu, Y., Chen, H., 2016. Dual targeting luminescent gold nanoclusters for tumor imaging and deep tissue therapy. Biomaterials 100, 1–16. https://doi.org/10.1016/j.biomaterials.2016.05.017

Chen, H., Li, Shulan, Li, B., Ren, X., Li, Shengnan, Mahounga, D.M., Cui, S., Gu, Y., Achilefu, S., 2012. Folate-modified gold nanoclusters as near-infrared fluorescent probes for tumor imaging and therapy. Nanoscale 4, 6050–6064. https://doi.org/10.1039/C2NR31616A

Chen, L.-D., Liu, J., Yu, X.-F., He, M., Pei, X.-F., Tang, Z.-Y., Wang, Q.-Q., Pang, D.-W., Li, Y., 2008. The biocompatibility of quantum dot probes used for the targeted imaging of hepatocellular carcinoma metastasis. Biomaterials 29, 4170–4176. https://doi.org/10.1016/j.biomaterials.2008.07.025

Chen, N.-T., Souris, J.S., Cheng, S.-H., Chu, C.-H., Wang, Y.-C., Konda, V., Dougherty, U., Bissonnette, M., Mou, C.-Y., Chen, C.-T., Lo, L.-W., 2017. Lectin-Functionalized Mesoporous Silica Nanoparticles for Endoscopic Detection of Premalignant Colonic Lesions. Nanomedicine Nanotechnol. Biol. Med. 13, 1941–1952. https://doi.org/10.1016/j.nano.2017.03.014

Chen, S.L., Bilchik, A.J., 2006. More extensive nodal dissection improves survival for stages I to III of colon cancer: a population-based study. Ann. Surg. 244, 602–610. https://doi.org/10.1097/01.sla.0000237655.11717.50

Chen, S.-Q., Zhang, H.-M., Li, J.-B., Jiang, H.-Y., Fan, L., Kong, L.-Z., Yao, S.-Z., 2014. Analyzing simultaneous positive expression of EZH2 and P53 protein to improve predictive value in cervical squamous cell carcinoma. Int. J. Gynecol. Cancer Off. J. Int. Gynecol. Cancer Soc. 24, 1653–1658. https://doi.org/10.1097/IGC.0000000000000273

Chen, Z., Li, Y., Zhang, C., Yi, H., Wu, C., Wang, J., Liu, Y., Tan, J., Wen, J., 2013. Downregulation of Beclin1 and Impairment of Autophagy in a Small Population of Colorectal Cancer. Dig. Dis. Sci. 58, 2887–2894. https://doi.org/10.1007/s10620-013-2732-8

Cho, D.-H., Jo, Y.K., Kim, S.C., Park, I.J., Kim, J.C., 2012. Down-regulated expression of ATG5 in colorectal cancer. Anticancer Res. 32, 4091–4096.

Choi, A.M.K., Ryter, S.W., Levine, B., 2013. Autophagy in Human Health and Disease. N. Engl. J. Med. 368, 651–662. https://doi.org/10.1056/NEJMra1205406

Choi, A.O., Brown, S.E., Szyf, M., Maysinger, D., 2008. Quantum dot-induced epigenetic and genotoxic changes in human breast cancer cells. J. Mol. Med. Berl. Ger. 86, 291–302. https://doi.org/10.1007/s00109-007-0274-2

Choi, H.S., Liu, W., Misra, P., Tanaka, E., Zimmer, J.P., Itty Ipe, B., Bawendi, M.G., Frangioni, J.V., 2007. Renal clearance of quantum dots. Nat. Biotechnol. 25, 1165–1170. https://doi.org/10.1038/nbt1340

Choi, J.H., Cho, Y.-S., Ko, Y.H., Hong, S.U., Park, J.H., Lee, M.A., 2014. Absence of autophagy-related proteins expression is associated with poor prognosis in patients with colorectal adenocarcinoma. Gastroenterol. Res. Pract. 2014, 179586. https://doi.org/10.1155/2014/179586

Choices, N.H.S., 2015. Bowel cancer screening - bowel scope screening - NHS Choices [WWW Document]. URL http://www.nhs.uk/conditions/bowel-cancer-screening/pages/bowel-scope-screening.aspx (accessed 9.29.16).

Christopoulos, P.F., Papageorgiou, E., Petraki, C., Koutsilieris, M., 2017. The COOH-terminus of the IGF-1Ec Isoform Enhances the Proliferation and Migration of Human MCF-7 Breast Cancer Cells. Anticancer Res. 37, 2899–2912.

Christopoulos, P.F., Philippou, A., Koutsilieris, M., 2015. Pattern of IGF-1 Variants' Expression in Human Cancer Cell Lines Using a Novel q-RT-PCR Approach. Anticancer Res. 35, 107–115.
Colorectal cancer: diagnosis and management | introduction | Guidance and guidelines | NICE [WWW Document], n.d. URL https://www.nice.org.uk/guidance/cg131/chapter/introduction (accessed 9.29.16).
Connor, E.E., Mwamuka, J., Gole, A., Murphy, C.J., Wyatt, M.D., 2005. Gold nanoparticles are taken up by human cells but do not cause acute cytotoxicity. Small Weinh. Bergstr. Ger. 1, 325–327. https://doi.org/10.1002/smll.200400093
Correa-Duarte, M.A., Giersig, M., Liz-Marzán, L.M., 1998. Stabilization of CdS semiconductor nanoparticles against photodegradation by a silica coating procedure. Chem. Phys. Lett. 286, 497–501. https://doi.org/10.1016/S0009-2614(98)00012-8
Cui, H., Hu, D., Zhang, J., Gao, G., Chen, Z., Li, W., Gong, P., Sheng, Z., Cai, L., 2017. Gold Nanoclusters–Indocyanine Green Nanoprobes for Synchronous Cancer Imaging, Treatment, and Real-Time Monitoring Based on Fluorescence Resonance Energy Transfer. ACS Appl. Mater. Interfaces 9, 25114–25127. https://doi.org/10.1021/acsami.7b06192
Dahabreh, I.J., Terasawa, T., Castaldi, P.J., Trikalinos, T.A., 2011. Systematic review: Anti-epidermal growth factor receptor treatment effect modification by KRAS mutations in advanced colorectal cancer. Ann. Intern. Med. 154, 37–49. https://doi.org/10.7326/0003-4819-154-1-201101040-00006
Dai, Z., Wu, F., Yeung, E.W., Li, Y., 2010. IGF-IEc expression, regulation and biological function in different tissues. Growth Horm. IGF Res. 20, 275–281. https://doi.org/10.1016/j.ghir.2010.03.005
Danhier, F., Feron, O., Préat, V., 2010. To exploit the tumor microenvironment: Passive and active tumor targeting of nanocarriers for anti-cancer drug delivery. J. Control. Release Off. J. Control. Release Soc. 148, 135–146. https://doi.org/10.1016/j.jconrel.2010.08.027
Daniels, T.R., Delgado, T., Rodriguez, J.A., Helguera, G., Penichet, M.L., 2006. The transferrin receptor part I: Biology and targeting with cytotoxic antibodies for the treatment of cancer. Clin. Immunol. Orlando Fla 121, 144–158. https://doi.org/10.1016/j.clim.2006.06.010
Davids, M.S., Letai, A., 2012. Targeting the B-Cell Lymphoma/Leukemia 2 Family in Cancer. J. Clin. Oncol. 30, 3127–3135. https://doi.org/10.1200/JCO.2011.37.0981
Davies, M., Arumugam, P.J., Shah, V.I., Watkins, A., Roger Morgan, A., Carr, N.D., Beynon, J., 2008. The clinical significance of lymph node micrometastasis in stage I and stage II colorectal cancer. Clin. Transl. Oncol. Off. Publ. Fed. Span. Oncol. Soc. Natl. Cancer Inst. Mex. 10, 175–179.
Denduluri, S.K., Idowu, O., Wang, Z., Liao, Z., Yan, Z., Mohammed, M.K., Ye, J., Wei, Q., Wang, J., Zhao, L., Luu, H.H., 2015. Insulin-like growth factor (IGF) signaling in tumorigenesis and the development of cancer drug resistance. Genes Dis. 2, 13–25. https://doi.org/10.1016/j.gendis.2014.10.004
Deng, M., Wang, Y., Zhang, B., Liu, P., Xiao, H., Zhao, J., 2012. New proangiogenic activity on vascular endothelial cells for C-terminal mechano growth factor. Acta Biochim. Biophys. Sin. 44, 316–322. https://doi.org/10.1093/abbs/gms012
Deng, M., Zhang, B., Wang, K., Liu, F., Xiao, H., Zhao, J., Liu, P., Li, Y., Lin, F., Wang, Y., 2011. Mechano growth factor E peptide promotes osteoblasts proliferation and bone-defect healing in rabbits. Int. Orthop. 35, 1099–1106. https://doi.org/10.1007/s00264-010-1141-2
Dequanter, D., VAN DE Velde, M., Bar, I., Nuyens, V., Rousseau, A., Nagy, N., Vanhamme, L., Vanhaeverbeek, M., Brohée, D., Delrée, P., Boudjeltia, K., Lothaire, P., Uzureau, P., 2016. Nuclear localization of glutamate-cysteine ligase is associated with proliferation in head and neck squamous cell carcinoma. Oncol. Lett. 11, 3660–3668. https://doi.org/10.3892/ol.2016.4458
Derfus, A.M., Chen, A.A., Min, D.-H., Ruoslahti, E., Bhatia, S.N., 2007. Targeted quantum dot conjugates for siRNA delivery. Bioconjug. Chem. 18, 1391–1396. https://doi.org/10.1021/bc060367e
Des Guetz, G., Schischmanoff, O., Nicolas, P., Perret, G.-Y., Morere, J.-F., Uzzan, B., 2009. Does microsatellite instability predict the efficacy of adjuvant chemotherapy in colorectal cancer? A systematic review with meta-analysis. Eur. J. Cancer Oxf. Engl. 1990 45, 1890–1896. https://doi.org/10.1016/j.ejca.2009.04.018
Di Nicolantonio, F., Martini, M., Molinari, F., Sartore-Bianchi, A., Arena, S., Saletti, P., De Dosso, S., Mazzucchelli, L., Frattini, M., Siena, S., Bardelli, A., 2008. Wild-type BRAF is required for response to panitumumab or cetuximab in metastatic colorectal cancer. J. Clin. Oncol. Off. J. Am. Soc. Clin. Oncol. 26, 5705–5712. https://doi.org/10.1200/JCO.2008.18.0786
Diagaradjane, P., Orenstein-Cardona, J.M., Colón-Casasnovas, N.E., Deorukhkar, A., Shentu, S., Kuno, N., Schwartz, D.L., Gelovani, J.G., Krishnan, S., 2008. Imaging epidermal growth factor receptor expression in vivo: pharmacokinetic and biodistribution characterization of a bioconjugated quantum

dot nanoprobe. Clin. Cancer Res. Off. J. Am. Assoc. Cancer Res. 14, 731–741. https://doi.org/10.1158/1078-0432.CCR-07-1958

Dickerson, E.B., Dreaden, E.C., Huang, X., El-Sayed, I.H., Chu, H., Pushpanketh, S., McDonald, J.F., El-Sayed, M.A., 2008. Gold nanorod assisted near-infrared plasmonic photothermal therapy (PPTT) of squamous cell carcinoma in mice. Cancer Lett. 269, 57–66. https://doi.org/10.1016/j.canlet.2008.04.026

Dienst, A., Grunow, A., Unruh, M., Rabausch, B., Nör, J.E., Fries, J.W.U., Gottstein, C., 2005. Specific occlusion of murine and human tumor vasculature by VCAM-1-targeted recombinant fusion proteins. J. Natl. Cancer Inst. 97, 733–747. https://doi.org/10.1093/jnci/dji130

Dluzniewska, J., Sarnowska, A., Beresewicz, M., Johnson, I., Srai, S.K.S., Ramesh, B., Goldspink, G., Górecki, D.C., Zabłocka, B., 2005. A strong neuroprotective effect of the autonomous C-terminal peptide of IGF-1 Ec (MGF) in brain ischemia. FASEB J. Off. Publ. Fed. Am. Soc. Exp. Biol. 19, 1896–1898. https://doi.org/10.1096/fj.05-3786fje

Dobrowolny, G., Giacinti, C., Pelosi, L., Nicoletti, C., Winn, N., Barberi, L., Molinaro, M., Rosenthal, N., Musarò, A., 2005. Muscle expression of a local Igf-1 isoform protects motor neurons in an ALS mouse model. J. Cell Biol. 168, 193–199. https://doi.org/10.1083/jcb.200407021

Doger, F.K., Meteoglu, I., Tuncyurek, P., Okyay, P., Cevikel, H., 2006. Does the EGFR and VEGF expression predict the prognosis in colon cancer? Eur. Surg. Res. Eur. Chir. Forsch. Rech. Chir. Eur. 38, 540–544. https://doi.org/10.1159/000096774

Duan, H., Nie, S., 2007. Etching Colloidal Gold Nanocrystals with Hyperbranched and Multivalent Polymers: A New Route to Fluorescent and Water-Soluble Atomic Clusters. J. Am. Chem. Soc. 129, 2412–2413. https://doi.org/10.1021/ja067727t

Duffy, A., Le, J., Sausville, E., Emadi, A., 2015. Autophagy modulation: a target for cancer treatment development. Cancer Chemother. Pharmacol. 75, 439–447. https://doi.org/10.1007/s00280-014-2637-z

Duffy, M.J., Lamerz, R., Haglund, C., Nicolini, A., Kalousová, M., Holubec, L., Sturgeon, C., 2014. Tumor markers in colorectal cancer, gastric cancer and gastrointestinal stromal cancers: European group on tumor markers 2014 guidelines update. Int. J. Cancer 134, 2513–2522. https://doi.org/10.1002/ijc.28384

Durzyńska, J., Barton, E., 2014a. IGF expression in HPV-related and HPV-unrelated human cancer cells. Oncol. Rep. 32, 893–900. https://doi.org/10.3892/or.2014.3329

Durzyńska, J., Barton, E., 2014b. IGF expression in HPV-related and HPV-unrelated human cancer cells. Oncol. Rep. 32, 893–900. https://doi.org/10.3892/or.2014.3329

EDC (1-ethyl-3-(3-dimethylaminopropyl)carbodiimide hydrochloride) - Thermo Fisher Scientific [WWW Document], n.d. URL https://www.thermofisher.com/order/catalog/product/22980 (accessed 10.2.16).

Elzahhar, P., Belal, A.S.F., Elamrawy, F., Helal, N.A., Nounou, M.I., 2019. Bioconjugation in Drug Delivery: Practical Perspectives and Future Perceptions, in: Weissig, V., Elbayoumi, T. (Eds.), Pharmaceutical Nanotechnology: Basic Protocols, Methods in Molecular Biology. Springer New York, New York, NY, pp. 125–182. https://doi.org/10.1007/978-1-4939-9516-5_11

Er, T.-K., Chen, C.-C., Bujanda, L., Herreros-Villanueva, M., 2014. Clinical relevance of KRAS mutations in codon 13: Where are we? Cancer Lett. 343, 1–5. https://doi.org/10.1016/j.canlet.2013.09.012

Erogbogbo, F., Yong, K.-T., Roy, I., Hu, R., Law, W.-C., Zhao, W., Ding, H., Wu, F., Kumar, R., Swihart, M.T., Prasad, P.N., 2011. In vivo targeted cancer imaging, sentinel lymph node mapping and multi-channel imaging with biocompatible silicon nanocrystals. ACS Nano 5, 413–423. https://doi.org/10.1021/nn1018945

Fact Sheets by Cancer [WWW Document], 2016. URL http://globocan.iarc.fr/Pages/fact_sheets_cancer.aspx (accessed 9.25.16).

Farooq, M.U., Novosad, V., Rozhkova, E.A., Wali, H., Ali, A., Fateh, A.A., Neogi, P.B., Neogi, A., Wang, Z., 2018. Gold Nanoparticles-enabled Efficient Dual Delivery of Anticancer Therapeutics to HeLa Cells. Sci. Rep. 8, 2907. https://doi.org/10.1038/s41598-018-21331-y

Fathollah, S., Mirpour, S., Mansouri, P., Dehpour, A.R., Ghoranneviss, M., Rahimi, N., Safaie Naraghi, Z., Chalangari, R., Chalangari, K.M., 2016. Investigation on the effects of the atmospheric pressure plasma on wound healing in diabetic rats. Sci. Rep. 6, 19144. https://doi.org/10.1038/srep19144

Fischer, C., Mazzone, M., Jonckx, B., Carmeliet, P., 2008. FLT1 and its ligands VEGFB and PlGF: drug targets for anti-angiogenic therapy? Nat. Rev. Cancer 8, 942–956. https://doi.org/10.1038/nrc2524

Fischer, H.C., Liu, L., Pang, K.S., Chan, W.C.W., 2006. Pharmacokinetics of Nanoscale Quantum Dots: In Vivo Distribution, Sequestration, and Clearance in the Rat. Adv. Funct. Mater. 16, 1299–1305. https://doi.org/10.1002/adfm.200500529

Fitzpatrick, J.A.J., Andreko, S.K., Ernst, L.A., Waggoner, A.S., Ballou, B., Bruchez, M.P., 2009. Long-term persistence and spectral blue shifting of quantum dots in vivo. Nano Lett. 9, 2736–2741. https://doi.org/10.1021/nl901534q

Folkman, J., 1971. Transplacental carcinogenesis by stilbestrol. N. Engl. J. Med. 285, 404–405. https://doi.org/10.1056/NEJM197108122850711

Fornaro, M., Hinken, A.C., Needle, S., Hu, E., Trendelenburg, A.-U., Mayer, A., Rosenstiel, A., Chang, C., Meier, V., Billin, A.N., Becherer, J.D., Brace, A.D., Evans, W.J., Glass, D.J., Russell, A.J., 2014. Mechano-growth factor peptide, the COOH terminus of unprocessed insulin-like growth factor 1, has no apparent effect on myoblasts or primary muscle stem cells. Am. J. Physiol. Endocrinol. Metab. 306, E150-156. https://doi.org/10.1152/ajpendo.00408.2013

Frangioni, J.V., Kim, S.-W., Ohnishi, S., Kim, S., Bawendi, M.G., 2007. Sentinel lymph node mapping with type-II quantum dots. Methods Mol. Biol. Clifton NJ 374, 147–159. https://doi.org/10.1385/1-59745-369-2:147

Fry, R., Maron, D., n.d. Colon and Rectum Robert D Fry NNM, David J Maron et al., in: Sabistan Textbook of Surgery, 19th Edition The Biological Basis of Modern Surgical Practice.

Galluzzi, L., Kepp, O., Kroemer, G., 2012. Mitochondria: master regulators of danger signalling. Nat. Rev. Mol. Cell Biol. 13, 780–788. https://doi.org/10.1038/nrm3479

Gao, S., Chen, D., Li, Q., Ye, J., Jiang, H., Amatore, C., Wang, X., 2014. Near-infrared fluorescence imaging of cancer cells and tumors through specific biosynthesis of silver nanoclusters. Sci. Rep. 4. https://doi.org/10.1038/srep04384

Gaponik, N., Talapin, D.V., Rogach, A.L., Hoppe, K., Shevchenko, E.V., Kornowski, A., Eychmüller, A., Weller, H., 2002. Thiol-Capping of CdTe Nanocrystals: An Alternative to Organometallic Synthetic Routes. J. Phys. Chem. B 106, 7177–7185. https://doi.org/10.1021/jp025541k

Gaumet, M., Vargas, A., Gurny, R., Delie, F., 2008. Nanoparticles for drug delivery: the need for precision in reporting particle size parameters. Eur. J. Pharm. Biopharm. Off. J. Arbeitsgemeinschaft Für Pharm. Verfahrenstechnik EV 69, 1–9. https://doi.org/10.1016/j.ejpb.2007.08.001

George, B., Kopetz, S., 2011. Predictive and prognostic markers in colorectal cancer. Curr. Oncol. Rep. 13, 206–215. https://doi.org/10.1007/s11912-011-0162-3

Ghaderi, S., Ramesh, B., Seifalian, A.M., 2012. Synthesis of mercaptosuccinic acid/MercaptoPolyhedral oligomeric silsesquioxane coated cadmium telluride quantum dots in cell labeling applications. J. Nanosci. Nanotechnol. 12, 4928–4935.

Glazebrook, H., Hatch, T., Brindle, N.P.J., 1998. Regulation of Insulin-Like Growth Factor-1 Expression in Vascular Endothelial Cells by the Inflammatory Cytokine Interleukin-1. J. Vasc. Res. 35. https://doi.org/10.1159/000025577

Godt, J., Scheidig, F., Grosse-Siestrup, C., Esche, V., Brandenburg, P., Reich, A., Groneberg, D.A., 2006. The toxicity of cadmium and resulting hazards for human health. J. Occup. Med. Toxicol. Lond. Engl. 1, 22. https://doi.org/10.1186/1745-6673-1-22

Goel, A., Nagasaka, T., Arnold, C.N., Inoue, T., Hamilton, C., Niedzwiecki, D., Compton, C., Mayer, R.J., Goldberg, R., Bertagnolli, M.M., Boland, C.R., 2007. The CpG island methylator phenotype and chromosomal instability are inversely correlated in sporadic colorectal cancer. Gastroenterology 132, 127–138. https://doi.org/10.1053/j.gastro.2006.09.018

Gold Preparations, 2012. , in: LiverTox: Clinical and Research Information on Drug-Induced Liver Injury. National Institute of Diabetes and Digestive and Kidney Diseases, Bethesda (MD).

Gonda, K., Miyashita, M., Higuchi, H., Tada, H., Watanabe, T.M., Watanabe, M., Ishida, T., Ohuchi, N., 2015. Predictive diagnosis of the risk of breast cancer recurrence after surgery by single-particle quantum dot imaging. Sci. Rep. 5, 14322. https://doi.org/10.1038/srep14322

Górecki, D.C., Beręsewicz, M., Zabłocka, B., 2007. Neuroprotective effects of short peptides derived from the Insulin-like growth factor 1. Neurochem. Int. 51, 451–458. https://doi.org/10.1016/j.neuint.2007.04.030

Gray, R.G., Quirke, P., Handley, K., Lopatin, M., Magill, L., Baehner, F.L., Beaumont, C., Clark-Langone, K.M., Yoshizawa, C.N., Lee, M., Watson, D., Shak, S., Kerr, D.J., 2011. Validation study of a quantitative multigene reverse transcriptase-polymerase chain reaction assay for assessment of recurrence risk in patients with stage II colon cancer. J. Clin. Oncol. Off. J. Am. Soc. Clin. Oncol. 29, 4611–4619. https://doi.org/10.1200/JCO.2010.32.8732

Green, M., Howman, E., 2005. Semiconductor quantum dots and free radical induced DNA nicking. Chem. Commun. 121–123. https://doi.org/10.1039/B413175D
Greene, F.L., Sobin, L.H., 2008. The staging of cancer: a retrospective and prospective appraisal. CA. Cancer J. Clin. 58, 180–190. https://doi.org/10.3322/CA.2008.0001
Greig, C.A., Hameed, M., Young, A., Goldspink, G., Noble, B., 2006. Skeletal muscle IGF-I isoform expression in healthy women after isometric exercise. Growth Horm. IGF Res. 16, 373–376. https://doi.org/10.1016/j.ghir.2006.09.005
Guastadisegni, C., Colafranceschi, M., Ottini, L., Dogliotti, E., 2010. Microsatellite instability as a marker of prognosis and response to therapy: a meta-analysis of colorectal cancer survival data. Eur. J. Cancer Oxf. Engl. 1990 46, 2788–2798. https://doi.org/10.1016/j.ejca.2010.05.009
Guével, X.L., Spies, C., Daum, N., Jung, G., Schneider, M., 2012. Highly fluorescent silver nanoclusters stabilized by glutathione: a promising fluorescent label for bioimaging. Nano Res. 5, 379–387. https://doi.org/10.1007/s12274-012-0218-1
Guo, W., Sun, X., Jacobson, O., Yan, X., Min, K., Srivatsan, A., Niu, G., Kiesewetter, D.O., Chang, J., Chen, X., 2015. Intrinsically radioactive [64Cu]CuInS/ZnS quantum dots for PET and optical imaging: improved radiochemical stability and controllable Cerenkov luminescence. ACS Nano 9, 488–495. https://doi.org/10.1021/nn505660r
Habeeb Muhammed, M.A., Verma, P.K., Pal, S.K., Retnakumari, A., Koyakutty, M., Nair, S., Pradeep, T., 2010. Luminescent Quantum Clusters of Gold in Bulk by Albumin-Induced Core Etching of Nanoparticles: Metal Ion Sensing, Metal-Enhanced Luminescence, and Biolabeling. Chem. – Eur. J. 16, 10103–10112. https://doi.org/10.1002/chem.201000841
Haggar, F.A., Boushey, R.P., 2009. Colorectal cancer epidemiology: incidence, mortality, survival, and risk factors. Clin. Colon Rectal Surg. 22, 191–197. https://doi.org/10.1055/s-0029-1242458
Hakim, M., Billan, S., Tisch, U., Peng, G., Dvrokind, I., Marom, O., Abdah-Bortnyak, R., Kuten, A., Haick, H., 2011. Diagnosis of head-and-neck cancer from exhaled breath. Br. J. Cancer 104, 1649–1655. https://doi.org/10.1038/bjc.2011.128
Hakuno, F., Takahashi, S.-I., 2018. IGF1 receptor signaling pathways. J. Mol. Endocrinol. 61, T69–T86. https://doi.org/10.1530/JME-17-0311
Han, H.-Y., Kim, H., Jeong, S.-H., Lim, D.-S., Ryu, M.H., 2014. Sulfasalazine induces autophagic cell death in oral cancer cells via Akt and ERK pathways. Asian Pac. J. Cancer Prev. APJCP 15, 6939–6944. https://doi.org/10.7314/apjcp.2014.15.16.6939
Han, Y., Xue, X.-F., Shen, H.-G., Guo, X.-B., Wang, X., Yuan, B., Guo, X.-P., Kuang, Y.-T., Zhi, Q.-M., Zhao, H., 2014. Prognostic significance of Beclin-1 expression in colorectal cancer: a meta-analysis. Asian Pac. J. Cancer Prev. APJCP 15, 4583–4587.
Hansson, H.A., Jennische, E., Skottner, A., 1987. Regenerating endothelial cells express insulin-like growth factor-I immunoreactivity after arterial injury. Cell Tissue Res. 250, 499–505.
Hauck, T.S., Anderson, R.E., Fischer, H.C., Newbigging, S., Chan, W.C.W., 2010. In vivo quantum-dot toxicity assessment. Small Weinh. Bergstr. Ger. 6, 138–144. https://doi.org/10.1002/smll.200900626
Helle, M., Cassette, E., Bezdetnaya, L., Pons, T., Leroux, A., Plénat, F., Guillemin, F., Dubertret, B., Marchal, F., 2012. Visualisation of Sentinel Lymph Node with Indium-Based near Infrared Emitting Quantum Dots in a Murine Metastatic Breast Cancer Model. PLoS ONE 7. https://doi.org/10.1371/journal.pone.0044433
Hembury, M., Chiappini, C., Bertazzo, S., Kalber, T.L., Drisko, G.L., Ogunlade, O., Walker-Samuel, S., Krishna, K.S., Jumeaux, C., Beard, P., Kumar, C.S.S.R., Porter, A.E., Lythgoe, M.F., Boissière, C., Sanchez, C., Stevens, M.M., 2015. Gold-silica quantum rattles for multimodal imaging and therapy. Proc. Natl. Acad. Sci. U. S. A. 112, 1959–1964. https://doi.org/10.1073/pnas.1419622112
Heneweer, C., Holland, J.P., Divilov, V., Carlin, S., Lewis, J.S., 2011. Magnitude of enhanced permeability and retention effect in tumors with different phenotypes: 89Zr-albumin as a model system. J. Nucl. Med. Off. Publ. Soc. Nucl. Med. 52, 625–633. https://doi.org/10.2967/jnumed.110.083998
Hernández-Breijo, B., Monserrat, J., Román, I.D., González-Rodríguez, Á., Fernández-Moreno, M.D., Lobo, M.V.T., Valverde, Á.M., Gisbert, J.P., Guijarro, L.G., 2013. Azathioprine desensitizes liver cancer cells to insulin-like growth factor 1 and causes apoptosis when it is combined with bafilomycin A1. Toxicol. Appl. Pharmacol. 272, 568–578. https://doi.org/10.1016/j.taap.2013.07.024
Hewish, M., Lord, C.J., Martin, S.A., Cunningham, D., Ashworth, A., 2010. Mismatch repair deficient colorectal cancer in the era of personalized treatment. Nat. Rev. Clin. Oncol. 7, 197–208. https://doi.org/10.1038/nrclinonc.2010.18

Hewitson, P., Glasziou, P., Watson, E., Towler, B., Irwig, L., 2008. Cochrane systematic review of colorectal cancer screening using the fecal occult blood test (hemoccult): an update. Am. J. Gastroenterol. 103, 1541–1549. https://doi.org/10.1111/j.1572-0241.2008.01875.x

Hill, M., Wernig, A., Goldspink, G., 2003. Muscle satellite (stem) cell activation during local tissue injury and repair. J. Anat. 203, 89–99. https://doi.org/10.1046/j.1469-7580.2003.00195.x

Hong, E.J., Choi, D.G., Shim, M.S., 2016. Targeted and effective photodynamic therapy for cancer using functionalized nanomaterials. Acta Pharm. Sin. B 6, 297–307. https://doi.org/10.1016/j.apsb.2016.01.007

Hou, W., Han, J., Lu, C., Goldstein, L.A., Rabinowich, H., 2010. Autophagic degradation of active caspase-8: a crosstalk mechanism between autophagy and apoptosis. Autophagy 6, 891–900. https://doi.org/10.4161/auto.6.7.13038

Hsu, C.-Y., Chen, C.-W., Yu, H.-P., Lin, Y.-F., Lai, P.-S., 2013. Bioluminescence resonance energy transfer using luciferase-immobilized quantum dots for self-illuminated photodynamic therapy. Biomaterials 34, 1204–1212. https://doi.org/10.1016/j.biomaterials.2012.08.044

HT-29 ATCC ® HTB-38™ Homo sapiens colon colorectal adenocar [WWW Document], 2019. URL https://www.lgcstandards-atcc.org/products/all/HTB-38.aspx (accessed 9.22.19).

Hu, Z., Qian, G., Müller, S., Xu, J., Saba, N.F., Kim, S., Chen, Z., Jiang, N., Wang, D., Zhang, H., Lane, K., Hoyt, C., Shin, D.M., Chen, Z.G., 2015. Biomarker quantification by multiplexed quantum dot technology for predicting lymph node metastasis and prognosis in head and neck cancer. Oncotarget. https://doi.org/10.18632/oncotarget.9225

Huang, X., Jain, P.K., El-Sayed, I.H., El-Sayed, M.A., 2007. Gold nanoparticles: interesting optical properties and recent applications in cancer diagnostics and therapy. Nanomed. 2, 681–693. https://doi.org/10.2217/17435889.2.5.681

Huh, J.W., Oh, B.R., Kim, H.R., Kim, Y.J., 2010. Preoperative carcinoembryonic antigen level as an independent prognostic factor in potentially curative colon cancer. J. Surg. Oncol. 101, 396–400. https://doi.org/10.1002/jso.21495

Hurwitz, H., Fehrenbacher, L., Novotny, W., Cartwright, T., Hainsworth, J., Heim, W., Berlin, J., Baron, A., Griffing, S., Holmgren, E., Ferrara, N., Fyfe, G., Rogers, B., Ross, R., Kabbinavar, F., 2004. Bevacizumab plus irinotecan, fluorouracil, and leucovorin for metastatic colorectal cancer. N. Engl. J. Med. 350, 2335–2342. https://doi.org/10.1056/NEJMoa032691

Hutchins, G., Southward, K., Handley, K., Magill, L., Beaumont, C., Stahlschmidt, J., Richman, S., Chambers, P., Seymour, M., Kerr, D., Gray, R., Quirke, P., 2011. Value of mismatch repair, KRAS, and BRAF mutations in predicting recurrence and benefits from chemotherapy in colorectal cancer. J. Clin. Oncol. Off. J. Am. Soc. Clin. Oncol. 29, 1261–1270. https://doi.org/10.1200/JCO.2010.30.1366

HUV-EC-C [HUVEC] ATCC ® CRL-1730™ Homo sapiens umbilical vei [WWW Document], 2019. URL https://www.lgcstandards-atcc.org/products/all/CRL-1730.aspx (accessed 9.22.19).

Iacopetta, B., Grieu, F., Amanuel, B., 2010. Microsatellite instability in colorectal cancer. Asia Pac. J. Clin. Oncol. 6, 260–269. https://doi.org/10.1111/j.1743-7563.2010.01335.x

Ivanecz, A., Kavalar, R., Palfy, M., Pivec, V., Sremec, M., Horvat, M., Potrč, S., 2014. Can we improve the clinical risk score? The prognostic value of p53, Ki-67 and thymidylate synthase in patients undergoing radical resection of colorectal liver metastases. HPB 16, 235–242. https://doi.org/10.1111/hpb.12089

Iyer, A.K., Khaled, G., Fang, J., Maeda, H., 2006. Exploiting the enhanced permeability and retention effect for tumor targeting. Drug Discov. Today 11, 812–818. https://doi.org/10.1016/j.drudis.2006.07.005

Jain, R.K., 1994. Barriers to drug delivery in solid tumors. Sci. Am. 271, 58–65.

Jass, J.R., 2004. HNPCC and sporadic MSI-H colorectal cancer: a review of the morphological similarities and differences. Fam. Cancer 3, 93–100. https://doi.org/10.1023/B:FAME.0000039849.86008.b7

Jiang, C., Zhong, Z., Liu, B., He, Z., Zou, J., Wang, L., Wang, J., Peng, J., Cao, Y., 2016. Coffee-Ring-Free Quantum Dot Thin Film Using Inkjet Printing from a Mixed-Solvent System on Modified ZnO Transport Layer for Light-Emitting Devices. ACS Appl. Mater. Interfaces. https://doi.org/10.1021/acsami.6b08679

Jiang, P., Mizushima, N., 2014. Autophagy and human diseases. Cell Res. 24, 69–79. https://doi.org/10.1038/cr.2013.161

Jin, T., Tiwari, D.K., Tanaka, S.-I., Inouye, Y., Yoshizawa, K., Watanabe, T.M., 2010. Antibody-protein A conjugated quantum dots for multiplexed imaging of surface receptors in living cells. Mol. Biosyst. 6, 2325–2331. https://doi.org/10.1039/c0mb00056f

Jing, X., Ye, Y., Bao, Y., Zhang, J., Huang, J., Wang, R., Guo, J., Guo, F., 2018. Mechano-growth factor protects against mechanical overload induced damage and promotes migration of growth plate chondrocytes through RhoA/YAP pathway. Exp. Cell Res. 366, 81–91. https://doi.org/10.1016/j.yexcr.2018.02.021

Juweid, M., Neumann, R., Paik, C., Perez-Bacete, M.J., Sato, J., van Osdol, W., Weinstein, J.N., 1992. Micropharmacology of monoclonal antibodies in solid tumors: direct experimental evidence for a binding site barrier. Cancer Res. 52, 5144–5153.

Kalyane, D., Raval, N., Maheshwari, R., Tambe, V., Kalia, K., Tekade, R.K., 2019. Employment of enhanced permeability and retention effect (EPR): Nanoparticle-based precision tools for targeting of therapeutic and diagnostic agent in cancer. Mater. Sci. Eng. C Mater. Biol. Appl. 98, 1252–1276. https://doi.org/10.1016/j.msec.2019.01.066

Kamila, S., McEwan, C., Costley, D., Atchison, J., Sheng, Y., Hamilton, G.R.C., Fowley, C., Callan, J.F., 2016. Diagnostic and Therapeutic Applications of Quantum Dots in Nanomedicine. Top. Curr. Chem. 370, 203–224. https://doi.org/10.1007/978-3-319-22942-3_7

Kang, E.-C., Ogura, A., Kataoka, K., Nagasaki, Y., 2004. Preparation of Water-soluble PEGylated Semiconductor Nanocrystals. Chem. Lett. 33, 840–841. https://doi.org/10.1246/cl.2004.840

Kang, S.H., Bozhilov, K.N., Myung, N.V., Mulchandani, A., Chen, W., 2008. Microbial synthesis of CdS nanocrystals in genetically engineered E. coli. Angew. Chem. Int. Ed Engl. 47, 5186–5189. https://doi.org/10.1002/anie.200705806

Kanthan, R., Senger, J.-L., Kanthan, S.C., 2012. Molecular events in primary and metastatic colorectal carcinoma: a review. Pathol. Res. Int. 2012, 597497. https://doi.org/10.1155/2012/597497

Kanzawa, T., Germano, I.M., Komata, T., Ito, H., Kondo, Y., Kondo, S., 2004. Role of autophagy in temozolomide-induced cytotoxicity for malignant glioma cells. Cell Death Differ. 11, 448–457. https://doi.org/10.1038/sj.cdd.4401359

Karakoti, A.S., Shukla, R., Shanker, R., Singh, S., 2015. Surface functionalization of quantum dots for biological applications. Adv. Colloid Interface Sci. 215, 28–45. https://doi.org/10.1016/j.cis.2014.11.004

Karapetis, C.S., Khambata-Ford, S., Jonker, D.J., O'Callaghan, C.J., Tu, D., Tebbutt, N.C., Simes, R.J., Chalchal, H., Shapiro, J.D., Robitaille, S., Price, T.J., Shepherd, L., Au, H.-J., Langer, C., Moore, M.J., Zalcberg, J.R., 2008. K-ras mutations and benefit from cetuximab in advanced colorectal cancer. N. Engl. J. Med. 359, 1757–1765. https://doi.org/10.1056/NEJMoa0804385

Kasprzak, A., Adamek, A., Przybyszewska, W., Pyda, P., Szmeja, J., Seraszek-Jaros, A., Lanzafame, A., Surdacka, A., Mozer-Lisewska, I., Koczorowska, M., 2015. Insulin-like growth factor-1 mRNA isoforms and insulin-like growth factor-1 receptor mRNA expression in chronic hepatitis C. World J. Gastroenterol. 21, 3867–3875. https://doi.org/10.3748/wjg.v21.i13.3867

Kasprzak, A., Szaflarski, W., Szmeja, J., Andrzejewska, M., Przybyszewska, W., Kaczmarek, E., Koczorowska, M., Kościński, T., Zabel, M., Drews, M., 2013. Differential expression of IGF-1 mRNA isoforms in colorectal carcinoma and normal colon tissue. Int. J. Oncol. 42, 305–316. https://doi.org/10.3892/ijo.2012.1706

Kasprzak, A., Szaflarski, W., Szmeja, J., Andrzejewska, M., Przybyszewska, W., Koczorowska, M., Drews, M., Kaczmarek, E., 2012. Expression of various insulin-like growth factor-1 mRNA isoforms in colorectal cancer. Contemp. Oncol. 16, 147–153. https://doi.org/10.5114/wo.2012.28794

Kaur, J., Debnath, J., 2015. Autophagy at the crossroads of catabolism and anabolism. Nat. Rev. Mol. Cell Biol. 16, 461–472. https://doi.org/10.1038/nrm4024

Ke, C.-Y., Yang, F.-L., Wu, W.-T., Chung, C.-H., Lee, R.-P., Yang, W.-T., Subeq, Y.-M., Liao, K.-W., 2016. Vitamin D3 Reduces Tissue Damage and Oxidative Stress Caused by Exhaustive Exercise. Int. J. Med. Sci. 13, 147–153. https://doi.org/10.7150/ijms.13746

Keil, E., Höcker, R., Schuster, M., Essmann, F., Ueffing, N., Hoffman, B., Liebermann, D.A., Pfeffer, K., Schulze-Osthoff, K., Schmitz, I., 2013. Phosphorylation of Atg5 by the Gadd45β–MEKK4-p38 pathway inhibits autophagy. Cell Death Differ. 20, 321–332. https://doi.org/10.1038/cdd.2012.129

Kessinger, C.W., Khemtong, C., Togao, O., Takahashi, M., Sumer, B.D., Gao, J., 2010. In vivo angiogenesis imaging of solid tumors by alpha(v)beta(3)-targeted, dual-modality micellar nanoprobes. Exp. Biol. Med. Maywood NJ 235, 957–965. https://doi.org/10.1258/ebm.2010.010096

Kharlamov, A.N., Tyurnina, A.E., Veselova, V.S., Kovtun, O.P., Shur, V.Y., Gabinsky, J.L., 2015. Silica–gold nanoparticles for atheroprotective management of plaques: results of the NANOM-FIM trial. Nanoscale 7, 8003–8015. https://doi.org/10.1039/C5NR01050K

Khorana, A.A., Ryan, C.K., Cox, C., Eberly, S., Sahasrabudhe, D.M., 2003. Vascular endothelial growth factor, CD68, and epidermal growth factor receptor expression and survival in patients with Stage II and Stage III colon carcinoma: a role for the host response in prognosis. Cancer 97, 960–968. https://doi.org/10.1002/cncr.11152

Kim, J.G., Suh, C.S., Kim, S.H., Choi, Y.M., Moon, S.Y., Lee, J.Y., 2000. Insulin-like growth factors (IGFs), IGF-binding proteins (IGFBPs), and IGFBP-3 protease activity in the peritoneal fluid of patients with and without endometriosis. Fertil. Steril. 73, 996–1000.

Kim, S., Fisher, B., Eisler, H.-J., Bawendi, M., 2003. Type-II Quantum Dots: CdTe/CdSe(Core/Shell) and CdSe/ZnTe(Core/Shell) Heterostructures. J. Am. Chem. Soc. 125, 11466–11467. https://doi.org/10.1021/ja0361749

Kimura, T., Tanaka, S., Haruma, K., Sumii, K., Kajiyama, G., Shimamoto, F., Kohno, N., 2000. Clinical significance of MUC1 and E-cadherin expression, cellular proliferation, and angiogenesis at the deepest invasive portion of colorectal cancer. Int. J. Oncol. 16, 55–64.

Kirchner, C., Liedl, T., Kudera, S., Pellegrino, T., Muñoz Javier, A., Gaub, H.E., Stölzle, S., Fertig, N., Parak, W.J., 2005. Cytotoxicity of colloidal CdSe and CdSe/ZnS nanoparticles. Nano Lett. 5, 331–338. https://doi.org/10.1021/nl047996m

Kirla, R., Salminen, E., Huhtala, S., Nuutinen, J., Talve, L., Haapasalo, H., Kalimo, H., n.d. Prognostic Value of the Expression of Tumor Suppressor Genes p53, p21, p16 and pRb, and Ki-67 Labelling in High Grade Astrocytomas Treated with Radiotherapy. J. Neurooncol. 46, 71–80. https://doi.org/10.1023/A:1006473320474

Klionsky, D.J., Abe, A., Abedin, M.J., Abeliovich, H., Acevedo Arozena, A., Adachi, H., et al, 2016. Guidelines for the use and interpretation of assays for monitoring autophagy (3rd edition). Autophagy 12, 1–222. https://doi.org/10.1080/15548627.2015.1100356

Koczorowska, M.M., Kwasniewksa, A., Gozdzicka-Jozefiak, A., 2011. IGF1 mRNA isoform expression in the cervix of HPV-positive women with pre-cancerous and cancer lesions. Exp. Ther. Med. 2, 149–156. https://doi.org/10.3892/etm.2010.174

Kogan-Zviagin, I., Shamay, Y., Nissan, A., Sella-Tavor, O., Golan, M., David, A., 2014. Intra-colonic administration of a polymer-bound NIRF probe for improved colorectal cancer detection during colonoscopy. J. Control. Release Off. J. Control. Release Soc. 192, 182–191. https://doi.org/10.1016/j.jconrel.2014.06.058

Kolitz-Domb, M., Grinberg, I., Corem-Salkmon, E., Margel, S., 2014. Engineering of near infrared fluorescent proteinoid-poly(L-lactic acid) particles for in vivo colon cancer detection. J. Nanobiotechnology 12, 30. https://doi.org/10.1186/s12951-014-0030-z

Kong, Y., Chen, J., Gao, F., Li, W., Xu, X., Pandoli, O., Yang, H., Ji, J., Cui, D., 2010. A multifunctional ribonuclease-A-conjugated CdTe quantum dot cluster nanosystem for synchronous cancer imaging and therapy. Small Weinh. Bergstr. Ger. 6, 2367–2373. https://doi.org/10.1002/smll.201001050

Koutsilieris, M., Mastrogamvrakis, G., Lembessis, P., Sourla, A., Miligos, S., Michalas, S., 2001. Increased insulin-like growth factor 1 activity can rescue KLE endometrial-like cells from apoptosis. Mol. Med. 7, 20–26.

Krag, D.N., Anderson, S.J., Julian, T.B., Brown, A.M., Harlow, S.P., Ashikaga, T., Weaver, D.L., Miller, B.J., Jalovec, L.M., Frazier, T.G., Noyes, R.D., Robidoux, A., Scarth, H.M.C., Mammolito, D.M., McCready, D.R., Mamounas, E.P., Costantino, J.P., Wolmark, N., National Surgical Adjuvant Breast and Bowel Project, 2007. Technical outcomes of sentinel-lymph-node resection and conventional axillary-lymph-node dissection in patients with clinically node-negative breast cancer: results from the NSABP B-32 randomised phase III trial. Lancet Oncol. 8, 881–888. https://doi.org/10.1016/S1470-2045(07)70278-4

Kumar, G., Tajpara, P., Bukhari, A.B., Ramchandani, A.G., De, A., Maru, G.B., 2014. Dietary curcumin post-treatment enhances the disappearance of B(a)P-derived DNA adducts in mouse liver and lungs. Toxicol. Rep. 1, 1181–1194. https://doi.org/10.1016/j.toxrep.2014.11.008

Kwon, H., Lee, Jiyeon, Song, R., Hwang, S.I., Lee, Junghan, Kim, Y.-H., Lee, H.J., 2013. In Vitro and In Vivo Imaging of Prostate Cancer Angiogenesis Using Anti-Vascular Endothelial Growth Factor Receptor 2 Antibody-Conjugated Quantum Dot. Korean J. Radiol. 14, 30–37. https://doi.org/10.3348/kjr.2013.14.1.30

Kwon, S., Cho, C.H., Lee, E.S., Park, J.-K., 2015. Automated Measurement of Multiple Cancer Biomarkers Using Quantum-Dot-Based Microfluidic Immunohistochemistry. Anal. Chem. 87, 4177–4183. https://doi.org/10.1021/acs.analchem.5b00199

Ladabaum, U., Wang, G., Terdiman, J., Blanco, A., Kuppermann, M., Boland, C.R., Ford, J., Elkin, E., Phillips, K.A., 2011. Strategies to identify the Lynch syndrome among patients with colorectal cancer: a cost-effectiveness analysis. Ann. Intern. Med. 155, 69–79. https://doi.org/10.7326/0003-4819-155-2-201107190-00002

Lane, D.P., 1992. Cancer. p53, guardian of the genome. Nature 358, 15–16. https://doi.org/10.1038/358015a0

Larson, D.R., Zipfel, W.R., Williams, R.M., Clark, S.W., Bruchez, M.P., Wise, F.W., Webb, W.W., 2003. Water-soluble quantum dots for multiphoton fluorescence imaging in vivo. Science 300, 1434–1436. https://doi.org/10.1126/science.1083780

Lee, Y.K., Choi, E.-J., Webster, T.J., Kim, S.-H., Khang, D., 2015. Effect of the protein corona on nanoparticles for modulating cytotoxicity and immunotoxicity. Int. J. Nanomedicine 10, 97–113. https://doi.org/10.2147/IJN.S72998

Leslie, A., Carey, F.A., Pratt, N.R., Steele, R.J.C., 2002. The colorectal adenoma–carcinoma sequence. Br. J. Surg. 89, 845–860. https://doi.org/10.1046/j.1365-2168.2002.02120.x

Li, C., Vu, K., Hazelgrove, K., Kuemmerle, J.F., 2015. Increased IGF-IEc expression and mechano-growth factor production in intestinal muscle of fibrostenotic Crohn's disease and smooth muscle hypertrophy. Am. J. Physiol. Gastrointest. Liver Physiol. 309, G888-899. https://doi.org/10.1152/ajpgi.00414.2014

Li, J., Hou, N., Faried, A., Tsutsumi, S., Kuwano, H., 2010. Inhibition of autophagy augments 5-fluorouracil chemotherapy in human colon cancer in vitro and in vivo model. Eur. J. Cancer Oxf. Engl. 1990 46, 1900–1909. https://doi.org/10.1016/j.ejca.2010.02.021

Li, J., Hou, N., Faried, A., Tsutsumi, S., Takeuchi, T., Kuwano, H., 2009a. Inhibition of autophagy by 3-MA enhances the effect of 5-FU-induced apoptosis in colon cancer cells. Ann. Surg. Oncol. 16, 761–771. https://doi.org/10.1245/s10434-008-0260-0

Li, J., Hou, N., Faried, A., Tsutsumi, S., Takeuchi, T., Kuwano, H., 2009b. Inhibition of autophagy by 3-MA enhances the effect of 5-FU-induced apoptosis in colon cancer cells. Ann. Surg. Oncol. 16, 761–771. https://doi.org/10.1245/s10434-008-0260-0

Li, P., Sun, P., Yang, W., Zhang, X., 2012. Real-time mapping of rat stomach lymph nodes by quantum dots. Scand. J. Gastroenterol. 47, 454–460. https://doi.org/10.3109/00365521.2012.654405

Libânio, D., Azevedo, L.F., 2016. Analysis of the Cochrane Review: Chromoscopy Versus Conventional Endoscopy for the Detection of Polyps in the Colon and Rectum. Cochrane Database Syst Rev. 2016;4:CD006439. Acta Médica Port. 29, 583–586. https://doi.org/10.20344/amp.7968

Libutti, S.K., Paciotti, G.F., Byrnes, A.A., Alexander, H.R., Gannon, W.E., Walker, M., Seidel, G.D., Yuldasheva, N., Tamarkin, L., 2010. Phase I and pharmacokinetic studies of CYT-6091, a novel PEGylated colloidal gold-rhTNF nanomedicine. Clin. Cancer Res. Off. J. Am. Assoc. Cancer Res. 16, 6139–6149. https://doi.org/10.1158/1078-0432.CCR-10-0978

Lin, C., Zhang, Z., Wang, L., Lin, N., Yang, W., Wu, W., Wang, W., Wang, R., Wang, Y., 2017. [Effect of nano carbon tattooing on the lesion localization in the early colon cancer for additional surgical procedure after endoscopic resection]. Zhonghua Wei Chang Wai Ke Za Zhi Chin. J. Gastrointest. Surg. 20, 910–913.

Lin, L., Baehrecke, E.H., 2015. Autophagy, cell death, and cancer. Mol. Cell. Oncol. 2. https://doi.org/10.4161/23723556.2014.985913

Linardou, H., Briasoulis, E., Dahabreh, I.J., Mountzios, G., Papadimitriou, C., Papadopoulos, S., Bafaloukos, D., Kosmidis, P., Murray, S., 2011. All about KRAS for clinical oncology practice: gene profile, clinical implications and laboratory recommendations for somatic mutational testing in colorectal cancer. Cancer Treat. Rev. 37, 221–233. https://doi.org/10.1016/j.ctrv.2010.07.008

Liu, J., Yu, M., Zhou, C., Yang, S., Ning, X., Zheng, J., 2013. Passive Tumor Targeting of Renal-Clearable Luminescent Gold Nanoparticles: Long Tumor Retention and Fast Normal Tissue Clearance. J. Am. Chem. Soc. 135, 4978–4981. https://doi.org/10.1021/ja401612x

Liu, J.P., Baker, J., Perkins, A.S., Robertson, E.J., Efstratiadis, A., 1993. Mice carrying null mutations of the genes encoding insulin-like growth factor I (Igf-1) and type 1 IGF receptor (Igf1r). Cell 75, 59–72.

Liu, Q., Guan, J.-Z., Sun, Y., Le, Z., Zhang, P., Yu, D., Liu, Y., 2017a. Insulin-like growth factor 1 receptor-mediated cell survival in hypoxia depends on the promotion of autophagy via suppression of the PI3K/Akt/mTOR signaling pathway. Mol. Med. Rep. 15, 2136–2142. https://doi.org/10.3892/mmr.2017.6265

Liu, Q., Guan, J.-Z., Sun, Y., Le, Z., Zhang, P., Yu, D., Liu, Y., 2017b. Insulin-like growth factor 1 receptor-mediated cell survival in hypoxia depends on the promotion of autophagy via suppression of the PI3K/Akt/mTOR signaling pathway. Mol. Med. Rep. 15, 2136–2142. https://doi.org/10.3892/mmr.2017.6265

Loo, C., Lowery, A., Halas, N., West, J., Drezek, R., 2005. Immunotargeted nanoshells for integrated cancer imaging and therapy. Nano Lett. 5, 709–711. https://doi.org/10.1021/nl050127s

Loupakis, F., Cremolini, C., Salvatore, L., Schirripa, M., Lonardi, S., Vaccaro, V., Cuppone, F., Giannarelli, D., Zagonel, V., Cognetti, F., Tortora, G., Falcone, A., Bria, E., 2012. Clinical impact of anti-epidermal growth factor receptor monoclonal antibodies in first-line treatment of metastatic colorectal cancer: meta-analytical estimation and implications for therapeutic strategies. Cancer 118, 1523–1532. https://doi.org/10.1002/cncr.26460

Low, P.S., Kularatne, S.A., 2009. Folate-targeted therapeutic and imaging agents for cancer. Curr. Opin. Chem. Biol. 13, 256–262. https://doi.org/10.1016/j.cbpa.2009.03.022
Ludwig, J.A., Weinstein, J.N., 2005. Biomarkers in Cancer Staging, Prognosis and Treatment Selection. Nat. Rev. Cancer 5, 845–856. https://doi.org/10.1038/nrc1739
Luo, Q., Wu, K., Zhang, B., Song, G., 2015. Mechano growth factor E peptide promotes rat bone marrow-derived mesenchymal stem cell migration through CXCR4-ERK1/2. Growth Factors Chur Switz. 33, 210–219.
Luo, Q.-Y., Lin, Y., Li, Y., Xiong, L.-H., Cui, R., Xie, Z.-X., Pang, D.-W., 2014. Nanomechanical analysis of yeast cells in CdSe quantum dot biosynthesis. Small Weinh. Bergstr. Ger. 10, 699–704. https://doi.org/10.1002/smll.201301940
Luo, Z., Jiang, L., Xu, Y., Li, H., Xu, W., Wu, S., Wang, Y., Tang, Z., Lv, Y., Yang, L., 2015. Mechano growth factor (MGF) and transforming growth factor (TGF)-β3 functionalized silk scaffolds enhance articular hyaline cartilage regeneration in rabbit model. Biomaterials 52, 463–475. https://doi.org/10.1016/j.biomaterials.2015.01.001
Lurje, G., Lenz, H.-J., 2009. EGFR signaling and drug discovery. Oncology 77, 400–410. https://doi.org/10.1159/000279388
Ma, Q., Su, X., 2010. Near-infrared quantum dots: synthesis, functionalization and analytical applications. The Analyst 135, 1867–1877. https://doi.org/10.1039/c0an00233j
Maeda, H., 2015. Toward a full understanding of the EPR effect in primary and metastatic tumors as well as issues related to its heterogeneity. Adv. Drug Deliv. Rev. 91, 3–6. https://doi.org/10.1016/j.addr.2015.01.002
Maeda, H., 2010. Tumor-selective delivery of macromolecular drugs via the EPR effect: background and future prospects. Bioconjug. Chem. 21, 797–802. https://doi.org/10.1021/bc100070g
Maiuri, M.C., Zalckvar, E., Kimchi, A., Kroemer, G., 2007. Self-eating and self-killing: crosstalk between autophagy and apoptosis. Nat. Rev. Mol. Cell Biol. 8, 741–752. https://doi.org/10.1038/nrm2239
Mamounas, E. (Terry) P., 2016. Optimal Management of the Axilla: A Look at the Evidence. Adv. Surg., Advances in Surgery 50, 29–40. https://doi.org/10.1016/j.yasu.2016.03.003
Mao, C., Huang, Y.-F., Yang, Z.-Y., Zheng, D.-Y., Chen, J.-Z., Tang, J.-L., 2013. KRAS p.G13D mutation and codon 12 mutations are not created equal in predicting clinical outcomes of cetuximab in metastatic colorectal cancer: a systematic review and meta-analysis. Cancer 119, 714–721. https://doi.org/10.1002/cncr.27804
Mariño, G., Niso-Santano, M., Baehrecke, E.H., Kroemer, G., 2014. Self-consumption: the interplay of autophagy and apoptosis. Nat. Rev. Mol. Cell Biol. 15, 81–94. https://doi.org/10.1038/nrm3735
Martynenko, I.V., Kuznetsova, V.A., Orlova, A.O., Kanaev, P.A., Maslov, V.G., Loudon, A., Zaharov, V., Parfenov, P., Gun'ko, Y.K., Baranov, A.V., Fedorov, A.V., 2015. Chlorin e6-ZnSe/ZnS quantum dots based system as reagent for photodynamic therapy. Nanotechnology 26, 055102. https://doi.org/10.1088/0957-4484/26/5/055102
Matheny, R.W., Nindl, B.C., Adamo, M.L., 2010. Minireview: Mechano-growth factor: a putative product of IGF-I gene expression involved in tissue repair and regeneration. Endocrinology 151, 865–875. https://doi.org/10.1210/en.2009-1217
Matsumura, Y., Maeda, H., 1986. A new concept for macromolecular therapeutics in cancer chemotherapy: mechanism of tumoritropic accumulation of proteins and the antitumor agent smancs. Cancer Res. 46, 6387–6392.
Mattoussi, H., Mauro, J.M., Goldman, E.R., Anderson, G.P., Sundar, V.C., Mikulec, F.V., Bawendi, M.G., 2000. Self-Assembly of CdSe−ZnS Quantum Dot Bioconjugates Using an Engineered Recombinant Protein. J. Am. Chem. Soc. 122, 12142–12150. https://doi.org/10.1021/ja002535y
Mavrommatis, E., Shioura, K.M., Los, T., Goldspink, P.H., 2013. The E-domain region of mechano-growth factor inhibits cellular apoptosis and preserves cardiac function during myocardial infarction. Mol. Cell. Biochem. 381, 69–83. https://doi.org/10.1007/s11010-013-1689-4
Mayer, I.A., Arteaga, C.L., 2016. The PI3K/AKT Pathway as a Target for Cancer Treatment. Annu. Rev. Med. 67, 11–28. https://doi.org/10.1146/annurev-med-062913-051343
Meng, H., Chen, J.-Y., Mi, L., Wang, P.-N., Ge, M.-Y., Yue, Y., Dai, N., 2011. Conjugates of folic acids with BSA-coated quantum dots for cancer cell targeting and imaging by single-photon and two-photon excitation. J. Biol. Inorg. Chem. JBIC Publ. Soc. Biol. Inorg. Chem. 16, 117–123. https://doi.org/10.1007/s00775-010-0709-z

Miki, H., Uehara, N., Kimura, A., Sasaki, T., Yuri, T., Yoshizawa, K., Tsubura, A., 2012. Resveratrol induces apoptosis via ROS-triggered autophagy in human colon cancer cells. Int. J. Oncol. 40, 1020–1028. https://doi.org/10.3892/ijo.2012.1325

Milingos, Dimitrios S, Philippou, A., Armakolas, A., Papageorgiou, E., Sourla, A., Protopapas, A., Liapi, A., Antsaklis, A., Mastrominas, M., Koutsilieris, M., 2011. Insulinlike Growth Factor-1Ec (MGF) Expression in Eutopic and Ectopic Endometrium: Characterization of the MGF E-Peptide Actions In Vitro. Mol. Med. 17, 21–28. https://doi.org/10.2119/molmed.2010.00043

Milingos, Dimitrios S., Philippou, A., Armakolas, A., Papageorgiou, E., Sourla, A., Protopapas, A., Liapi, A., Antsaklis, A., Mastrominas, M., Koutsilieris, M., 2011. Insulinlike growth factor-1Ec (MGF) expression in eutopic and ectopic endometrium: characterization of the MGF E-peptide actions in vitro. Mol. Med. Camb. Mass 17, 21–28. https://doi.org/10.2119/molmed.2010.00043

Mills, P., Dominique, J.C., Lafrenière, J.F., Bouchentouf, M., Tremblay, J.P., 2007. A synthetic mechano growth factor E Peptide enhances myogenic precursor cell transplantation success. Am. J. Transplant. Off. J. Am. Soc. Transplant. Am. Soc. Transpl. Surg. 7, 2247–2259. https://doi.org/10.1111/j.1600-6143.2007.01927.x

Moghimi, S.M., Hunter, A.C., Murray, J.C., 2001. Long-circulating and target-specific nanoparticles: theory to practice. Pharmacol. Rev. 53, 283–318.

Molecular testing strategies for Lynch syndrome in people with colorectal cancer | Guidance and guidelines | NICE [WWW Document], n.d. URL https://www.nice.org.uk/guidance/dg27 (accessed 9.28.17).

Molnar, B., Sipos, F., Galamb, O., Tulassay, Z., 2003. Molecular detection of circulating cancer cells. Role in diagnosis, prognosis and follow-up of colon cancer patients. Dig. Dis. Basel Switz. 21, 320–325. https://doi.org/75355

Moreira, L., Balaguer, F., Lindor, N., de la Chapelle, A., Hampel, H., Aaltonen, L.A., Hopper, J.L., Le Marchand, L., Gallinger, S., Newcomb, P.A., Haile, R., Thibodeau, S.N., Gunawardena, S., Jenkins, M.A., Buchanan, D.D., Potter, J.D., Baron, J.A., Ahnen, D.J., Moreno, V., Andreu, M., Ponz de Leon, M., Rustgi, A.K., Castells, A., EPICOLON Consortium, 2012. Identification of Lynch syndrome among patients with colorectal cancer. JAMA 308, 1555–1565. https://doi.org/10.1001/jama.2012.13088

Mouradov, D., Domingo, E., Gibbs, P., Jorissen, R.N., Li, S., Soo, P.Y., Lipton, L., Desai, J., Danielsen, H.E., Oukrif, D., Novelli, M., Yau, C., Holmes, C.C., Jones, I.T., McLaughlin, S., Molloy, P., Hawkins, N.J., Ward, R., Midgely, R., Kerr, D., Tomlinson, I.P.M., Sieber, O.M., 2013. Survival in stage II/III colorectal cancer is independently predicted by chromosomal and microsatellite instability, but not by specific driver mutations. Am. J. Gastroenterol. 108, 1785–1793. https://doi.org/10.1038/ajg.2013.292

Mourmouras, N., Philippou, A., Christopoulos, P., Kostoglou, K., Grivaki, C., Konstantinidis, C., Serafetinides, E., Delakas, D., Koutsilieris, M., 2018. Differential Expression of IGF-I Transcripts in Bladder Cancer. Anticancer Res. 38, 3453–3459. https://doi.org/10.21873/anticanres.12614

Murray, C.B., Norris, D.J., Bawendi, M.G., 1993. Synthesis and characterization of nearly monodisperse CdE (E = sulfur, selenium, tellurium) semiconductor nanocrystallites. J. Am. Chem. Soc. 115, 8706–8715. https://doi.org/10.1021/ja00072a025

Mussa Farkhani, S., Valizadeh, A., 2014. Review: three synthesis methods of CdX (X = Se, S or Te) quantum dots. IET Nanobiotechnology IET 8, 59–76. https://doi.org/10.1049/iet-nbt.2012.0028

Nagamitsu, A., Greish, K., Maeda, H., 2009. Elevating blood pressure as a strategy to increase tumor-targeted delivery of macromolecular drug SMANCS: cases of advanced solid tumors. Jpn. J. Clin. Oncol. 39, 756–766. https://doi.org/10.1093/jjco/hyp074

Nair, L.V., Nazeer, S.S., Jayasree, R.S., Ajayaghosh, A., 2015. Fluorescence Imaging Assisted Photodynamic Therapy Using Photosensitizer-Linked Gold Quantum Clusters. ACS Nano 9, 5825–5832. https://doi.org/10.1021/acsnano.5b00406

Nakase, H., Sakuma, S., Fukuchi, T., Yoshino, T., Mohri, K., Miyata, K., Kumagai, H., Hiwatari, K.-I., Tsubaki, K., Ikejima, T., Tobita, E., Zhu, M., Wilson, K.J., Washington, K., Gore, J.C., Pham, W., 2017. Evaluation of a novel fluorescent nanobeacon for targeted imaging of Thomsen-Friedenreich associated colorectal cancer. Int. J. Nanomedicine 12, 1747–1755. https://doi.org/10.2147/IJN.S124174

Nanda, N., Dhawan, D.K., Bhatia, A., Mahmood, A., Mahmood, S., 2016. Doxycycline Promotes Carcinogenesis & Metastasis via Chronic Inflammatory Pathway: An In Vivo Approach. PLOS ONE 11, e0151539. https://doi.org/10.1371/journal.pone.0151539

Nanomedicine : European Science Foundation [WWW Document], 2019. URL http://archives.esf.org/coordinating-research/forward-looks/biomedical-sciences-med/completed-forward-looks-in-biomedical-sciences/nanomedicine.html (accessed 9.12.19).

Nezis, I.P., Shravage, B.V., Sagona, A.P., Lamark, T., Bjørkøy, G., Johansen, T., Rusten, T.E., Brech, A., Baehrecke, E.H., Stenmark, H., 2010. Autophagic degradation of dBruce controls DNA fragmentation in nurse cells during late Drosophila melanogaster oogenesis. J. Cell Biol. 190, 523–531. https://doi.org/10.1083/jcb.201002035

Nikoletopoulou, V., Markaki, M., Palikaras, K., Tavernarakis, N., 2013. Crosstalk between apoptosis, necrosis and autophagy. Biochim. Biophys. Acta 1833, 3448–3459. https://doi.org/10.1016/j.bbamcr.2013.06.001

Nizam, R., Siddiqi, N., Landas, S.K., Kaplan, D.S., Holtzapple, P.G., 1996. Colonic tattooing with India ink: benefits, risks, and alternatives. Am. J. Gastroenterol. 91, 1804–1808.

Noorolyai, S., Shajari, N., Baghbani, E., Sadreddini, S., Baradaran, B., 2019. The relation between PI3K/AKT signalling pathway and cancer. Gene 698, 120–128. https://doi.org/10.1016/j.gene.2019.02.076

Nurunnabi, M., Cho, K.J., Choi, J.S., Huh, K.M., Lee, Y., 2010. Targeted near-IR QDs-loaded micelles for cancer therapy and imaging. Biomaterials 31, 5436–5444. https://doi.org/10.1016/j.biomaterials.2010.03.057

Oberbauer, A.M., 2013. The Regulation of IGF-1 Gene Transcription and Splicing during Development and Aging. Front. Endocrinol. 4, 39. https://doi.org/10.3389/fendo.2013.00039

Obonyo, O., Fisher, E., Edwards, M., Douroumis, D., 2010. Quantum dots synthesis and biological applications as imaging and drug delivery systems. Crit. Rev. Biotechnol. 30, 283–301. https://doi.org/10.3109/07388551.2010.487184

Ogino, S., Nosho, K., Kirkner, G.J., Shima, K., Irahara, N., Kure, S., Chan, A.T., Engelman, J.A., Kraft, P., Cantley, L.C., Giovannucci, E.L., Fuchs, C.S., 2009. PIK3CA mutation is associated with poor prognosis among patients with curatively resected colon cancer. J. Clin. Oncol. Off. J. Am. Soc. Clin. Oncol. 27, 1477–1484. https://doi.org/10.1200/JCO.2008.18.6544

Oniszczuk, A., Wojtunik-Kulesza, K.A., Oniszczuk, T., Kasprzak, K., 2016. The potential of photodynamic therapy (PDT)-Experimental investigations and clinical use. Biomed. Pharmacother. Biomedecine Pharmacother. 83, 912–929. https://doi.org/10.1016/j.biopha.2016.07.058

Onoshima, D., Yukawa, H., Baba, Y., 2015. Multifunctional quantum dots-based cancer diagnostics and stem cell therapeutics for regenerative medicine. Adv. Drug Deliv. Rev., Multifunctional Nanodevices and Nanobots for Bioimaging, Cancer Diagnosis/Therapy, Stem Cell Therapy, and Regenerative Medicine 95, 2–14. https://doi.org/10.1016/j.addr.2015.08.004

Osborn, L., Hession, C., Tizard, R., Vassallo, C., Luhowskyj, S., Chi-Rosso, G., Lobb, R., 1989. Direct expression cloning of vascular cell adhesion molecule 1, a cytokine-induced endothelial protein that binds to lymphocytes. Cell 59, 1203–1211.

Overview | Colorectal cancer: diagnosis and management | Guidance | NICE [WWW Document], n.d. URL https://www.nice.org.uk/guidance/cg131 (accessed 7.23.19).

Park, I.J., Choi, G.-S., Lim, K.H., Kang, B.M., Jun, S.H., 2009. Serum carcinoembryonic antigen monitoring after curative resection for colorectal cancer: clinical significance of the preoperative level. Ann. Surg. Oncol. 16, 3087–3093. https://doi.org/10.1245/s10434-009-0625-z

Park, J.M., Huang, S., Wu, T.-T., Foster, N.R., Sinicrope, F.A., 2013. Prognostic impact of Beclin 1, p62/sequestosome 1 and LC3 protein expression in colon carcinomas from patients receiving 5-fluorouracil as adjuvant chemotherapy. Cancer Biol. Ther. 14, 100–107. https://doi.org/10.4161/cbt.22954

Parsons, R., Myeroff, L.L., Liu, B., Willson, J.K., Markowitz, S.D., Kinzler, K.W., Vogelstein, B., 1995. Microsatellite instability and mutations of the transforming growth factor beta type II receptor gene in colorectal cancer. Cancer Res. 55, 5548–5550.

Pattabi, M., Pattabi, R.M., 2014. Photoluminescence from Gold and Silver Nanoparticles. Nano Hybrids 6, 1–35. https://doi.org/10.4028/www.scientific.net/NH.6.1

Pattingre, S., Tassa, A., Qu, X., Garuti, R., Liang, X.H., Mizushima, N., Packer, M., Schneider, M.D., Levine, B., 2005. Bcl-2 antiapoptotic proteins inhibit Beclin 1-dependent autophagy. Cell 122, 927–939. https://doi.org/10.1016/j.cell.2005.07.002

PC-3 ATCC ® CRL-1435™ Homo sapiens prostate; derived from me [WWW Document], 2019. URL https://www.lgcstandards-atcc.org/products/all/CRL-1435.aspx (accessed 9.22.19).

Peer, D., Karp, J.M., Hong, S., Farokhzad, O.C., Margalit, R., Langer, R., 2007. Nanocarriers as an emerging platform for cancer therapy. Nat. Nanotechnol. 2, 751–760. https://doi.org/10.1038/nnano.2007.387

Peña, J.R., Pinney, J., Ayala, P., Desai, T., Goldspink, P.H., 2015. Localized Delivery of Mechano-Growth Factor E-domain Peptide via Polymeric Microstructures Improves Cardiac Function following Myocardial Infarction. Biomaterials 0, 26–34. https://doi.org/10.1016/j.biomaterials.2014.12.050

Peng, C., Liu, J., Yang, G., Li, Y., 2017. Lysyl oxidase activates cancer stromal cells and promotes gastric cancer progression: quantum dot-based identification of biomarkers in cancer stromal cells. Int. J. Nanomedicine 13, 161–174. https://doi.org/10.2147/IJN.S143871

Peng, Y., Wang, L., Gu, J., 2013. Elevated preoperative carcinoembryonic antigen (CEA) and Ki67 is predictor of decreased survival in IIA stage colon cancer. World J. Surg. 37, 208–213. https://doi.org/10.1007/s00268-012-1814-7

Peng, Z.A., Peng, X., 2001. Formation of High-Quality CdTe, CdSe, and CdS Nanocrystals Using CdO as Precursor. J. Am. Chem. Soc. 123, 183–184. https://doi.org/10.1021/ja003633m

Pereira, M., Lai, E.P., 2008. Capillary electrophoresis for the characterization of quantum dots after non-selective or selective bioconjugation with antibodies for immunoassay. J. Nanobiotechnology 6, 10. https://doi.org/10.1186/1477-3155-6-10

Petitjean, A., Mathe, E., Kato, S., Ishioka, C., Tavtigian, S.V., Hainaut, P., Olivier, M., 2007. Impact of mutant p53 functional properties on TP53 mutation patterns and tumor phenotype: lessons from recent developments in the IARC TP53 database. Hum. Mutat. 28, 622–629. https://doi.org/10.1002/humu.20495

Petros, R.A., DeSimone, J.M., 2010. Strategies in the design of nanoparticles for therapeutic applications. Nat. Rev. Drug Discov. 9, 615–627. https://doi.org/10.1038/nrd2591

Philippou, A., Armakolas, A., Koutsilieris, M., 2013. Evidence for the Possible Biological Significance of the igf-1 Gene Alternative Splicing in Prostate Cancer. Front. Endocrinol. 4, 31. https://doi.org/10.3389/fendo.2013.00031

Philippou, A., Armakolas, A., Panteleakou, Z., Pissimissis, N., Nezos, A., Theos, A., Kaparelou, M., Armakolas, N., Pneumaticos, S.G., Koutsilieris, M., 2011. IGF1Ec expression in MG-63 human osteoblast-like osteosarcoma cells. Anticancer Res. 31, 4259–4265.

Philippou, A., Maridaki, M., Halapas, A., Koutsilieris, M., 2007. The role of the insulin-like growth factor 1 (IGF-1) in skeletal muscle physiology. Vivo Athens Greece 21, 45–54.

Philippou, A., Maridaki, M., Pneumaticos, S., Koutsilieris, M., 2014. The complexity of the IGF1 gene splicing, posttranslational modification and bioactivity. Mol. Med. Camb. Mass 20, 202–214. https://doi.org/10.2119/molmed.2014.00011

Photodynamic Therapy for Cancer [WWW Document], 2016. . Natl. Cancer Inst. URL https://www.cancer.gov/about-cancer/treatment/types/surgery/photodynamic-fact-sheet (accessed 9.28.16).

Pic, E., Pons, T., Bezdetnaya, L., Leroux, A., Guillemin, F., Dubertret, B., Marchal, F., 2010. Fluorescence imaging and whole-body biodistribution of near-infrared-emitting quantum dots after subcutaneous injection for regional lymph node mapping in mice. Mol. Imaging Biol. MIB Off. Publ. Acad. Mol. Imaging 12, 394–405. https://doi.org/10.1007/s11307-009-0288-y

Pino, M.S., Chung, D.C., 2010. The chromosomal instability pathway in colon cancer. Gastroenterology 138, 2059–2072. https://doi.org/10.1053/j.gastro.2009.12.065

Plumb, A.A., Halligan, S., Pendsé, D.A., Taylor, S.A., Mallett, S., 2014. Sensitivity and specificity of CT colonography for the detection of colonic neoplasia after positive faecal occult blood testing: systematic review and meta-analysis. Eur. Radiol. 24, 1049–1058. https://doi.org/10.1007/s00330-014-3106-0

Qu, L., Peng, Z.A., Peng, X., 2001. Alternative Routes toward High Quality CdSe Nanocrystals. Nano Lett. 1, 333–337. https://doi.org/10.1021/nl0155532

Qu, X., Wang, J., Zhang, Z., Koop, N., Rahmanzadeh, R., Hüttmann, G., 2008. Imaging of cancer cells by multiphoton microscopy using gold nanoparticles and fluorescent dyes. J. Biomed. Opt. 13, 031217. https://doi.org/10.1117/1.2942373

Quesada, A., Micevych, P., Handforth, A., 2009. C-terminal mechano growth factor protects dopamine neurons: a novel peptide that induces heme oxygenase-1. Exp. Neurol. 220, 255–266. https://doi.org/10.1016/j.expneurol.2009.08.029

Radenkovic, D., Kobayashi, H., Remsey-Semmelweis, E., Seifalian, A.M., 2016. Quantum dot nanoparticle for optimization of breast cancer diagnostics and therapy in a clinical setting. Nanomedicine Nanotechnol. Biol. Med. 12, 1581–1592. https://doi.org/10.1016/j.nano.2016.02.014

Ramalingam, V., Varunkumar, K., Ravikumar, V., Rajaram, R., 2018. Target delivery of doxorubicin tethered with PVP stabilized gold nanoparticles for effective treatment of lung cancer. Sci. Rep. 8, 3815. https://doi.org/10.1038/s41598-018-22172-5

Ramesh, B.S., Giorgakis, E., Lopez-Davila, V., Dashtarzheneha, A.K., Loizidou, M., 2016. Detection of cell surface calreticulin as a potential cancer biomarker using near-infrared emitting gold nanoclusters. Nanotechnology 27, 285101. https://doi.org/10.1088/0957-4484/27/28/285101
Reimers, M.S., Zeestraten, E.C.M., Kuppen, P.J.K., Liefers, G.J., van de Velde, C.J.H., 2013. Biomarkers in precision therapy in colorectal cancer. Gastroenterol. Rep. 1, 166–183. https://doi.org/10.1093/gastro/got022
Reiss, P., Protière, M., Li, L., 2009. Core/Shell semiconductor nanocrystals. Small Weinh. Bergstr. Ger. 5, 154–168. https://doi.org/10.1002/smll.200800841
Resch-Genger, U., Grabolle, M., Cavaliere-Jaricot, S., Nitschke, R., Nann, T., 2008. Quantum dots versus organic dyes as fluorescent labels. Nat. Methods 5, 763–775. https://doi.org/10.1038/nmeth.1248
Retnakumari, A., Setua, S., Menon, D., Ravindran, P., Muhammed, H., Pradeep, T., Nair, S., Koyakutty, M., 2010. Molecular-receptor-specific, non-toxic, near-infrared-emitting Au cluster-protein nanoconjugates for targeted cancer imaging. Nanotechnology 21, 055103. https://doi.org/10.1088/0957-4484/21/5/055103
Rezatabar, S., Karimian, A., Rameshknia, V., Parsian, H., Majidinia, M., Kopi, T.A., Bishayee, A., Sadeghinia, A., Yousefi, M., Monirialamdari, M., Yousefi, B., 2019. RAS/MAPK signaling functions in oxidative stress, DNA damage response and cancer progression: REZATABAR ET AL. J. Cell. Physiol. https://doi.org/10.1002/jcp.28334
Rhee, Y.-Y., Kim, K.-J., Kang, G.H., 2017. CpG Island Methylator Phenotype-High Colorectal Cancers and Their Prognostic Implications and Relationships with the Serrated Neoplasia Pathway. Gut Liver 11, 38–46. https://doi.org/10.5009/gnl15535
Rosenthal, S.J., McBride, J., Pennycook, S.J., Feldman, L.C., 2007. Synthesis, Surface Studies, Composition and Structural Characterization of CdSe, Core/Shell, and Biologically Active Nanocrystals. Surf. Sci. Rep. 62, 111–157. https://doi.org/10.1016/j.surfrep.2007.02.001
Roth, A.D., Delorenzi, M., Tejpar, S., Yan, P., Klingbiel, D., Fiocca, R., d'Ario, G., Cisar, L., Labianca, R., Cunningham, D., Nordlinger, B., Bosman, F., Van Cutsem, E., 2012. Integrated analysis of molecular and clinical prognostic factors in stage II/III colon cancer. J. Natl. Cancer Inst. 104, 1635–1646. https://doi.org/10.1093/jnci/djs427
Roth, A.D., Tejpar, S., Delorenzi, M., Yan, P., Fiocca, R., Klingbiel, D., Dietrich, D., Biesmans, B., Bodoky, G., Barone, C., Aranda, E., Nordlinger, B., Cisar, L., Labianca, R., Cunningham, D., Van Cutsem, E., Bosman, F., 2010. Prognostic role of KRAS and BRAF in stage II and III resected colon cancer: results of the translational study on the PETACC-3, EORTC 40993, SAKK 60-00 trial. J. Clin. Oncol. Off. J. Am. Soc. Clin. Oncol. 28, 466–474. https://doi.org/10.1200/JCO.2009.23.3452
Rotoli, D., Morales, M., Maeso, M., Garcï¿½a, M., Morales, A., ï¿½vila, J., Martï¿½n-Vasallo, P., 2016. Expression and localization of the immunophilin FKBP51 in colorectal carcinomas and primary metastases, and alterations following oxaliplatin-based chemotherapy. Oncol. Lett. https://doi.org/10.3892/ol.2016.4772
Sachdev, D., Yee, D., 2007. Disrupting insulin-like growth factor signaling as a potential cancer therapy. Mol. Cancer Ther. 6, 1–12. https://doi.org/10.1158/1535-7163.MCT-06-0080
Sakuma, S., Yu, J.Y.H., Quang, T., Hiwatari, K.-I., Kumagai, H., Kao, S., Holt, A., Erskind, J., McClure, R., Siuta, M., Kitamura, T., Tobita, E., Koike, S., Wilson, K., Richards-Kortum, R., Liu, E., Washington, K., Omary, R., Gore, J.C., Pham, W., 2015. Fluorescence-Based Endoscopic Imaging of Thomsen-Friedenreich Antigen to Improve Early Detection of Colorectal Cancer. Int. J. Cancer J. Int. Cancer 136, 1095–1103. https://doi.org/10.1002/ijc.29093
Salminen, E., Palmu, S., Vahlberg, T., Roberts, P.-J., Söderström, K.-O., 2005. Increased proliferation activity measured by immunoreactive Ki67 is associated with survival improvement in rectal/recto sigmoid cancer. World J. Gastroenterol. 11, 3245–3249.
Saltz, L.B., Clarke, S., Díaz-Rubio, E., Scheithauer, W., Figer, A., Wong, R., Koski, S., Lichinitser, M., Yang, T.-S., Rivera, F., Couture, F., Sirzén, F., Cassidy, J., 2008. Bevacizumab in combination with oxaliplatin-based chemotherapy as first-line therapy in metastatic colorectal cancer: a randomized phase III study. J. Clin. Oncol. Off. J. Am. Soc. Clin. Oncol. 26, 2013–2019. https://doi.org/10.1200/JCO.2007.14.9930
Samuels, Y., Wang, Z., Bardelli, A., Silliman, N., Ptak, J., Szabo, S., Yan, H., Gazdar, A., Powell, S.M., Riggins, G.J., Willson, J.K.V., Markowitz, S., Kinzler, K.W., Vogelstein, B., Velculescu, V.E., 2004. High frequency of mutations of the PIK3CA gene in human cancers. Science 304, 554. https://doi.org/10.1126/science.1096502
Sargent, D.J., Marsoni, S., Monges, G., Thibodeau, S.N., Labianca, R., Hamilton, S.R., French, A.J., Kabat, B., Foster, N.R., Torri, V., Ribic, C., Grothey, A., Moore, M., Zaniboni, A., Seitz, J.-F., Sinicrope, F.,

Gallinger, S., 2010. Defective mismatch repair as a predictive marker for lack of efficacy of fluorouracil-based adjuvant therapy in colon cancer. J. Clin. Oncol. Off. J. Am. Soc. Clin. Oncol. 28, 3219–3226. https://doi.org/10.1200/JCO.2009.27.1825

Sartore-Bianchi, A., Martini, M., Molinari, F., Veronese, S., Nichelatti, M., Artale, S., Di Nicolantonio, F., Saletti, P., De Dosso, S., Mazzucchelli, L., Frattini, M., Siena, S., Bardelli, A., 2009. PIK3CA mutations in colorectal cancer are associated with clinical resistance to EGFR-targeted monoclonal antibodies. Cancer Res. 69, 1851–1857. https://doi.org/10.1158/0008-5472.CAN-08-2466

Sato, H., Takino, T., Miyamori, H., 2005. Roles of membrane-type matrix metalloproteinase-1 in tumor invasion and metastasis. Cancer Sci. 96, 212–217. https://doi.org/10.1111/j.1349-7006.2005.00039.x

Sato, K., Sasaki, R., Ogura, Y., Shimoda, N., Togashi, H., Terada, K., Sugiyama, T., Kakinuma, H., Ogawa, O., Kato, T., 1998. Expression of vascular endothelial growth factor gene and its receptor (flt-1) gene in urinary bladder cancer. Tohoku J. Exp. Med. 185, 173–184.

Savvani, A., Petraki, C., Msaouel, P., Diamanti, E., Xoxakos, I., Koutsilieris, M., 2013. IGF-IEc Expression Is Associated with Advanced Clinical and Pathological Stage of Prostate Cancer. Anticancer Res. 33, 2441–2445.

Schweichel, J.U., Merker, H.J., 1973. The morphology of various types of cell death in prenatal tissues. Teratology 7, 253–266. https://doi.org/10.1002/tera.1420070306

Second Expert Report | World Cancer Research Fund International [WWW Document], 2016. URL http://www.wcrf.org/int/research-we-fund/continuous-update-project-cup/second-expert-report (accessed 9.29.16).

Sha, Y., Afandi, R., Zhang, B., Yang, L., Lv, Y., 2017a. MGF E peptide pretreatment improves collagen synthesis and cell proliferation of injured human ACL fibroblasts via MEK-ERK1/2 signaling pathway. Growth Factors Chur Switz. 35, 29–38. https://doi.org/10.1080/08977194.2017.1327856

Sha, Y., Lv, Y., Xu, Z., Yang, L., Hao, X., Afandi, R., 2017b. MGF E peptide pretreatment improves the proliferation and osteogenic differentiation of BMSCs via MEK-ERK1/2 and PI3K-Akt pathway under severe hypoxia. Life Sci. 189, 52–62. https://doi.org/10.1016/j.lfs.2017.09.017

Sha, Y., Yang, L., Lv, Y., 2019. MGF E peptide improves anterior cruciate ligament repair by inhibiting hypoxia-induced cell apoptosis and accelerating angiogenesis. J. Cell. Physiol. 234, 8846–8861. https://doi.org/10.1002/jcp.27546

Shang, J., Fan, X., Liu, H., 2015. The role of mechano-growth factor E peptide in the regulation of osteosarcoma. Oncol. Lett. 10, 697–704. https://doi.org/10.3892/ol.2015.3339

Shi, Q., Mandrekar, S.J., Sargent, D.J., 2012. Predictive biomarkers in colorectal cancer: usage, validation, and design in clinical trials. Scand. J. Gastroenterol. 47, 356–362. https://doi.org/10.3109/00365521.2012.640836

Shiota, G., Ishida, M., Noguchi, N., Oyama, K., Takano, Y., Okubo, M., Katayama, S., Tomie, Y., Harada, K., Hori, K., Ashida, K., Kishimoto, Y., Hosoda, A., Suou, T., Kanbe, T., Tanaka, K., Nosaka, K., Tanida, O., Kojo, H., Miura, K., Ito, H., Kaibara, N., Kawasaki, H., 2000. Circulating p53 antibody in patients with colorectal cancer: relation to clinicopathologic features and survival. Dig. Dis. Sci. 45, 122–128.

Si, C., Zhang, Y., Lv, X., Yang, W., Ran, Z., Sun, P., 2014. In vivo lymph node mapping by Cadmium Tellurium quantum dots in rats. J. Surg. Res. 192, 305–311. https://doi.org/10.1016/j.jss.2014.07.028

Singh, P., Kim, Y.J., Singh, H., Mathiyalagan, R., Wang, C., Yang, D.C., 2015. Biosynthesis of Anisotropic Silver Nanoparticles by Bhargavaea indica and Their Synergistic Effect with Antibiotics against Pathogenic Microorganisms [WWW Document]. J. Nanomater. https://doi.org/10.1155/2015/234741

Singh, P., Pandit, S., Mokkapati, V.R.S.S., Garg, A., Ravikumar, V., Mijakovic, I., 2018. Gold Nanoparticles in Diagnostics and Therapeutics for Human Cancer. Int. J. Mol. Sci. 19. https://doi.org/10.3390/ijms19071979

Singh, P., Singh, H., Kim, Y.J., Mathiyalagan, R., Wang, C., Yang, D.C., 2016. Extracellular synthesis of silver and gold nanoparticles by Sporosarcina koreensis DC4 and their biological applications. Enzyme Microb. Technol. 86, 75–83. https://doi.org/10.1016/j.enzmictec.2016.02.005

Singh, S., Sharma, A., Robertson, G.P., 2012. Realizing the clinical potential of cancer nanotechnology by minimizing toxicologic and targeted delivery concerns. Cancer Res. 72, 5663–5668. https://doi.org/10.1158/0008-5472.CAN-12-1527

Sipos, F., Székely, H., Kis, I.D., Tulassay, Z., Műzes, G., 2017. Relation of the IGF/IGF1R system to autophagy in colitis and colorectal cancer. World J. Gastroenterol. 23, 8109–8119. https://doi.org/10.3748/wjg.v23.i46.8109

Skinner, S.A., Tutton, P.J., O'Brien, P.E., 1990. Microvascular architecture of experimental colon tumors in the rat. Cancer Res. 50, 2411–2417.

Snover, D.C., 2011. Update on the serrated pathway to colorectal carcinoma. Hum. Pathol. 42, 1–10. https://doi.org/10.1016/j.humpath.2010.06.002
So, M.-K., Xu, C., Loening, A.M., Gambhir, S.S., Rao, J., 2006. Self-illuminating quantum dot conjugates for in vivo imaging. Nat. Biotechnol. 24, 339–343. https://doi.org/10.1038/nbt1188
Song, X.-R., Goswami, N., Yang, H.-H., Xie, J., 2016. Functionalization of metal nanoclusters for biomedical applications. Analyst 141, 3126–3140. https://doi.org/10.1039/C6AN00773B
Song, Y., Xu, K., Yu, C., Dong, L., Chen, P., Lv, Y., Chiang, M.Y.M., Li, L., Liu, W., Yang, L., 2017. The use of mechano growth factor to prevent cartilage degeneration in knee osteoarthritis. J. Tissue Eng. Regen. Med. https://doi.org/10.1002/term.2493
Stavropoulou, A., Halapas, A., Sourla, A., Philippou, A., Papageorgiou, E., Papalois, A., Koutsilieris, M., 2009. IGF-1 Expression in Infarcted Myocardium and MGF E Peptide Actions in Rat Cardiomyocytes in Vitro. Mol. Med. 15, 127–135. https://doi.org/10.2119/molmed.2009.00012
Steigerwald, M.L., Brus, L.E., 1990. Semiconductor crystallites: a class of large molecules. Acc. Chem. Res. 23, 183–188. https://doi.org/10.1021/ar00174a003
Stern, J.M., Kibanov Solomonov, V.V., Sazykina, E., Schwartz, J.A., Gad, S.C., Goodrich, G.P., 2016. Initial Evaluation of the Safety of Nanoshell-Directed Photothermal Therapy in the Treatment of Prostate Disease. Int. J. Toxicol. 35, 38–46. https://doi.org/10.1177/1091581815600170
Stürzenbaum, S.R., Höckner, M., Panneerselvam, A., Levitt, J., Bouillard, J.-S., Taniguchi, S., Dailey, L.-A., Ahmad Khanbeigi, R., Rosca, E.V., Thanou, M., Suhling, K., Zayats, A.V., Green, M., 2013. Biosynthesis of luminescent quantum dots in an earthworm. Nat. Nanotechnol. 8, 57–60. https://doi.org/10.1038/nnano.2012.232
Sun, L.-C., Chu, K.-S., Cheng, S.-C., Lu, C.-Y., Kuo, C.-H., Hsieh, J.-S., Shih, Y.-L., Chang, S.-J., Wang, J.-Y., 2009. Preoperative serum carcinoembryonic antigen, albumin and age are supplementary to UICC staging systems in predicting survival for colorectal cancer patients undergoing surgical treatment. BMC Cancer 9, 288. https://doi.org/10.1186/1471-2407-9-288
Suppiah, A., Alabi, A., Madden, L., Hartley, J.E., Monson, J.R.T., Greenman, J., 2008. Anti-p53 autoantibody in colorectal cancer: prognostic significance in long-term follow-up. Int. J. Colorectal Dis. 23, 595–600. https://doi.org/10.1007/s00384-008-0458-4
Suppiah, A., Greenman, J., 2013. Clinical utility of anti-p53 auto-antibody: Systematic review and focus on colorectal cancer. World J. Gastroenterol. WJG 19, 4651–4670. https://doi.org/10.3748/wjg.v19.i29.4651
SW620 [SW-620] ATCC ® CCL-227™ Homo sapiens colon; derived f [WWW Document], 2019. URL http://www.lgcstandards-atcc.org/products/all/CCL-227.aspx?geo_country=gb#history (accessed 9.22.19).
Swart, C., Du Toit, A., Loos, B., 2016. Autophagy and the invisible line between life and death. Eur. J. Cell Biol. 95, 598–610. https://doi.org/10.1016/j.ejcb.2016.10.005
Tan, Y.-Q., Zhang, J., Zhou, G., 2017. Autophagy and its implication in human oral diseases. Autophagy 13, 225–236. https://doi.org/10.1080/15548627.2016.1234563
Tang, J.-C., Feng, Y.-L., Liang, X., Cai, X.-J., 2016. Autophagy in 5-Fluorouracil Therapy in Gastrointestinal Cancer: Trends and Challenges. Chin. Med. J. (Engl.) 129, 456–463. https://doi.org/10.4103/0366-6999.176069
Tang, J.J., Podratz, J.L., Lange, M., Scrable, H.J., Jang, M.-H., Windebank, A.J., 2017. Mechano growth factor, a splice variant of IGF-1, promotes neurogenesis in the aging mouse brain. Mol. Brain 10, 23. https://doi.org/10.1186/s13041-017-0304-0
Tang, L.-L., Xian, C.-Y., Wang, Y.-L., 2006. The MGF expression of osteoblasts in response to mechanical overload. Arch. Oral Biol. 51, 1080–1085. https://doi.org/10.1016/j.archoralbio.2006.06.009
Tasdemir, E., Maiuri, M.C., Galluzzi, L., Vitale, I., Djavaheri-Mergny, M., D'Amelio, M., Criollo, A., Morselli, E., Zhu, C., Harper, F., Nannmark, U., Samara, C., Pinton, P., Vicencio, J.M., Carnuccio, R., Moll, U.M., Madeo, F., Paterlini-Brechot, P., Rizzuto, R., Szabadkai, G., Pierron, G., Blomgren, K., Tavernarakis, N., Codogno, P., Cecconi, F., Kroemer, G., 2008. Regulation of autophagy by cytoplasmic p53. Nat. Cell Biol. 10, 676–687. https://doi.org/10.1038/ncb1730
Tessmer, I., Kaur, P., Lin, J., Wang, H., 2013. Investigating bioconjugation by atomic force microscopy. J. Nanobiotechnology 11, 25. https://doi.org/10.1186/1477-3155-11-25
Thanh, N.T.K., Green, L.A.W., 2010. Functionalisation of nanoparticles for biomedical applications. Nano Today 5, 213–230. https://doi.org/10.1016/j.nantod.2010.05.003
Thirunavukarasu, P., Sukumar, S., Sathaiah, M., Mahan, M., Pragatheeshwar, K.D., Pingpank, J.F., Zeh, H., Bartels, C.J., Lee, K.K.W., Bartlett, D.L., 2011. C-stage in colon cancer: implications of

carcinoembryonic antigen biomarker in staging, prognosis, and management. J. Natl. Cancer Inst. 103, 689–697. https://doi.org/10.1093/jnci/djr078
Tjandra, J.J., Chan, M.K.Y., 2007. Follow-up after curative resection of colorectal cancer: a meta-analysis. Dis. Colon Rectum 50, 1783–1799. https://doi.org/10.1007/s10350-007-9030-5
Tong, Y., Feng, W., Wu, Y., Lv, H., Jia, Y., Jiang, D., 2015. Mechano-growth factor accelerates the proliferation and osteogenic differentiation of rabbit mesenchymal stem cells through the PI3K/AKT pathway. BMC Biochem. 16, 1. https://doi.org/10.1186/s12858-015-0031-z
Trakarnsanga, A., Akaraviputh, T., 2011. Endoscopic tattooing of colorectal lesions: Is it a risk-free procedure? World J. Gastrointest. Endosc. 3, 256–260. https://doi.org/10.4253/wjge.v3.i12.256
Troncoso, R., Vicencio, J.M., Parra, V., Nemchenko, A., Kawashima, Y., Del Campo, A., Toro, B., Battiprolu, P.K., Aranguiz, P., Chiong, M., Yakar, S., Gillette, T.G., Hill, J.A., Abel, E.D., Leroith, D., Lavandero, S., 2012. Energy-preserving effects of IGF-1 antagonize starvation-induced cardiac autophagy. Cardiovasc. Res. 93, 320–329. https://doi.org/10.1093/cvr/cvr321
Tsikitis, V.L., Malireddy, K., Green, E.A., Christensen, B., Whelan, R., Hyder, J., Marcello, P., Larach, S., Lauter, D., Sargent, D.J., Nelson, H., 2009. Postoperative surveillance recommendations for early stage colon cancer based on results from the clinical outcomes of surgical therapy trial. J. Clin. Oncol. Off. J. Am. Soc. Clin. Oncol. 27, 3671–3676. https://doi.org/10.1200/JCO.2008.20.7050
Tsoi, K.M., Dai, Q., Alman, B.A., Chan, W.C.W., 2013. Are quantum dots toxic? Exploring the discrepancy between cell culture and animal studies. Acc. Chem. Res. 46, 662–671. https://doi.org/10.1021/ar300040z
Turner, J., 2009. The Gastrointestinal Tract, in: Robins and Cotran Pathologic Basis of Disease.
Umar, A., Boland, C.R., Terdiman, J.P., Syngal, S., de la Chapelle, A., Rüschoff, J., Fishel, R., Lindor, N.M., Burgart, L.J., Hamelin, R., Hamilton, S.R., Hiatt, R.A., Jass, J., Lindblom, A., Lynch, H.T., Peltomaki, P., Ramsey, S.D., Rodriguez-Bigas, M.A., Vasen, H.F.A., Hawk, E.T., Barrett, J.C., Freedman, A.N., Srivastava, S., 2004. Revised Bethesda Guidelines for hereditary nonpolyposis colorectal cancer (Lynch syndrome) and microsatellite instability. J. Natl. Cancer Inst. 96, 261–268.
Vaklavas, C., Blume, S.W., Grizzle, W.E., 2017. Translational Dysregulation in Cancer: Molecular Insights and Potential Clinical Applications in Biomarker Development. Front. Oncol. 7. https://doi.org/10.3389/fonc.2017.00158
Van Cutsem, E., Nordlinger, B., Cervantes, A., ESMO Guidelines Working Group, 2010. Advanced colorectal cancer: ESMO Clinical Practice Guidelines for treatment. Ann. Oncol. Off. J. Eur. Soc. Med. Oncol. ESMO 21 Suppl 5, v93-97. https://doi.org/10.1093/annonc/mdq222
Vankayala, R., Lin, C.-C., Kalluru, P., Chiang, C.-S., Hwang, K.C., 2014. Gold nanoshells-mediated bimodal photodynamic and photothermal cancer treatment using ultra-low doses of near infra-red light. Biomaterials 35, 5527–5538. https://doi.org/10.1016/j.biomaterials.2014.03.065
Varghese, F., Bukhari, A.B., Malhotra, R., De, A., 2014. IHC Profiler: An Open Source Plugin for the Quantitative Evaluation and Automated Scoring of Immunohistochemistry Images of Human Tissue Samples. PLOS ONE 9, e96801. https://doi.org/10.1371/journal.pone.0096801
Vasen, H.F., Watson, P., Mecklin, J.P., Lynch, H.T., 1999. New clinical criteria for hereditary nonpolyposis colorectal cancer (HNPCC, Lynch syndrome) proposed by the International Collaborative group on HNPCC. Gastroenterology 116, 1453–1456.
Vassilakos, G., Philippou, A., Koutsilieris, M., 2017. Identification of the IGF-1 processing product human Ec/rodent Eb peptide in various tissues: Evidence for its differential regulation after exercise-induced muscle damage in humans. Growth Horm. IGF Res. Off. J. Growth Horm. Res. Soc. Int. IGF Res. Soc. 32, 22–28. https://doi.org/10.1016/j.ghir.2016.11.001
Vassilakos, G., Philippou, A., Tsakiroglou, P., Koutsilieris, M., 2014. Biological activity of the e domain of the IGF-1Ec as addressed by synthetic peptides. Horm. Athens Greece 13, 182–196.
Vihinen, P., Ala-aho, R., Kähäri, V.-M., 2005. Matrix metalloproteinases as therapeutic targets in cancer. Curr. Cancer Drug Targets 5, 203–220.
Vivanco, I., Sawyers, C.L., 2002. The phosphatidylinositol 3-Kinase AKT pathway in human cancer. Nat. Rev. Cancer 2, 489–501. https://doi.org/10.1038/nrc839
Volkov, Y., 2015. Quantum dots in nanomedicine: recent trends, advances and unresolved issues. Biochem. Biophys. Res. Commun., Nanomedicine 468, 419–427. https://doi.org/10.1016/j.bbrc.2015.07.039
Vousden, K.H., Lane, D.P., 2007. p53 in health and disease. Nat. Rev. Mol. Cell Biol. 8, 275–283. https://doi.org/10.1038/nrm2147
Vu, T.Q., Lam, W.Y., Hatch, E.W., Lidke, D.S., 2015. Quantum dots for quantitative imaging: from single molecules to tissue. Cell Tissue Res. 360, 71–86. https://doi.org/10.1007/s00441-014-2087-2

Walther, A., Johnstone, E., Swanton, C., Midgley, R., Tomlinson, I., Kerr, D., 2009. Genetic prognostic and predictive markers in colorectal cancer. Nat. Rev. Cancer 9, 489–499. https://doi.org/10.1038/nrc2645

Walther, C., Meyer, K., Rennert, R., Neundorf, I., 2008. Quantum dot-carrier peptide conjugates suitable for imaging and delivery applications. Bioconjug. Chem. 19, 2346–2356. https://doi.org/10.1021/bc800172q

Wang, C., Ma, Q., Su, X., 2008. Synthesis of CdTe nanocrystals with mercaptosuccinic acid as stabilizer. J. Nanosci. Nanotechnol. 8, 4408–4414.

Wang, J.-Y., Chen, J., Yang, J., Wang, H., Shen, X., Sun, Y.-M., Guo, M., Zhang, X.-D., 2016. Effects of surface charges of gold nanoclusters on long-term in vivo biodistribution, toxicity, and cancer radiation therapy. Int. J. Nanomedicine 11, 3475–3485. https://doi.org/10.2147/IJN.S106073

Wang, R., Wang, Y., Li, D., Yu, L., Liu, G., Ma, J., Wang, W., 2016. Application of carbon nanoparticles to mark locations for re-inspection after colonic polypectomy. Surg. Endosc. 30, 1530–1533. https://doi.org/10.1007/s00464-015-4367-7

Wang, S., Gu, K., 2018. Insulin-like growth factor 1 inhibits autophagy of human colorectal carcinoma drug-resistant cells via the protein kinase B/mammalian target of rapamycin signaling pathway. Mol. Med. Rep. 17, 2952–2956. https://doi.org/10.3892/mmr.2017.8272

Wang, S., Li, W., Yuan, D., Song, J., Fang, J., 2016. Quantitative detection of the tumor-associated antigen large external antigen in colorectal cancer tissues and cells using quantum dot probe. Int. J. Nanomedicine 11, 235–247. https://doi.org/10.2147/IJN.S97509

Wang, W., Wang, R., Wang, Y., Yu, L., Li, D., Huang, S., Ma, J., Lin, N., Yang, W., Chen, X., Liu, B., Lv, R., Liao, L., 2013. Preoperative Colonic Lesion Localization with Charcoal Nanoparticle Tattooing for Laparoscopic Colorectal Surgery [WWW Document]. https://doi.org/info:doi/10.1166/jbn.2013.1767

Wang, Y., Wang, W., Li, D., Li, M., Wang, P., Wen, J., Liang, M., Su, B., Yin, Y., 2014. IGF-1 alleviates NMDA-induced excitotoxicity in cultured hippocampal neurons against autophagy via the NR2B/PI3K-AKT-mTOR pathway. J. Cell. Physiol. 229, 1618–1629. https://doi.org/10.1002/jcp.24607

Weber, J.C., Nakano, H., Bachellier, P., Oussoultzoglou, E., Inoue, K., Shimura, H., Wolf, P., Chenard-Neu, M.P., Jaeck, D., 2001. Is a proliferation index of cancer cells a reliable prognostic factor after hepatectomy in patients with colorectal liver metastases? Am. J. Surg. 182, 81–88.

Weng, K.C., Noble, C.O., Papahadjopoulos-Sternberg, B., Chen, F.F., Drummond, D.C., Kirpotin, D.B., Wang, D., Hom, Y.K., Hann, B., Park, J.W., 2008. Targeted tumor cell internalization and imaging of multifunctional quantum dot-conjugated immunoliposomes in vitro and in vivo. Nano Lett. 8, 2851–2857. https://doi.org/10.1021/nl801488u

Winawer, S.J., Zauber, A.G., Ho, M.N., O'Brien, M.J., Gottlieb, L.S., Sternberg, S.S., Waye, J.D., Schapiro, M., Bond, J.H., Panish, J.F., 1993. Prevention of colorectal cancer by colonoscopic polypectomy. The National Polyp Study Workgroup. N. Engl. J. Med. 329, 1977–1981. https://doi.org/10.1056/NEJM199312303292701

Wirawan, E., Vande Walle, L., Kersse, K., Cornelis, S., Claerhout, S., Vanoverberghe, I., Roelandt, R., De Rycke, R., Verspurten, J., Declercq, W., Agostinis, P., Vanden Berghe, T., Lippens, S., Vandenabeele, P., 2010. Caspase-mediated cleavage of Beclin-1 inactivates Beclin-1-induced autophagy and enhances apoptosis by promoting the release of proapoptotic factors from mitochondria. Cell Death Dis. 1, e18. https://doi.org/10.1038/cddis.2009.16

Wirth, G.J., Schandelmaier, K., Smith, V., Burger, A.M., Fiebig, H.-H., 2006. Microarrays of 41 human tumor cell lines for the characterization of new molecular targets: expression patterns of cathepsin B and the transferrin receptor. Oncology 71, 86–94. https://doi.org/10.1159/000100476

Wolcott, A., Gerion, D., Visconte, M., Sun, J., Schwartzberg, A., Chen, S., Zhang, J.Z., 2006. Silica-Coated CdTe Quantum Dots Functionalized with Thiols for Bioconjugation to IgG Proteins. J. Phys. Chem. B 110, 5779–5789. https://doi.org/10.1021/jp057435z

Worthley, D.L., Leggett, B.A., 2010. Colorectal cancer: molecular features and clinical opportunities. Clin. Biochem. Rev. Aust. Assoc. Clin. Biochem. 31, 31–38.

Wrigley, S., Arafa, D., Tropea, D., 2017. Insulin-Like Growth Factor 1: At the Crossroads of Brain Development and Aging. Front. Cell. Neurosci. 11, 14. https://doi.org/10.3389/fncel.2017.00014

Wu, H., Che, X., Zheng, Q., Wu, A., Pan, K., Shao, A., Wu, Q., Zhang, J., Hong, Y., 2014. Caspases: a molecular switch node in the crosstalk between autophagy and apoptosis. Int. J. Biol. Sci. 10, 1072–1083. https://doi.org/10.7150/ijbs.9719

Wu, J., Wu, K., Lin, F., Luo, Q., Yang, L., Shi, Y., Song, G., Sung, K.-L.P., 2013. Mechano-growth factor induces migration of rat mesenchymal stem cells by altering its mechanical properties and activating ERK

pathway. Biochem. Biophys. Res. Commun. 441, 202–207. https://doi.org/10.1016/j.bbrc.2013.10.031
Wu, Q., Chu, M., 2012. Self-illuminating quantum dots for highly sensitive in vivo real-time luminescent mapping of sentinel lymph nodes. Int. J. Nanomedicine 7, 3433–3443. https://doi.org/10.2147/IJN.S30709
Wu, X., He, X., Wang, K., Xie, C., Zhou, B., Qing, Z., 2010. Ultrasmall near-infrared gold nanoclusters for tumor fluorescence imaging in vivo. Nanoscale 2, 2244–2249. https://doi.org/10.1039/C0NR00359J
Wu, Y., Qu, J.Y., 2006. Autofluorescence spectroscopy of epithelial tissues. J. Biomed. Opt. 11, 054023. https://doi.org/10.1117/1.2362741
Xin, C., Bingbing, Z., Yuanliang, W., Chengyu, X., Li, Y., Moyuan, D., Qin, P., Yuxiao, L., 2012. Mechano-growth factor E peptide inhibits the differentiation and mineralization of osteoblasts. Arch. Oral Biol. 57, 720–727. https://doi.org/10.1016/j.archoralbio.2011.11.016
Xiong, L.-H., Cui, R., Zhang, Z.-L., Yu, X., Xie, Z., Shi, Y.-B., Pang, D.-W., 2014. Uniform fluorescent nanobioprobes for pathogen detection. ACS Nano 8, 5116–5124. https://doi.org/10.1021/nn501174g
Xu, J., Shang, L., 2018. Emerging applications of near-infrared fluorescent metal nanoclusters for biological imaging. Chin. Chem. Lett. https://doi.org/10.1016/j.cclet.2017.12.020
Xue, L., Yan, B., Li, Y., Tan, Y., Luo, X., Wang, M., 2018. Surface-enhanced Raman spectroscopy of blood serum based on gold nanoparticles for tumor stages detection and histologic grades classification of oral squamous cell carcinoma. Int. J. Nanomedicine 13, 4977–4986. https://doi.org/10.2147/IJN.S167996
Yaghini, E., Turner, H.D., Le Marois, A.M., Suhling, K., Naasani, I., MacRobert, A.J., 2016. In vivo biodistribution studies and ex vivo lymph node imaging using heavy metal-free quantum dots. Biomaterials 104, 182–191. https://doi.org/10.1016/j.biomaterials.2016.07.014
Yan, Y., Jiang, K., Liu, P., Zhang, X., Dong, X., Gao, J., Liu, Q., Barr, M.P., Zhang, Q., Hou, X., Meng, S., Gong, P., 2016. Bafilomycin A1 induces caspase-independent cell death in hepatocellular carcinoma cells via targeting of autophagy and MAPK pathways. Sci. Rep. 6, 37052. https://doi.org/10.1038/srep37052
Yang, L., Mao, H., Wang, Y.A., Cao, Z., Peng, X., Wang, X., Duan, H., Ni, C., Yuan, Q., Adams, G., Smith, M.Q., Wood, W.C., Gao, X., Nie, S., 2009. Single chain epidermal growth factor receptor antibody conjugated nanoparticles for in vivo tumor targeting and imaging. Small Weinh. Bergstr. Ger. 5, 235–243. https://doi.org/10.1002/smll.200800714
Yang, M., Wen, T., Chen, H., Deng, J., Yang, C., Zhang, Z., 2018. Knockdown of insulin-like growth factor 1 exerts a protective effect on hypoxic injury of aged BM-MSCs: role of autophagy. Stem Cell Res. Ther. 9, 284. https://doi.org/10.1186/s13287-018-1028-5
Yang, P., Lipowsky, R., Dimova, R., 2009. Nanoparticle formation in giant vesicles: synthesis in biomimetic compartments. Small Weinh. Bergstr. Ger. 5, 2033–2037. https://doi.org/10.1002/smll.200900560
Yang, S., Alnaqeeb, M., Simpson, H., Goldspink, G., 1996. Cloning and characterization of an IGF-1 isoform expressed in skeletal muscle subjected to stretch. J. Muscle Res. Cell Motil. 17, 487–495.
Yang, S.Y., Goldspink, G., 2002. Different roles of the IGF-I Ec peptide (MGF) and mature IGF-I in myoblast proliferation and differentiation. FEBS Lett. 522, 156–160.
Yang, X., Stein, E.W., Ashkenazi, S., Wang, L.V., 2009. Nanoparticles for photoacoustic imaging. Wiley Interdiscip. Rev. Nanomed. Nanobiotechnol. 1, 360–368. https://doi.org/10.1002/wnan.42
Yang, Y., Hu, L., Zheng, H., Mao, C., Hu, W., Xiong, K., Wang, F., Liu, C., 2013. Application and interpretation of current autophagy inhibitors and activators. Acta Pharmacol. Sin. 34, 625–635. https://doi.org/10.1038/aps.2013.5
Yang, Z., Ghoorun, R.A., Fan, X., Wu, P., Bai, Y., Li, J., Chen, H., Wang, L., Wang, J., 2015. High expression of Beclin-1 predicts favorable prognosis for patients with colorectal cancer. Clin. Res. Hepatol. Gastroenterol. 39, 98–106. https://doi.org/10.1016/j.clinre.2014.06.014
Yang, Zhang, Y., 2004. Encapsulation of Quantum Nanodots in Polystyrene and Silica Micro-/Nanoparticles. Langmuir 20, 6071–6073. https://doi.org/10.1021/la049610t
Yap, R., Ianno, D., Burgess, A., 2016. Colonoscopic localization accuracy for colorectal resections in the laparoscopic era. Am. J. Surg. 212, 258–263. https://doi.org/10.1016/j.amjsurg.2015.12.014
Yeh, C.-Y., Hsiao, J.-K., Wang, Y.-P., Lan, C.-H., Wu, H.-C., 2016. Peptide-conjugated nanoparticles for targeted imaging and therapy of prostate cancer. Biomaterials 99, 1–15. https://doi.org/10.1016/j.biomaterials.2016.05.015
Yi, Q., Feng, J., He, L., Wan, R., Zeng, H., Yang, L., Wu, S., Tang, L., 2017. The structure-function relationships of insulin-like growth factor 1 Ec in C2C12 cells. Cell Adhes. Migr. 12, 47–55. https://doi.org/10.1080/19336918.2017.1318240

Ying, E., Li, D., Guo, S., Dong, S., Wang, J., 2008. Synthesis and bio-imaging application of highly luminescent mercaptosuccinic acid-coated CdTe nanocrystals. PloS One 3, e2222. https://doi.org/10.1371/journal.pone.0002222

Yong, K.-T., Law, W.-C., Roy, I., Jing, Z., Huang, H., Swihart, M.T., Prasad, P.N., 2011. Aqueous phase synthesis of CdTe quantum dots for biophotonics. J. Biophotonics 4, 9–20. https://doi.org/10.1002/jbio.201000080

Yong, K.-T., Swihart, M.T., 2012. In vivo toxicity of quantum dots: no cause for concern? Nanomed. 7, 1641–1643. https://doi.org/10.2217/nnm.12.152

Yong, K.-T., Wang, Y., Roy, I., Rui, H., Swihart, M.T., Law, W.-C., Kwak, S.K., Ye, L., Liu, J., Mahajan, S.D., Reynolds, J.L., 2012. Preparation of quantum dot/drug nanoparticle formulations for traceable targeted delivery and therapy. Theranostics 2, 681–694. https://doi.org/10.7150/thno.3692

Yothers, G., O'Connell, M.J., Lee, M., Lopatin, M., Clark-Langone, K.M., Millward, C., Paik, S., Sharif, S., Shak, S., Wolmark, N., 2013. Validation of the 12-gene colon cancer recurrence score in NSABP C-07 as a predictor of recurrence in patients with stage II and III colon cancer treated with fluorouracil and leucovorin (FU/LV) and FU/LV plus oxaliplatin. J. Clin. Oncol. Off. J. Am. Soc. Clin. Oncol. 31, 4512–4519. https://doi.org/10.1200/JCO.2012.47.3116

Young, M.M., Takahashi, Y., Khan, O., Park, S., Hori, T., Yun, J., Sharma, A.K., Amin, S., Hu, C.-D., Zhang, J., Kester, M., Wang, H.-G., 2012. Autophagosomal membrane serves as platform for intracellular death-inducing signaling complex (iDISC)-mediated caspase-8 activation and apoptosis. J. Biol. Chem. 287, 12455–12468. https://doi.org/10.1074/jbc.M111.309104

Yu, H., Rao, B., Jiang, W., Yang, S., Zhu, M., 2017. The photoluminescent metal nanoclusters with atomic precision. Coord. Chem. Rev. https://doi.org/10.1016/j.ccr.2017.12.005

Yu, M., Zheng, J., 2015. Clearance Pathways and Tumor Targeting of Imaging Nanoparticles. ACS Nano 9, 6655–6674. https://doi.org/10.1021/acsnano.5b01320

Yu, W.W., Chang, E., Drezek, R., Colvin, V.L., 2006. Water-soluble quantum dots for biomedical applications. Biochem. Biophys. Res. Commun. 348, 781–786. https://doi.org/10.1016/j.bbrc.2006.07.160

Yuan, N., Song, L., Zhang, S., Lin, W., Cao, Y., Xu, F., Fang, Y., Wang, Zhen, Zhang, H., Li, X., Wang, Zhijian, Cai, J., Wang, Jian, Zhang, Y., Mao, X., Zhao, W., Hu, S., Chen, S., Wang, Jianrong, 2015. Bafilomycin A1 targets both autophagy and apoptosis pathways in pediatric B-cell acute lymphoblastic leukemia. Haematologica 100, 345–356. https://doi.org/10.3324/haematol.2014.113324

Yuan, X., Luo, Z., Zhang, Q., Zhang, X., Zheng, Y., Lee, J.Y., Xie, J., 2011. Synthesis of highly fluorescent metal (Ag, Au, Pt, and Cu) nanoclusters by electrostatically induced reversible phase transfer. ACS Nano 5, 8800–8808. https://doi.org/10.1021/nn202860s

Yuan, Z.-X., Wang, X.-Y., Qin, Q.-Y., Chen, D.-F., Zhong, Q.-H., Wang, L., Wang, J.-P., 2013. The prognostic role of BRAF mutation in metastatic colorectal cancer receiving anti-EGFR monoclonal antibodies: a meta-analysis. PloS One 8, e65995. https://doi.org/10.1371/journal.pone.0065995

Zanou, N., Gailly, P., 2013. Skeletal muscle hypertrophy and regeneration: interplay between the myogenic regulatory factors (MRFs) and insulin-like growth factors (IGFs) pathways. Cell. Mol. Life Sci. CMLS 70, 4117–4130. https://doi.org/10.1007/s00018-013-1330-4

Zeestraten, E.C.M., Benard, A., Reimers, M.S., Schouten, P.C., Liefers, G.J., van de Velde, C.J.H., Kuppen, P.J.K., 2013. The Prognostic Value of the Apoptosis Pathway in Colorectal Cancer: A Review of the Literature on Biomarkers Identified by Immunohistochemistry. Biomark. Cancer 5, 13–29. https://doi.org/10.4137/BIC.S11475

Zeng, Q., Zhang, Y., Song, K., Kong, X., Aalders, M.C.G., Zhang, H., 2009. Enhancement of sensitivity and specificity of the fluoroimmunoassay of Hepatitis B virus surface antigen through "flexible" coupling between quantum dots and antibody. Talanta 80, 307–312. https://doi.org/10.1016/j.talanta.2009.06.061

Zeng, Y., Tian, X., Wang, Q., He, W., Fan, J., Gou, X., 2018. Attenuation of everolimus-induced cytotoxicity by a protective autophagic pathway involving ERK activation in renal cell carcinoma cells. Drug Des. Devel. Ther. 12, 911–920. https://doi.org/10.2147/DDDT.S160557

Zhang, B., Luo, Q., Chen, Z., Shi, Y., Ju, Y., Yang, L., Song, G., 2016. Increased nuclear stiffness via FAK-ERK1/2 signaling is necessary for synthetic mechano-growth factor E peptide-induced tenocyte migration. Sci. Rep. 6, 18809. https://doi.org/10.1038/srep18809

Zhang, B., Luo, Q., Mao, X., Xu, B., Yang, L., Ju, Y., Song, G., 2014. A synthetic mechano-growth factor E peptide promotes rat tenocyte migration by lessening cell stiffness and increasing F-actin formation via the FAK-ERK1/2 signaling pathway. Exp. Cell Res. 322, 208–216. https://doi.org/10.1016/j.yexcr.2014.01.005

Zhang, C., Arentz, G., Winderbaum, L., Lokman, N.A., Klingler-Hoffmann, M., Mittal, P., Carter, C., Oehler, M.K., Hoffmann, P., 2016. MALDI Mass Spectrometry Imaging Reveals Decreased CK5 Levels in Vulvar Squamous Cell Carcinomas Compared to the Precursor Lesion Differentiated Vulvar Intraepithelial Neoplasia. Int. J. Mol. Sci. 17, 1088. https://doi.org/10.3390/ijms17071088

Zhang, C., Yan, J., Liu, C., Ji, X., He, Z., 2014. One-pot synthesis of DNA-CdTe:Zn2+ nanocrystals using Na2TeO3 as the Te source. ACS Appl. Mater. Interfaces 6, 3189–3194. https://doi.org/10.1021/am405864z

Zhang, H., Zeng, X., Li, Q., Gaillard-Kelly, M., Wagner, C.R., Yee, D., 2009. Fluorescent tumour imaging of type I IGF receptor in vivo: comparison of antibody-conjugated quantum dots and small-molecule fluorophore. Br. J. Cancer 101, 71–79. https://doi.org/10.1038/sj.bjc.6605103

Zhang, S., Huang, J., Zhang, J., Liu, Y., Wang, Y., Jin, Q., Wang, W., Zhu, H., Huang, H., Qiu, M., Wu, H., 2015. Automatic Immunoscoring of Immunohistochemistry Images of Human Lung Cancer Tissue Samples: A Screening Tool, in: 2015 Seventh International Conference on Measuring Technology and Mechatronics Automation. Presented at the 2015 Seventh International Conference on Measuring Technology and Mechatronics Automation, pp. 217–220. https://doi.org/10.1109/ICMTMA.2015.60

Zhang, X., Wang, Y., Yan, W., Mao, J., Wang, J., Jiang, J., Dai, Y., 2015. [Application of lymph node labeling with carbon nanoparticles in laparoscopic colorectal cancer surgery]. Zhonghua Yi Xue Za Zhi 95, 2612–2615.

Zhang, X.-D., Luo, Z., Chen, J., Shen, X., Song, S., Sun, Y., Fan, S., Fan, F., Leong, D.T., Xie, J., 2014. Ultrasmall Au10−12(SG)10−12 Nanomolecules for High Tumor Specificity and Cancer Radiotherapy. Adv. Mater. 26, 4565–4568. https://doi.org/10.1002/adma.201400866

Zhang, X.-D., Luo, Z., Chen, J., Song, S., Yuan, X., Shen, X., Wang, H., Sun, Y., Gao, K., Zhang, L., Fan, S., Leong, D.T., Guo, M., Xie, J., 2015. Ultrasmall Glutathione-Protected Gold Nanoclusters as Next Generation Radiotherapy Sensitizers with High Tumor Uptake and High Renal Clearance. Sci. Rep. 5. https://doi.org/10.1038/srep08669

Zhao, M.-X., Zhu, B.-J., Yao, W.-J., Chen, D.-F., Wang, C., 2018. The delivery of doxorubicin of multifunctional β-cyclodextrin-modified CdSe/ZnS quantum dots for bioactivity and nano-probing. Chem. Biol. Drug Des. 91, 285–293. https://doi.org/10.1111/cbdd.13080

Zhao, S., Wang, S., Pan, P., Xia, T., Chang, X., Yang, X., Guo, L., Meng, Q., Yang, F., Qian, W., Xu, Z., Wang, Y., Wang, Z., Gu, L., Wang, R., Jia, F., Yao, J., Li, Z., Bai, Y., 2019. Magnitude, Risk Factors, and Factors Associated With Adenoma Miss Rate of Tandem Colonoscopy: A Systematic Review and Meta-analysis. Gastroenterology 156, 1661-1674.e11. https://doi.org/10.1053/j.gastro.2019.01.260

Zheng, H., Li, X., Chen, C., Chen, J., Sun, J., Sun, Si, Jin, L., Li, J., Sun, Shengrong, Wu, X., 2016. Quantum dot-based immunofluorescent imaging and quantitative detection of TOP2A and prognostic value in triple-negative breast cancer. Int. J. Nanomedicine 11, 5519–5529. https://doi.org/10.2147/IJN.S111594

Zheng, H., Zhang, X., Wang, X., Sun, B., 2012. Autophagy Enhances the Aggressiveness of Human Colorectal Cancer Cells and Their Ability to Adapt to Apoptotic Stimulus. Cancer Biol. Med. 9, 105–110. https://doi.org/10.3969/j.issn.2095-3941.2012.02.004

Zheng, J., Zhou, C., Yu, M., Liu, J., 2012. Different Sized Luminescent Gold Nanoparticles. Nanoscale 4, 4073–4083. https://doi.org/10.1039/c2nr31192e

Zheng, Y., Lai, L., Liu, W., Jiang, H., Wang, X., 2017. Recent advances in biomedical applications of fluorescent gold nanoclusters. Adv. Colloid Interface Sci. 242, 1–16. https://doi.org/10.1016/j.cis.2017.02.005

Zhou, J., Yang, Y., Zhang, C., 2015. Toward Biocompatible Semiconductor Quantum Dots: From Biosynthesis and Bioconjugation to Biomedical Application. Chem. Rev. 115, 11669–11717. https://doi.org/10.1021/acs.chemrev.5b00049

Zimmer, J.P., Kim, S.-W., Ohnishi, S., Tanaka, E., Frangioni, J.V., Bawendi, M.G., 2006. Size series of small indium arsenide-zinc selenide core-shell nanocrystals and their application to in vivo imaging. J. Am. Chem. Soc. 128, 2526–2527. https://doi.org/10.1021/ja0579816

Zinevich, L.S., Goncharova, N.O., Uruvaeva, I.V., Delone, G.V., Mikaelian, A.S., 2013. [Igf-1 and its isoform expression in hepatic cell tumors and the surrounding tissue in mice liver carcinogenesis induced by diethylnitrozamine]. Izv. Akad. Nauk Seriia Biol. Ross. Akad. Nauk 673–681.

9 Chapter 9: Appendix

9.1 Western blot results – preliminary data

9.1.1 Introduction

This chapter briefly outlines preliminary western blot work on tissues and cell lines investigating the expression of the MGF peptide. The techniques and limitations are described and further experiments required before drawing acceptable conclusions from this work.

9.1.2 Method

9.1.3 Western blot technique

9.1.3.1 Lysate extraction from the cell lines

The cell lines were seeded in 6 well plates at a density of 1x 10^6/well with the DMEM medium containing 10% FBS and 1% Penstrep at 37^{o}C, in 5% CO2 for 48 hours. Following this, the culture medium was removed, and the cells were washed twice with cold PBS. The cells were detached using cell scrapers in 1ml cold PBS, and the cell suspension was transferred to microcentrifuge tubes. The tubes were centrifuged at 3000 rpm for 5 minutes, and the supernatant discarded. The pelleted cells were suspended in 1 ml cold RIPA buffer (Radio Immuno Precipitation Assay) with freshly added inhibitor cocktail (Roche). Freeze-thawing cycles were carried out to enhance cell lysis. The resulting mixture was centrifuged at 14000 xg for 15 minutes, and the supernatant containing the protein transferred to another tube. Total protein concentration was measured using a modified Lowry protein assay kit (Pierce Biotechnology, USA), following the manufacture's protocol. The final protein concentrations for the cell lysates used were 2.1 mg/ml for 3T3 cell line, 2.4 mg/ml for MCF7 cell line, 0.8 mg/ml for the HT29 cell line and 1.8 mg/ml for the SW629 cell line.

9.1.3.2 Lysis extraction from tissues

Tissue samples, stored in liquid nitrogen, were sliced to small pieces using a clean razor blade. These samples were thawed in RIPA buffer and inhibitor cocktail (Roche). The tissue was transferred to a grinder and 20 strokes used to grind the tissues. This tissue was then collected in a microcentrifuge tube and centrifuged at 4500 xg for 4 minutes, and the supernatant collected, and protein concentration measured using a modified Lowry protein assay kit (Pierce Biotechnology, USA) following the manufacturer's protocol. The final protein concentrations for the tissue lysates were 0.5 mg/ml for the lane one colorectal liver metastasis, 3mg/ml for the second lane colorectal liver metastasis, and 3mg/ml for the normal liver tissues.

9.1.3.3 Denaturing samples and performing electrophoresis

Following the preparation of the lysates from the cell lines and the tissues, 10µL of PBS was added to 10µL of the lysate salutation. This was mixed with 20µL of loading buffer (NuPage® LDS sample buffer, which contains sodium dodecyl sulphate (SDS) and subjected to the Vortex mixer for 5 seconds. Subsequently, the solutions were subject to a water bath at 90^{o}c for 5 minutes and subjected to the Vortex mixer for a further few seconds.
The chambers were filled with the NuPage® SDS running buffer, and the NuPage® gel plate was used for the electrophoresis. 20µL of each sample lysate was placed in the wells with a 12µL standard protein ladder in the 1st slot. The remaining wells were allocated as follows: (2) and (3) Colorectal liver metastatic tissue (4) and (5) normal liver tissue (6) Fibroblast 3T3 cell line (7) MCF7 breast cancer cell line (8) SW620 cell line treated with autophagy inducing agent (9) SW620 cell line (10) HT29 cell line treated with autophagy inducing agent. The Xcell II™ Mini-Cell system was used on an automated 44 program of 90 min at 35 mA (125 V, 5 W) using a PowerEase® 500 power supply (Invitrogen). Following electrophoresis proteins were

transferred to polyvinylidene difluoride (PVDF) membrane (Bio-Rad Laboratories Ltd), pre-treated by soaking in methanol for 10 min. Gels were sandwiched with the PVDF membrane between several sheets of pre-wetted chromatography filter paper (Whatmen, Maidstone, UK) and sponges. This was submerged in an XCell II Blot Module (Invitrogen) filled with 1x Transfer buffer. Proteins were transferred using an automated program of 90 min at 125 mA (25 V, 17 W). Following electro-transfer, PVDF membranes were blocked in 5% (w/v) Marvel skimmed milk powder (Marvel, UK) in PBS for at least 1 hr. The blocked blots were washed in PBS and incubated on a rocker at room temperature for 1 hour in the primary MGF antibody diluted in 1% (w/v) Marvel/PBS. The blots were then washed with 3x 0.1% (v/v) Tween-20 in PBS, then 3x PBS followed by incubation on a rocker at room temperature for 1 hour in the secondary horseradish peroxidase (HRP)-conjugate antibody diluted in 1% (w/v) Marvel/PBS. Following incubation, the blots were washed as before and proteins visualised with DAB substrate solution (0.25 mg/ml 3, 3'-Diaminobenzidine tetrahydrochloride, 0.5 µl/ml H2O2 in dH2O).

9.1.4 Results

Western blotting, within limitations (discussed below), suggested expression of MGF in colorectal liver metastatic tissue, breast cancer cell line and the colorectal cancer cell lines and not demonstrated in normal liver tissue, and mildly in fibroblast cell line 3T3. (Figure 9.1). Lane 7 with the HT29 cell line did not demonstrate any signals.

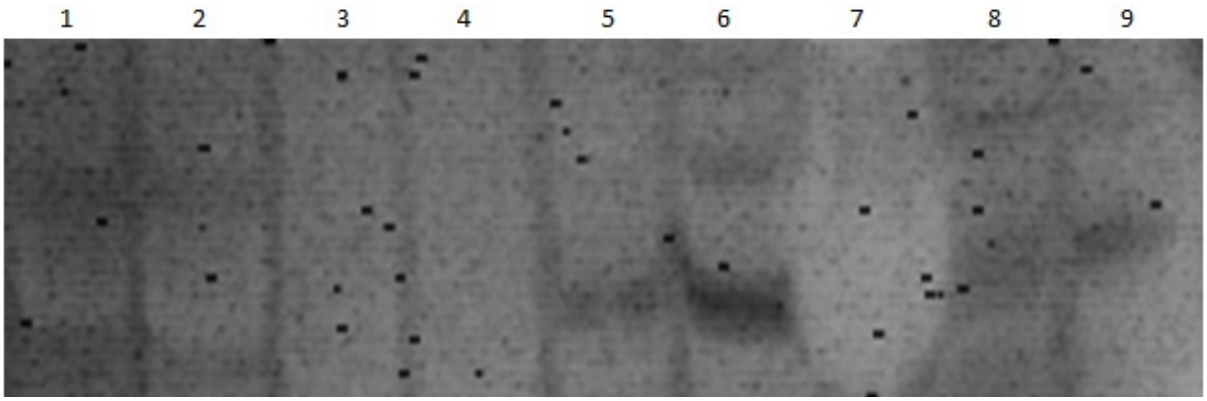

Figure 9.1*:* Western blotting for MGF. 1, 2 --Colorectal liver metastasis (tissue) 3,4 --Normal liver (tissue) 5– Fibroblast (cell line) 6-- Breast Cancer (cell line) 7, 8, 9—Colorectal cancer (cell lines HT29 and SW620)

9.1.5 Discussion

The results demonstrated are limited due to the lack of positive controls and the absence of the reference protein ladder. It is also unclear as to why lane 7, which included the colorectal cancer cell line HT29, did not demonstrate any signals with an empty lane. Interestingly, the breast cancer cell line MCF7 demonstrated the strongest signal. Overall, due to the significant limitations of the methodology, this will be required to be repeated with a positive control such as prostate cancer or skeletal muscle before firm conclusions can be reached.

9.2 Quantum dot conjugated with MGF application in colorectal cancer cell lines: preliminary data in assessing suitability for quantification

9.2.1 Introduction

Since initial reports of quantum dot-based immunohistochemistry in 2001, an increasing number of protocols have been reported in the literature (Akhtar et al., 2007; Vu et al., 2015). Recent studies are in Table 2.4, demonstrating the efficacy of quantum dot immunohistochemistry to have equal or superior ability to quantify the expression of single and multiple antigens in different cancer tissues. I describe preliminary work investigating the quantification of semiconductor quantum dot fluorescence which would be useful in quantitative immunofluorescent techniques.

9.2.2 Supplementary methods

9.2.2.1.1 Ultraviolet-visible absorbance spectroscopy

The JASCO FP-8300 Spectrofluorometer was used to measure emission spectra of the quantum dots when excited at wavelengths of 355 nm and 390 nm. The quantum dots were diluted in distilled water and the absorbance and emission of serially diluted quantum dots measured. Serial dilutions of the quantum dot and the conjugated MGF antibody quantum dots in PBS was performed in six groups of 3 wells each. Group 1 contained 100 µL of the undiluted quantum dot, group 2 contained 50 µL of quantum dot and 50 µL of PBS, group 3 contained 25 µL of the quantum dot, and 25 µL of quantum dot and this dilution continued to 6 groups.

9.2.3 Results

9.2.3.1.1 Ultraviolet-visible absorbance spectroscopy

The intensity of the emission spectrum of serially diluted unconjugated CdTe/MSA quantum dot is illustrated in Figure 9.2. Using the pre-set wavelengths of excitation at 355nm and 390nm, and the strength of the emission at 620nm was measured with the JASCO FP-8300 Spectrofluorometer. The emission was higher at 355nm compared to 390nm excitation and increasing the lag time and integration time produced the maximum emission from the unconjugated CdTe/MSA quantum dots. Figure 9.3 demonstrates CdTe/MSA quantum dots conjugated with the MGF antibody subjected to the same procedure. The serially diluted quantum dots demonstrated an exponential decrease in the fluorescence and therefore provided a good standard for quantification.

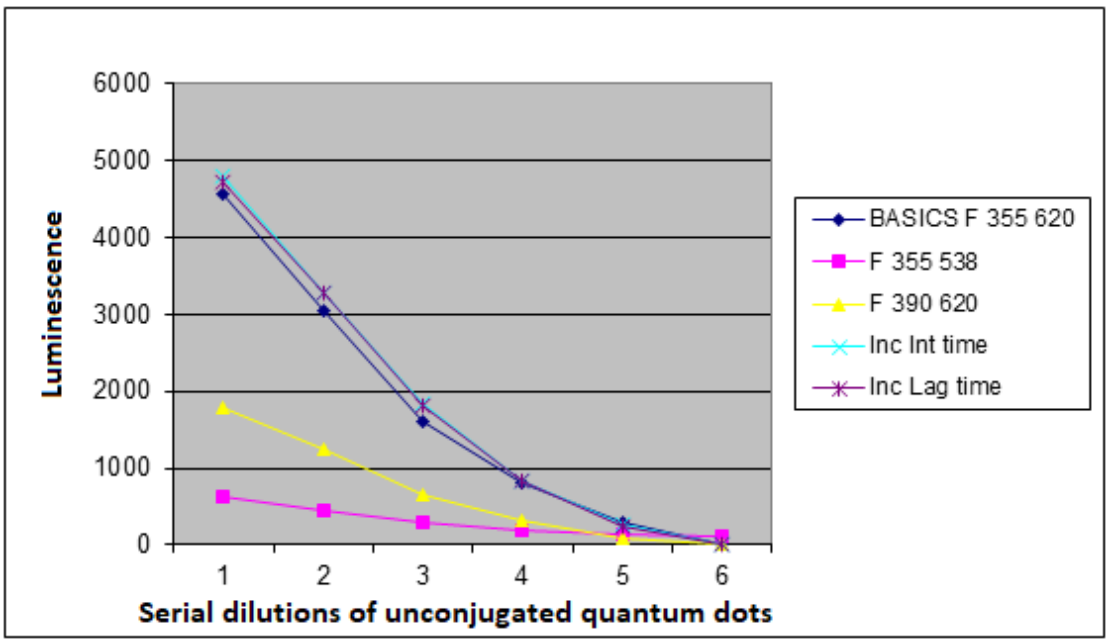

Figure 9.2: Emission strength of serially diluted unconjugated quantum dots. The different lines represent the different settings on filters used. Group 1 – 1:1000 unconjugated quantum dot concentration with serial dilutions x2 progressively to group 6.

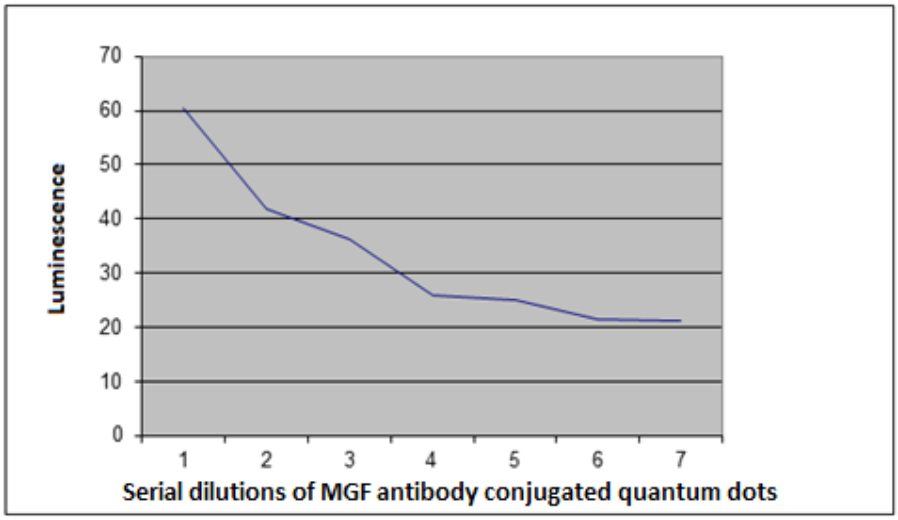

Figure 9.3: Emission strength of serially diluted quantum dots conjugated with MGF antibody. Filter at 355 excitation 620 absorbance. Group 1 – 1:1000 MGF antibody conjugated quantum dot concentration with serial dilutions x2 progressively to group 7.

9.2.4 Discussion

These results demonstrate the fluorescence intensity of the quantum dots can be predicted from the concentration of quantum dots subjected to external excitation, suggesting that automation of quantification of immunohistochemistry slides assessment is feasible. The additional benefit of quantum dot immunofluorescence is the ability to use quantum dots with different excitation spectra targeting different proteins on the slides and therefore enable rapid assessment with a smaller volume of tissues which is particularly of use in biopsies from tissues which are limited by small volumes. Table 2.4 outlines recent studies confirming the ability of quantum dots to achieve this purpose.

Further work would include experiments involving the application of MGF antibody-conjugated quantum dots of tissue slides and comparing the results generated compared to the current gold standard of histopathologist scoring. This work will include the feasibility of identifying spectrofluorometers which are sensitive enough to detect the fluorescence of the quantum dots in tissues which have low levels of expression of proteins of interest.

9.3 The validity of cell viability assay used for the autophagy experiments

Figure 9.4 demonstrates the standardisation of the cell viability assay using six different concentrations of the SW620 cell line incubated for 24 hours with CellTiter-Blue®. The graph demonstrated a predictable drop in measurements with the reducing cell densities, thereby confirming the validity of the assay.

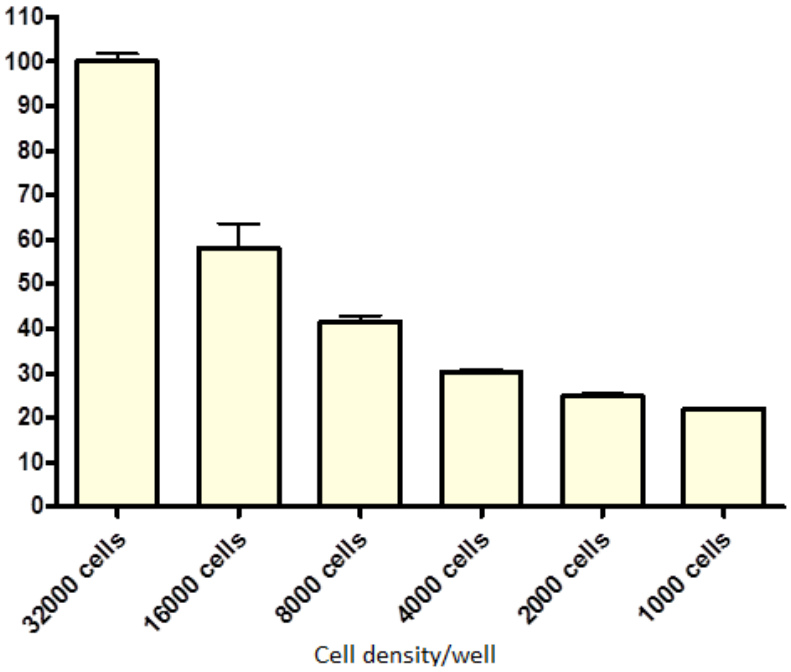

Figure 9.4*:* Cell viability assay validation using reducing concentrations of SW620 cells

9.4 Publications

9.4.1 Manuscript accepted for publication

- Mechano-growth Factor Expression in Colorectal Cancer Investigated with Fluorescent Gold Nanoparticles. S Alagaratnam, SY Yang, M Loizidou, B Fuller, B Ramesh. Anticancer Res. 2019 Apr;39(4):1705-1710

9.4.2 Abstracts published from poster presentations at the 2012 British Association of Surgical Oncology and Association of Cancer Surgery conference

- The Mechanogrowth factor expression in colorectal cancer: a potential new target for nanoparticles. S Alagaratnam, A Johnson, A Seifalian, M Winslet, S Yang. European Journal of Surgical Oncology 2012 Nov;38(11):1122
- The role of autophagy in colorectal cancer cells: a pro-survival mechanism**.** S Alagaratnam, A Johnson, J Coppell, A Seifalian, S Yang. European Journal of Surgical Oncology 2012 Nov;38(11):1120

9.4.3 Manuscripts being submitted for publication

- ***Review paper*** **-** Mechanogrowth factor (IGF1-1Ec) in cancer. S Alagaratnam, B Ramesh, B Fuller, S Yang. *Submitted to the Journal of cellular pathology*

- ***Research paper*** **–** Increased expression of IGF-1Ec with increasing colonic polyp dysplasia and colorectal cancer. S Alagaratnam, S Yang, B Ramesh, TV Luong, M Loizidou, B Fuller. *Being submitted to Growth Hormone and IGF Research Journal*